



Isolation, Characterization and Anticancer Evaluation of Alkaloids from *Eumachia montana* (Rubiaceae)

Thesis submitted to the University of Nottingham for the degree of

Doctor of Philosophy

March 2025

Yuye Shuai

20216520

Supervisor:

Tracey D. Bradshaw, Kuan Hon Lim, Premanand Krishnan, Dong-Hyun Kim

School of Pharmacy, Faculty of Science

University of Nottingham

Table of Contents

ABSTRACT	4
ACKNOWLEDGEMENTS.....	5
LIST OF ABBREVIATIONS	6
CHAPTER 1 INTRODUCTION	13
1.1 NATURAL PRODUCTS AND DRUG DISCOVERY	13
<i>Classification of Anticancer Drugs Derived from NPs</i>	<i>13</i>
<i>Methodologies for Natural Product Drug Discovery.....</i>	<i>21</i>
<i>Challenges in Natural Product Drug Discovery</i>	<i>25</i>
1.2 ALKALOIDS AND THE GENUS <i>EUMACHIA</i>	25
<i>Classification, occurrence, biosynthesis, and bioactivities of Alkaloids.....</i>	<i>25</i>
<i>The Genus Eumachia (syn. Psychotria)</i>	<i>38</i>
1.3 CANCERS.....	47
<i>Breast cancer.....</i>	<i>48</i>
<i>Colorectal cancer</i>	<i>50</i>
<i>Brain cancer (glioblastoma multiforme)</i>	<i>53</i>
<i>Lung cancer.....</i>	<i>55</i>
1.4 METABOLOMICS	57
<i>Metabolomics Techniques.....</i>	<i>58</i>
<i>Metabolomics in Drug Discovery, Cellular Mechanism</i>	<i>59</i>
<i>Metabolomics in Biomarkers' Identification</i>	<i>60</i>
<i>Targeting Metabolic Pathways in Cancer Cells.....</i>	<i>61</i>
<i>Challenges and Future Directions.....</i>	<i>66</i>
1.5 RESEARCH OBJECTIVES.....	69
CHAPTER 2 ISOLATION, CHARACTERIZATION OF ALKALOIDS FROM <i>EUMACHIA MONTANA</i>	71
2.1 INTRODUCTION.....	71
<i>The Genus Eumachia.....</i>	<i>72</i>
<i>Bioactivity of Oligocyclotryptamine Alkaloids from Eumachia</i>	<i>73</i>
<i>Advancements in Structural Characterization and Synthesis</i>	<i>74</i>
<i>Exploring Eumachia montana as a Source of Novel Alkaloids.....</i>	<i>75</i>
2.2 RESULTS AND DISCUSSION	78
2.2.1(-)- Calycanthine (1).....	78
2.2.2 Inseparable oligocyclotryptamine alkaloids from <i>Eumachia montana</i>	81
2.2.3 Eumatricine (5).....	91
2.3 CONCLUSION	96
CHAPTER 3 ANTICANCER EVALUATION OF OLEOIDINE (2), CALEDONINE (3) AND EUMATANINE (4).....	97
3.1 INTRODUCTION.....	97
3.2 RESULTS AND DISCUSSION	98
3.2.1 Preliminary screening of oleoidine (2), caledonine (3) and eumatanine (4)	98
3.2.2 Cellular Mechanism of caledonine (3) and eumatanine (4).....	110
3.3 CONCLUSION	131
CHAPTER 4 METABOLOMICS STUDIES	133
4.1 INTRODUCTION.....	133
4.2 RESULTS AND DISCUSSION.....	137

4.2.1 LC-HRMS-based data processing and metabolite identification	137
4.2.2 The analytical performance of LC-HRMS and Multivariate Analysis	139
4.2.3 Metabolite Comparison	142
4.2.4 Pathway Analysis.....	143
4.3 CONCLUSION AND FUTURE WORK.....	162
CHAPTER 5 GENERAL CONCLUSION	165
CHAPTER 6 MATERIALS AND METHODS	167
6.1 ISOLATION AND CHARACTERISATION OF ALKALOIDS	167
6.1.1 Plant Source and Authentication	167
6.1.2 General Experimental Procedures	167
6.1.3 Chromatography Techniques.....	168
6.1.4 Spray Reagent (Dragendorff's reagent)	171
6.1.5 Extraction of alkaloids	172
6.1.6 Isolation of alkaloids	173
6.1.7 Compound Data.....	176
6.2 CELL CULTURE ASSAYS.....	177
6.2.1 General Cell Culture	177
6.2.2 MTT cell viability assay.....	182
6.2.3 Cell counting assay.....	185
6.2.4 Clonogenic assay.....	186
6.2.5 Flow cytometry studies.....	187
6.2.6 Fluorescent microscopy.....	191
6.2.7 Caspase 3/7 assay.....	192
6.2.8 Reactive oxygen species assay.....	194
6.2.9 Metabolomics study.....	196
Statistical analysis	199
REFERENCES.....	200
APPENDICES	257

Abstract

The dimeric (-)-calycanthine (**1**), the hexameric (+)-oleoidine (**2**), the heptameric (+)-caledonine (**3**), the octameric (+)-eumatanine (**4**) and a tricyclic pyrroloquinoline alkaloid, eumatricine (**5**) are alkaloids isolated from the leaves of *Eumachia montana*; compounds **4** and **5** are previously uncharacterized alkaloids. Preliminary anticancer assays, including MTT, cell count and clonogenic assays, revealed potent inhibition of cell growth and colony formation by compounds **2-4** against seven carcinoma cell lines (including breast, colorectal, lung and glioblastoma multiforme cell lines). The GI₅₀ values of compounds **2-4** ranged from 0.1 to 2.7 μM, and potent cytotoxic activity against HCT-116 and MCF-7 was observed (**3** > **4** > **2**). Cell cycle analysis and apoptosis assays revealed that compound **3** and **4** evokes profound apoptosis without cell cycle phase-specific arrest (under most circumstance except in MCF-7 cells when against **4** at 1 × GI₅₀ for 24h). Additionally, compound **4** also activated caspase, further corroborating the conclusion of apoptosis-induction. Detection of ROS induced by **4** infers a role for oxidative stress in anticancer activity, while γH2AX detection indicates the presence of DNA double strand breaks. Visualization of **4**-treated cells by fluorescence microscopy implies multiple cell death pathways are simultaneously triggered (e.g., apoptosis, autophagy, necrosis and paraptosis). Furthermore, metabolomic analysis of **3** and **4** highlights their disruption of membrane integrity through the upregulation of glycerophosphoethanolamine (GPE), glycerophosphocholine (GPC), and acetylcholine (ACh), reinforcing their role in apoptosis induction. These findings provide valuable insights into the mechanism of action of these compounds and their potential as anticancer agents.

Acknowledgements

First and foremost, I would like to express my deepest gratitude to my supervisor, Tracey, for her unwavering support, encouragement, and invaluable guidance throughout my PhD journey. Her continuous belief in me and her constructive insights have been instrumental in shaping both my research and personal growth.

I am sincerely thankful to Kuan Hon for his generous mentorship and support during my time at the University of Nottingham Malaysia Campus. His patience and dedication in teaching me have had a lasting impact on my academic development. I would also like to thank Hyun for his expert guidance on metabolomics, which significantly enriched the scientific depth of my research. Special thanks to Prem, whose help and support in Malaysia were pivotal to the early stages of my PhD and who continued to support me even after I relocated to the UK.

My heartfelt appreciation goes to my colleagues Rui, Haojie, Dilsu, Amelia, and Rasha for their technical assistance and camaraderie in the lab. Their help made the research process not only more efficient but also enjoyable.

Finally, I am deeply grateful to my parents for their constant love and encouragement, which have been the foundation of my perseverance. To my husband, Xiang—thank you for always standing by my side and being my greatest source of strength and support.

List of Abbreviations

^{13}C	Carbon-13
^1H	Proton
5-HT	5-hydroxytryptamine
ABS	Access and benefit-sharing
ACC	Acetyl co-a carboxylase
ACDs	Antibody-drug conjugates
ACGs	Annonaceous acetogenins
ACh	Acetylcholine
AChE	Acetylcholinesterase
ACLY	ATP-citrate lyase
ADCs	Antibody-drug conjugates
ADI	Enzyme arginine deiminase
AFt	Apoferitin
AI	Artificial intelligence
AML	Acute myeloid leukemia
AMPK	Adenosine monophosphate-activated protein kinase
ANM	Amino sugar and nucleotide sugar metabolism
APC	Adenomatous polyposis coli
APCI	Atmospheric pressure chemical ionization
ASA	Acetylsalicylic acid
ATCC	American type tissue culture collection
B-CLL	B-cell chronic lymphocytic leukemia
BBB	Blood-brain barrier
BC	Breast cancer
BChE	Butyrylcholinesterase
BER	Base excision repair
BGCs	Biosynthetic gene clusters
BP	Bromopyruvate
BSA	Bovine serum albumin
calcd	Calculated
CAR	Chimeric antigen receptor

CC	Column chromatography
ccRCC	Clear cell-renal cell carcinoma
CDCl ₃	Deuterated chloroform
CD ₃ OH	Deuterated methanol
CDKs	Cyclin-dependent kinases
ChAT	Choline acetyltransferase
CIMP	CpG island methylator phenotype
CIN	Chromosomal instability
CK	Creatine kinase
CKI	Compound kushen injection
CKi	Creatine kinase inhibitors
CLL	Chronic lymphocytic leukemia
COSY	Correlation spectroscopy
Cr	Creatine
CRC	Colorectal cancer
CRPC	Castration-resistant prostate cancer
CTLC	Centrifugal thin layer chromatography
CTZ	Clotrimazole
Cyt c	Cytochrome c
DCIS	Ductal carcinoma in situ
DFMO	Difluoromethylornithine
DG	Deoxyglucose
<i>DHFR</i>	Dihydrofolate reductase
DISC	Death-inducing signaling complex
DMSO	Dimethylsulfoxide
DMT	Dimethyltryptamine
DOX	Doxorubicin
DSB	Double-strand breaks
DTP	Drug-tolerant persister
<i>E.</i>	<i>Eumachia</i>
ECD	Electronic circular dichroism
EDI3	Endometrial differential 3
EDTA	Ethylenediaminetetraacetic acid

EGFR	Epidermal growth factor receptor
EMT	Epithelial–mesenchymal transition
EPR	Enhanced permeation and retention
ER	Endoplasmic reticulum
ESCC	Esophageal squamous cell carcinoma
ESI	Electrospray ionization
F1,6BP	Fructose-1,6-bisphosphate
F6P	Fructose-6-phosphate
FADD	<i>FAS</i> -associated death domain
<i>FAO</i>	Fatty acid oxidation
FAP	Familial adenomatous polyposis
FASN	Fatty acid synthase
FBDD	Fragment-based drug design
FBS	Foetal bovine serum
FDA	Food and drug administration
FT-ICR	Fourier transform ion cyclotron resonance
g	Gram
G3P	Glycerol 3-phosphate
G6PDH	Glucose 6-phosphate dehydrogenase
GBM	Glioblastoma multiforme
GC	Gas chromatography
GFAT	Glutamine:fructose-6-phosphate amidotransferase
GLS	Glutaminase
GPC	Glycerophosphocholine
GPE	Glycerophosphoethanolamine
HBP	Hexosamine biosynthetic pathway
HCC	Hepatocellular carcinoma
HEPES	N-2-hydroxyethylpiperazine-n'-2-ethanesulfonic acid
HER2	Human epidermal growth factor 2 receptor
HG	Hydroxyglutarate
HK	Hexokinase
HMBC	Heteronuclear multiple bond spectroscopy
HNPCCS	Hereditary nonpolyposis colorectal cancer

HPLC	High-performance liquid chromatography
HR	Homologous recombination
HR-DART-MS	High-resolution direct analysis in real-time mass spectrometry
HRESIMS	High-resolution electrospray ionization mass spectrometry
HTC	Hepatoma cell
HTS	High-throughput screening
IAA	Indole-3-acetic-acid
IBC	Inherited breast cancer
ICI	Immune checkpoint inhibition
IDH	Isocitrate dehydrogenase
IMS	Industrial methylated spirit
KEGG	Kyoto encyclopedia of genes and genomes
LARC	Locally advanced rectal cancer
LC	Liquid chromatography
LLC	Lewis lung carcinoma
Log ₂ FC	Log ₂ fold changes
<i>LPCAT1</i>	Lysophosphatidylcholine acyltransferase 1
lyso PC	Lysophosphatidylcholine
M	Molar
m/z	Accurate masses
MAO	Monoamine oxidase
MAPKs	Mitogen-activated protein kinases
<i>MCM3/5</i>	Minichromosome maintenance complex component 3 and 5
MDA	Microtubule-destabilizing agent
MDR	Multidrug resistance
MEM	Minimum essential medium
MeOH	Methanol
MGMT	Methylguanine dna-methyltransferase
MIAs	Monoterpenoid indole alkaloids
MIP	Molecularly imprinted polymers
miR	Microrna
ML	Machine learning
mM	Millimolar

MMR	Mismatch repair
MOMP	Mitochondrial outer membrane permeabilization
MS	Mass spectrometry
MSA	Microtubule-stabilizing agent
MSI	Microsatellite instability
MTA	Microtubule-targeting agent
MTT	3-[4,5-dimethylthiazol-2-yl]-2,5-diphenyl tetrazolium bromide
NCCD	The nomenclature committee on cell death
NCEs	New chemical entities
NCI	National cancer institute
NCRT	Neoadjuvant chemoradiation therapy
NEAA	Non-essential amino acids
NETs	Neuroendocrine tumours
NK	Natural killer
NMDA	N-methyl-d-aspartate
NMR	Nuclear magnetic resonance
NOESY	Nuclear overhauser effect spectroscopy
NP	Natural product
NPDD	Natural product drug discovery
NSCLC	Non-small cell lung cancer
NST	No special type
O6MG	O6 methyl guanine
OAT	Ornithine aminotransferase
OD	Optical density
ODC	Ornithine decarboxylase
OPLS-DA	Orthogonal partial least squares – discriminant analysis
OXPHOS	Oxidative phosphorylation
PARP	Poly (ADP-ribose) polymerase
PBS	Phosphate-buffered saline
PC	Product code
PCA	Principal component analysis
PD-L1	Programmed death ligand 1
PDA	Photodiode array

PDAC	Pancreatic ductal adenocarcinoma
PDC	Pyruvate dehydrogenase complex
PE	Plating efficiency
PFK	Phosphofructokinase
Pgp	P-glycoprotein
PI	Propidium iodide
PK	Pharmacokinetic
PLS-DA	Partial least squares discriminant analysis
PPP	Pentose phosphate pathway
PR	Progesterone receptor
PS	Phosphatidylserine
<i>PTDSSI</i>	Phosphatidylserine synthase 1
QC	Quality control
R5P	Ribose 5-phosphate
RB	Retinoblastoma
RES	Reticuloendothelial system
RNA	Ribonuclease A
ROS	Reactive oxygen species
RPMI	Rosewell park memorial institute
RT	Retention time
SA	Salicylic acid
SASP	Senescence-associated secretory phenotype
SCC	Skin squamous cell carcinoma
SCD1	Stearoyl-coa desaturase 1
SCLC	Small cell lung cancer
SDs	Standard derivations
SEC	Size-exclusion chromatography
SERMs	Selective estrogen receptor modulators
SF	Survival fraction
SPD	Styrylpyrone derivative
SPE	Solid-phase extraction
TCA	Tricarboxylic acid
TCM	Traditional chinese medicine

TEM	Transmission electron microscopy
TERT	Telomerase reverse transcriptase
TGI	Total growth inhibition
THH	Tetrahydroharmine
TKIs	Tyrosine kinase inhibitors
TLC	Thin layer chromatography
TMS	Tetramethylsilane
TMZ	Temozolomide
TNBC	Triple negative breast cancer
TOF	Time-of-flight
Topo	Topoisomerase
Topo Iccs	Topo I-DNA cleavage complexes
UDP-GlcNAc	Uridine-5'-diphospho-n-acetyl-d-glucosamine
UHPLC	Ultra high performance liquid chromatography
VCR	Vincristine
VEGF	Vascular endothelial growth factor
VIP	Variable importance
VLB	Vinblastine
XIAP	X-linked inhibitor of apoptosis

Chapter 1 Introduction

1.1 Natural Products and Drug Discovery

Natural products (NP), as the result of natural evolutionary fine-tuning, are defined as secondary metabolites produced by living organisms and regarded as an invaluable source of therapeutic agents. This is especially true with regard to anticancer drugs, the vast structural complexity and diversity of natural products provides numerous possibilities for discovery. Indeed, 50% of Food and Drug Administration (FDA)-approved drugs from 1940 to 2012 were natural product-derived or inspired by natural compounds, and > 60% of marketed anti-cancer agents within the time frame between 1981 and 2019 were derived from natural products. Their structural complexity and biological relevance make them invaluable in oncology, where they have been the basis for many approved anticancer drugs, including paclitaxel and doxorubicin.

Although extensive data indicate that natural products, including structures derived from or related to natural products, still represent a dominant source of novel drugs for the treatment of human diseases (e.g., infectious diseases (microbial, parasitic, and viral), cancers, antihypertensives, and anti-inflammatory), the pharmaceutical industry has placed more emphasis on combinatorial chemical techniques to identify and optimise lead compounds for drug discovery (Newman and Cragg, 2020). However, to date, only three combinatorial drugs have been approved as new chemical entities (NCEs), and two of them are anticancer drugs, namely sorafenib tosylate (approved by the FDA in 2005), for the treatment of advanced renal cancer; vemurafenib (approved by the FDA in 2011), which for the first-time engaged techniques of fragment screening and model fitting to design and construct an anticancer drug (Newman and Cragg, 2020).

Classification of Anticancer Drugs Derived from NPs

Cancer remains one of the leading causes of mortality worldwide, necessitating the discovery of innovative and effective therapeutic agents. Natural products, derived from plants, microbes, and marine organisms, have played a pivotal role in oncology, forming the basis of numerous chemotherapeutic agents (Newman and Cragg, 2020). They are characterized by their complex molecular architectures, which are difficult to replicate synthetically. This structural

complexity often correlates with high specificity for biological targets, making them ideal for anticancer drug discovery (Atanasov et al., 2021).

Antitumour antibiotics, one of the significant classes of anticancer agents produced by micro-organisms (or plants, or marine invertebrates), exert anticancer activity by DNA interaction, e.g., Actinomycin D, Doxorubicin (DOX), Mitomycin C, Etoposide, Irinotecan, and Bleomycin (**Figure 1.1**). These agents have multiple modes of action, hence may be subject to alternative classifications, i.e., alkylating agents, DNA cleavage agents, antimetabolites, topoisomerase inhibitors, antimicrotubule agents and others. Alkylating agents such as mitomycin C from *Streptomyces caespitosus* induce DNA cross-linking and alkylation-mediated damage. DNA cleavage agents like bleomycin from *Streptomyces verticillus* induce strand breaks through oxidative mechanisms. Antimetabolites disrupt nucleotide biosynthesis and function, exemplified methotrexate, derived from the natural folate analogue aminopterin. Topoisomerase inhibitors interfere with DNA replication and repair by targeting topoisomerase enzymes, which are essential for maintaining DNA supercoiling. Camptothecin, derived from *Camptotheca acuminata*, inhibits topoisomerase I (Topo I), leading to DNA strand breaks, while anthracycline antibiotic such as DOX, from *Streptomyces peucetius*, target topoisomerase II (Topo II), preventing religation of DNA strands and inducing apoptosis (Furuta et al., 2003, Lüpertz et al., 2010). Antimicrotubule agents disrupt mitotic spindle dynamics, thereby inhibiting cell division. Microtubule stabilizers like eribulin, a potent naturally occurring mitotic inhibitor targeting β -tubulin, is a synthetic macrocyclic ketone analogue of the marine sponge natural product *halichondrin B* (Towle et al., 2001). Eribulin is effective in treating metastatic breast cancer (BC) by causing prolonged and irreversible mitotic blockade, which triggers apoptosis (Towle et al., 2011, Kuznetsov et al., 2004). Other important anticancer drugs that derived from nature includes the topoisomerase inhibitors irinotecan (*Camptotheca acuminata*, Topo I) and etoposide (*Podophyllum peltatum*, Topo II), as well as the antimicrotubule agents paclitaxel (Taxol®) (*Taxus brevifolia*), vincristine (VCR), and vinblastine (VBL) (*Catharanthus roseus*) (Wang, 1985, Donehower, 1996, Gidding et al., 1999).

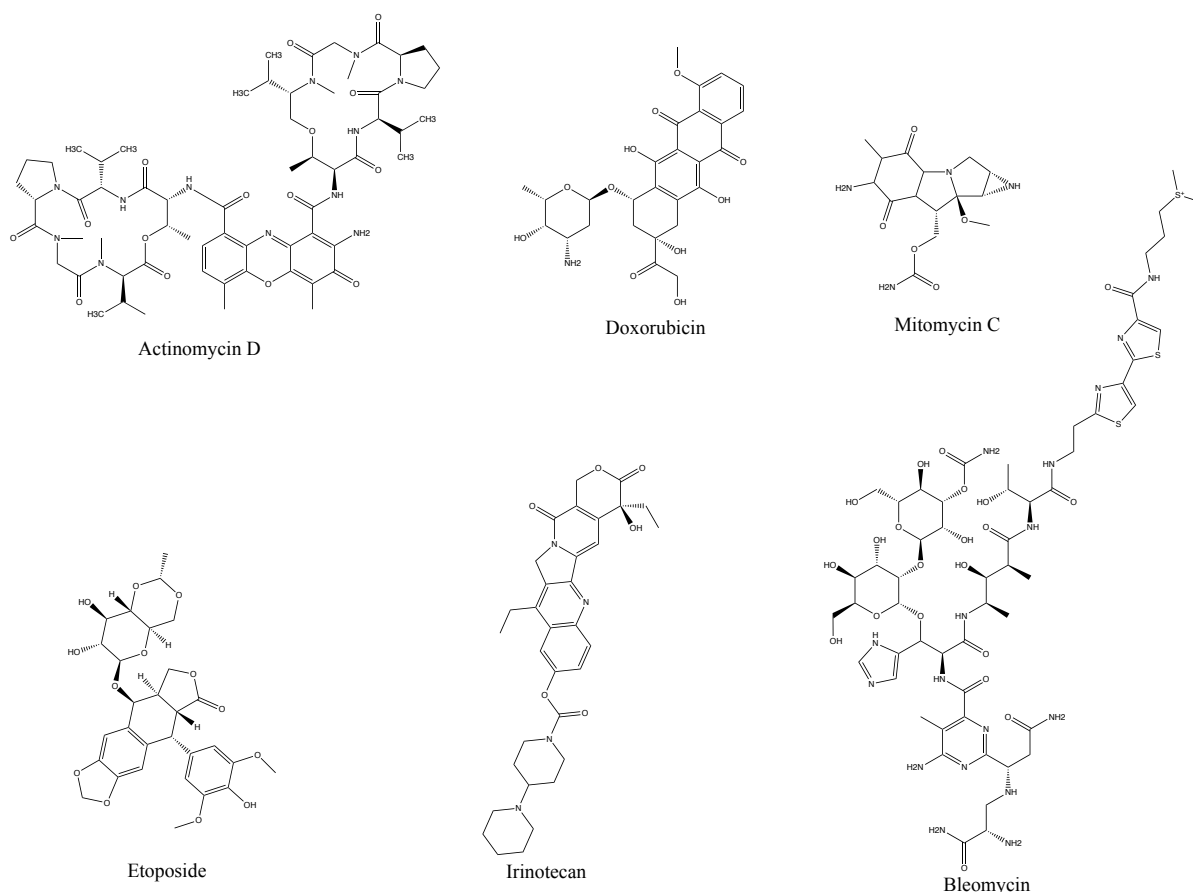


Figure 1. 1 Molecular structure of antitumour antibiotics from NP

Topoisomerase inhibitors

Topoisomerases (type I and II) are essential enzymes that are responsible for DNA supercoil relaxation by generating transient breaks in DNA strands/or prevent religation during replication, transcription, and repair, leading to apoptosis (D'Arpa and Liu, 1989, Froelich-Ammon and Osheroff, 1995). Topo I) introduces single-strand breaks to relax DNA, while Topo II) creates double-strand breaks to facilitate DNA passage, supercoil relaxation, and chromosome segregation; these processes (e.g. the catalytic cycle of Topo II) are mediated through ATP-dependent mechanisms (e.g. ATP hydrolysis) (D'Arpa and Liu, 1989, Robinson et al., 1993). Topoisomerase inhibitors function through two primary mechanisms. Specifically, Topo I inhibitors, such as camptothecin, irinotecan and topotecan, induce single-strand breaks, while Topo II inhibitors generate double-strand breaks by targeting DNA cleavage (e.g. etoposide, teniposide, and anthracyclines (idarubicin, daunorubicin, and DOX)) or ATP hydrolysis (e.g. novobiocin) (Wang, 1985, Robinson et al., 1993).

Topo I inhibitors primarily work by stabilizing the single-strand cleavage complex, resulting in DNA damage and cell death. For example, camptothecin, a natural alkaloid isolated from the bark of the Chinese tree *Camptotheca acuminata*, was first identified in the 1960s by researchers at the US National Cancer Institute (NCI), presenting potent antitumour activity by interacting noncovalently with the interface of the Topo I-DNA complex and thus preventing DNA religation (Hsiang et al., 1985, Wall and Wani, 1996). Therefore, camptothecins are both noncovalent binding agents and topoisomerase inhibitors. The mechanism of action of camptothecin involves the selective stabilization of transient Topo I-DNA cleavage complexes (Topo Iccs)(Hsiang et al., 1985, Pommier, 2006). By preventing the religation of DNA strands, camptothecin promotes the accumulation of single-strand breaks, which are converted into lethal double-strand breaks during DNA replication (Furuta et al., 2003).

Camptothecin specifically targets Topo I, as demonstrated by the resistance conferred by Topo I deletion or mutations in both yeast and vertebrate cells (Nitiss and Wang, 1988, Eng et al., 1988, Pommier et al., 1999). Structurally, the activity of camptothecin depends on the stereochemistry of the natural 20-S enantiomer, as inversion of its chiral centre to the 20-R configuration abolishes activity (Pommier, 2006). Since camptothecin binds reversibly Topo Iccs, it is considered a highly precise pharmacological tool, enabling controlled drug exposure and selective trapping of Topo Iccs (Pommier, 2006). To sum up, camptothecin is a valuable tool for exploring cellular responses to replication-associated DNA damage, as well as checkpoint and repair mechanisms (Pommier, 2013, Pommier et al., 2003, Pommier et al., 2006). However, camptothecins as anticancer drugs also cause severe side effects, which has led to the subsequent development of water-soluble derivatives of camptothecins, including topotecan and irinotecan, which are now widely used in clinical oncology (Hsiang et al., 1985, Wall and Wani, 1996). Additionally, liposomal formulations of camptothecin analogues, such as Onivyde (irinotecan liposome injection), have been developed to enhance anti-tumour efficacy and reduce toxicity by improving drug loading, permeability, and retention effect (Ko, 2016, Milano et al., 2022).

Another example DOX (Adriamycin) is an anthracycline antibiotic isolated from the microorganism (*Streptomyces peucetius*) (Lomovskaya et al., 1999). It exhibits a range of bioactivities, including antibacterial, immunosuppressive, antiparasitic, and wide-spectrum

antitumour activity (Tacar et al., 2013, Friedman and Caflisch, 2009, Gamo et al., 2010, Johansson et al., 2006, Saha et al., 2021). As an anticancer agent, DOX employs multiple mechanisms of action, with its primary mode of activity being the inhibition of Topo II (Kciuk et al., 2023). DOX exert its anticancer activity by stabilizing the DNA-Topo II cleavage complex, which prevents the relegation of double strand breaks, ultimately leading to cell cycle arrest and apoptosis in rapidly proliferating cancer cells (Pommier et al., 2010, Lüpertz et al., 2010). In addition to its activity as a Topoisomerase inhibitor, DOX enhances its cytotoxicity by generating reactive oxygen species (ROS) through direct binding to cardiolipin on the inner mitochondrial membrane, the primary site of ROS production, ultimately leading to oxidative DNA damage (Gilliam et al., 2012, Montalvo et al., 2020). Moreover, DOX is a DNA intercalator that binds to G-C-rich regions of duplex DNA, forming DOX-DNA adducts in response to chemotherapy, which can subsequently induce DNA damage and cell death through a non-Topo II-mediated mechanism (Swift et al., 2006, Forrest et al., 2012, Coldwell et al., 2008).

DOX together with its semisynthetic product daunorubicin, are amongst the most efficient antitumour drugs, which have been used clinically for >4 decades. As a wide spectrum antitumour drug, it can be used for breast, ovarian, transitional cell bladder cancer, bronchogenic lung cancer, thyroid and gastric cancer, soft tissue and osteogenic sarcomas, neuroblastoma, Wilms' tumour, and malignant lymphoma .

Antimicrotubule agents

Antimicrotubule agents that are derived from NPs represent a critical class of anticancer drugs and are notable for their role in supressing microtubule dynamics, which are crucial for mitosis and cell division, thereby inducing mitotic block and subsequent apoptosis in cancer cells (Jordan and Wilson, 2004). Prominent antimicrotubule agents include paclitaxel (Taxol®) and the vinca alkaloids (VCR and VBL) (Donehower, 1996, Gidding et al., 1999).

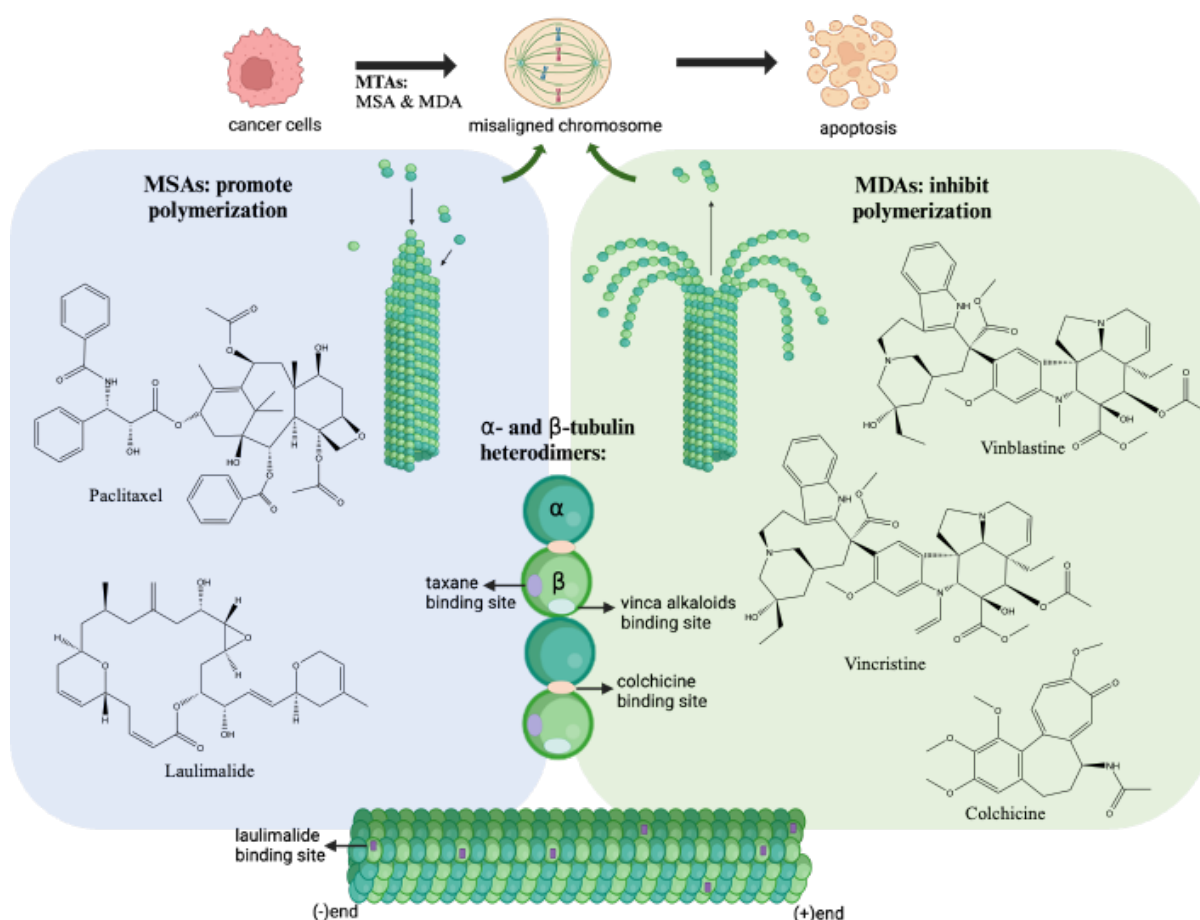


Figure 1. 2 Mechanism of action of MTAs and the binding sites of MSAs and MDAs. MSAs, such as paclitaxel and lulimalide, promote polymerization, preventing microtubule depolymerization and leading to mitotic arrest. Conversely, MDAs, including vinblastine, vincristine, and colchicine, inhibit polymerization, disrupting spindle formation and inducing apoptosis. The disruption of microtubule dynamics ultimately impairs proper chromosome segregation and induces apoptosis, making MTAs effective anticancer agents. The specific binding sites of these agents has presented on tubulin heterodimers, which are formed by α - and β -subunits of the protein tubulin. The taxane binding site has been mapped to β -tubulin on the interior lumen of the microtubule, while the lulimalide binding site is on the exterior of the microtubule. The vinca binding site is located on the β -subunit at the boundary between two heterodimers, whereas the colchicine binding site is located at the interface of the α/β -subunits within a tubulin heterodimer. Each microtubule has a plus (+) end, where β -tubulin faces the solvent and undergoes dynamic growth, and a minus (-) end, where α -tubulin faces the solvent and is typically anchored for stability. MDA, microtubule-destabilizing agent; MSA, microtubule-stabilizing agent; MTA, microtubule-targeting agent. (Draw by BioRender and ChemDraw.)

Substances that bind to soluble tubulin or tubulin within microtubules function as antimetabolic agents, inhibiting cell proliferation by disrupting the polymerization dynamics of spindle microtubules, whose rapid and dynamic behaviour is essential for proper spindle function. Microtubule-targeting agents are broadly categorized into microtubule-destabilizing (MDA) and microtubule-stabilizing agents (MSA). MDA inhibit microtubule polymerization, leading

to a reduction in microtubule mass (**Figure 1.2**). This group includes clinically utilized drugs such as vinca alkaloids (e.g., VBL, VCR, vinorelbine), cryptophycins, halichondrins, colchicine, estramustine, and combretastatins. In contrast, MSA promote microtubule polymerization and enhance stability (**Figure 1.2**). Key drugs in this category include paclitaxel, docetaxel, epothilones, discodermolide, laulimalide, sarcodictyins, and certain steroids and polyisoprenyl benzophenones (Jordan, 2002, Jesus et al., 2002). Both classes disrupt microtubule dynamics critical for mitosis, making them effective tools in cancer therapy. However, current understanding indicates that their primary and most potent mechanism of action is the suppression of microtubule dynamics, rather than the modulation of microtubule polymer mass through increases or decreases (Jordan and Wilson, 2004).

The promising activity of microtubule-targeting drugs to suppress microtubule dynamics depends on their direct interaction with microtubules or their interaction with soluble tubulin. Furthermore, the extent to which a drug binds to soluble tubulin versus microtubules, as well as the specific location of its binding site (**Figure 1.2**), plays a crucial role in determining its overall impact on the microtubule system (Jordan and Wilson, 2004). The vinca alkaloids (e.g. VCR, VBL) for example, target tubulin and microtubules primarily, depolymerizing microtubules, disrupting mitotic spindle assembly, and effectively arresting dividing cancer cells in mitosis with condensed chromosomes at high concentrations (e.g., 10-100nM in HeLa cells), while effective apoptosis was induced by solely suppressing microtubule dynamics at relevant lower concentrations (e.g., IC_{50} of 0.8nM in HeLa cells) (Jordan, 2002, Jordan et al., 1991). The binding between VBL and soluble tubulin is rapid and reversible (Wilson et al., 1982). VBL also directly interacts with microtubules, preferentially binding to tubulin at microtubule plus ends with high affinity, while exhibiting reduced binding to tubulin buried within the lattice (**Figure 1.2**) (Jordan et al., 1986, Singer et al., 1989). The binding of one or two VBL molecules to the plus end of a microtubule suppresses treadmilling and dynamic instability by approximately 50%, without significant microtubule depolymerization (Jordan and Wilson, 2004). Treadmilling and dynamic instability are two key non-equilibrium dynamics of microtubules. Treadmilling maintains microtubule length by adding tubulin subunits at the plus end and removing them at the minus end, while dynamic instability involves alternating phases of growth and shrinkage, driven by transitions between catastrophe and rescue (Jordan and Wilson, 2004). VBL reduces microtubule growth and shortening rates while increasing time spent in a paused state (Jordan and Wilson, 2004). In mitotic spindles,

this suppression disrupts spindle assembly and kinetochore tension, misaligning chromosomes and delaying the metaphase-to-anaphase transition by inhibiting the anaphase-promoting complex. Prolonged mitotic arrest ultimately induces apoptosis, making vinblastine effective against rapidly dividing cancer cells.

The vinca alkaloids were introduced clinically 40 years ago and have been pivotal in cancer chemotherapy. VBL and VCR, derived from the periwinkle plant (*Catharanthus roseus*), were first identified for their antimitotic properties in the late 1950s by researchers at Eli Lilly and the University of Western Ontario. These agents were highly effective in treating childhood leukaemia, earning them recognition as "wonder drugs," and were later applied to adult haematological cancers. Their success also spurred the development of semi-synthetic analogues, including vindesine, vinorelbine, and vinflunine. The principal side effects of Vinca alkaloids are peripheral neuropathy and reversible myelosuppression (Gidding et al., 1999). Neurotoxicity, linked to their effects on microtubules, may result from disrupted axonal transport, altered microtubule dynamics, neuronal retraction, or demyelination (Sahenk et al., 1994, Quasthoff and Hartung, 2002). Despite these challenges, vinca alkaloids remain crucial in combination chemotherapy regimens.

Other examples include paclitaxel and its semi-synthetic derivative, docetaxel, which were pivotal additions to chemotherapy in the late twentieth century. Paclitaxel, a complex compound isolated from the stem bark of the Pacific yew, *Taxus brevifolia* in 1967 by Monroe Wall and Mansukh Wani, gained prominence in 1979 when Schiff and Horwitz discovered its ability to promote microtubule polymerization, contrasting with the depolymerizing effects of vinca alkaloids (Wani et al., 1971, Schiff et al., 1979). Clinical development was initially hindered by limited natural supply, but semi-synthetic production enabled its approval in 1995 (Horwitz, 1994). It is now widely used to treat breast, ovarian, and non-small-cell lung cancers, as well as Kaposi's sarcoma, with neurotoxicity and myelosuppression as primary side effects (Markman, 2003).

Taxanes bind with high affinity to the β -subunit of tubulin on the inner surface of microtubules (**Figure 1.2**), stabilizing their structure and enhancing polymerization by inducing

conformational changes in tubulin; effective polymerization requires the binding of thousands of paclitaxel molecules per microtubule (Nogales et al., 1995, Nogales, 2001). However, low level binding of paclitaxel achieves stabilization and suppression of microtubule dynamics in the absence of microtubule polymerization, ultimately blocking mitotic progression at metaphase and leading to apoptosis without significant microtubule bundling (Derry et al., 1995, Yvon et al., 1999). For example, mitosis in HeLa cells is inhibited at 8 nM paclitaxel, while polymer mass increases at concentrations >10nM (Jordan et al., 1993). The successful drug discovery of taxanes has driven the discovery of other microtubule-stabilizing agents, including epothilones, discodermolide, sarcodictyins, eleutherobin, and laulimalide, among which, laulimalide targets distinct sites on the microtubule, while others compete with paclitaxel for binding at similar sites (**Figure 1.2**) (Pryor et al., 2002).

Methodologies for Natural Product Drug Discovery

The discovery of anti-cancer drugs can be directed in varied ways, including phenotypic research, to study agents with activity while the target requires elucidation, as well as target-directed research, to study the unknown activity of a molecule with a known target (pertinent to tumourigenesis). Either way, natural products are regarded as the most important molecule resources, other resources include synthetic agents, biological agents, and vaccines. However, challenges such as complex isolation processes and the rediscovery of known compounds have boosted the development of innovative methodologies. Modern approaches to natural product drug discovery (NPDD) integrate traditional methods of isolation and characterization (bioassay-guided) with advanced techniques such as high-throughput screening, -omics technologies (e.g. metabolomics, proteomics, as well as genome mining and engineering), and computational tools (e.g. RetroPath, Kyoto Encyclopedia of Genes and Genomes (KEGG), fragment-based drug design (FBDD), synthetic intelligence, and virtual screening) so as to enhance the efficiency and success rate of drug discovery (Najjar et al., 2019, Ren et al., 2020, Bülbül et al., 2025). Additionally, the combination of NPDD and synthetic chemistry methods, such as virtual screening, offers a promising approach in drug design and development, addressing the challenges of time-consuming processes and high costs (Tzvetkov et al., 2023).

Traditional Extraction and Screening

Traditionally, the discovery process often begins with the collection of biological samples from diverse environments, such as terrestrial and marine ecosystems. These samples are subjected to extraction and fractionation to isolate secondary metabolites. Traditional methods employ bioassay-guided fractionation, where biological activity is monitored throughout the isolation process, ensuring that the active compounds are identified (Atanasov et al., 2021). For anticancer agents, bioassays typically focus on cytotoxicity against cancer cell lines or inhibition of specific molecular targets, such as kinases or topoisomerases. However, bioassay-guided isolation has disadvantages: they are of labour-intensive, time-consuming, and prone to lead to rediscovery of known compounds. To address these issues, pre-fractionation techniques, such as high-throughput screening (HTS), have been employed and enabling rapid evaluation of large compound libraries against specific biological targets and streamlining identification of novel compounds (Wagenaar, 2008).

Pre-fractionation is an advanced technique used in NPDD to enhance the efficiency of identifying bioactive compounds, particularly for HTS. Crude plant extracts often contain a vast array of metabolites, including secondary compounds, pigments, and sugars, many of which may mask or interfere with the detection of active molecules. Pre-fractionation addresses these challenges by separating the extract into chemically distinct and less complex sub-fractions, increasing the likelihood of detecting bioactive "hits" during HTS. Additionally, fractionation protocols can be tailored to enrich sub-fractions with compounds exhibiting drug-like properties, such as moderate hydrophilicity. These approaches not only enhance the compatibility of natural product libraries with high-throughput screening but also improve the efficiency of identifying and following up on promising hits, thereby increasing the likelihood of discovering novel bioactive compounds. High-throughput screening has significantly accelerated the identification of potential drug candidates from complex natural matrices. For example, the discovery of platensimycin, a selective inhibitor of β -ketoacyl-(acyl-carrier-protein) synthase I/II (FabF/B), was achieved through the screening of 250,000 microbial extracts derived from 83,000 strains under three different growth conditions by Merck (Wang et al., 2006). The NCI Program for NPDD has developed a publicly accessible, HTS-compatible library comprising over 1,000,000 fractions derived from 125,000 natural product extracts (Thornburg et al., 2018). This initiative aims to advance natural product-based drug

discovery by providing a valuable resource for screening against various diseases, ultimately accelerating the drug development process.

Pre-fractionation typically employs chromatographic and spectroscopic methods, including liquid-liquid partitioning, solid-phase extraction (SPE), thin-layer chromatography (TLC), size-exclusion chromatography (SEC) and column chromatography. By dividing crude plant extracts into smaller, more manageable sub-fractions enriched with bioactive components, pre-fractionation helps overcome the challenges of complexity, redundancy, and poor compatibility with automated systems. For example, sequential liquid-liquid partitioning was employed for the discovery of paclitaxel, where solvents of varying polarity (e.g. chloroform and water) were utilized to create distinct fractions enriched with hydrophobic or hydrophilic compounds, ultimately facilitating the concentration of bioactive taxane class from *Taxus brevifolia* extracts (Wani et al., 1971). Prior to analysis, SPE uses solid-phase materials (e.g. cartridge or sorbent) to separate compounds based on polarity, charge, or affinity, facilitating the removal of interfering compounds from samples and the enrichment of analytes of interest in the sample. For instance, using tailor-made molecularly imprinted polymers (MIP) as SPE absorbents, VBL was separated from *Catharanthus roseus* extracts with high selectivity and high yield (89%) (Zhu et al., 2007). TLC-based pre-fractionation allows visual identification of compound classes in extracts. For example, the existence of alkaloids can be visualized by spraying Dragendorff's reagent on the TLC plate, where yellow colour represents positive results. SEC is valuable for separating plant extracts by molecular size. For instance, this method has been used to pre-fractionate extracts of *Tinospora cordifolia*, leading to the isolation of the active compound α -D-glucan (RR1) with immunomodulatory and anticancer properties (Raveendran Nair et al., 2004). For the antimalarial and potential anticancer agent artemisinin (isolated from *Artemisia annua*), pre-fractionation using column chromatography enriched fractions containing sesquiterpene lactones, facilitating its isolation (Ivanescu et al., 2015). In the discovery of resveratrol (from *Vitis vinifera*), SPE and liquid-liquid extraction enabled the simultaneous enrichment and purification of sample, while the selective isolation of phenolic fractions facilitated its subsequent bioactivity screening effectively (Li et al., 2024).

Genomic and Metabolomic Approaches

Omics technologies, including genomics, transcriptomics, proteomics, and metabolomics, have revolutionized NPDD. Genomic approaches, such as genome mining, enable the identification of biosynthetic gene clusters (BGCs) responsible for the production of bioactive secondary metabolites (Rutledge and Challis, 2015). This approach is particularly valuable for microorganisms, such as actinomycetes, which harbour vast untapped biosynthetic potential (Bentley et al., 2002). Metabolomics facilitates target-oriented drug discovery by providing comprehensive profiling of secondary metabolites, aiding in the identification of novel compounds and their structural characterization. Transcriptomics and proteomics further contribute by elucidating gene expression and protein interactions associated with secondary metabolism, providing insights into the regulation of bioactive compound production.

Semi-synthesis and Chemical Modification

NPs often serve as scaffolds for chemical modification to improve their pharmacokinetic (PK) properties and efficacy. For example, semisynthetic derivatives of paclitaxel, such as docetaxel, exhibit improved solubility and potency. Synthetic biology has emerged as a powerful tool for harnessing the biosynthetic potential of natural products (Smanski et al., 2016). By engineering microbial hosts, researchers can optimize the production of rare or structurally complex compounds that are difficult to obtain from their native sources. This approach also enables the generation of novel analogues with enhanced pharmacological properties. Bioprospecting, particularly in underexplored ecosystems such as deep-sea environments and extreme habitats, continues to yield novel bioactive compounds. Advances in metagenomics and single-cell sequencing have expanded access to genetic material from unculturable microorganisms, further enhancing the scope of natural product discovery.

Computational Tools

Computational approaches, including cheminformatics, molecular docking, and artificial intelligence (AI), have become integral to NP research. Cheminformatics tools aid in the dereplication process by comparing compounds against known databases, minimizing the rediscovery of previously identified molecules (Booth et al., 2013). Molecular docking and virtual screening allow researchers to predict the binding affinity of NPs to specific biological targets, streamlining the prioritization of compounds for experimental validation. AI and

machine learning algorithms further enhance the efficiency of drug discovery by identifying patterns in large datasets and predicting novel bioactivities based on structural features.

Challenges in Natural Product Drug Discovery

Despite advancements, NPDD faces several challenges, including the rediscovery of known compounds, difficulties in scaling up production, the complexity of natural product structures and drug resistance mechanisms. However, the integration of multidisciplinary approaches offers promising solutions. For instance, combining omics technologies with computational tools enables the efficient prioritization of bioactive compounds. Additionally, advances in synthetic biology and engineered biosynthesis provide opportunities to overcome supply limitations and enhance pharmacological properties. For example, overharvesting of plants like *Taxus brevifolia* has led to resource depletion of Taxol, in which case the synthetic biology and plant cell cultures offer potential solutions (Eibl et al., 2018, Tabata, 2004). Additionally, more abundant and accessible species, such as *Corylus avellana* L., have been explored as alternative sources, as taxanes have been successfully isolated from hazel shells (Ottaggio et al., 2008). The structural intricacy of natural products can hinder large-scale production, highlighting the demand of developing advanced synthetic methodologies and biotechnological approaches to possibly address this limitation. The emergence of resistance in cancer cells often limits the long-term efficacy of natural product-based therapies, while combination therapies, next-generation derivatives and nano-formulations are being explored to overcome this challenge.

1.2 Alkaloids and the genus *Eumachia*

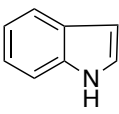
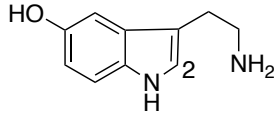
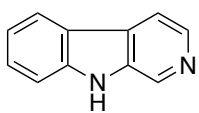
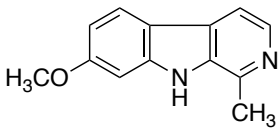
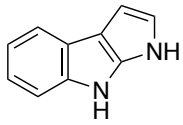
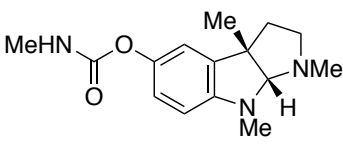
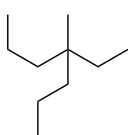
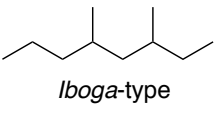
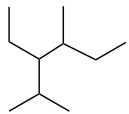
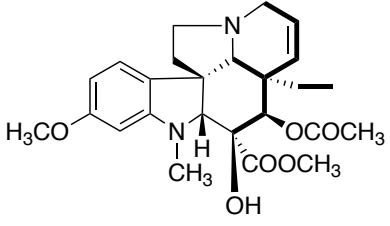
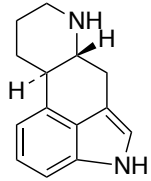
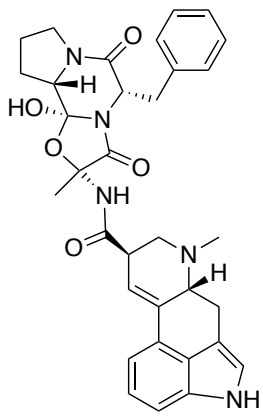
Classification, occurrence, biosynthesis, and bioactivities of Alkaloids

Alkaloids are a class of nitrogen-containing compounds with low molecule weight that are mainly of plant origin. They occur as salts, free state bases or alkaloid N-oxides and are usually biosynthesized in metabolically active tissues (e.g., roots and shoots) and are stored in vacuoles, where they are sequestered (thus non-toxic to the host plant). Functionally, plant alkaloids could play the role of chemical defence against plant herbivores and parasites, insects, and bacteria. However, a small number of alkaloids are also produced by fungi, bacteria, and animal (such as the amphibians, insects and marine invertebrates). Since the discovery of the first bioactive alkaloid, morphine in 1803, to date >27,000 different alkaloids have been

identified and classified (Dewick, 2009a). Alkaloids contain at least one nitrogen (typically as amines), which makes the majority of alkaloids possess an alkaline property. This unique property enables alkaloids to form water-soluble salts in the presence of mineral acid, thus facilitating their isolation and purification. The vast structural diversity of alkaloids led to a lack of uniform classification for alkaloids. As such, several classifications have been proposed. Firstly, alkaloids can be classified according to the ring system that contains the nitrogen atom, e.g., pyrrolidine, piperidine, quinoline, isoquinoline, indolizidine and indole alkaloids. The biochemical precursors of alkaloids are usually amino acids (e.g., ornithine, lysine, nicotinic acid, tyrosine, tryptophan, anthranilic acid and histidine), which give rise to the basic carbon-nitrogen skeleton in most cases. Thus, this represents another approach for alkaloid classification, i.e., based on the amino acid precursors. Indole alkaloids are attributed to tryptophan-derived alkaloids.

According to the structural complexity of the heterocyclic rings, indole alkaloids can be divided into simple indole alkaloids, simple β -carboline alkaloids, pyrroloindoline alkaloids, terpenoid indole alkaloids, and ergot alkaloids (**Table 1.1**). The biosynthesis of indole alkaloids can be discussed in terms of the tryptophan-derived moiety and non-tryptophan-derived moieties, which include isoprene, secoiridoid units and polyketide moieties. Tryptophan is a significant precursor of a variety of indole alkaloids. Additionally, tryptophan can also be regarded as the precursor of some quinoline alkaloids as the indole ring system can rearrange into a quinoline ring system.

Table 1. 1 Structure classification of indole alkaloids.

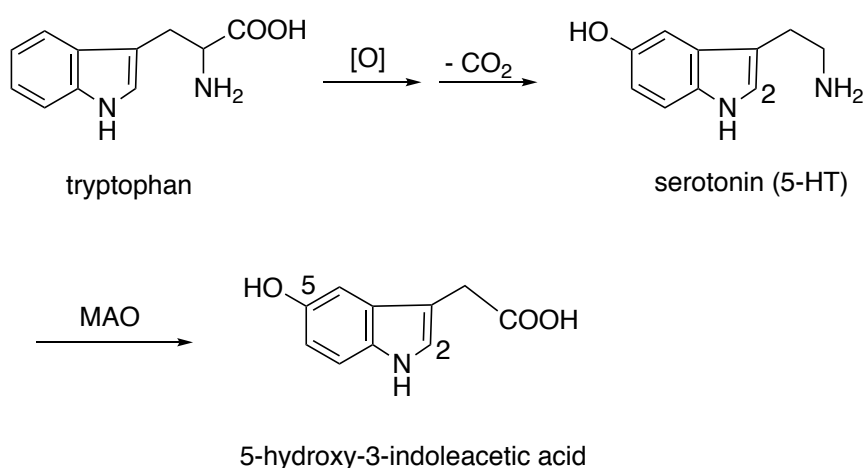
Class	Core structure	Structure examples
Simple indole alkaloids		 Serotonin
Simple β -carboline alkaloids		 Harmine
Pyrroloindole alkaloids		 physostigmine (eserine)
Terpenoid alkaloids	 <i>Aspidosperma</i> -type  <i>Iboga</i> -type  <i>Corynanthe</i> -type	 vindoline
Ergot alkaloids		 ergotamine

Simple indole alkaloids

Indole alkaloids have a comparatively simple chemical structure, in which the skeleton of tryptophan remains almost completely intact, while the carboxyl group is never present and most substitution occurs at C-5 of the benzene ring. The alkaloids serotonin and indole-3-acetic-acid (IAA) are included in this group and their formation can be achieved by three steps from tryptophan (**Scheme 1.1**).

Serotonin, an important neurotransmitter also known as 5-hydroxytryptamine (5-HT), is formed directly from tryptophan via hydroxylation and decarboxylation, and finally is excreted before being metabolized to indole-3-acetic-acid by monoamine oxidase (MAO) (**Scheme 1.1**) (Funayama and Cordell, 2014). The vasocontraction effect of serotonin in capillary vessels was first discovered by Rapport et al. in 1948 in the blood of cows (Rapport et al., 1948).

IAA (indole- β -acetic acid), also known as heteroauxin, has been widely used in agricultural practice for its growth-promoting activity, while psilocin is isolated as an hallucinogenic substance along with psilocybin from the *Psilocybe* mushroom (Fritz Kögl, 1933, Schultes and Hofmann, 1979). These two simple alkaloids are also known as protoalkaloids, which may serve as biosynthetic precursors of other alkaloids.



Scheme 1. 1 Formation and Metabolism of Serotonin (5-HT)

Simple β -carboline alkaloids

β -Carboline is a nitrogen-containing heterocycle that consists of a series of indole alkaloids such as tryptoline, pinoline, harmane, harmine, harmaline, tetrahydroharmine (THH) and 9-methyl- β -carboline. Its basic structure is a pyridine ring fused to an indole skeleton (**Figure 1.3**). The various β -carboline alkaloids mainly differ in their saturation level in the third ring and the varied R groups indicated in the **Figure 1.2.1**. It is proposed that the skeleton of β -carboline is formed by the condensation of an aldehyde or keto acid with tryptamine or its derivatives via a Mannich/Pictet-Spengler-type reaction to furnish the third six-membered heterocyclic ring (**Scheme 1.2**) (Dewick, 2009a).

Different kinds of β -carboline alkaloids have been discovered in the plant families Rubiaceae (e.g., *Psychotria barbiflora*, *Galianthe thalictroides*) (de Oliveira et al., 2013, de Oliveira Figueiredo et al., 2014), Malpighiaceae (e.g., *Banisteriopsis caapi*) (Callaway et al., 2005), Zygophyllaceae (e.g., *Peganum harmala* L.) (Hemmateenejad et al., 2006), Annonaceae (e.g., *Annona foetida*) (Costa et al., 2011), Caryophyllaceae (e.g., *Gypsophila oldhamiana*) (Zhang et al., 2015), Simarubaceae (e.g., *Picrasma quassioides*) (Zhao et al., 2012), Euphorbiaceae (e.g., *Trigonostemon lii*) (Li et al., 2012), and Elaeagnaceae (e.g., *Elaeagnus*) (Abizov and Tolkachev, 2012). Additionally, β -carboline alkaloids have been isolated from animals and marine creatures, including scorpions, ascidians, and freshwater cyanobacterium. The skin of scorpions will fluoresce when exposed to certain wavelengths of UV due to the presence of β -carboline alkaloids (Stachel et al., 1999, Davis et al., 1998).

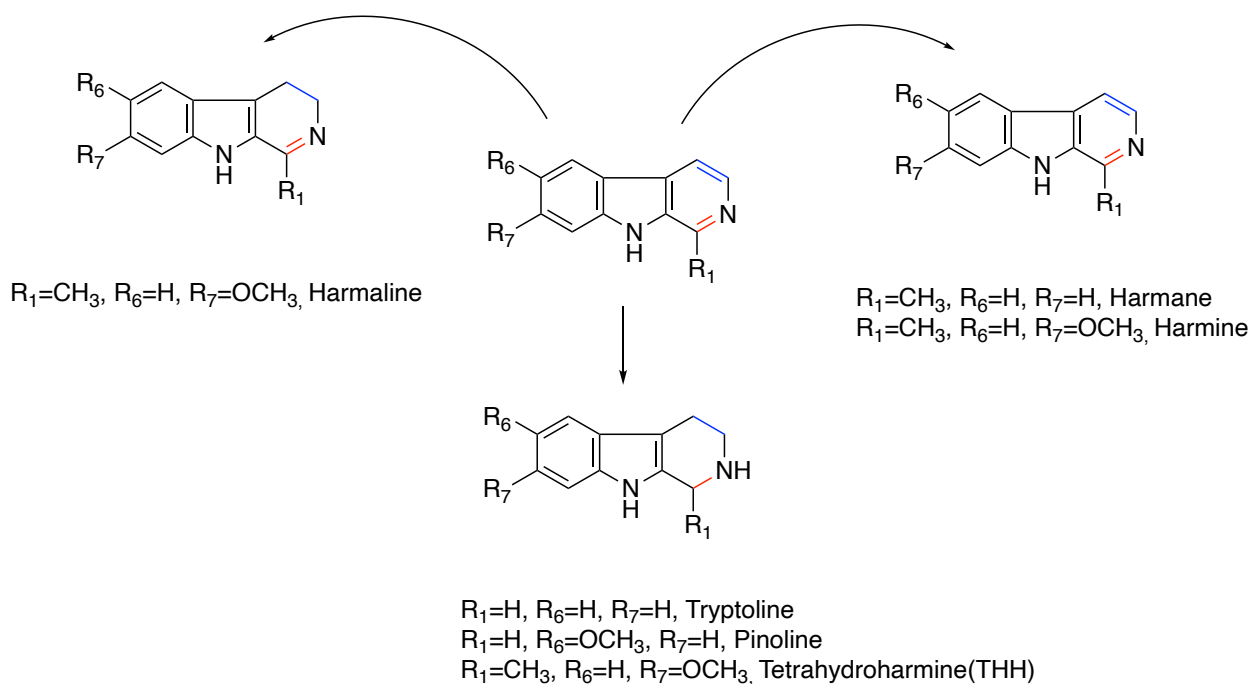
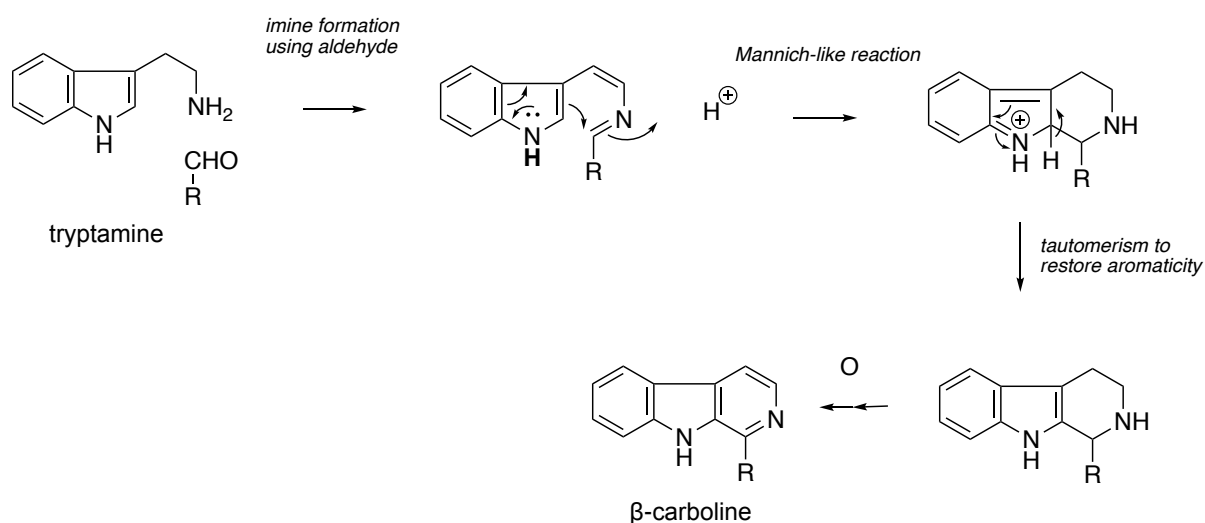


Figure 1. 3 Structures of β -carboline alkaloids: harmaline, harmine, harmine, tryptoline, pinoline, and THH



Scheme 1. 2 Formation of β -carboline from tryptamine

Many isolated β -carboline alkaloids show cytotoxic activities. For example, two cytotoxic β -carboline alkaloids from *Galianthe thalictroides* (Rubiaceae) were reported as potent inhibitors of DNA topoisomerase I and II α , which are important enzymes for cell division and key targets for anticancer drugs (de Oliveira Figueiredo et al., 2014). The β -carboline alkaloids from the plant *Trigonostemon lii* and marine tunicates (*E. glaucus*) also exhibited potent cytotoxic

activity against several human cancer cell lines (HL-60, SMMC-7721, A549, MCF-7, and SW480) and murine leukaemia cells (P388 and L1210), respectively (Li et al., 2012, Suzuki et al., 2011).

Additionally, harmine and harmaline are β -carboline alkaloids that were isolated from *Banisteriopsis caapi* (Malpighiaceae), serving as active constituents in the hallucinogenic beverage ayahuasca, along with another potent psychoactive agent (N-N-dimethyltryptamine) from *Psychotria viridis* (Rubiaceae) (McKenna et al., 1984). It is proposed that the β -carbolines contribute psychoactive effects by reversibly inhibiting MAO to prevent the degradation of dimethyltryptamine in the gut (McKenna et al., 1984). As widely utilized Traditional Chinese Medicine (TCM), *Gypsophila oldhamiana* (Shan Yin Chai Hu) is used for treating fever, consumptive diseases, and infantile malnutrition syndrome, while *Picrasma quassioides* is known for its heat-clearing and detoxifying properties, with its β -carbolines exhibiting potent anti-inflammatory activity (Zhang et al., 2015, Zhao et al., 2012).

Pyrroloindoleline alkaloids

The pyrroloindole skeleton (**Figure 1.4**) can be characterized by physostigmine (also known as eserine), which is deduced to be formed by methylation of C-3 (nucleophilic character) in the tryptamine molecule (**Scheme 1.3**). Pyrroloindole alkaloids are relatively rare and have been discovered in plants, amphibians, and marine algae.

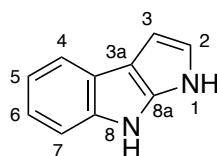
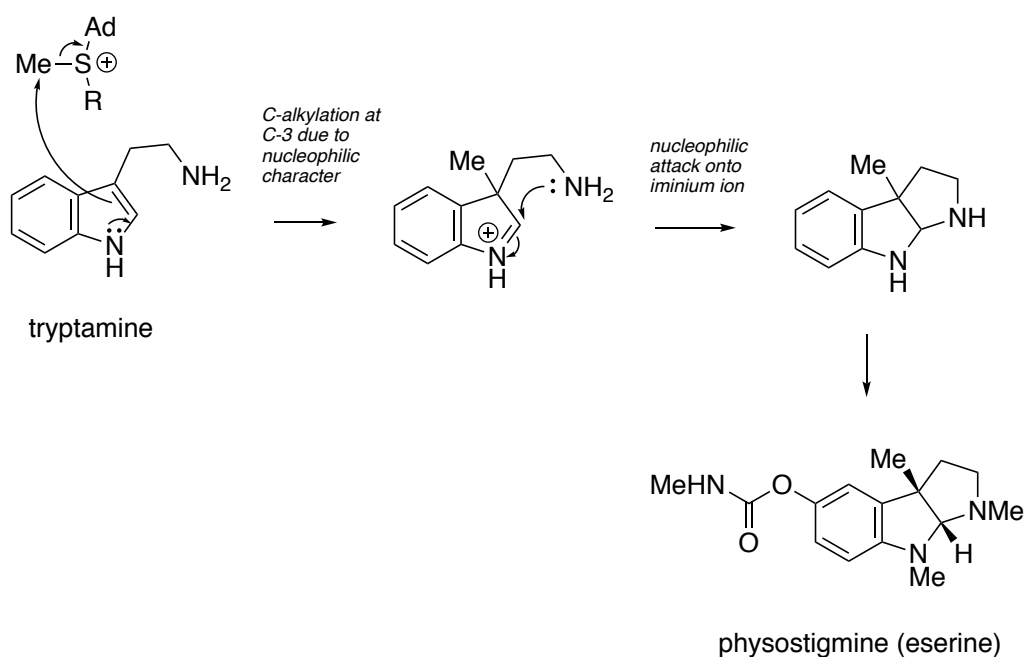


Figure 1. 4 Basic structure of pyrroloindole



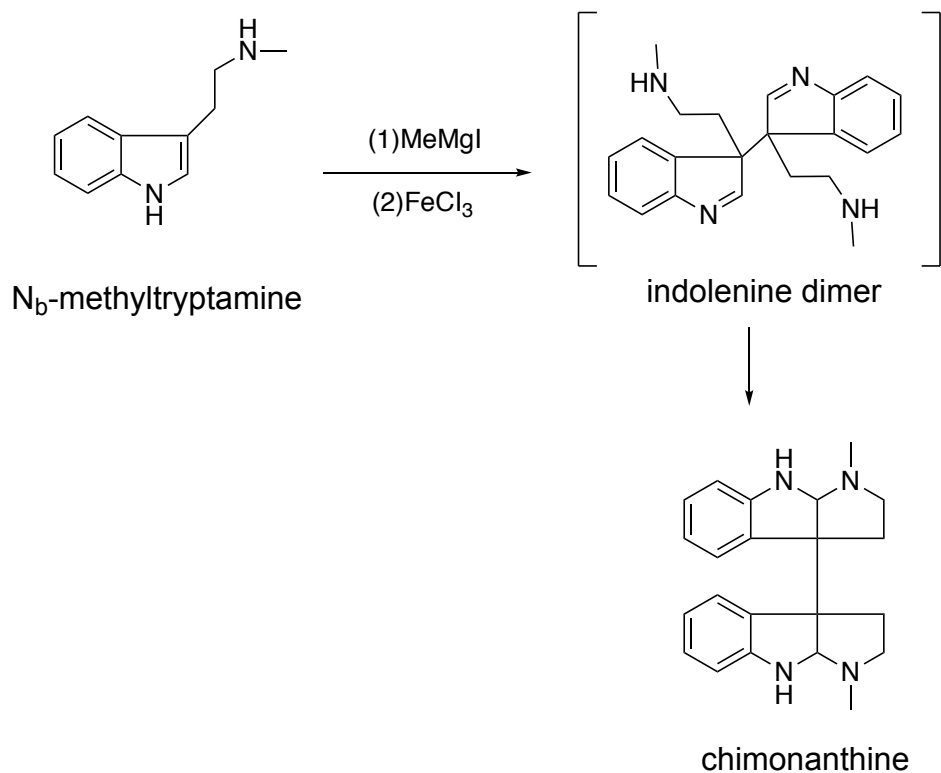
Scheme 1.3 A plausible biosynthetic pathway of physostigmine (eserine)

Physostigmine is detected in the vine *Physostigma venenosum* (Fabaceae), whose seeds are also known as Calabar beans, while physostigmine is responsible for the poisonous property of Calabar beans (Funayama and Cordell, 2014). It is also reported that physostigmine has the ability to excite the parasympathetic nervous system and contract skeletal muscles as an anticholinesterase agent (Dewick, 2009a).

Chimonanthine is a dimeric pyrroloindole alkaloid, isolated from *Chimonanthus praecox* (wintersweet) (Calycanthaceae) and *Psychotria rostrata* (Rubiaceae) (Wang et al., 2011, Verotta et al., 1998). The biomimetic synthesis of chimonanthine proposed by Scott in 1964 used N₆-methyltryptamine as the precursor, which was subsequently treated with methyl magnesium iodide (CH₃MgI) and iron (III) chloride to produce the indolenine dimer, followed by one step transformation to produce meso- and (±)-chimonanthine (**Scheme 1.4**). The further treatment of (±)-chimonanthine with aqueous acid provided the quinoline alkaloids (±)-calycanthine (**Figure 1.5**) (Scott et al., 1964).

Similar to chimonanthine, calycanthine mainly exists in plants from two families, Calycanthaceae and Rubiaceae (Gordin, 1905, Zhang et al., 2009a, Duke et al., 1995, Adjibade

et al., 1992, Verotta et al., 1998, do Nascimento et al., 2006, Woo-Ming and Stuart, 1975, Lajis et al., 1993). The biological activities of calycanthine have been widely studied and it was shown to possess anti-convulsant, antifungal, and melanogenesis inhibitory properties (Chebib et al., 2003, Zhang et al., 2009a, Morikawa et al., 2014).



Scheme 1. 4 A one-step synthesis and biosynthetic model of chimonanthine

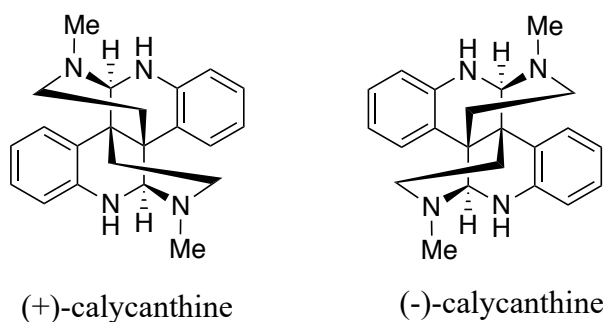


Figure 1. 5 Structures of (\pm) -calycanthine

Oligocyclotryptamine alkaloids (also terms as polypyrroloindoline alkaloids, cyclotryptamine alkaloids)

Oligocyclotryptamine alkaloids are a subclass of pyrroloindoline natural products distinguished by their complex oligomeric structures, which are formed through the C–C linkage of multiple basic building blocks of *cis*-pyrrolidino[2,3-*b*]indoline (also referred to as cyclotryptamine), which are either linked at their benzylic carbon atoms, or by the union of the benzylic carbon atom of one fragment with the aromatic C7 *peri* carbon atom of another. Higher-order oligomers in this family are primarily formed by attaching additional 3a*R*-*cis*-pyrrolidino[2,3-*b*]indoline units at the benzylic carbon (position-3a) to the aromatic carbon (position-7) of the preceding structure. These compounds are typically characterized by their highly intricate polycyclic frameworks, including the dimeric 3a-3a'-bispyrrolidino[2,3-*b*]indoline core unit and multiple C3a quaternary stereocenters, with at least one being a vicinal C3a–C3a' bond, up to seven C3a–C7' linkages, and numerous basic nitrogen centres (Steven and Overman, 2007). These oligocyclotryptamine alkaloids, particularly those based on the meso-chimonanthine core, can be further categorised into the [n+1] and [n+2] series. Representative alkaloids of these series are illustrated in **Figure 1.6** (Jannic et al., 1999, Scott and Movassaghi, 2024). The combination of severe steric crowding and structural complexity poses significant challenges for their stereochemical characterization and total synthetic reproduction. These features highlight the structural uniqueness of oligocyclotryptamine alkaloids and underscore the difficulties associated with their study and synthesis.

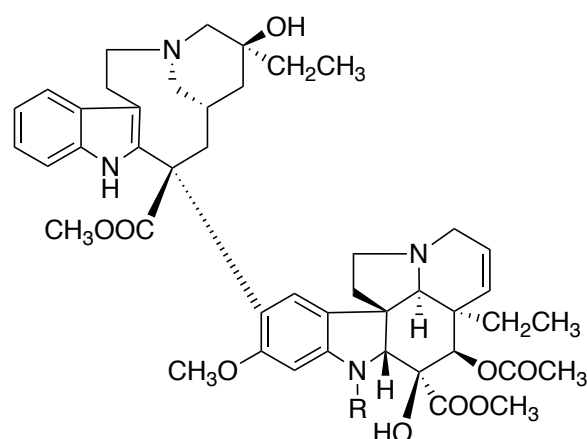
The structural and stereochemical characterization of some higher-order oligocyclotryptamines have previously been complicated by atropisomerism leading to signal broadening in NMR spectra. However, mass spectrometry has been invaluable, as the characteristic fragmentation of the C3a–C3a' σ bond provides crucial insights into the positioning of this linkage within each oligomer (Jannic et al., 1999, Guéritte-Voegelein et al., 1992). Recent advancements in chemical synthesis, which enable stereocontrolled coupling of cyclotryptamine monomers, have helped overcome longstanding challenges in determining and validating the structures and stereochemistry of these complex alkaloids, including (–)-hodgkinsine, (+)-quadrigemine H, (+)-isopsychotridine, (+)-oleoidine, (+)-caledonine, (–)-hodgkinsine B, (–)-quadrigemine C, and (–)-psychotidine (**Figure 2.1**) (Steven and Overman, 2007, Scott and Movassaghi, 2024).

Oligocyclotryptamine alkaloids are primarily isolated from the genus of *Eumachia* (syn. *Psychotria*), representing a fascinating family of NPs known for their diverse therapeutic bioactivities, including anticancer (quadrigemine H, quadrigemine C, psychotridine, isopsychotridine C from *Eumachia forsteriana*), analgesic ((+)-chimonanthine, hodgkinsine, quadrigemine C, psychotridine from *Palicourea colorata*), antimicrobial (psychotrimine from *Eumachia rostrata*) and antithrombotic (Psm2 from *Selaginella moellendorffii*) effects, (Roth et al., 1986, Nascimento et al., 2015, Saad et al., 1995, Adjibadé et al., 1990, Amador et al., 2001, Elisabetsky et al., 1995, Amador et al., 2000, Schallenberger et al., 2010, Shi et al., 2012, Su et al., 2016).

Terpenoid indole alkaloids

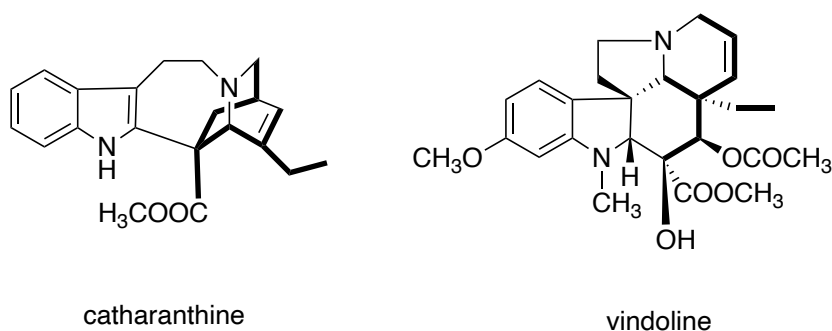
Terpenoid indole alkaloids mainly consist of a tryptamine and a C₉ or C₁₀ monoterpene secologanin unit. Terpenoid indole alkaloids could be divided into several structural types based on the rearrangement of the monoterpene fragment, e.g., the *Corynanthe*-type (ajmalicine and akuammicine), *Ipoga*-type (Ipogaine, catharanthine), and *Aspidosperma*-type (tabersonine) (Dewick, 2009a).

The *Catharanthus* alkaloids, VBL and VCR, also referred to as *Vinca* alkaloids (**Figure 1.6**), were initially isolated from the leaves of *Catharanthus roseus*; they possess potent antitumour activity (2015). The *Vinca* alkaloids are essentially bisindoles that are composed of an *Ipoga*-type alkaloid unit, catharanthine, and an *Aspidosperma*-type alkaloid unit, vindoline (**Scheme 1.5**) (Taylor and Farnsworth, 1975). Clinically, both VCR and VBL are used as anti-tumour drugs, while VCR is used more frequently, for example for the treatment of leukaemia, malignant lymphatic tumour, and childhood cancer.



vinblastine (VLB) R = CH₃
 vincristine (VCR) R = CHO

Figure 1. 6 Structures of vinblastine (VLB) and vincristine (VCR)



catharanthine

vindoline

Scheme 1. 5 The monoterpenoid C10 units are highlighted in the structures of catharanthine and vindoline

The terpenoid indole alkaloid, reserpine, was used clinically as a hypotensive drug (possessing a sedative side effect) until the presence of the phenothiazine-type drugs (McQueen et al., 1954). It was isolated from the roots of *Rauvolfia serpentina* (Apocynaceae). *Rauvolfia serpentina* also contains another *Corynanthe*-type alkaloid ajmaline, which is clinically used for its antiarrhythmic activity (**Figure 1.7**) (McQueen et al., 1954).

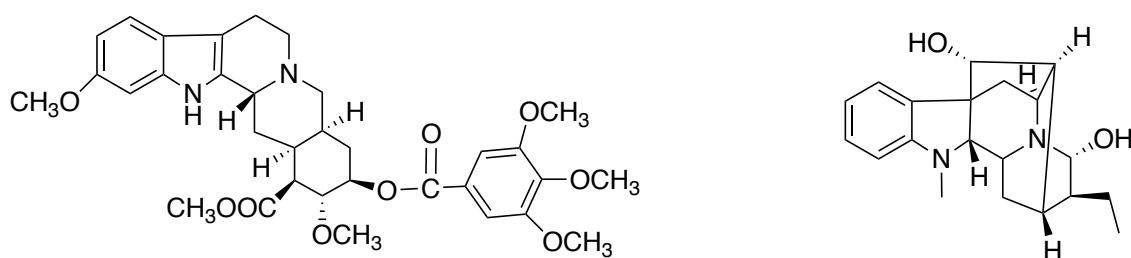


Figure 1. 7 Structures of reserpine and ajmaline

Ergot Alkaloids

It is known that ergot from the parasitic fungus *Claviceps purpurea* is very dangerous as it can contract the blood vessels of arms and legs, preventing the circulation of blood, and may eventually cause the loss of these limbs (Funayama and Cordell, 2014). The biologically active alkaloids isolated from ergot comprise ergocristin, ergocornine and ergotamine (Figure 1.8) (Řeháček and Sajdl, 1990, Stoll, 1945). These ergot alkaloids possess a common skeleton of lysergic acid, among which ergotamine consist of a structure based on lysergic acid coupled with a small polypeptide structure. Ergot alkaloids are typically discovered in fungi genera, including *Aspergillus*, *Rhizopus*, and *Penicillium* (Dewick, 2009a). The skeleton of ergot alkaloids is also known as the ergoline nucleus, which is biosynthesised from L-tryptophan, a C5 unit of mevalonic acid and methionine (Floss, 1976).

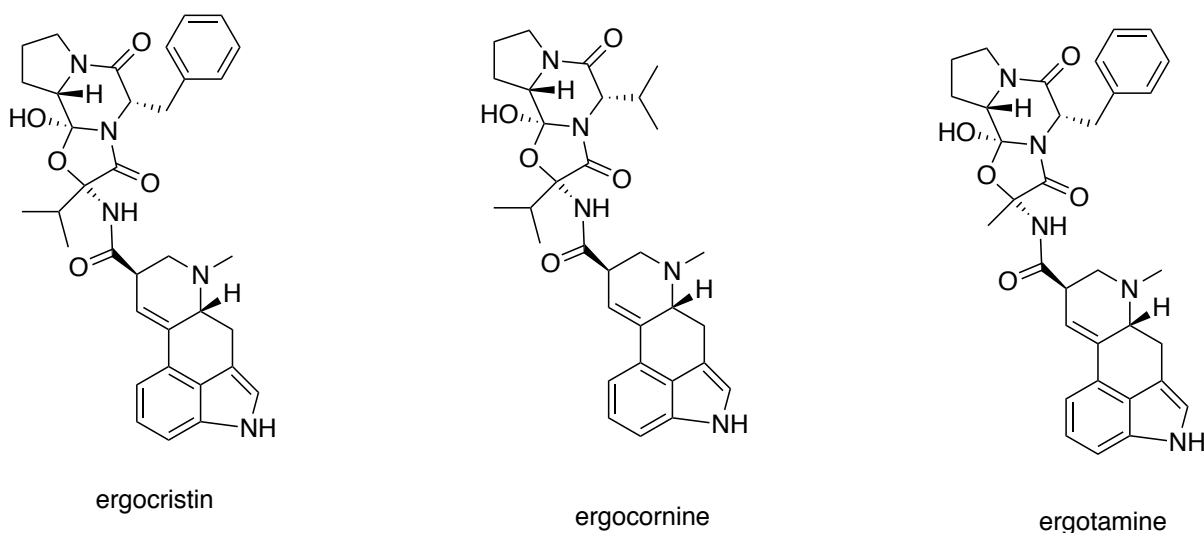


Figure 1. 8 Structures of ergocristin, ergocornine and ergotamine

The Genus *Eumachia* (syn. *Psychotria*)

The genera *Psychotria* and *Eumachia* are integral components of the Rubiaceae family, specifically within the tribes Psychotrieae and Palicoureeae. Recent taxonomic revisions have refined their classifications, leading to a clearer understanding of their species diversity, morphological characteristics, alkaloid profiles, and bioactivities (Berger et al., 2022, Turner, 2019).

Traditionally, *Psychotria* was considered a large, pantropical genus encompassing numerous species. However, phylogenetic studies have revealed that *Psychotria* in its broad sense was polyphyletic, prompting taxonomists to segregate distinct lineages into separate genera. One notable outcome of these revisions is the expansion of the genus *Eumachia*, which was previously underrepresented in taxonomic treatments. This expansion involved the transfer of certain species from *Psychotria* to *Eumachia*, based on shared morphological characteristics and genetic evidence. For instance, *Psychotria montana* and *Psychotria rostrata* were transferred to the genus of *Eumachia* (Turner, 2019). These taxonomic refinements have implications for the classification of related genera within the tribes Palicoureeae and Psychotrieae. Genera such as *Eumachia*, *Palicourea*, *Notopleura*, *Carapicha*, *Geophila*, and *Rudgea* have been attributed to the tribe Palicoureeae, and they have also been subjects of recent studies aiming to clarify their phylogenetic relationships and morphological boundaries, and these genera (Berger et al., 2022, Taylor et al., 2017).

The genus *Eumachia* (tribe Palicoureeae, family Rubiaceae) has been expanded through recent taxonomic revisions to include species formerly classified under *Psychotria*, though the exact number of species within *Eumachia* remains under investigation (Turner, 2019). Recent studies suggest it is a pantropical genus with including > 83 species distributed across the Neotropics, Africa, Asia, and the Pacific region (Taylor et al., 2017, Berger et al., 2022). Initially, most species were classified within the broadly defined genus *Psychotria*. Species in both genera exhibit typical Rubiaceae traits, including simple, opposite leaves, interpetiolar stipules, and small tubular flowers arranged in inflorescences. *Psychotria* species are generally small understory trees or shrubs, while *Eumachia* species share similar morphological traits, particularly in their stipules and fruit morphology, which have been key in distinguishing the genus (Taylor et al., 2017).

Traditional Uses

Many *Psychotria* or its relative genera *Palicourea* and *Notopleura* species have been used in various local traditional medicine to treat various diseases, while some are even utilised for religious or recreational purposes. For example, both *Psychotria viridis* and *Psychotria carthagenensis* are able to act as the admixtures to prepare the intoxicating beverage called ayahuasca due to the presence of the potent hallucinogen, N,N-dimethyltryptamine (McKenna et al., 1984). Ayahuasca is also known as caapi or yage in various aboriginal tribes endemic to the Amazon Basin, and it is well-known as a psychoactive brew that has been widely used for medicinal, religious and recreational purposes by the native inhabitants. Ayahuasca is prepared by boiling or soaking the bark of *Banisteriopsis caapi*, together with the leaves of admixtures *Psychotria viridis* or *Psychotria carthagenensis* (McKenna et al., 1984).

In the tribes of the Amazon and India, *Psychotria* plants are regarded as useful traditional medicines for treating diseases include bronchitis, gastrointestinal disorders (e.g., cough, ulcer and stomach ache), as well as female reproductive diseases (Calixto et al., 2016). An indigenous tribe in Panama relies heavily on herbal remedies for their therapeutic effects, with the leaves of *Psychotria emetica* serving as a traditional medicine for the treatment of chickenpox and fever (Gupta et al., 2005). It is also recorded that a cold-water infusion made by the crushed leaves of *Notopleura uliginosa* is useful for stomach ache and fever (Joly et al., 1987). In Brazil, the different plant parts of *Palicourea colorata* are utilized as analgesics to alleviate earache (flower) and abdominal pain (roots and fruits) (Elisabetsky et al., 1995). In the Malay society, the leaves of both *Eumachia rostrata* and *Psychotria calocarpa* have been made into a decoction for the treatment of constipation (Lajis et al., 1993, Zhou et al., 2010).

Multiple *Psychotria* species from China have shown great medicinal value in TCM for the treatment of various ailments. The stems, leaves and roots of *Psychotria rubra* are used to treat a wide range of diseases (including tonsillitis, diphtheria, sore swelling, rheumatism pain, bruises, colds and fever, sore throat, stomach ache, dysentery and haemorrhoids) due to its function of clearing away heat and toxins, reducing swelling, as well as hydroscopic effect. The whole plant of the vine *Psychotria serpens* is used in TCM for the treatment of rheumatic arthralgia, sciatica, carbuncle swelling and poison, sore throat, with functions of relaxing muscles and collaterals, strengthening muscles and bones, dispelling wind and pain.

Indole alkaloids from the Eumachia genus

Both genera of *Eumachia* and *Psychotria* are well-known for their production of secondary metabolites, including various alkaloids, terpenoids, flavonoids, coumarins, tannins, and cyclic peptides, among which, alkaloids are considered the most abundant. *Psychotria* species are rich in indole alkaloids, with notable examples including dimethyltryptamine (DMT) found in *Psychotria viridis*, a species traditionally used in South American shamanic practices (Rivier and Lindgren, 1972). In comparison, it is reported that the *Eumachia* species are abundant in pyrrolidinoindoline alkaloids, while most of them are polyindoline alkaloids that are structurally complex and likely exhibit bioactivity, although comprehensive phytochemical studies are needed to elucidate their full potential (**Table 1.2**) (Taylor et al., 2017, de Carvalho et al., 2016).

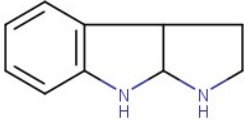
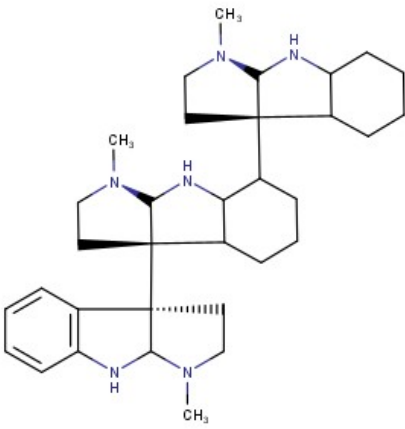
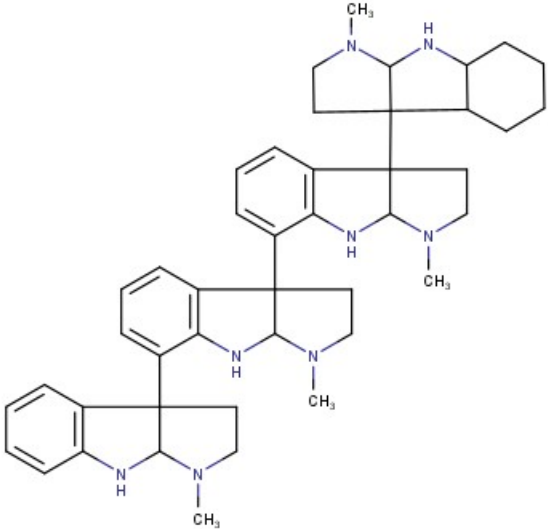
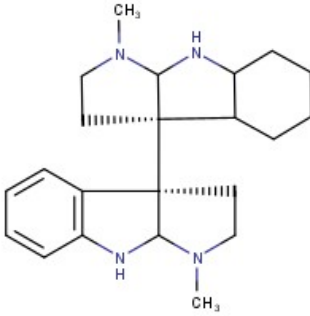
To date, nine species of *Eumachia* have been subjected to phytochemical investigation, primarily originating from Asia, Australasia, and the Pacific region. Notably, pyrrolidinoindoline alkaloids were isolated in eight of these studies, with only the study about *Eumachia straminea* (syn. *Psychotria straminea*) failing to report their presence (**Table 1.3**) (Fu et al., 2015). The genus is notable for accumulating polypyrroloindoline alkaloids, also known as cyclotryptamine, oligocyclotryptamine alkaloids, or cis-pyrrolidino[2,3-b]indoline alkaloids (Jamison et al., 2017). These compounds are typically oligomers, consisting of monomeric units joined by quaternary carbon stereocenters, resulting in diverse stereoisomers. Common dimers include (+)-chimonanthine and (–)-calycanthine, while larger oligomers have also been identified (e.g. hodgkinsine, psychotridine, and quadrigemines A-C) (Adjibade et al., 1992, Lajis et al., 1993, Roth et al., 1986, Libot et al., 1987). For example, psychotridine, which is a pentameric pyrroloindoline alkaloid that consists of five indole units, has also been isolated from *E. forsteriana*, *E. oleoides*, and *E. leptothyrsa* (previously known as *Psychotria beccarioides*) (Libot et al., 1987, Roth et al., 1986, Hart et al., 1974). Other complex polyindolinic alkaloids that contain four or more indole units include quadrigemines A-C, oleidine and caledonine, have also been isolated from *Eumachia* genus (Libot et al., 1987, Roth et al., 1986, Jannic et al., 1999).

Polypyrroloindoline alkaloids are also reported in species of *Psychotria* and *Palicourea*, highlighting their distribution across related genera (Takayama et al., 2004). To be specific,

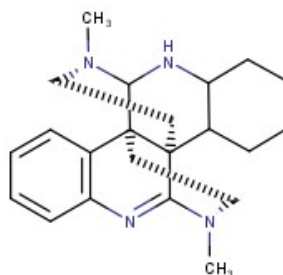
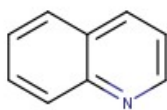
Palicourea colorata contains various pyrroloindoline alkaloids such as calycanthine, hodgekinsine, psychotridine and quadrigemines, while psychotrimine was isolated from *Psychotria calocarpa* (Verotta et al., 1998, Zhou et al., 2010). Within *Eumachia*, oligomers often feature specific C3a–C7' linkages interrupted by a single C3a–C3a' linkage, forming chimonanthine subunits (Guéritte-Voegelein et al., 1992, Jannic et al., 1999). The location of labile bonds within these structures influences their fragmentation patterns, as observed in compounds such as quadrigemine B and quadrigemine C, which exhibit distinct mass spectrometric fragmentation modes (Jamison et al., 2017).

Additionally, monoterpene indole alkaloids (MIAs) are mainly isolated from *Palicourea* and *Psychotria* species (especially from neotropical areas), namely, *Palicourea correae*, *Palicourea prunifolia*, *Psychotria stachyoides*, *Palicourea suterella*, *Psychotria branchyceras*, and *Palicourea didymocarpos* (Achenbach et al., 1995b, Lucilia et al., 2012, Pimenta et al., 2010, Van De Santos et al., 2001, Kerber et al., 2001, Paul et al., 2003). Other examples of indole alkaloids isolated from *Eumachia*, along with alkaloids aforementioned, are summarized in Tables 1.3 and Table 1.4.

Table 1. 2 Examples of alkaloids from *Eumachia* genus.

Class	Core structure	Examples
Pyrrolidinoindoline alkaloids		 <p>Hodgkinsine</p>
		 <p>Quadrigemine B</p>
		 <p>(+)-Chimonanthine</p>

Quinoline alkaloid



(-)-Calycanthine

Table 1. 3 Pyrrolidinoindoline and quinoline alkaloids from *Eumachia* species.

Compound	Species	Reference
(-)-calycanthine	<i>Eumachia rostrata</i>	(Lajis et al., 1993)
	<i>Eumachia forsteriana</i>	(Adjibade et al., 1992)
iso-calycanthine	<i>Eumachia forsteriana</i>	(Adjibade et al., 1992)
calycosidine	<i>Eumachia rostrata</i>	(Lajis et al., 1993)
(+)-chimonanthine	<i>Eumachia rostrata</i>	(Lajis et al., 1993)
meso-chimonanthine	<i>Eumachia forsteriana</i>	(Adjibade et al., 1992)
	<i>Eumachia lyciiflora</i>	(Jannic et al., 1999)
	<i>Eumachia rostrata</i>	(Lajis et al., 1993)
hodgkinsine	<i>Eumachia oleoides</i>	(Libot et al., 1987, Jannic et al., 1999)
	<i>Eumachia cymuligera</i>	(Brand et al., 2012)
	<i>Eumachia depauperate</i>	(Nascimento et al., 2015)
	<i>Eumachia frutescens</i>	(Anet et al., 1961)
psychotridine	<i>Eumachia oleoides</i>	(Jannic et al., 1999)
	<i>Eumachia leptothyrsa</i>	(Hart et al., 1974)

isopsychotridine A	<i>Eumachia oleoides</i>	(Libot et al., 1987)
isopsychotridine B	<i>Eumachia oleoides</i>	(Libot et al., 1987, Jannic et al., 1999)
isopsychotridine C	<i>Eumachia forsteriana</i>	(Roth et al., 1986)
psychopentamine	<i>Eumachia rostrata</i>	(Takayama et al., 2004)
psychotrimine	<i>Eumachia rostrata</i>	(Takayama et al., 2004)
quadrigenines A	<i>Eumachia forsteriana</i>	(Roth et al., 1986)
	<i>Eumachia frutescens</i>	(Parry and Smith, 1978)
quadrigenines B	<i>Eumachia forsteriana</i>	(Roth et al., 1986)
	<i>Eumachia cymuligera</i>	(Brand et al., 2012)
	<i>Eumachia frutescens</i>	(Parry and Smith, 1978)
quadrigenines C	<i>Eumachia oleoides</i>	(Libot et al., 1987, Jannic et al., 1999)
oleidine	<i>Eumachia oleoides</i>	(Jannic et al., 1999)
caledonine	<i>Eumachia oleoides</i>	(Jannic et al., 1999)

Table 1. 4 Monoterpenoid indole alkaloids from *Psychotria* and *Palicourea* species.

Species	Compound	Reference
<i>Palicourea correae</i>	Correantoside	
	10-Hydroxycorreantoside	
	Correantine B	(Achenbach et al., 1995b)
	20- <i>epi</i> -Correantine B	
	Correantine A	
	Correantine C	

<i>Palicourea prunifolia</i>	10-Hydroxy- <i>iso</i> -deppeaninol	
	10-Hydroxy-antirrhine	(Lucilia et al., 2012)
	N-Oxide-10-hydroxyantirrhine	
<i>Psychotria branchyceras</i>	Brachycerine	(Kerber et al., 2001)
<i>Psychotria stachyoides</i>	Correantosine E	(Pimenta et al., 2010)
	Correantosine F	
<i>Psychotria suterella</i>	Naucleatine	(Van De Santos et al., 2001)
<i>Palicourea didymocarpos</i>	Bahienoside A	(Paul et al., 2003)
	Bahienoside B	

Bioactivities of Eumachia and its relative genus

The polyindoline alkaloids (including quadrigemines A and B, psychotridine, and isopsychotridine C) isolated from *E. forsteriana* have shown higher cytotoxicity than vincristine against rat hepatoma cells (HTC line). It is concluded that a cellular mortality of 100% was obtained within 24h of incubation at the concentration of 2.5, 5, 5 and 10 μ M for the alkaloids psychotridine, isopsychotridine C, quadrigemines A, and quadrigemine B, respectively (Roth et al., 1986). Another study also described the time- and dose-dependent relationship of the cytotoxic activity of quadrigemine B against HEp-2 cells (Mahmud et al., 1993).

The genus *Psychotria* has also been extensively studied for its diverse pharmacological potential. Previous reports described the significant cytotoxicity of the extracts of *Psychotria rubra* against KB cells (initially thought to originate from an oral epidermal carcinoma, was later identified as a HeLa cell derivative), as well as the moderate toxicity level and potent clot lysis activity of the extracts of *Psychotria calocarpa* (Hayashi et al., 1987, Bristy et al., 2020, ATCC). Subsequent studies were also carried out to investigate other pharmacological properties of the leaves of *Psychotria calocarpa*, including antinociceptive (may possibly suppress the inflammatory mediators), antidiarrheal (significant and dose-dependent) and antioxidant activities (strong) (Bristy et al., 2020). Furthermore, the pyrrolidine indole

alkaloids isolated from the leaves and flowers of *Psychotria colorata* have marked opioid-like analgesic activity, and further research indicated hodgekinsine, psychotridine (pentamer), quadrigemine C and (+)-chimonanthine (dimer) played a major role for their potent analgesic effects (Elisabetsky et al., 1995, Verotta et al., 1998, Amador et al., 2000, Amador et al., 2001, Verotta et al., 2002).

Additionally, *Psychotria* species have been investigated for their effects on the central nervous system (CNS). Multiple studies have reported that the quaternary β -carboline alkaloids, MIAs, and azepine-indole alkaloids from the *Psychotria* genus (e.g. *Psychotria suterella*, *Psychotria laciniata*, and *Psychotria nemorosa*) have the capacity to modulate acetylcholinesterase (AChE), butyrylcholinesterase (BChE), and monoamine oxidases A (MAO-A), which are key enzymes related with neurodegenerative diseases (e.g., depression and dementia) (Passos et al., 2013, Klein-Júnior et al., 2020a).

The Eumachia species in Malaysia and Eumachia montana

Malaysia, with its diverse tropical ecosystems, is home to several species from these genera. However, the distribution and bioactivity of *Eumachia* species in Malaysia remain relatively understudied. Previous studies on the bark and twigs of the Malaysian plant *Eumachia rostrata* have reported the isolation of polyindoline alkaloids, including the quinoline alkaloid (-)-calycanthine (dimer) and the pyrrolidinoindoline alkaloids (+)-chimonanthine (dimer), hodgekinsine (trimer), and the major component quadrigemine B (tetramer), which were reported to be cytotoxic (Lajis et al., 1993, Roth et al., 1986). More recently, additional two indole alkaloids, namely, psychotrimine (trimer) and psychopentamine (pentamer) were isolated from the leaves of *Eumachia rostrata* (Takayama et al., 2004).

Another species within the genus, *Eumachia montana* (Blume) I.M.Turner (syn. *Psychotria montana*) is an evergreen herb grown in Malaysia. It has opposite decussate leaves with a shape of elliptic or oblong-lanceolate (Hutan et al., 1989). Traditionally, the roots of *E. montana* are applied externally for poulticing ulcer and swellings, or to be made into a decoction that is consumed orally to treat constipation (1989, Ong et al., 2012). However, to the best of our knowledge, there have been no prior phytochemical or biological studies on *E. montana*, as verified through searches in Web of Science and Reaxys. This recognition has motivated the

search for alkaloid-containing *Eumachia* species in Malaysia that have not yet been investigated. Identifying such species holds significant potential for the discovery of novel alkaloids with valuable pharmacological properties.

In contrast to the relatively understudied *Eumachia*, the closely related genus *Psychotria* is well-represented in Malaysian forests. Several species, including *Psychotria calocarpa*, *Psychotria sarmentosa*, *Psychotria griffithii*, and *Psychotria malayana*, have been documented in the region, among which, two species have been phytochemically investigated for their alkaloidal composition (*Psychotria calocarpa* and *Psychotria malayana*) (Verotta et al., 1998, Hadi et al., 2014). For example, species such as *Psychotria malayana* have been documented in the region, previous studies of its leaves indicated the presence of hodgekinsine as the major alkaloid, together with other alkaloids, namely, calycanthine, (\pm)-chimonanthine, and meso-chimonanthine (Hadi et al., 2014). Additionally, from the flowers and leaves of another Malaysian species *Psychotria calocarpa* (Rubiaceae), various pyrroloindoline alkaloids such as calycanthine, hodgekinsine, psychotridine, quadrigemines, and psychotriasine was obtained (Zhou et al., 2010). Additionally, from the leaves of another Malaysian species *Psychotria calocarpa*, various pyrroloindoline alkaloids such as calycanthine, hodgekinsine, psychotridine, quadrigemines, and psychotriasine were obtained (Zhou et al., 2010, Verotta et al., 1998).

1.3 Cancers

Cancer is a generic term for a large group of diseases that can affect any part of the body. Other terms used are malignant tumours and neoplasms. A defining characteristic of most malignant cancers is the abnormal cells divide uncontrollably, which invade adjacent tissues and spread to other organs, a process known as metastasis. However, certain malignancies, such as chronic lymphocytic leukaemia (CLL), deviate from the typical cancer paradigm by evading apoptosis rather than proliferating rapidly, with prolonged MCL1 overexpression enhancing cell survival and leading to their accumulation in the bloodstream despite a low proliferative rate (Johnston et al., 2004). In 2020, cancer was the leading cause of death worldwide, accounting for approximately 10 million fatalities (Organization, 2022). Lung, breast, colorectal, liver, and stomach cancers were the most common causes of cancer-related mortality, responsible for around 50% of cancer deaths, while lung, breast, colorectal, and prostate cancers were the most

frequently diagnosed, comprising over 70% of new cases globally (Organization, 2022). The risk factors of cancer include tobacco use, alcohol consumption, unhealthy diet, physical inactivity and air pollution. In 2020, around one-third of deaths from cancer worldwide were due to tobacco use, high body mass index, alcohol consumption, low fruit and vegetable intake, and lack of physical activity (Organization, 2022).

Breast cancer

Globally, Breast cancer (BC) was the most commonly diagnosed cancer in 2020, with 2.26 million new cases, and one of the leading causes of cancer-related mortality, accounting for 685,000 deaths, or approximately 7% of all cancer deaths (Organization, 2022). Although the exact causes of BC are not fully understood, according to numerous studies in recent decades, factors that may lead to BC have been indicated, comprising genetic mutations, oestrogen exposure, overexpression of leptin, or abnormal growth factor signalling (Cavalieri et al., 2006, Haslam and Woodward, 2003, Jardé et al., 2011). However, the survival rate is improving. In the last 40 years, UK BC survival beyond 10 years has doubled from 4 in 10 women to ~8 in 10 (UK). Additionally, early diagnoses of BC tends to improve the survival rates significantly; the 5-year survival rate for people when the disease is diagnosed at the early stage is 98%, while that for people receiving disease diagnoses at the latest stage is ~26% (UK).

There are three important receptors, namely oestrogen receptor (ER), progesterone receptor (PR), and human epidermal growth factor 2 receptor (HER2), and the presence or absence of these receptors can define subtypes of BC into ER⁺, PR⁺ and HER2⁺ BC, and thus targeted treatment for different receptor-positive BC are developed. For example, ER⁺ cancer cells have oestrogen receptors and rely on oestrogen for growth, and therefore they can be treated with hormone therapy to lower the levels of oestrogen in the body or block its binding and stimulatory effects (e.g. tamoxifen, anastrozole) (UK). ER⁺ accounts for the majority of BC cases (~70%) and tamoxifen is one of the most commonly used hormone therapies for BC (UK). The expression of PR can be activated by ER gene, and ER⁺ PR⁺ tumours generally exhibit better prognoses than ER⁺ PR⁻ tumours, as PR expression reflects an active ER signalling complex, enhancing sensitivity to endocrine therapies such as tamoxifen and aromatase inhibitors (e.g. anastrozole) (Kaneko et al., 1993, Bardou et al., 2003). However, clinical and laboratory evidence suggests that ER⁺PR⁻ BC may exhibit specific resistance to

selective oestrogen receptor modulators (SERMs) while responding more favourably to oestrogen withdrawal via aromatase inhibitors, suggesting that PR loss does not necessarily signify a nonfunctional ER complex (Cui et al., 2005, Mohammed et al., 2015).

The current first-line therapy for HER2⁺ BC includes the pertuzumab-trastuzumab-docetaxel combination, in which pertuzumab and trastuzumab are monoclonal antibodies targeting different extracellular domains of the HER2 protein (Keating, 2012). Monoclonal antibodies are capable of recognising and targeting specific proteins on cancer cells and hence stop particular proteins from binding to cancer cells or block the proteins from triggering the cancer cells to divide and grow (UK). However, due to the high molecular weight, trastuzumab cannot penetrate the blood-brain barrier (BBB), leading to a high incidence of CNS metastases (28–43%) in patients receiving trastuzumab-based HER2-targeted therapy, posing a major challenge in treating HER2-positive metastatic BC (Bendell et al., 2003). Although small-molecule HER2 inhibitors such as lapatinib have been developed, their therapeutic efficacy remains limited, highlighting the urgent need for novel small-molecule agents capable of crossing the BBB and exerting anti-metastatic effects in HER2-positive BC (Taskar et al., 2012). Additionally, HER2 overexpression activates the PI3K/AKT/mTOR and Ras/Raf/MAPK signalling pathways, driving tumour progression and drug resistance in HER2-positive BC, suggesting that targeting key components such as AKT and mTOR holds significant therapeutic potential (Adamczyk et al., 2017). Notably, actein, a cycloartane triterpenoid from *Cimicifuga foetida*, has demonstrated anticancer activity across various malignancies and has exhibited significant anti-metastatic effects in HER2-positive BC cells *in vitro* by modulating the AKT/mTOR and Ras/Raf/MAPK signalling pathways (Wu et al., 2020b).

Furthermore, triple negative breast cancer (TNBC) is a type of BC that characterized by the absence of expression of these three receptors (ER, PR and HER2) and the presence of overexpression of epidermal growth factor receptor (EGFR). Notably, ER⁺ PR⁺ HER2[–] tumours are associated with the most favourable clinical outcomes, while the triple negative subtype has the worst overall and disease free survival, as the absence of hormones receptors (ER and PR) and HER2 make the treatment of TNBC a challenge due to the lack of response to standard hormonal therapy or therapies targeted at HER2 (Onitilo et al., 2009).

Nevertheless, drugs that target EGFR are potential treatments for TNBC, for example the tyrosine kinase inhibitors such as gefitinib, erlotinib and lapatinib (UK). The tyrosine kinase inhibitors belong to a group of cancer growth blockers that specifically work by blocking the signalling of EGFR, which ultimately impairs cell growth and metastasis (UK). Poly (ADP-ribose) polymerase (PARP) inhibitors (e.g. olaparib and rucaparib) are another type of anticancer therapy, which are used in the targeted treatment of BRCA-mutant BC. Since PARP is an important protein in DNA repair especially base excision repair (BER), PARP inhibition can lead to cell death by preventing cancer cells from repairing their damaged DNA (Chen, 2011). In the UK, ~5-10% diagnosed BC are inherited breast cancers (IBC) due to a faulty gene in family, for instance *BRCA1* or *BRCA2* genes (UK). *BRCA1* or *BRCA2*-mutant BC can interfere with the repair of DNA damage including DNA cross links and double strand breaks by homologous recombination (HR). As a result, the *BRCA*-mutant cells that are already deficient in DNA HR, are particularly sensitive to PARP inhibitors due to the synthetic lethal relationship between BER and HR (Chen, 2011).

Based on the different histological appearance of carcinoma cells, other types of BC comprise invasive BC (no special type or NST), invasive lobular BC, inflammatory BC, ductal carcinoma in situ (DCIS), and the other rare types of BC. Among all these types of BC, NST is the most common, in this condition cancer cells with no special features have grown through the lining of the ducts into the surrounding breast tissue. DCIS, which is contained within the ducts has the potential to develop into NST. The second most common type is invasive lobular BC, which begins in the cells that line the lobules (the glands that make milk when breastfeeding) and spreads into the surrounding breast tissue (UK). Numerous research programmes are currently underway to evaluate treatments for BC, which include surgery, radiotherapy, chemotherapy, hormone therapy, as well as targeted drugs and immunotherapies.

Colorectal cancer

Colorectal cancer (CRC) is also known as bowel cancer, which starts in the large bowel (colon) and the back passage (rectum), arising from complex genetic and epigenetic alterations (Fearon and Vogelstein, 1990). It is a leading cause of cancer-related mortality worldwide, ranking

second among top 10 most common cancers in 2020, and being the 4th most common cancer in UK, with the highest incidence rates in people aged 85 to 89 between 2016 and 2018 (Sung et al., 2021, UK, 2022). CRC may be classified according to origin or type, and may including adenocarcinoma, squamous cell tumours, carcinoid tumours, sarcomas, lymphomas and melanoma. The risk factors of CRC include older age, high intakes of red, processed meat, low intakes of fibre, obesity, lack of physical exercise, smoking and genetic disorders (e.g. familial adenomatous polyposis (FAP), hereditary nonpolyposis colorectal cancer (HNPCCS)) (Fearon and Vogelstein, 1990). Specifically, FAP is characterized by the inherited loss of the adenomatous polyposis coli (APC) tumour suppressor gene on chromosome 5q, while HNPCC, also known as Lynch syndrome, results from deleterious mutations in mismatch repair (MMR) genes such as *hMSH2* and *hMLH1* (Ashton-Rickardt et al., 1989, Lynch and Lynch, 2000). The disease progresses through distinct molecular pathways, including chromosomal instability (CIN), microsatellite instability (MSI), and the CpG island methylator phenotype (CIMP), all of which contribute to tumour development and therapeutic resistance (Nazemalhosseini Mojarad et al., 2013).

Nevertheless, CRC survival has more than doubled in the last 40 years in the UK, and an early diagnoses of bowel cancer tends to improve the survival rates significantly (10 year or more survival rates from 21.8% to 56.6%) (UK, 2022). Numerous research programmes around the world aim to evaluate the causes and improve diagnosis and treatment of bowel cancer. Specific research aspects include the relationship of bowel cancer and gene expression, the development of chemotherapy drugs, targeted drugs, and immunotherapy. The monoclonal antibodies cetuximab, panitumumab, and bevacizumab are a type of targeted therapy for bowel cancer. Cetuximab, panitumumab are EGFR inhibitors, which work by blocking the signalling of EGFR that encourage cancer cells to grow and divide (UK). Bevacizumab is anti-angiogenesis agent which can block cancer blood vessel growth and metastasis (UK).

Conventional treatments, including surgery, chemotherapy, and targeted therapies, have shown efficacy but are often limited by drug resistance and adverse effects. Recent research has focused on natural product-derived drugs as potential alternatives or adjuncts to standard treatments. These compounds (e.g. camptothecin, berberine, curcumin) exert anticancer effects through diverse mechanisms, including apoptosis induction, inhibition of proliferation, and

modulation of signalling pathways such as Wnt/ β -catenin, PI3K/AKT, and NF- κ B (Wall and Wani, 1996, Wu et al., 2012, Ismail et al., 2019). Understanding the pathology, therapeutic approaches, and molecular mechanisms governing CRC progression is essential for developing novel treatment strategies.

The molecular mechanisms governing CRC progression and therapeutic response are highly intricate, involving multiple deregulated signalling pathways. One of the most critical pathways in CRC is Wnt/ β -catenin signalling, which is frequently accompanied by APC mutations (Vermeulen et al., 2010). This aberrant activation leads to nuclear translocation of β -catenin, where it drives the transcription of genes involved in proliferation and survival (MacDonald et al., 2009). Therapeutic NPs targeting this pathway, including curcumin and berberine, have shown promise in preclinical models by reducing β -catenin transcriptional activity and inducing tumour cell apoptosis (Ismail et al., 2019, Wu et al., 2012).

The PI3K/AKT/mTOR pathway is another major driver of CRC progression, regulating cell proliferation, metastasis, survival, and angiogenesis. Mutations in PIK3CA, a key component of this pathway, contribute to enhanced tumour cell proliferation and resistance to chemotherapy (e.g. EGFR-targeted treatment) (Custodio and Feliu, 2013, Stefani et al., 2021). Natural compounds such as quercetin and resveratrol have been demonstrated to suppress AKT phosphorylation, thereby restoring apoptotic sensitivity in CRC cells (Yang et al., 2015, Neamtu et al., 2022). The NF- κ B pathway plays a crucial role in CRC cell proliferation, apoptosis, angiogenesis, inflammation, and metastasis, with its persistent activation promoting immune evasion and resistance to therapy (Soleimani et al., 2020). Inhibition of NF- κ B signalling by quercetin and curcumin has been shown to enhance the efficacy of standard chemotherapeutic agents (Neamtu et al., 2022, Ismail et al., 2019).

CRC remains a significant global health burden, with complex molecular pathologies that drive tumourigenesis and therapeutic resistance. While conventional treatments have improved patient outcomes, limitations such as drug resistance and adverse side effects necessitate the exploration of alternative strategies (i.e. novel chemical elements and formulations). Natural product-derived compounds offer promising avenues for CRC therapy by targeting key

signalling pathways involved in tumour progression and drug resistance. Their ability to modulate Wnt/ β -catenin, PI3K/AKT, and NF- κ B pathways highlights their therapeutic potential in overcoming the limitations of current treatments. Further research is essential to optimize the efficacy and clinical applicability of these natural compounds, paving the way for novel interventions in CRC management.

Brain cancer (glioblastoma multiforme)

Brain cancer encompasses a diverse group of malignant tumours affecting the brain and central nervous system (CNS), with varying degrees of malignancy, aggressiveness, and treatment responsiveness. Among these, glioblastoma multiforme (GBM) is the most aggressive and prevalent primary malignant brain tumour in adults, classified as grade IV astrocytoma by the World Health Organization (WHO) (Brennan et al., 2013, Louis et al., 2021). Despite advances in neurosurgery, radiotherapy, and chemotherapy, GBM remains incurable, with a median survival time of approximately 15 months following diagnosis (Grochans et al., 2022). GBM typically arises in the cerebral hemispheres and may develop from pre-existing diffuse WHO grade II astrocytomas or anaplastic astrocytomas, progressing to secondary GBM. However, in most cases, GBM develops *de novo* following a short clinical history, without evidence of a preceding lower-grade malignancy (Brandes et al., 2008).

Pathology of GBM

GBM exhibits elusive risk factors and significant genetic and histopathological heterogeneity, which contribute to its aggressive behavior and drug resistance. The diagnosis of GBM is based on histopathological features, which includes cellular polymorphism, nuclear atypia, mitotic activity, vascular thrombosis, microvascular proliferation and necrosis (Kleihues et al., 2002). Notably, microvascular proliferation and/or necrosis are essential diagnostic criteria distinguishing GBM from lower-grade gliomas. Additionally, genetic and molecular alterations are regarded as the hallmark of GBM, including mutations in isocitrate dehydrogenase (IDH)-wildtype, telomerase reverse transcriptase (TERT) promoter, chromosomes 7/10, and *EGFR* (Louis et al., 2021). In particular, *EGFR* amplification occurs in approximately half of all GBM cases, driving uncontrolled cell proliferation (Brennan et al., 2013). Mutations in IDH are associated with better prognosis but are less common in primary GBM (Parsons et al., 2008). Tumour suppressor genes such as *TP53* and *PTEN* frequently undergo mutations, leading to

unchecked tumour growth (Brennan et al., 2013). The epigenetic modification of MGMT (O[6]-methylguanine-DNA methyltransferase) promoter methylation affects direct DNA repair mechanisms and serves as a predictive biomarker for responsiveness to temozolomide (TMZ) (Hegi et al., 2005). Clinical research has demonstrated that mutations in *EGFR* or *PTEN* result in the sustained activation of the PI3K/AKT/mTOR signalling pathway, thereby promoting tumourigenesis and contributing to therapy-resistance (Li et al., 2016).

Additionally, GBM cells have evolved multiple mechanisms to evade apoptotic cell death, contributing to the failure of standard therapies. Apoptosis resistance is one of the most prominent hallmarks of GBM, with tumour cells frequently overexpressing anti-apoptotic proteins such as BCL2 and BCL-XL while downregulating pro-apoptotic factors like BAX and p53 (Van Meir et al., 2010). Beyond apoptosis resistance, GBM cells utilize autophagy as a survival mechanism under metabolic stress or therapeutic pressure (particularly in the hypoxic tumour microenvironment), balancing cell survival through organelle degradation or inducing autophagic/apoptotic cell death under extreme conditions (Pawlowska et al., 2018). Hypoxia and angiogenesis are induced through overexpression of vascular endothelial growth factor (VEGF), supporting tumour growth and invasion (Jain et al., 2007, Fukumura et al., 2001, Nagy et al., 2002). Additionally, metabolic adaptations such as reliance on aerobic glycolysis, known as the Warburg effect, provide tumour cells with the energy required for rapid proliferation (Hanahan and Weinberg, 2017).

Treatment of GBM

GBM can be characterized by rapid proliferation, significant heterogeneity—including diffuse infiltration, necrosis, extensive angiogenesis, pronounced treatment resistance, and widespread genomic aberrations—and an invariably fatal clinical course, posing major challenges for therapeutic strategies.

The treatment of GBM is multimodal, incorporating surgery, radiation therapy, and chemotherapy, with TMZ as the first-line chemotherapeutic agent. TMZ exerts its effect by alkylating DNA, inducing apoptotic or autophagic tumour cell death. The *MGMT* promoter methylation status is a key predictor of TMZ response, with methylated tumours demonstrating

TMZ-sensitivity and better outcomes (Hegi et al., 2005). Bevacizumab, an anti-VEGF monoclonal antibody, is used for recurrent GBM, though its benefit in newly diagnosed cases remains controversial (Norden et al., 2008). Despite aggressive management, the median survival remains approximately 12–15 months (Stupp et al., 2005). Additionally, studies have demonstrated that natural compounds, such as resveratrol, can enhance the anticancer effects of TMZ in GBM cells by abrogating G2 arrest and inducing mitotic catastrophe, ultimately leading to cellular senescence and reduced clonogenic activity (Filippi-Chiela et al., 2013).

Various innovative therapies are under investigation to improve GBM treatment outcomes. Immunotherapy approaches, including checkpoint inhibitors, dendritic cell vaccines, and chimeric antigen receptor (CAR) T-cell therapy, are being explored, with ongoing research evaluating their efficacy (Lim et al., 2018). Gene therapy strategies are also being studied, focusing on targeting oncogenic drivers and restoring tumour suppressor function to inhibit tumour progression (Kwiatkowska et al., 2013). Additionally, targeted therapies are being developed to interfere with molecular pathways such as EGFR (e.g. Gefitinib, Erlotinib), VEGFR (e.g. Aflibercept, Cediranib), and mTOR (e.g. Sirolimus (rapamycin), Everolimus) signalling, though their clinical efficacy has been limited so far (Van Meir et al., 2010).

GBM remains one of the most formidable challenges in neuro-oncology due to its aggressive nature, resistance to therapy, and poor prognosis. Advances in molecular diagnostics and emerging therapeutic strategies offer hope for improved outcomes. Future research should focus on personalized treatment approaches based on tumour-specific molecular signatures.

Lung cancer

The latest global report identifies lung cancer as the leading cause of cancer-related mortality and the second most diagnosed malignancy, with approximately 2,206,771 new cases (11.4%) and 1,796,144 deaths (18.0%) reported in 2020 across 185 countries (Sung et al., 2021). It primarily arises from the epithelial cells of the lung and is strongly associated with environmental risk factors such as smoking, pollution, and occupational exposures. Despite advances in diagnosis and treatment, lung cancer remains a major public health concern due to its high incidence, late-stage presentation, and aggressive nature.

Lung cancer is broadly classified into two major categories: non-small cell lung cancer (NSCLC) and small cell lung cancer (SCLC). NSCLC accounts for approximately 85% of lung cancer cases and is further subdivided into adenocarcinoma (40%), squamous cell carcinoma (25%), and large cell carcinoma (Otegui et al., 2023). Adenocarcinoma is the most common subtype, frequently occurring in non-smokers and associated with genetic mutations such as EGFR, ALK, and KRAS (Otegui et al., 2023).

The pathogenesis of lung cancer involves multiple genetic and epigenetic changes that promote tumour growth and metastasis. Mutations in key oncogenes, including EGFR and KRAS, and ALK, play a critical role in NSCLC tumourigenesis via multiple significant signalling pathways (e.g. the PI3K/AKT/mTOR signalling pathway), while the loss of tumour suppressor genes such as *TP53* and *STK11* contributes to disease progression and immune checkpoint inhibition (ICI) resistance (Lastwika et al., 2016, Hallberg and Palmer, 2013, Skoulidis et al., 2018). In addition to genetic mutations, epigenetic modifications such as DNA methylation and antigen presentation machinery regulate gene expression and tumour behaviour (Rother et al., 2024). The tumour microenvironment further influences lung cancer progression through regulating tumour growth, immune evasion, and therapy resistance (Rother et al., 2024).

Treatment strategies for lung cancer vary depending on the stage and molecular characteristics of the tumour, while the advent of targeted therapy has revolutionized lung cancer treatment, with EGFR inhibitors (such as osimertinib), ALK inhibitors (such as crizotinib), and KRAS inhibitors (such as sotorasib) offering personalized treatment approaches (Rodak et al., 2021). Targeted therapy aims to inhibit key proteins associated with these mutations, with *EGFR* being the most studied. EGFR mutations, present in approximately 20% of lung adenocarcinomas, drive oncogenic signalling and are targeted by tyrosine kinase inhibitors (TKIs) (Dogan et al., 2012). While first- and second-generation TKIs improve survival, resistance mechanisms such as the T790M mutation necessitated the development of third-generation inhibitors like osimertinib, now a first-line treatment (Bell et al., 2005, Rodak et al., 2021). Additionally, immunotherapy has complemented targeted therapies by overcoming immune evasion mechanisms. To be specific, immune checkpoint inhibitors (ICIs) target CTLA-4 (ipilimumab), PD-1 (pembrolizumab), and PD-L1 (Cemiplimab), and thus enhance antitumour immunity by disrupting inhibitory pathways used by cancer cells (Tang et al., 2020, Hoos,

2016, Reck et al., 2016, Sezer et al., 2021). While ICIs have shown clinical efficacy, response rates remain relatively low, leading to the development of combination strategies with chemotherapy, radiotherapy, or TKIs to improve outcomes (Rother et al., 2024). Recent advancements include the FDA approval of cemiplimab for first-line treatment of PD-L1-positive advanced NSCLC, demonstrating significant survival benefits (Sezer et al., 2021). Combination approaches, such as pembrolizumab with chemotherapy (KEYNOTE trials) and atezolizumab with chemotherapy (IMpower trials), have shown improved progression-free and overall survival (Reck et al., 2019, Rodak et al., 2021). In these cases, the natural product derived chemotherapy drug paclitaxel is utilized in combination with atezolizumab (Reck et al., 2019).

Lung cancer continues to be a major global health burden, but ongoing research is driving improvements in early detection, personalized medicine, and novel therapeutic strategies. The integration of drug discovery, natural product research, and cell-based models has provided valuable insights into lung cancer biology, paving the way for more effective treatments. Future directions in lung cancer research include AI-driven drug discovery, the development of immunotherapy combinations, and the application of nanotechnology-based drug delivery systems. These advancements hold promise for improving patient outcomes and overcoming the challenges associated with lung cancer treatment.

1.4 Metabolomics

Metabolomics is an emerging field that systematically studies large-scale metabolites, which are small molecules (<1500 Da) that serve as the end products of gene expression and cellular metabolic activities (Johnson and Gonzalez, 2012). This rapidly growing discipline provides a comprehensive profile of the chemical fingerprints left by cellular processes, offering a dynamic snapshot of metabolic changes induced by biotic factors (e.g., disease onset and progression) or abiotic perturbations (e.g., drug treatment and xenobiotic exposure). In medicinal chemistry and molecular sciences, metabolomics has become an essential tool for drug discovery, elucidating cellular mechanisms, and identifying biomarkers by detecting subtle alterations in biological pathways. It provides critical insights into metabolically relevant perturbations arising from genetic mutations, environmental influences, and pharmacological interventions at the molecular level (Clish, 2015, Johnson et al., 2012, Johnson et al., 2016).

In the context of cancer research, natural products (NPs) exhibit diverse mechanisms of action, including apoptosis-induction, cell cycle arrest, inhibition of angiogenesis, epigenetic modulation, and metabolic reprogramming. Notably, metabolic reprogramming is a hallmark of cancer, characterized by alterations in cellular metabolism, including enhanced glycolysis, increased glucose uptake, disrupted oxidative phosphorylation (OXPHOS), and aberrant lipid metabolism (Wang et al., 2021a). By analyzing intracellular and extracellular metabolites, metabolomics enables the identification of metabolic pathways influenced by cytotoxic NPs, facilitates biomarker discovery for anticancer responses, and reveals metabolic vulnerabilities that can be exploited for therapeutic interventions.

Metabolomics Techniques

Metabolomics studies acquire sophisticated analytical platforms to measuring and analysing the metabolome, the complete set of metabolites within a biological sample. Among the most commonly used analytical methods for metabolomics are mass spectrometry (MS) and nuclear magnetic resonance (NMR). To achieve highly sensitive and accurate metabolite identification and quantification, MS is typically coupled with chromatographic techniques such as gas chromatography (GC) and liquid chromatography (LC). The development of high-resolution, accurate mass instruments has advanced MS-based metabolomics, enabling the detection of thousands of metabolites in a single run.

Advanced metabolomics platforms, including LC-MS and GC-MS, offer unparalleled sensitivity and resolution, making them particularly effective in detecting low-abundance metabolites that may be critical for understanding complex biological processes, such as cancer development and progression. LC-MS is especially useful for profiling complex, non-volatile biological samples, as it is capable of analysing both polar and non-polar metabolites with minimal sample preparation. In contrast, GC-MS is ideal for the identification of volatile and thermally stable metabolites, providing high sensitivity for these types of compounds (Fiehn, 2016). These platforms enable detailed analysis of cellular metabolic alterations, allowing researchers to uncover pathways that are dysregulated in diseases like cancer.

Following raw data collection, robust data analysis is essential to interpret the large volumes of information generated. Multivariate statistical methods such as principal component analysis (PCA) and partial least squares discriminant analysis (PLS-DA) are commonly employed to differentiate metabolic profiles and identify significant alterations in metabolic pathways. Additionally, pathway analysis tools, such as MetaboAnalyst and KEGG pathways, provide insights into the biochemical networks that are affected by these metabolic changes.

In NPDD, to gain a more comprehensive understanding of how NPs exert their cytotoxic effects on cancer cells, metabolomics can be integrated with other omics approaches, including proteomics, genomics, and transcriptomics. This integrated approach offers a more holistic view of cellular mechanisms and provides valuable insights into how metabolic reprogramming in cancer cells can be targeted therapeutically, ultimately enhancing our understanding of complex biological systems and improving therapeutic strategies.

Metabolomics in Drug Discovery, Cellular Mechanism

The application of metabolomics in drug discovery is wide-ranging, spanning identification of drug targets to pharmacokinetics and cytotoxicity assessments. Metabolomics enables researchers to track the effects of potential drug candidates on metabolic pathways, providing insights into how drugs interact with biological systems and their impact on metabolic homeostasis.

This approach is particularly valuable in studying NPs, which often consist of complex mixtures containing structurally diverse compounds, making the identification of bioactive molecules challenging. Metabolomics addresses this challenge by integrating advanced analytical techniques such as LC-MS and NMR spectroscopy with computational tools, which facilitate the profiling and identification of bioactive metabolites from natural sources such as plants, fungi, and marine organisms. Additionally, metabolomics provides a systems-level perspective on the biochemical changes induced by NP, enabling the elucidation of NP-affected metabolic pathways, such as those involved in energy production, lipid metabolism, and amino acid processing. Instead of focusing on isolated pathways like the traditional methods, metabolomics captures the global metabolic shifts caused by tested agents, revealing their

mechanisms of action. For example, berberine, a plant-derived alkaloid, demonstrates anticancer activity by inducing cell cycle arrest, inhibiting cancer cell proliferation, as well as disrupting glycolysis and OXPHOS (Fan et al., 2013). Similarly, paclitaxel, a microtubule-stabilizing agent, not only induces cell cycle arrest and apoptosis but also alters cancer cell lipid metabolism by downregulating *CPT1B* and fatty acid oxidation (*FAO*) in BC cells (McGrogan et al., 2008, Wang et al., 2018).

Metabolomics in Biomarkers' Identification

Beyond mechanisms' elucidation, metabolomics can be used to identify disease-associated biomarkers, which can serve as potential drug targets for small molecules or biologics. By analyzing metabolomic changes following drug treatment, researchers can gain deeper insights into drug mechanisms of action and thus optimize drug efficacy and minimize adverse effects through personalized treatment strategies. Cancer studies have demonstrated that certain anticancer agents alter tumour metabolomic profiles, unveiling novel therapeutic targets and exploiting cancer-specific metabolic vulnerabilities (Tian et al., 2020, Zhang et al., 2024). One such metabolic vulnerability is the Warburg effect, a hallmark of cancer metabolism characterized by high glucose consumption and lactate production under aerobic conditions, which supports the biosynthetic and energetic demands of rapid tumour proliferation (Hosios and Manning, 2021). Through the application of metabolomics, it has been demonstrated that noscapine, an opium alkaloid, and FUZI alkaloidal extracts, a TCM, target the Warburg effect via the PI3K/mTOR signalling pathway in colon cancer cells and non-small NSCLC cells, respectively, thereby providing a framework for precision medicine (Tian et al., 2020, Zhang et al., 2024).

One of the most promising applications of metabolomics is biomarker discovery, which enables early disease detection, facilitates disease progression and therapy monitoring, as well as aids in stratifying patients most likely to benefit from specific anticancer treatments (Danzi et al., 2023). This is attributed to the ability of metabolomics to indicate therapeutic responses to anticancer agents, predict patient-specific benefits, and assess drug resistance. For example, resveratrol treatment alters glucose and amino acid metabolism in BC cells, with serotonin, kynurenine, and spermidine levels increasing up to 61-fold in MCF-7 and MDA-MB-231 cells, highlighting potential biomarkers of response (Zambrano et al., 2019, Jäger et al., 2011).

Targeting Metabolic Pathways in Cancer Cells

Cancer cells exhibit unique metabolic reprogramming, characterized by elevated glucose and glutamine metabolism, which facilitate rapid proliferation, increased biosynthesis, and survival under stressful conditions by providing and redirecting these crucial external carbon sources to synthesize DNA, proteins, and lipids, thereby meeting the bioenergetic and anabolic demands (Tennant et al., 2010). Cancer-specific isoforms of enzymes involved in energy metabolism, biosynthesis, and adaptation to hypoxic conditions present promising novel drug targets for cancer therapy, potentially improving therapeutic outcomes and enhancing the efficacy and specificity of treatments compared to current therapies. In addition to glycolysis and glutamine metabolism, several other metabolic pathways, including the tricarboxylic acid (TCA) cycle, lipid metabolism, are significantly altered to support the demands of cancer cells.

Given the crucial role of altered metabolic pathways in cancer progression, targeting these pathways has become a promising strategy for cancer treatment. NPs have historically played an important role in the development of cancer therapeutics, and several natural compounds (e.g. matrine and berberine) have been found to modulate metabolic pathways (e.g. glycolysis, glucose uptake, OXPHOS, and lipid metabolism) in cancer cells (Wang et al., 2021a, Fan et al., 2013).

Glycolysis and the Warburg Effect (aerobic glycolysis)

Cancer cells predominantly rely on glycolysis for energy production, a process that generates ATP and supplies key biosynthetic precursors in the form of glycolytic intermediates. These intermediates serve as building blocks for cellular proteins, membranes, and nucleic acids via metabolic pathways involved in amino acid, lipid, and nucleotide synthesis. The Warburg effect, also known as aerobic glycolysis, describes the phenomenon where cancer cells continue glycolysis even in the presence of oxygen. Instead of fully metabolizing glucose through mitochondrial oxidation to carbon dioxide, cancer cells convert glucose into lactate from pyruvate, leading to lactate secretion and regeneration of NAD⁺ (Hosios and Manning, 2021, Luengo et al., 2021). This metabolic shift allows for sustained glucose uptake and continued entry into glycolysis, with a portion of the carbon being directed into biosynthetic branches of glycolysis (Luengo et al., 2021). Consequently, macromolecular synthesis is promoted to support rapid cell growth, while glycolysis becomes the primary ATP source, meeting the

energy demands of rapidly dividing cancer cells. The key enzymes involved in glycolysis that are typically upregulated in cancer cells include hexokinase (HK), phosphofructokinase (PFK), and pyruvate kinase (Mathupala et al., 2009, Hasawi et al., 2014). Inhibition of these enzymes can disrupt glycolytic flux, impairing cancer cell growth.

HK, which has four isoenzymes, including cancer-overexpressed type II (HK-2), phosphorylates glucose in the initial step of glycolysis (Mathupala et al., 2009). The small molecule 3-bromopyruvate (3-BP) selectively targets tumour cells by inhibiting HK-2 and the mitochondrial ATP synthasome, leading to rapid ATP depletion and tumour destruction without harming the animals (Ko et al., 2004). HK has also been targeted therapeutically with 2-deoxyglucose (2-DG), a non-metabolized glucose analog, in clinical trials for advanced cancers, along with other compounds such as 5-thioglucofuranose and mannoheptulose (Tennant et al., 2010, Pelicano et al., 2006).

Phosphofructokinase (PFK) is a key rate-limiting enzyme in glycolysis and a promising target for cancer therapy due to its role in regulating glycolytic flux (Jenkins et al., 2011). PFK catalyzes the phosphorylation of fructose-6-phosphate (F6P) to fructose-1,6-bisphosphate (F1,6BP), a critical step in glycolysis (Yalcin et al., 2009). Direct inhibition of PFK can be achieved by dissociating its tetrameric form into dimers using compounds like clotrimazole (CTZ), salicylic acid (SA), or acetylsalicylic acid (ASA) (Coelho et al., 2011, Zancan et al., 2007). Additionally, oncogenic RAS activation increases F2,6BP levels, which enhance PFK activity, suggesting that reducing F2,6BP in RAS-transformed cells could effectively inhibit PFK (Jenkins et al., 2011). For instance, F2,6BP activates PFK by shifting its conformational equilibrium from dimeric to tetrameric form, thereby relieving ATP-mediated allosteric inhibition (Wu et al., 2006).

The final step of glycolysis is catalyzed by pyruvate kinase, which converts phosphoenolpyruvate to pyruvate and ATP, while being allosterically regulated by F1,6BP. F1,6BP activates the *PKM2* isoform, linking the two rate-limiting steps of glycolysis and enabling coordinated flux in *PKM2*-expressing cancer cells (Tennant et al., 2010). Inhibition of *PKM2* expression and ectopic expression of *PKM1* reduce lactate production, suggesting

that *PKM2* may replace *PKM1* in cancer cells, offering a potential target for tumour therapy (Christofk et al., 2008). However, a study found *PKM2* to be the predominant isoform in both normal and cancer cells, challenging the notion that *PKM2* is specific to cancer cells (Bluemlein et al., 2011).

NP-derived compounds also have demonstrated significant potential in modulating the glycolytic pathway in cancer cells, offering new avenues for cancer treatment. As alluded to, berberine, a plant-derived alkaloid, has been shown to exert anticancer effects by inducing cell cycle arrest, inhibiting cancer cell proliferation, and disrupting key metabolic processes such as glycolysis and OXPHOS (Fan et al., 2013). This disruption leads to a shift in the energy metabolism of cancer cells, impairing their ability to rapidly proliferate. Additionally, the application of metabolomics has provided further insights into how other natural products, such as noscapine (an opium alkaloid) and FUZI (a TCM derived from the secondary root of *Aconitum carmichaeli* Debx. from the *Ranunculaceae* family) alkaloidal extracts, affect cancer metabolism (Tian et al., 2020, Zhang et al., 2024). Noscapine has been found to target the Warburg effect, a metabolic hallmark of cancer cells, by modulating the PI3K/mTOR signalling pathway in colon cancer cells (Tian et al., 2020). Similarly, FUZI alkaloidal extracts have shown efficacy in targeting the same metabolic pathway in NSCLC cells, underscoring the potential of these compounds in disrupting the altered metabolic states characteristic of cancer (Zhang et al., 2024). By targeting the Warburg effect, these natural products may help reverse the dysregulated metabolic processes in cancer cells, providing a promising framework for precision medicine.

Glutaminolysis

Glutamine, which is actively transported into proliferating cells, plays a crucial role in cancer cell metabolism, providing not only a major source of energy but also nitrogen for nucleotide biosynthesis and a carbon substrate for various anabolic processes (e.g. the TCA cycle, NADPH production and glutathione synthesis (Reitzer et al., 1979, Gallagher et al., 2008, DeBerardinis et al., 2007). Glutaminolysis, the metabolic pathway that converts glutamine into glutamate by the phosphate-dependent enzyme glutaminase, and subsequently into α -KG, which is integral to these functions (Tapiero et al., 2002, DeBerardinis et al., 2007). In many cancers, particularly those driven by MYC overexpression, glutaminase (GLS) is increased,

which enhances the rate of glutamine metabolism and supports the high metabolic demands of rapidly proliferating tumour cells (Gao et al., 2009). This dysregulation of glutamine metabolism makes GLS a promising therapeutic target for cancer treatment, with strategies aimed at inhibiting GLS showing potential to disrupt tumour growth and survival. For example, curcumin, a NP derived from turmeric, has been shown to enhance cisplatin sensitivity by inhibiting glutamine metabolism, through its effects on increasing microRNA (miR)-37 expression, which directly targets the 3' UTR of GLS mRNA, thereby reducing GLS activity (Fan et al., 2022). These findings suggest that curcumin, via miR-137-mediated inhibition of glutamine metabolism, could serve as an effective strategy to overcome cisplatin resistance in CRC.

Tricarboxylic Acid (TCA) Cycle

Although glycolysis is upregulated, many cancer cells maintain an active TCA cycle by utilizing alternative carbon sources, such as glutamine. The TCA cycle intermediates are diverted to anabolic processes, fueling biosynthesis and tumour growth (DeBerardinis et al., 2007). However, cancer cells may also exhibit mutations in TCA cycle enzymes (e.g. IDH), leading to the production of oncometabolites like 2-hydroxyglutarate (2-HG), which can cause epigenetic alterations and promote tumourigenesis (Losman and Kaelin, 2013). The observation that (R)-2HG alone is sufficient to induce cellular transformation, along with the finding that this transformation is reversible, strongly suggests that targeting and inhibiting the production of (R)-2HG by mutant IDH could provide a therapeutic strategy for treating IDH-mutant cancers (Losman and Kaelin, 2013, Losman et al., 2013). In support of this, recent studies have reported the development of first-generation inhibitors of mutant IDH that can reduce the levels of (R)-2HG in both *in vitro* models and *in vivo* (Popovici-Muller et al., 2012, Wang et al., 2013). These inhibitors show promise as potential therapeutic agents, as they not only block the production of (R)-2HG but also attenuate the metabolic and epigenetic changes associated with IDH mutations, offering a targeted approach for treating cancers driven by IDH mutations.

Natural products have been reported to affect TCA cycle function. Berberine, an alkaloid isolated from plants such as *Berberis*, an isoquinoline alkaloid that widely produced by multiple Chinese medicinal plants, has been shown to inhibit citrate biosynthesis and

transportation, thereby disrupting mitochondrial metabolism and the TCA cycle, as well as inducing apoptosis in pancreatic cancer cells (Liu et al., 2020a). Similarly, curcumin, the active compound in turmeric, has been shown to redirect pyruvate metabolism via the upregulation of pyruvate dehydrogenase complex (PDC), leading to increased TCA cycle function and apoptosis, as well as decreased cell survival and cell growth in TNBC cancer cells (Mittal et al., 2020).

Lipid Metabolism

Alterations in lipid metabolism are common in cancer, as lipids are essential for membrane synthesis, energy storage, and signalling. Key enzymes involved in lipid biosynthesis, such as ATP-citrate lyase (ACLY), acetyl Co-A carboxylase (ACC), fatty acid synthase (FASN), and stearoyl-CoA desaturase 1 (SCD1), are frequently more abundant in cancer cells (Nambiar et al., 2014). Increased lipid synthesis is essential for rapid cell division and tumour growth.

Several natural products have been found to target lipid metabolism in cancer cells. Silibinin, a flavonoid derived from *Silybum marianum* (milk thistle), has been shown to inhibit FASN, ACC, and disrupt the phosphorylation of ACLY, leading to a reduction in lipid biosynthesis and slowed tumour growth in prostate cancer cells (Nambiar et al., 2014). Similarly, genistein, an isoflavonoid found in soy, reduces lipid accumulation and impairs cancer cell growth by inhibiting SCD1 and FASN activity in lung and BC, respectively (Hess and Igal, 2011, Ra et al., 2007).

One-Carbon Metabolism

One-carbon metabolism is essential for maintaining nucleotide synthesis, methylation reactions, and cellular epigenetic regulation. Cancer cells exhibit increased flux through folate and methionine cycles, supporting DNA replication, epigenetic regulation and tumourigenesis. This includes increased activity of enzymes like methionine synthase and dihydrofolate reductase (*DHFR*), which are involved in folate and methionine metabolism. Inhibitors targeting this pathway, folate-derived compounds such as methotrexate exert its cell proliferation inhibitor effects by inhibiting *DHFR* and blocking folate metabolism, have been widely used in various cancer therapy (Huennekens, 1994, Drugs.com). Therefore, targeting

enzymes such as *DHFR* in cancer may be a crucial way to explore underlying cellular mechanisms and identify potential inhibitors to one-carbon metabolism, ultimately contribute to cancer therapy.

Cancer cells depend on the reprogramming of key metabolic pathways to support rapid proliferation and survival. These pathways, including glycolysis, glutaminolysis, the TCA cycle, lipid metabolism, and one-carbon metabolism, are crucial for tumourigenesis. NPs have emerged as valuable modulators of metabolic pathways or may have co-evolved to fulfil this role, offering novel therapeutic strategies for cancer treatment. Compounds such as curcumin, resveratrol, silibinin, and berberine have shown the ability to target cancer cell metabolism, disrupt metabolic reprogramming, and inhibit tumour growth. However, further research is necessary to fully elucidate the molecular mechanisms through which these natural product-derived drugs affect cancer metabolism and to translate these findings into effective clinical therapies.

Metabolomics technologies have significantly advanced medicinal chemistry and molecular science by offering detailed insights into drug mechanisms, disease biomarkers, and alterations in metabolic pathways. Cancer metabolism, marked by distinct metabolic reprogramming, presents promising targets for therapeutic intervention. Despite challenges in data analysis and standardization, the integration of metabolomics with other omics technologies holds the potential to enhance precision medicine and drug discovery.

Challenges and Future Directions

Metabolomics is emerging as an indispensable approach for studying the effects of NPs in cancer therapy. It offers a unique capability to profile small molecules and capture the dynamic changes in metabolic pathways that occur in response to NP treatment. Unlike genomics and proteomics, which primarily focus on static features like gene expression or protein abundance, metabolomics reflects the actual functional state of cells, providing real-time insights into metabolic activity. This enables the investigation of the immediate downstream effects of NPs on cancer cell metabolism, which is central to understanding how these compounds modulate cellular processes involved in tumour growth, survival, and metastasis.

Furthermore, metabolomics plays a crucial role in identifying potential biomarkers that can predict both therapeutic responses and resistance to treatment. These biomarkers are vital for the development of precision medicine in cancer therapy, as they enable clinicians to tailor treatments to the specific metabolic profiles of individual tumours. The ability to monitor how a tumour's metabolic landscape shifts in response to NP treatment opens the door for more personalized, effective therapeutic strategies.

Despite its advantages, metabolomics faces significant challenges in the study of NPs. NPs, often composed of complex mixtures of bioactive compounds, pose difficulties for analysis due to the chemical diversity and variability of their constituents. This complexity, combined with low reproducibility across different cell lines, models, and analytical platforms, creates challenges for consistent data interpretation. Variability in experimental design, such as differences in treatment protocols, sample collection methods, and analytical techniques, can further complicate the reproducibility of results. Additionally, the limited availability of comprehensive spectral libraries for NPs hampers the identification of metabolites, especially when dealing with poorly characterized or novel compounds.

To address these challenges, future research should focus on integrating metabolomics with multi-omics approaches—such as genomics, transcriptomics, and proteomics. By combining data from these various omics layers, researchers can gain a more comprehensive understanding of the molecular mechanisms through which NPs exert their effects on cancer cells. This integrated approach can provide insights into how changes in gene expression or protein levels impact metabolic pathways, and vice versa, creating a more holistic view of cancer biology.

Moreover, the application of AI and machine learning (ML) techniques has the potential to greatly enhance metabolite identification and pathway prediction. AI and ML algorithms can analyze vast amounts of metabolomics data to uncover patterns, predict metabolic alterations, and provide deeper insights into how NPs modulate cancer metabolism. These technologies

can also aid in improving the accuracy of metabolite identification and quantification, addressing one of the key limitations of current metabolomics workflows.

Another promising avenue is the application of metabolomics in precision medicine. By profiling the metabolic states of tumours before, during, and after NP treatment, it becomes possible to identify specific metabolic vulnerabilities within individual cancer types. This information can be used to design more targeted and personalized anticancer therapies. By exploiting the specific metabolic alterations in tumours, NP-derived therapies can be fine-tuned to maximize therapeutic efficacy while minimizing toxicity. In this context, metabolomics could be used not only to track the effects of NP treatments but also to predict the development of resistance and guide therapeutic decisions.

Metabolomics-guided research is especially crucial in the discovery of novel natural product-based anticancer agents. Natural products have historically provided a rich source of bioactive compounds with therapeutic potential, yet the mechanisms through which these compounds exert their anticancer effects are often poorly understood. Metabolomics can illuminate the metabolic pathways modulated by these compounds, revealing how they disrupt cancer cell metabolism and identifying potential targets for future drug development. In addition, metabolomics can uncover metabolic shifts that contribute to resistance mechanisms, thereby informing strategies to overcome such resistance.

In summary, metabolomics is uniquely positioned to transform the study of natural products in cancer research by providing detailed insights into their molecular mechanisms of action and their impact on cancer metabolism. By identifying novel therapeutic targets, uncovering biomarkers for predicting responses, and accelerating the development of effective anticancer agents, metabolomics holds great promise for enhancing cancer treatment. Moreover, the integration of metabolomics with genomics, transcriptomics, proteomics, and computational tools like AI and ML will further enhance our ability to discover and develop personalized cancer therapies. With these advancements, metabolomics is poised to play a central role in the development of precision medicine strategies, guiding the effective use of natural product-derived drugs in clinical oncology.

1.5 Research Objectives

Malaysia is one of the most biodiverse regions in the world, hosting multiple *Eumachia* species in Peninsular Malaysia, including *Eumachia rostrata* and *Eumachia montana*, both of which are listed on Malaysia's Plant Red List (mybis, mybis). Traditionally, *Eumachia* species have been used in Malay society to treat constipation (*Eumachia rostrata* and *Eumachia montana*) and sores (*Eumachia montana*) (1989, Ong et al., 2012). *E. rostrata* has been phytochemically investigated for its alkaloidal composition, leading to the isolation of polyindole alkaloids with demonstrated cytotoxic activity (Lajis et al., 1993, Roth et al., 1986). However, a comprehensive literature search using Web of Science and Reaxys revealed that *E. montana* has not been previously studied for its phytochemical or biological properties. Given the limited discoveries to date, the ongoing expansion of this genus suggests that further research may reveal additional *Eumachia* species within the Malaysian flora. This has led to the search of alkaloid containing *Eumachia* species in Malaysia that was not previously investigated. This will provide tremendous potential for the discovery of alkaloids with useful pharmacological properties. Therefore, this study aims to investigate the alkaloid composition of *Eumachia montana* leaves collected in Malaysia and subsequently evaluate the cytotoxicity of the isolated pure alkaloids.

The specific objectives of this project are as below:

1. To extract and isolate pure alkaloids from the dried leaf material of *Eumachia montana*;
2. To spectroscopically characterize the structures of the pure alkaloids isolated;
3. To determine *in vitro* cytotoxic properties of pure alkaloids obtained by conducting preliminary screening assays on 8 different human-derived cell lines (MCF-7, MDA-MB-468 (breast), HCT-116, HT-29 (colon), U373 (GBM, vector control), U373M (GBM, MGMT-transfected), A549 (non-small cell lung cancer) and non-transformed lung fibroblasts MRC-5);
4. To investigate the cellular mechanism of action of selected alkaloids with promising cytotoxic properties via bioassays such as cell cycle, apoptosis, microscopy, and metabolomics.

This project was a collaboration between the Malaysia and UK campuses of the University of Nottingham. Experimental work for points 1 and 2 was conducted in Malaysia, while points 3

and 4 were undertaken in the UK. Compound isolation and preliminary characterisation were carried out in Malaysia; however, the quantities obtained were insufficient for subsequent bioassays in the UK. During this period, additional isolations were performed by my co-supervisor, Prem, at the Malaysia campus. All isolation and structure elucidation techniques were conducted in Malaysia, except for low-temperature NMR and full MS scans, which were performed in the UK due to limited availability of these facilities in Malaysia. On the basis of these data, the chemical structures of compounds **2–4** were subsequently elucidated and confirmed while I was based at the UK campus.

Chapter 2 Isolation, Characterization of alkaloids from *Eumachia montana*

2.1 Introduction

The isolation and characterization of alkaloids from plant sources have long been fundamental to the fields of pharmacognosy, drug discovery, and natural product research. Alkaloids, a diverse group of nitrogen-containing organic compounds, are produced by various plant species as secondary metabolites and have historically been a rich source of therapeutic agents (Newman and Cragg, 2020). Their structural diversity and bioactivity have made them the focus of extensive studies, with numerous alkaloids having been developed into clinically used drugs. From the early discovery of morphine to the more recent identification of anticancer agents such as vincristine and vinblastine, alkaloids have played a significant role in modern medicine (Dewick, 2009a, Funayama and Cordell, 2014). The pharmacological properties of alkaloids, including analgesic, antimicrobial, anticancer, and antiinflammatory effects, have made them indispensable in the development of novel therapeutic agents (Amador et al., 2000, Elisabetsky et al., 1995, Schallenberger et al., 2010, Saad et al., 1995, Nascimento et al., 2015, Roth et al., 1986, Frisvad et al., 2004).

In recent decades, the exploration of alkaloids as drug leads has gained renewed interest, particularly with advances in chemical analysis and biotechnology, which have enabled more efficient isolation and structural elucidation of these complex molecules. The intricate structures of alkaloids, particularly those derived from plants, have spurred the development of advanced techniques such as high-performance liquid chromatography (HPLC), MS, and NMR spectroscopy for their isolation and characterization. These techniques allow for the identification of not only the parent alkaloid but also its derivatives and potential modifications that may enhance pharmacological activity or reduce toxicity.

The Genus *Eumachia*

Recent taxonomic revisions have expanded the genus *Eumachia* (E.) (tribe Palicoureeae, family Rubiaceae) to include species formerly classified under *Psychotria*, refining its classification and species diversity (Turner, 2019). For example, *Psychotria montana* and *Psychotria rostrata* were reassigned to *Eumachia* based on morphological and genetic evidence (Turner, 2019). *Eumachia* is now recognized as a pantropical genus with over 83 species distributed across the Neotropics, Africa, Asia, and the Pacific (Taylor et al., 2017, Berger et al., 2022). *Psychotria* was previously considered a large, cosmopolitan genus; however, phylogenetic analyses revealed its polyphyletic nature, leading to the reclassification of distinct lineages into separate genera. These taxonomic refinements also impact the classification of related genera within the tribes Palicoureeae and Psychotrieae, such as *Palicourea*, *Notopleura*, *Carapicha*, *Geophila*, and *Rudgea*, which have been the focus of recent phylogenetic and morphological studies (Berger et al., 2022, Taylor et al., 2017).

Both *Eumachia* and *Psychotria* share typical Rubiaceae traits, such as simple, opposite leaves and small tubular flowers. While *Psychotria* species are mostly understory trees or shrubs, *Eumachia* species also display similar morphological traits, particularly in stipules and fruit morphology (Taylor et al., 2017). Numerous species of *Psychotria* and its relatives have been used in traditional medicine, treating ailments such as bronchitis, gastrointestinal disorders, and reproductive diseases. *Psychotria viridis* and *Psychotria carthagenensis* are key ingredients in the preparation of ayahuasca, a psychoactive beverage used in South American shamanic practices (McKenna et al., 1984). Other species, such as *Psychotria emetica*, are used to treat chickenpox and fever (Gupta et al., 2005), while *Palicourea colorata* is utilized as an analgesic for earaches and abdominal pain (Elisabetsky et al., 1995).

Both *Eumachia* and *Psychotria* are well known for their rich alkaloid content, with secondary metabolites exhibiting significant pharmacological properties. Both genera predominantly produce oligocyclotryptamine alkaloids (also termed cyclotryptamine or pyrrolidinoindoline alkaloids), a subclass of indole alkaloids, with closely related structures also reported in its relative genus *Palicourea* (Verotta et al., 1998, Zhou et al., 2010, Jamison et al., 2017). These structurally complex alkaloids are likely bioactive, though further investigation is required to

fully elucidate their pharmacological potential (Rivier and Lindgren, 1972, de Carvalho et al., 2016, Taylor et al., 2017).

Bioactivity of Oligocyclotryptamine Alkaloids from *Eumachia*

Oligocyclotryptamine alkaloids are structurally complex secondary metabolites found abundantly in *Eumachia* species. To date, nine *Eumachia* species, primarily distributed across Asia, Australasia, and the Pacific, have been studied, with eight yielding oligocyclotryptamine alkaloids. These alkaloids, derived from tryptamine precursors, form dimeric and oligomeric structures, such as (+)-chimonanthine, (–)-calycanthine, hodgkinsine, psychotridine, and quadrigemines A–C (Adjibade et al., 1992, Lajis et al., 1993, Roth et al., 1986, Libot et al., 1987). Their biosynthesis involves the formation of a core cis-pyrrolidino[2,3-b]indoline scaffold, commonly featuring a dimeric 3a-3a'-bispyrrolidino[2,3-b]indoline structure (Steven and Overman, 2007). Higher-order oligomers in this class are primarily formed through the attachment of additional 3aR-cis-pyrrolidino[2,3-b]indoline units at the benzylic carbon (position-3a) to the aromatic carbon (position-7) of the preceding structure. Meso-chimonanthine often serves as the core structure for these alkaloids (**Figure 2.1**). Based on this core, oligocyclotryptamine alkaloids can be further categorized into the [n+1] and [n+2] series, with representative alkaloids illustrated in **Figure 2.1** (Jannic et al., 1999, Scott and Movassaghi, 2024).

These alkaloids exhibit a diverse range of pharmacological properties, including anticancer, analgesic, antimicrobial, and antithrombotic activities (Roth et al., 1986, Nascimento et al., 2015, Saad et al., 1995, Adjibadé et al., 1990, Amador et al., 2001, Elisabetsky et al., 1995, Amador et al., 2000, Schallenberger et al., 2010, Shi et al., 2012, Su et al., 2016). Notably, quadrigemine H, quadrigemine C, psychotridine, and isopsychotridine C (isolated from *Eumachia forsteriana*) have demonstrated cytotoxicity surpassing that of vincristine in rat hepatoma cells (Roth et al., 1986). In addition, oligocyclotryptamine alkaloids isolated from *Psychotria colorata* display opioid-like analgesic properties, with compounds such as hodgkinsine, psychotridine, and quadrigemine C playing key roles (Verotta et al., 1998, Amador et al., 2001, Elisabetsky et al., 1995, Amador et al., 2000, Verotta et al., 2002). Other notable biological activities include antimicrobial effects of psychotrimine from *Eumachia*

rostrata and antithrombotic properties of Psm2 from *Selaginella moellendorffii* (Schallenberger et al., 2010, Su et al., 2016). The significance of these alkaloids in drug discovery is further underscored by their ability to modulate critical biological pathways. They have been shown to interact with serotonin and N-methyl-D-aspartate (NMDA) receptors, as well as key signaling cascades such as PI3K/AKT, which are implicated in cancer progression and neurological disorders (Elisabetsky et al., 1995, Amador et al., 2001, Su et al., 2016).

In Malaysia, *Eumachia* species remain relatively unexplored. However, research on *Eumachia rostrata* has identified several bioactive oligocyclotryptamine alkaloids, including (–)-calycanthine, (+)-chimonanthine, and quadrigemine B, all of which exhibit cytotoxic properties (Lajis et al., 1993, Roth et al., 1986). More recently, psychotrimine and psychopentamine were isolated from *E. rostrata* leaves (Takayama et al., 2004). In contrast, *Psychotria* species have been extensively studied in Malaysia, with *Psychotria calocarpa* and *Psychotria malayana* among those characterized for their alkaloid content. For instance, *Psychotria malayana* contains alkaloids such as hodgkinsine and calycanthine (Hadi et al., 2014), while *Psychotria calocarpa* yields diverse oligocyclotryptamine alkaloids, including psychotridine and quadrigemines (Verotta et al., 1998, Zhou et al., 2010).

Advancements in Structural Characterization and Synthesis

Historically, the structural and stereochemical characterization of higher-order oligocyclotryptamine alkaloids has been challenging due to atropisomerism, which causes signal broadening in NMR spectra. However, mass spectrometry has played a crucial role in elucidating these structures, as characteristic fragmentation of the C3a-C3a' σ bond provides valuable insights into connectivity within each oligomer (Jannic et al., 1999, Guéritte-Voegelein et al., 1992).

Recent advancements in chemical synthesis have further contributed to overcoming longstanding challenges in the stereocontrolled assembly of cyclotryptamine monomers. These innovations have enabled the structural determination and validation of several complex oligocyclotryptamine alkaloids, including (–)-hodgkinsine, (+)-quadrigemine H, (+)-

isopsychotridine, (+)-oleoidine, (+)-caledonine, (-)-hodgkinsine B, (-)-quadrigemine C, and (-)-psychotidine (**Figure 2.1**) (Steven and Overman, 2007, Scott and Movassaghi, 2024).

Exploring *Eumachia montana* as a Source of Novel Alkaloids

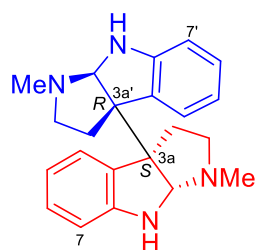
The growing understanding of alkaloid biosynthesis, chemical diversity, and mechanisms of action, particularly of oligocyclotryptamine alkaloids, highlights the continued significance of natural products in modern drug discovery. Their capacity to serve as leads for the development of novel therapeutics, alongside advancements in synthetic biology and combinatorial chemistry, facilitates the discovery of next-generation drugs with the potential to address unmet medical needs (Bülbül et al., 2025). Despite the increasing focus on synthetic compounds, the exploration of plant-derived alkaloids remains essential for identifying new bioactive compounds, promoting the sustainable use of natural resources, and maintaining the relevance of natural products in contemporary medicinal chemistry (Newman and Cragg, 2020).

While the genus *Eumachia* has been recognized for its production of bioactive alkaloids, individual species within this genus remain largely unexplored. *Eumachia montana* has not been previously investigated for its phytochemical or biological properties, as determined by a search in Web of Science and Reaxys. However, its traditional medicinal uses suggest significant pharmacological potential. Historically, the roots of *E. montana* have been applied externally for treating ulcers and swellings, while decoctions have been consumed for the treatment of constipation (Ong et al., 2012, Mahmud, 1989). Given its unexplored chemical profile and the promising bioactivity observed in related species, such as *Eumachia rostrata*, further phytochemical investigation of *E. montana* may yield novel alkaloids with significant therapeutic potential.

This gap in research has motivated the search for alkaloid-containing *Eumachia* species in Malaysia that have not yet been investigated. Identifying bioactive alkaloids from this species offers tremendous potential for the discovery of compounds with valuable pharmacological properties. Therefore, this study aims to investigate the alkaloid composition of *E. montana* leaves collected in Malaysia and subsequently evaluate the cytotoxicity of the isolated pure alkaloids. Our initial interest in *E. montana* was driven by the detection of potent cytotoxic

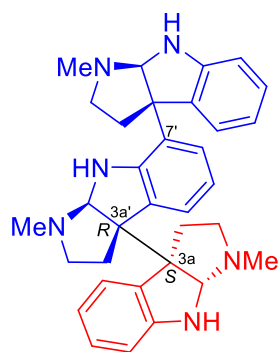
activity in its leaf alkaloid extract against a panel of cancer cell lines. Subsequent preliminary screening assays, including MTT, cell count, and clonogenic assays, demonstrated the potent cytotoxic effects of isolated oligocyclotryptamine alkaloids against eight human-derived cell lines, encompassing BC (MCF-7, MDA-MB-468), CRC (HCT-116, HT-29), glioblastoma (U373 vector control, U373M MGMT-transfected), and non-small cell lung cancer (A549), as well as non-transformed lung fibroblasts (MRC-5).

By addressing the existing knowledge gap regarding *E. montana*, this study not only aims to identify novel bioactive alkaloids but also contributes to the broader field of natural product and oncology research. The findings may support the development of potential therapeutic candidates for cancer treatment or provide insights into the cellular mechanisms underlying the cytotoxic effects of *E. montana*-derived alkaloids.

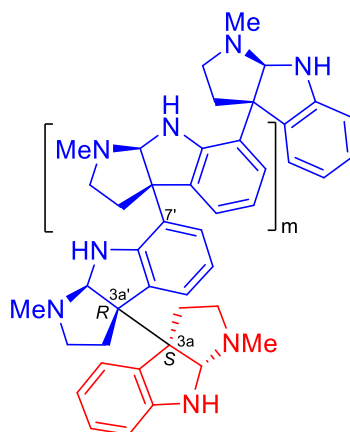


meso-chimonanthine

[n+1] series

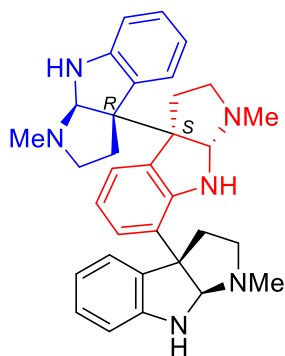


(-)-hodgkinsine
(*n* = 2)

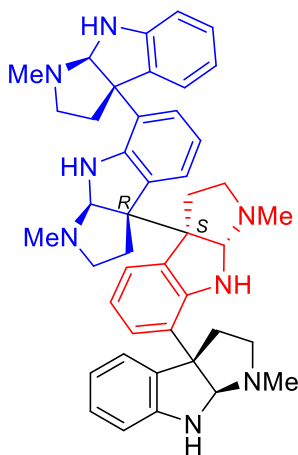


m = 1, (+)-quadrigemine H (*n* = 3)
m = 2, (+)-isopsychotridine (*n* = 4)
m = 3, (+)-oleoidine (*n* = 5)
m = 4, (+)-caledonine (*n* = 6)

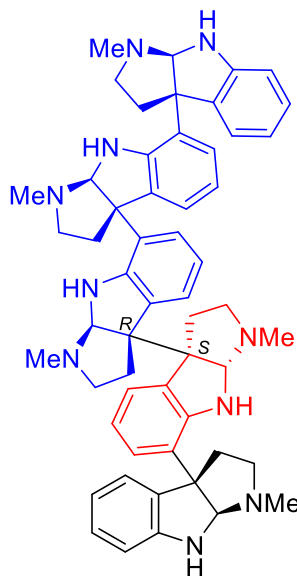
[n+2] series



(-)-hodgkinsine B
(*n* = 1)



(-)-quadrigemine C
(*n* = 2)



(-)-psychotridine
(*n* = 3)

Figure2. 1 Representative [n+1] and [n+2] series of oligocyclotryptamine alkaloids

2.2 Results and Discussion

The dried leaves (980g) of *Eumachia montana* (sample code: UNMC110) were exhaustively extracted using ethanol and the crude ethanolic extract subjected to acid-based extraction to eventually yield approximately 15.2g of crude alkaloidal mixture. A preliminary column chromatography of the crude alkaloidal mixture furnished nine combined fractions, namely, PML-A to PML-I (Table 2.1).

Table 2. 1 Main combined fractions of the leaf crude alkaloid of *Eumachia montana*

Fraction	Weight
PML-A	69.2 mg
PML-B	70.2 mg
PML-C	364.8 mg
PML-D	4.4285 g
PML-E	4.9569 g
PML-F	481.3 mg
PML-G	1.095 g
PML-H	199.2 mg
PML-I	1.031 g

Five pure alkaloids have been successfully isolated and purified, namely the dimeric (–)-calycanthine (**1**), the hexameric (+)-oleoidine (**2**), the heptameric (+)-caledonine (**3**), the octameric (+)-eumatanine (**4**), and a tricyclic pyrroloquinoline alkaloid, eumatricine (**5**). Of these, compounds **4** and **5** are newly described. Eumatanine (**4**) was determined as a new octameric cyclotryptamine alkaloid, while eumatricine (**5**) was elucidated as a new quinoline alkaloid. The detailed structure elucidation of the pure alkaloids isolated are described in the following subsections.

2.2.1(–)- Calycanthine (**1**)

Compound **1** was obtained as light yellowish crystals from fraction PML-C-F34. Since suitable crystals of compound **1** were obtained, an X-ray diffraction analysis was carried out. The X-ray structure of **1** revealed it as calycanthine, along with the results of optical rotation measurement ($[\alpha]_D +106$ (c 0.43, EtOH)), it is identified as (–)-calycanthine, which is in

agreement with the molecular formula based on the high-resolution electrospray ionization mass spectrometry (HRESIMS) data (m/z : 347.2250 $[M+H]^+$, $C_{22}H_{26}N_4+H$) (**Figure 2.2**). The 1H NMR spectrum of calycanthine (**1**) is shown in **Table 2.2**, which shows the comparison of (-)-calycanthine (**1**) and those (-)-calycanthine obtained from the literature (Adjibade et al., 1992). Both data are in good agreement, thus confirming the identification.

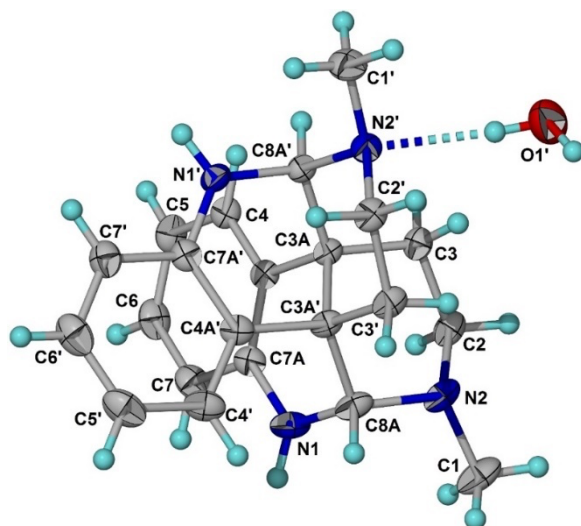


Figure2. 2 X-ray crystal structure of (-)-calycanthine (**1**)

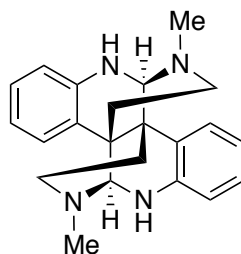


Figure2. 3 Chemical structure of (-)-calycanthine (**1**)

Table 2. 2 Comparison of NMR Spectroscopic Data of (-)-calycanthine (1)^a and (-)-calycanthine^b (Adjibade et al., 1992).

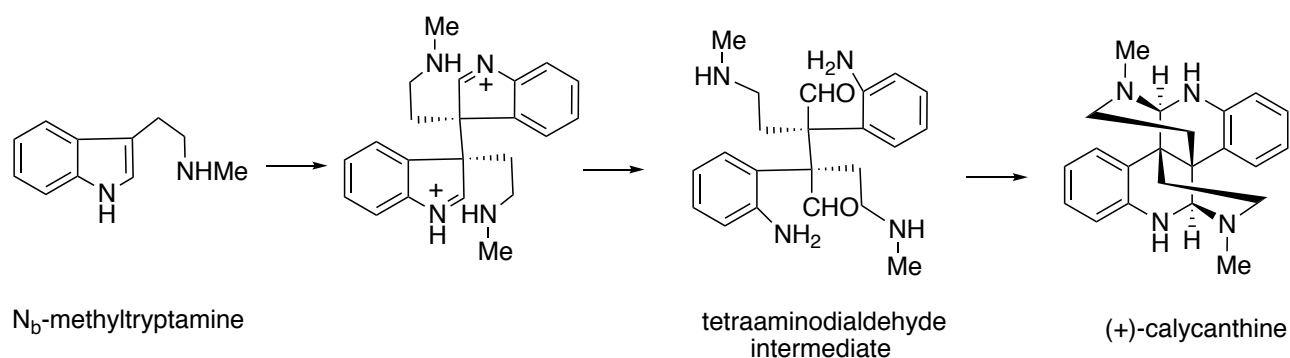
Position	(-)-calycanthine (1) ^a	(-)-calycanthine ^b
	δ_H (ppm, <i>J</i> in Hz)	δ_H (ppm, <i>J</i> in Hz)
N-Me	2.40, s, 6H	2.41, s, 6H
8a	4.30, s, 2H	4.31, s, 2H
Aromatic protons	6.26, dd (8.0, 1.2); 2H	6.25 to 7.03; dd, td, td, dd (1,7.5); 8H
	6.53, td (7.5, 1.2 Hz); 1H	
	6.81, td (7.6); 2H	
	7.00, dd (7.8, 1.5); 2H	

^aMeasured in CDCl₃, ¹H 600 MHz

^bMeasured in CDCl₃, ¹H 200 MHz

The crystalline alkaloid, calycanthine, was first isolated from the seeds of *Calycanthus glaucus*, and the ensuing studies indicated that calycanthine occurs mainly in plants from the families Calycanthaceae and Rubiaceae. The isolation of (+)-calycanthine was previously reported from the seeds and rinds of *Chimonanthus praecox*, while the optical antipode (-)-calycanthine was isolated from *Eumachia forsteriana*, *Eumachia rostrata* and *Palicourea colorata* (Kitajima et al., 2006, Adjibade et al., 1992, Verotta et al., 1998, Lajis et al., 1993). Several studies have been carried out on calycanthine regarding its biological activity. For example, calycanthine was found to show anti-convulsant, antifungal, and melanogenesis inhibitory activities (Chebib et al., 2003, Zhang et al., 2009a, Morikawa et al., 2014).

It was proposed that calycanthine is originated from N₆-methyltryptamine, which could form the key tetraaminodialdehyde intermediate via oxidative dimerisation. The tetraaminodialdehyde undergoes multiple enzyme-catalysed reactions and modifications to eventually yield calycanthine (Kitajima et al., 2006).



Scheme 2. 1 The biosynthetic pathway of calycanthine.

2.2.2 Inseparable oligocyclotryptamine alkaloids from *Eumachia montana*

Besides the main fraction of PML-C (70mg) that yielded the pure compound, (-)-calycanthine (**1**), another main fraction PML-D (4.43g) yielded several fractions that appeared to be a single spot based on their TLC profiles, namely, fractions PML-4 to PML-11. These fractions were further inspected with ¹H NMR experiment. However, their ¹H NMR spectra showed broadened/unresolved signals (**Figure 2.4**). Initially, the signal broadening issue was attributed to the presence of mixture of compounds (with similar *R_f* values in the TLC) in the samples sent for ¹H NMR measurements. Sample degradation was also thought of as a possible reason for the observed signal broadening. However, the possibility of sample degradation being the issue was eventually ruled out since the broadened signals persisted in the ¹H NMR spectra of PML-4 and PML-5 despite passing these samples through a patch of silica gel (silica 60, Merck 9385, 230-400mesh), which would normally remove contaminants that might be responsible for the signal broadening issue.

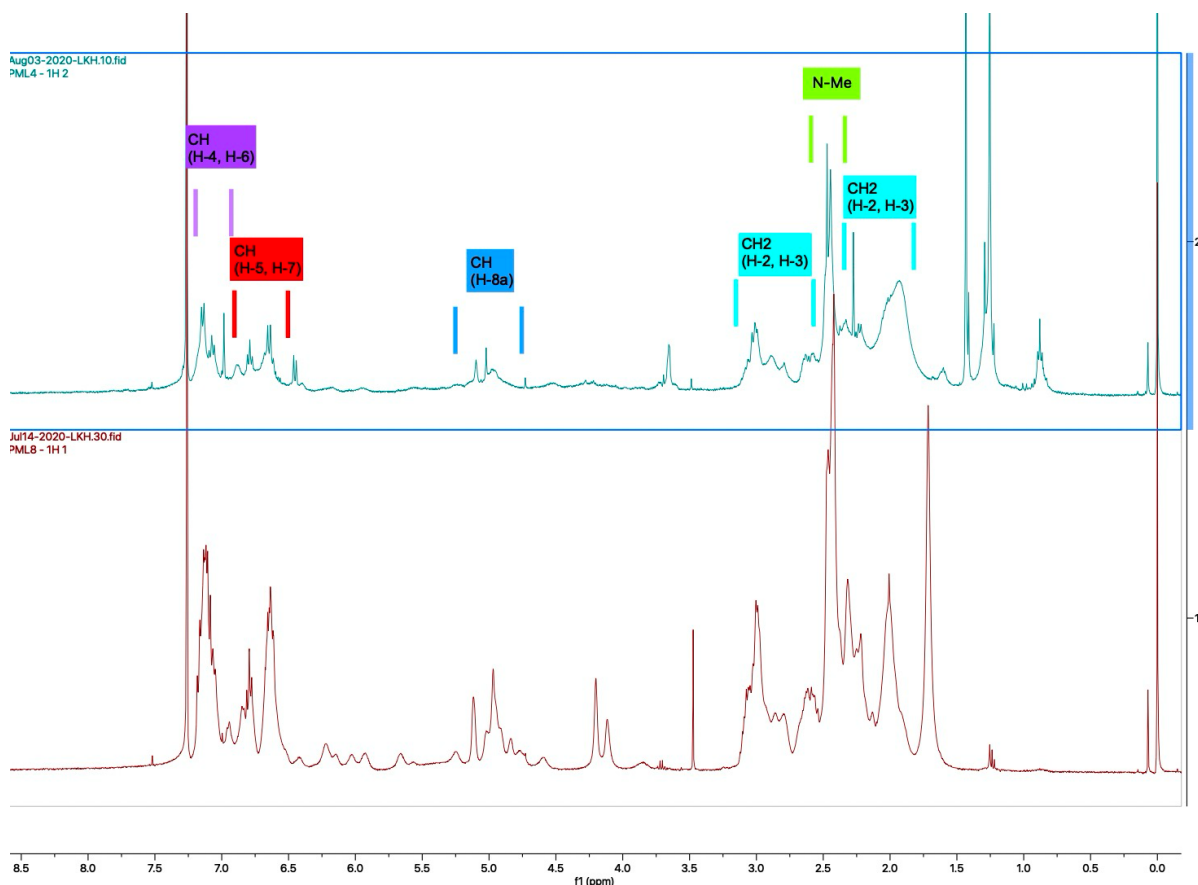


Figure 2. 4 Representative ^1H NMR spectra with broaden signals. The above shows the ^1H NMR spectra of PML-4 (top) and PML-8 (bottom) (measured in CDCl_3 600MHz); both PML-4 and PML-8 are composed of compounds 2-4.

Additionally, the situation became more complicated when most of these fractions with broadened ^1H NMR signals showed similar or identical R_f values on TLC (**Figure 2.5**). To further investigate the purity of each fraction obtained, the fractions were subjected to HPLC analysis. Based on the HPLC analysis, it was immediately apparent that there were 3 major compounds present in different compositions in the fractions that were submitted for ^1H NMR measurements. The HPLC chromatograms of selected fractions are presented in **Figure 2.6**, showing each fraction to compose of three major compound peaks (labelled as **2**, **3**, **4**) corresponding to the approximate retention times (R_t) of 7.5min, 14.5min, and 18min, respectively. Based on these retention times, the following pure fractions were separated and collected via semi-preparative HPLC (**Figure 2.6**).

When the TLC profiles of compound **2**, **3** and **4** (possessing different retention times in HPLC) were compared on the same plate, three spots with virtually identical R_f values were observed. This confirmed the earlier observation that these compounds could not be resolved on TLC

(**Figure 2.7**). To further confirm the purity of these fractions, compounds **2-4** were re-analysed using analytical and chiral HPLC, which showed **2-4** to be pure compounds and exist as single enantiomers. It was therefore established that the signal broadening issue was not due to the presence of a mixture of inseparable compounds in the NMR samples.

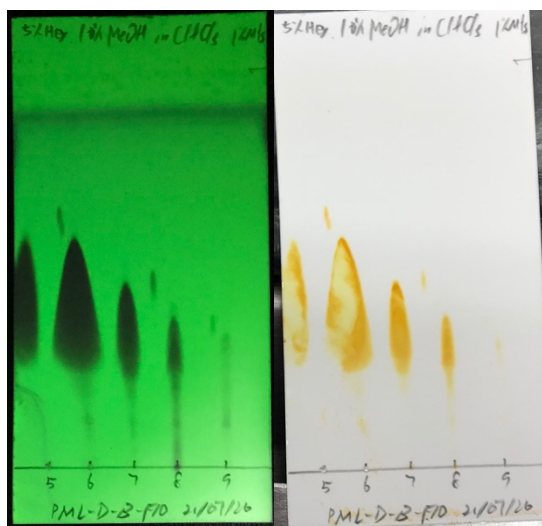


Figure 2.5 A representative TLC profile of fractions from PML-D-B-F10 (mobile phase: 10% MeOH, 5% hexane in CHCl_3 , with 1% NH_3 ; visualizing method: UV light (left) and Dragendorff's reagent (right).)

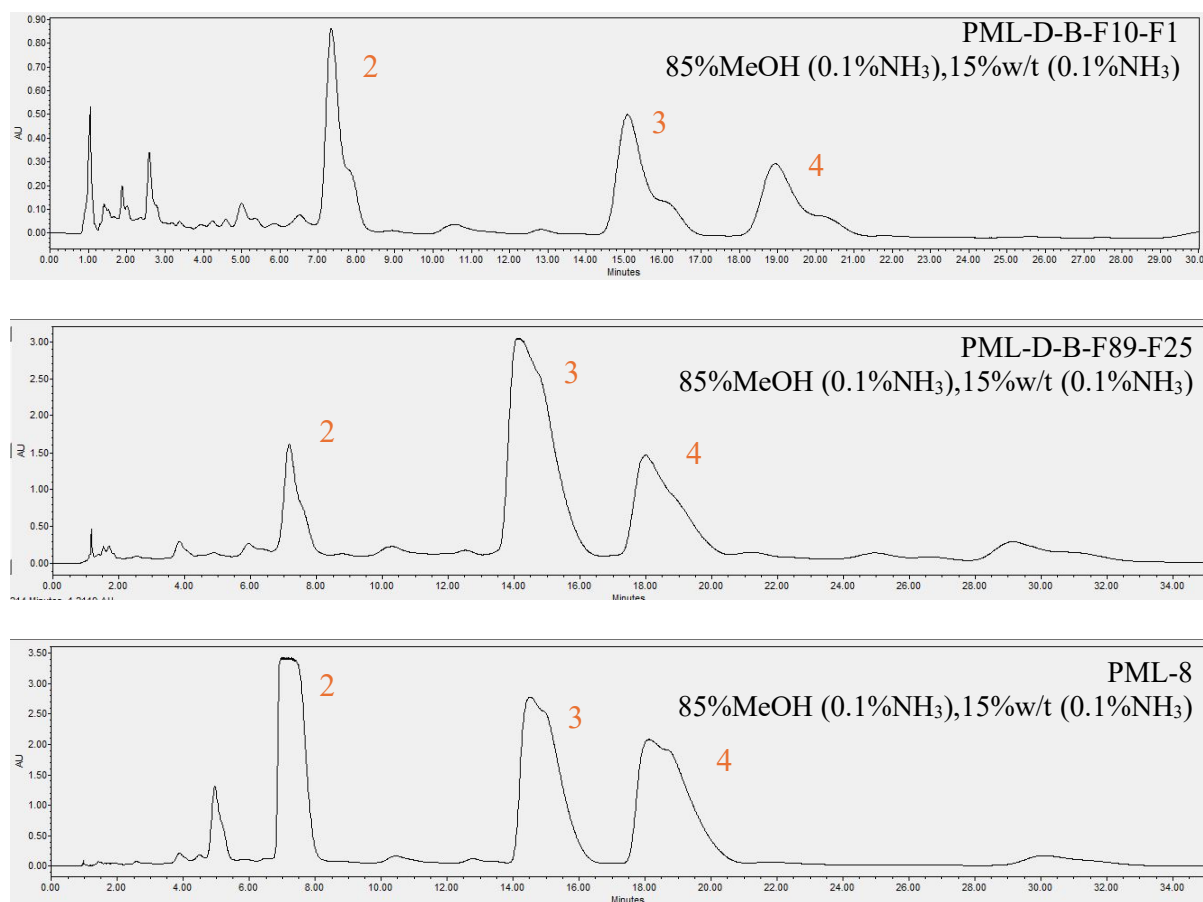


Figure 2.6 Representative HPLC chromatograms of fractions PML-D-B and PML-8

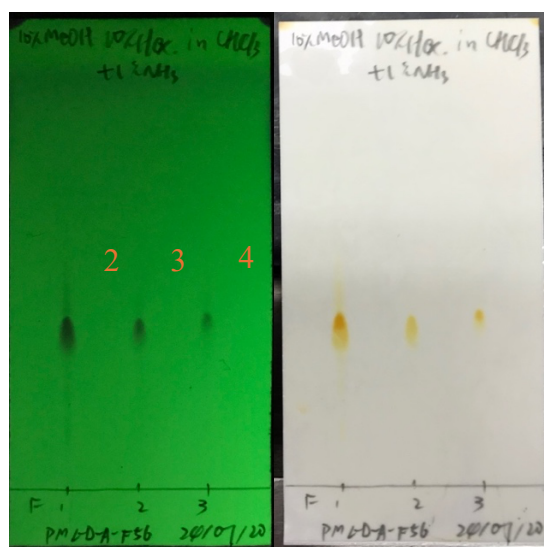


Figure 2. 7 TLC profile of compounds 2-4 (mobile phase: 10% MeOH, 10% Hexane in CHCl_3 , with 1% NH_3 ; visualizing method: UV light (left) and Dragendorff's reagent (right))

(+)-Oleoidine (2) and (+)-Caledonine (3)

(+)-Oleoidine (2) and (+)-caledonine (3) were both obtained as light yellowish powder from the main fraction PML-D using semi-preparative HPLC following successively column chromatography and centrifugal thin-layer chromatography (CTLC). To improve NMR signal resolution, the solvent used was changed from CDCl_3 to CD_3OD , while the temperature was raised from 25°C to 55°C when the ^1H NMR spectrum of 3 was measured. Surprisingly, the overall resolution of the signals in CD_3OD at 55°C improved tremendously, although majority of the signals remained unresolved (**Figure 2.9**).

Deuterated chloroform (CDCl_3) is widely regarded as the standard NMR solvent for small organic molecules, as its low polarity makes it suitable for hydrophobic and moderately polar compounds, while its volatility allows easy removal after analysis. In addition, it produces sharp, well-resolved spectra, with simple residual peaks (δ 7.26ppm in ^1H and δ 77.0ppm in ^{13}C). However, CDCl_3 has limited ability to dissolve more polar compounds, is prone to decomposition under light and oxygen, and requires stabilisation, which may interfere with sensitive samples.

In contrast, CD_3OD , owing to its higher polarity, provided superior solubility and spectral quality for highly polar compounds. Notably, through trial and error, it was found that the

overall spectral resolution of cyclotryptamine alkaloids was better in CD₃OD than in CDCl₃. CD₃OD exhibits characteristic residual solvent peaks at δ 3.31ppm in ¹H and δ 49.0ppm in ¹³C, along with a variable broad signal around δ 4.8ppm arising from HOD formed by exchange with residual water.

Improvement of signal resolution by variable temperature NMR is usually associated with the presence of a rotameric effect in a molecule. The rotameric effect is due to restricted rotation about one or more single bonds within the molecule, which gives rise to the presence of several conformations at room temperature. This supposition was supported by similar observations reported for quadrigemine C and hodgkinsine, which represent a tetrameric and a trimeric pyrrolidinoindoline alkaloid, respectively, and previously isolated from *Eumachia oleoides* (Guéritte-Voegelein et al., 1992). The ¹H NMR spectra of both the compounds were unresolved at room temperature. However, at 241K (-32°C), two sets of distinctive ¹H NMR signals corresponding to two conformers were clearly observed for both the compounds. Therefore, the issue of unresolved ¹H NMR signals encountered at the beginning of this project was primarily due to the presence of rotamers.

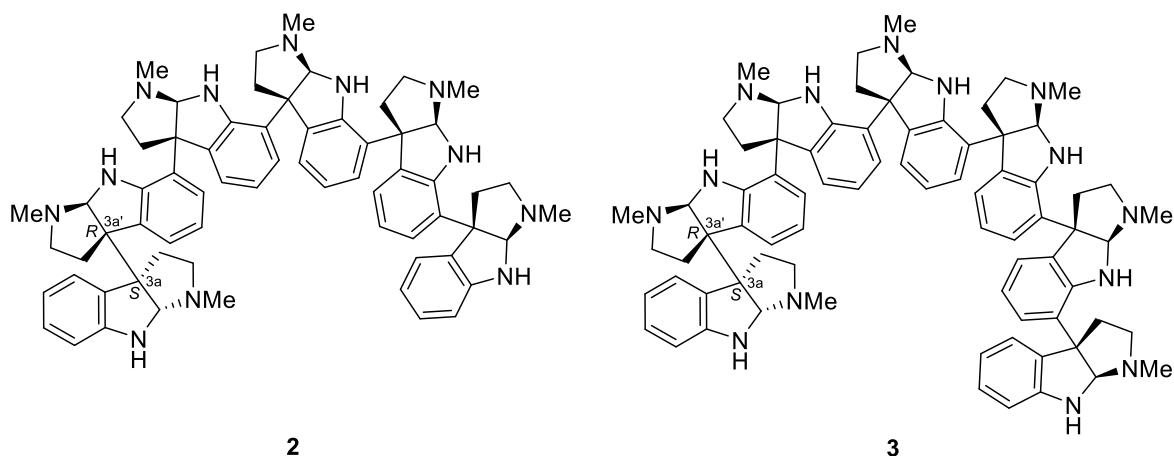


Figure 2.8 Chemical structures of (+)-oleoidine (**2**) and (+)-caledonine (**3**)

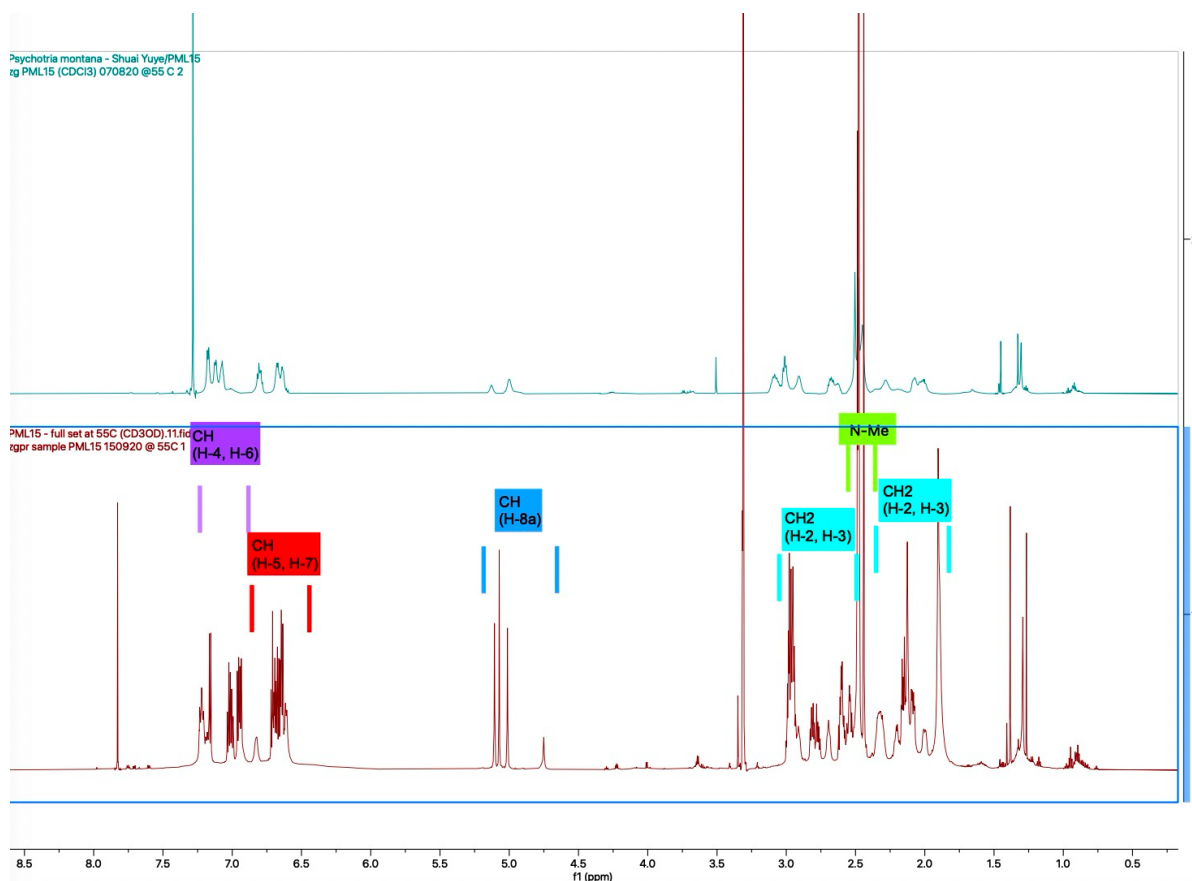


Figure 2.9 ^1H NMR spectra of compound (**3**) (600 MHz); measured in CHCl_3 at 55°C (top) and CD_3OH at 55°C (bottom)

Unfortunately, the 1D and 2D NMR spectra obtained for compounds **2** and **3** were still unsatisfactory, complex and unresolved even at low temperatures (-30°C). However, high-resolution electrospray ionization mass spectrometry (HRESIMS) data indicated that **2** and **3** are hexameric and heptameric cyclotryptamine alkaloids, with the molecular weight of ~ 1035 (m/z : 1035.6217 $[\text{M}+\text{H}]^+$) and ~ 1207 (m/z : 1207.7219 $[\text{M}+\text{H}]^+$), respectively. Additionally, HRESIMS data for compound **2** exhibited a $[\text{M} + \text{H}]^+$ peak at m/z 1035.6217 ($\text{C}_{66}\text{H}_{74}\text{N}_{12} + \text{H}^+$), accompanied by $[\text{M} + 2\text{H}]^{2+}$ and $[\text{M} + 3\text{H}]^{3+}$ peaks at m/z 518.3155 ($\text{C}_{66}\text{H}_{74}\text{N}_{12} + 2\text{H}^+$) and 345.8791 ($\text{C}_{66}\text{H}_{74}\text{N}_{12} + 3\text{H}^+$), respectively. Similarly, compound **3** displayed a $[\text{M} + \text{H}]^+$ peak at m/z 1207.7219 ($\text{C}_{77}\text{H}_{86}\text{N}_{14} + \text{H}^+$), with corresponding $[\text{M} + 2\text{H}]^{2+}$ and $[\text{M} + 3\text{H}]^{3+}$ peaks at m/z 604.3649 ($\text{C}_{77}\text{H}_{86}\text{N}_{14} + 2\text{H}^+$) and 403.2457 ($\text{C}_{77}\text{H}_{86}\text{N}_{14} + 3\text{H}^+$). Furthermore, the $[\text{MH} - 172]^+$ peaks observed in the mass spectra of both compounds indicated fragmentation patterns characteristic of the $[\text{n}+1]$ series of pyrrolidino[2,3-*b*]indoline alkaloids, suggesting their structures to be those of oleoidine and caledonine (Jannic et al., 1999, Guéritte-Voegelein et al., 1992). This suggestion was supported by the fact that the electronic

circular dichroism (ECD) curves of both compounds matched those reported for (–)-hodgkinsine, (+)-oleoidine, and (+)-caledonine (**Figure 2.10**). Additionally, the specific optical rotation data, as well as the ^1H and ^{13}C NMR spectra, of compounds **2** ($[\alpha]_{\text{D}} +106$ (c 0.43, EtOH)) and **3** ($[\alpha]_{\text{D}} +139$ (c 0.80, EtOH)) were broadly consistent with those reported for oleoidine ($[\alpha]_{\text{D}} +371^\circ$ (c 0.2, EtOH)) and caledonine ($[\alpha]_{\text{D}} +462^\circ$ (c 0.2, EtOH)) respectively (Jannic et al., 1999, Scott and Movassaghi, 2024).

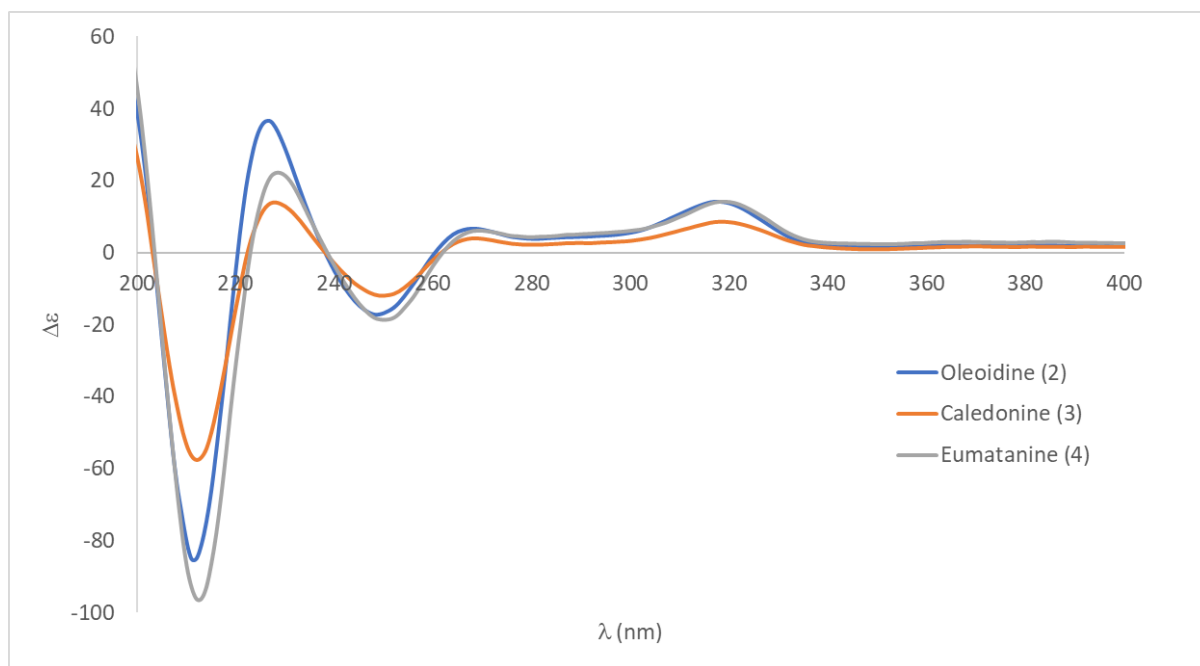


Figure 2.10 ECD spectra of Oleoidine (**2**), Caledonine (**3**), and Eumatanine (**4**)

Eumatanine (4)

Eumatanine (**4**) was isolated as a colourless oil, $[\alpha]_{\text{D}} +122$ (c 0.33, EtOH). The NMR spectra of eumatanine (**4**) were also unresolved, even at low temperatures, and showed a general resemblance to those of compounds **2** and **3** (**Figure 2.12-2.15**). However, its HRESIMS data provided crucial insights into its structure. The mass spectrum exhibited a $[\text{M} + \text{H}]^+$ peak at m/z 1379.8215 ($\text{C}_{88}\text{H}_{98}\text{N}_{16} + \text{H}^+$), indicative of an octameric cyclotryptamine alkaloid, along with multiple charged ion peaks at m/z 690.9153 ($[\text{M} + 2\text{H}]^{2+}$), 460.6125 ($[\text{M} + 3\text{H}]^{3+}$), and 345.7102 ($[\text{M} + 4\text{H}]^{4+}$) (**Figure 2.16**). Furthermore, fragment ion peaks at m/z 1207.7217 ($[\text{MH} - 172]^+$) and 604.3643 ($[\text{M} + 2\text{H} - 172]^+$) indicated that the terminal cyclotryptamine unit is connected to seven other units via a C3a-C3a' σ bond, concluding that **4** has a [7+1] arrangement of cyclotryptamine units.

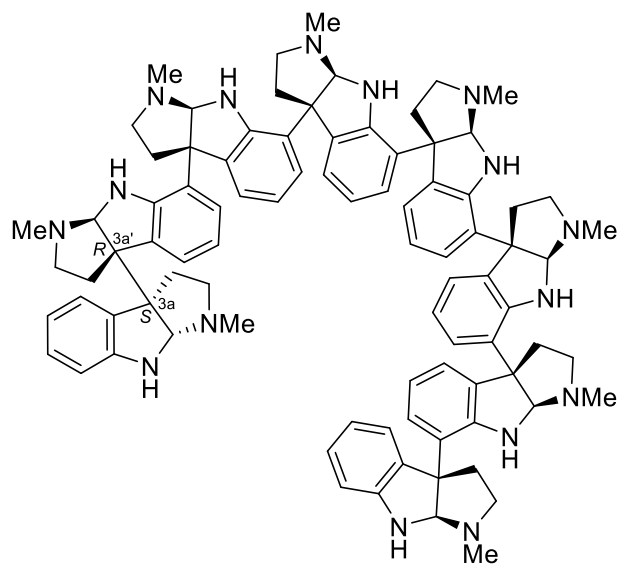


Figure 2.11 Chemical structure of (+)-eumatanine (**4**)

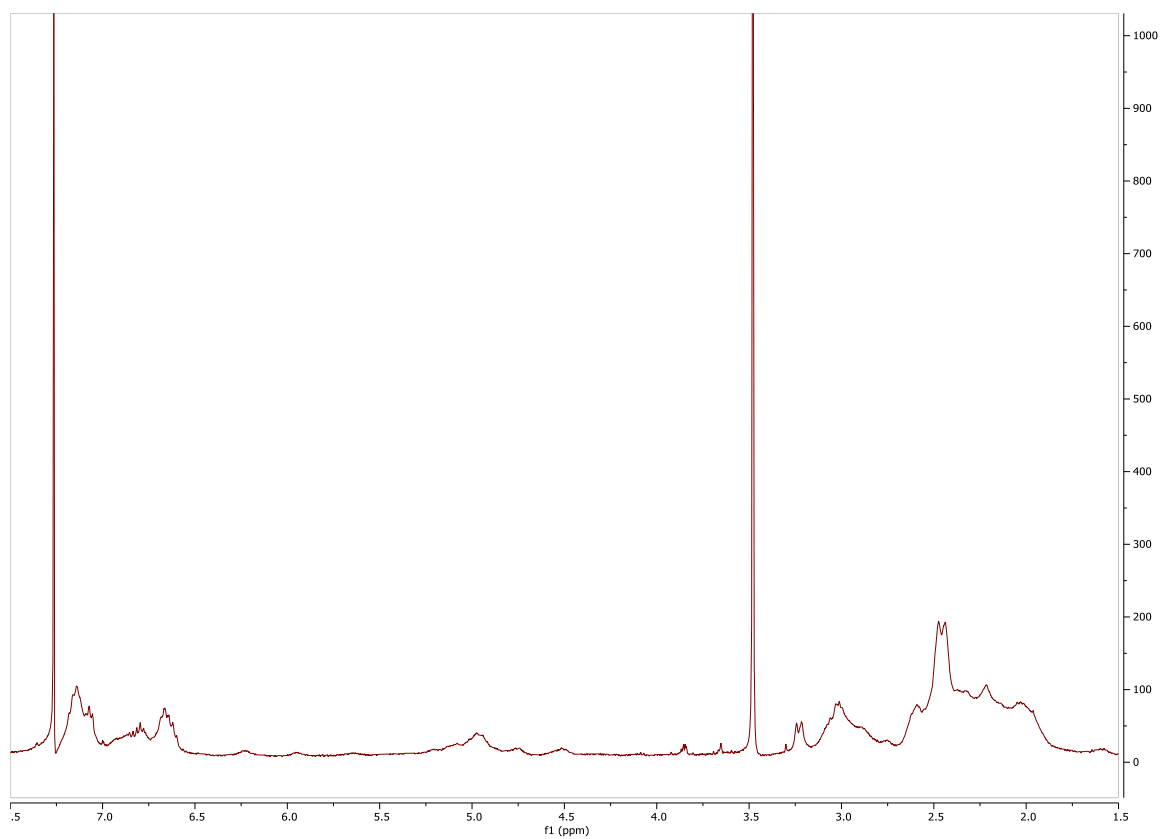


Figure 2.12 ^1H NMR Spectrum of Eumatanine (**4**) at rt in CDCl_3

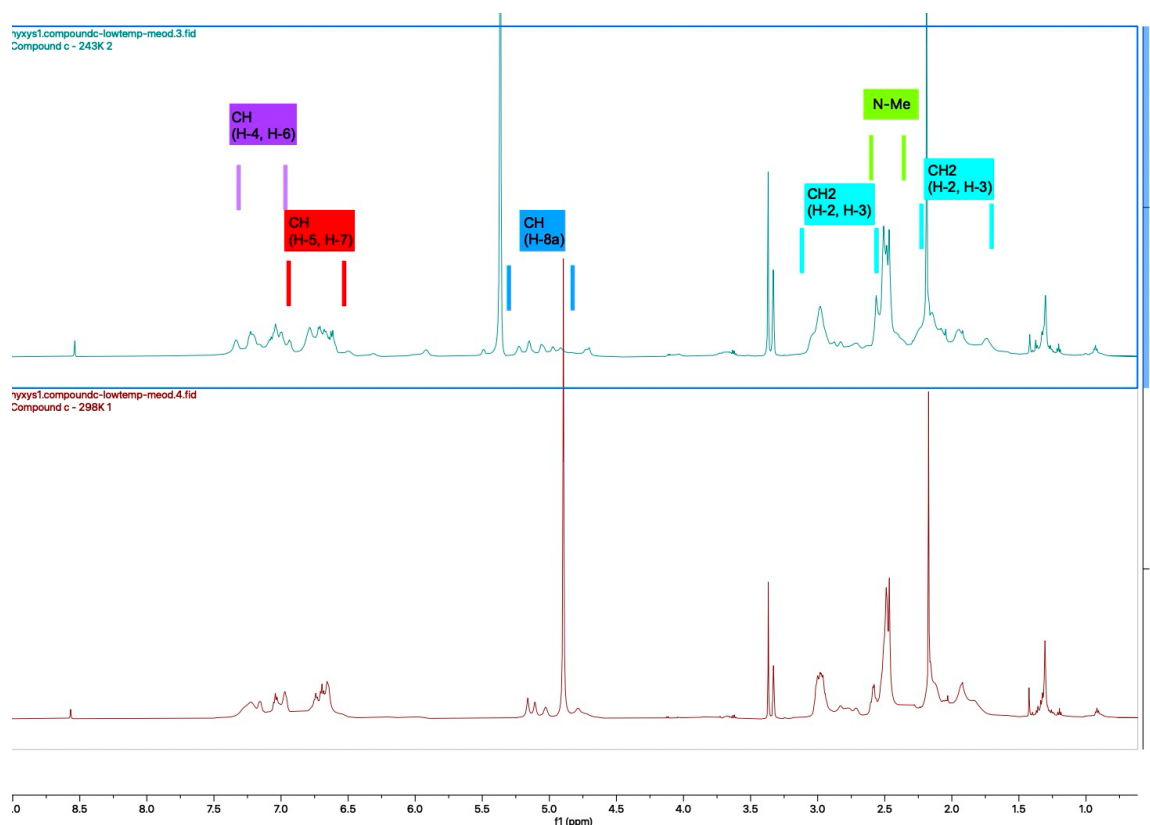


Figure 2.13 ^1H NMR Spectra of Eumatanine (**4**) at 243 K and 298 K in CD_3OD

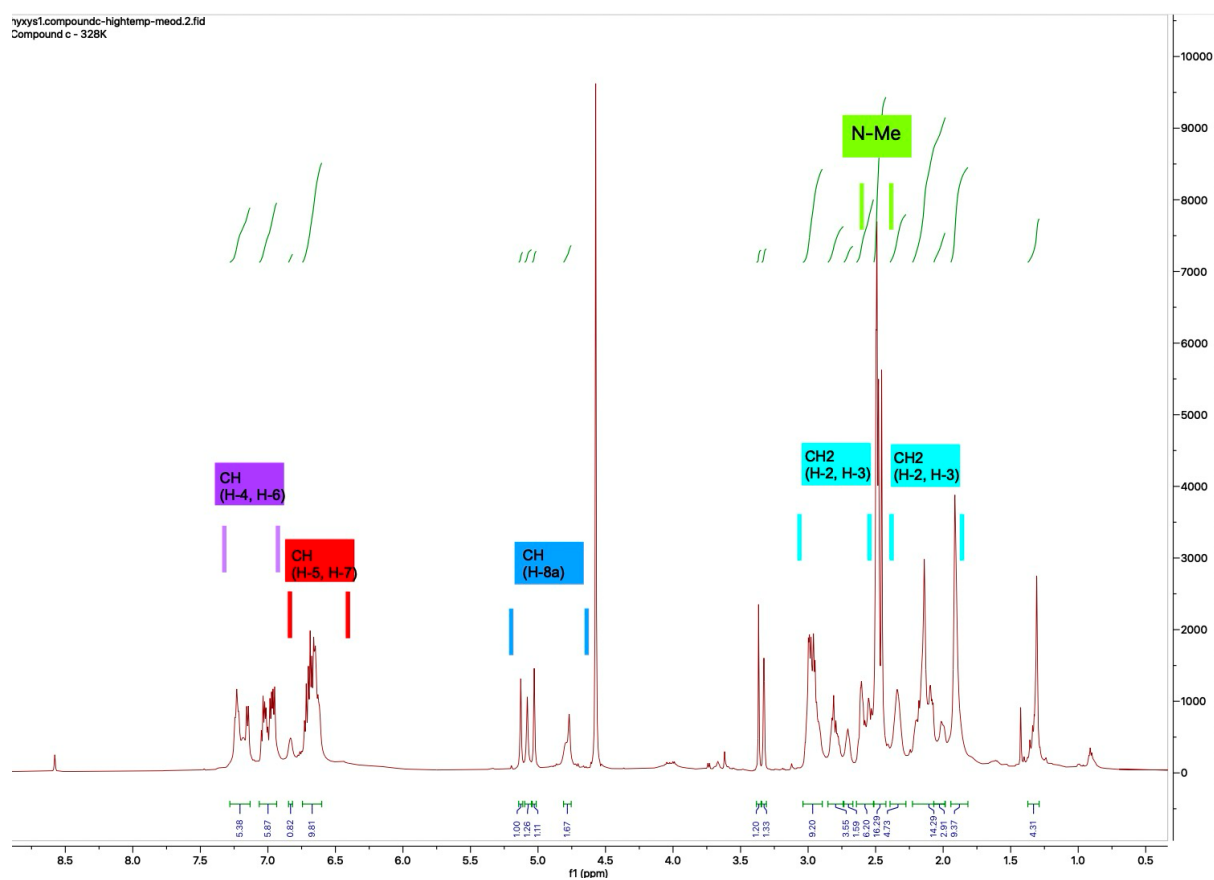
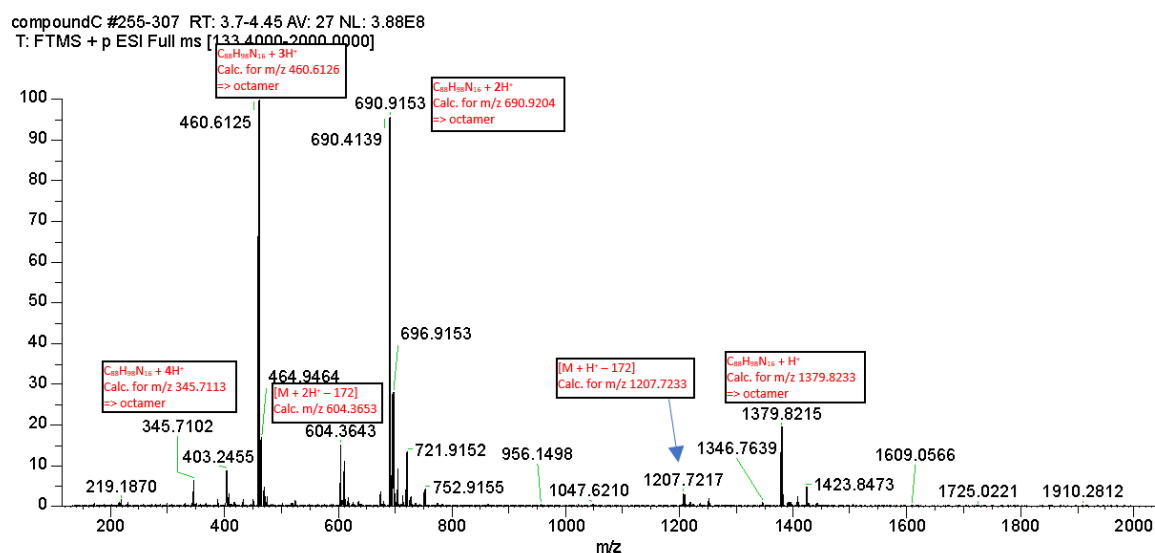
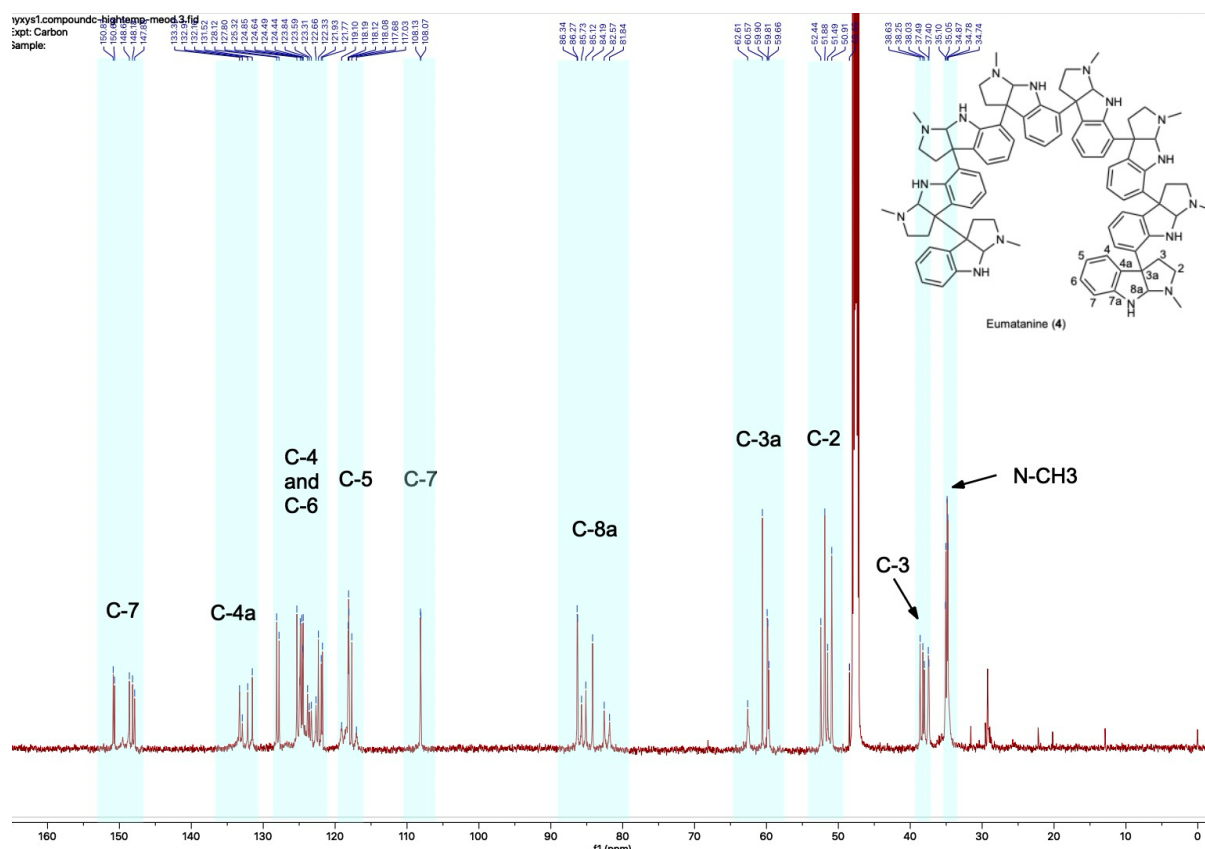


Figure 2.14 ^1H NMR Spectra of Eumatanine (**4**) at 328 K in CD_3OD



According to the biosynthetic pathway proposed by Scott and Mossavaghi, these alkaloids are formed by sequentially adding 3a*R*-configured *cis*-pyrrolidino[2,3-*b*]indoline units to the C-7 position of a preceding structure, with *meso*-chimonanthine as the core unit (Scott and Movassaghi, 2024). Based on this pathway, a plausible stereochemical assignment for eumatanine (4) can be proposed, which maintains the regio- and stereochemical integrity

observed in previously characterized oligomers. This proposal suggests that **4** consists of seven *R* and one *S* cyclotryptamine units (**Figure 2.11**). The identical ECD spectrum of **4**, compared to those of compounds **2** and **3** (**Figure 2.10**), further supports this stereochemical assignment. Eumatanine (**4**) thus represents the second reported octameric cyclotryptamine alkaloid, following vatamidine, which exhibits a [6+2] arrangement of cyclotryptamine units (Scott and Movassaghi, 2024, Adjibadé et al., 1990). Although both alkaloids contain eight units, they differ in connectivity: in vatamidine, a β - β' bond links a group of six units to a group of two, whereas in eumatanine (**4**), the same bond connects seven units to a single residual unit.

A similar series of oligocyclotryptamine alkaloids has been isolated from *Eumachia forsteriana*, including the hexamer vatine, the heptamer vatamine, and the octamer vatamidine. Notably, these larger alkaloids exhibit significant cytotoxicity against hepatoma (HTC) cells compared to their lower-molecular-weight counterparts (Adjibadé et al., 1990). The cytotoxicity of these oligocyclotryptamine alkaloids is influenced by both their molecular weight and structural isomerism. Alkaloids with higher molecular weights and more than five basic units demonstrate markedly greater cytotoxic activity, with toxicity increasing over prolonged incubation periods (Adjibadé et al., 1990). Additionally, the structural isomerism observed in compounds such as psychotridine C and isopsychotridine D plays a critical role in their differential cytotoxic effects (Adjibadé et al., 1990). Isopsychotridines D and E display greater potency than psychotridine C, emphasizing the importance of molecular configuration in determining biological activity. These findings underscore the need for further investigation into the relationship between molecular structure, size, and cytotoxic potential, which could inform the design of more effective therapeutic compounds.

2.2.3 Eumatricine (**5**)

Eumatricine (**5**) (**Figure 2.17**) was obtained as a light yellowish powder. The HRESIMS data of **5** showed a $[M + H]^+$ peak at m/z 183.0932, allowing for the deduction of the molecular formula $C_{12}H_{10}N_2$, which corresponds to nine degrees of unsaturation.

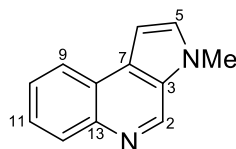


Figure 2.17 Chemical structure of eumatrinine (**5**)

The ^{13}C NMR data of **1** (Table 2.2.3) showed the presence of 12 carbons, which agrees with the molecular formula established by the HRESIMS data. Of the 12 carbons detected, 11 were due to aromatic resonances, while one was due to an aliphatic resonance. The ^1H NMR data of **5** (Table 2.2.3) indicated the presence of seven aromatic methines and a methyl group. The molecular formula of **5**, which showed the presence of 10 hydrogen atoms, suggested that the structure of **1** is mostly aromatic with the methyl group being the only aliphatic group in the molecule. The methyl group was observed to resonate at δ_{H} 4.04 and since the molecular formula is devoid of oxygen atom, this suggested the presence of an N-methyl group. The distinctive methine signal observed at δ_{H} 9.04 suggested the presence of a hydrogen due to an imine C-H. The ^1H NMR also revealed the presence of a pair of AB doublets at δ_{H} 7.00 and 7.27 with a coupling constant value of 2.9 Hz. This pair of signals was shown by the COSY data to be attributed to a CH-CH fragment (Figure 2.18). Additionally, the COSY data revealed that the remaining methine signals at δ_{H} 8.20, 8.18, 7.60 and 7.58 were due to the presence of a CH-CH-CH-CH partial structure of a 1,2-disubstituted benzene ring (Figure 2.18).

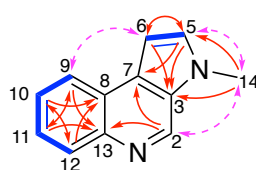


Figure 2.18 Selected COSY (blue bold bonds), HMBC (red arrows), and NOESY (pink dotted arrows) correlations of **1**

The HMBC data were instrumental in constructing the possible gross structure of **5** (Figure 2.17). The presence of an N-methyl pyrrole partial structure in **5**, which incorporated the C-5–C-6 fragment revealed by the ^1H NMR and COSY data, was supported by the HMBC three-bond correlations observed from H-5 to C-3 and C-7; from H-6 to C-3; and from CH_3 -14 to C-3 and C-5 (Figure 2.18). The most downfield carbon resonance at δ_{C} 142.43, which was attributable to an N-substituted aromatic carbon, correlated with H-9 and H-11 in the HMBC spectrum, thus allowing this carbon to be assigned to C-13. Furthermore, the presence of a

quinoline partial structure substituted at C-3 and C-7 was supported by the HMBC three-bond correlations observed from H-2 (δ_{H} 9.04) to C-7 and C-13; from H-9 to C-11 and C-13; from H-10 to C-8 and C-12; from H-11 to C-9 and C-13; from H-12 to C-8 and C-10. On the other hand, the pyrrole unit was deduced to be fused to the quinoline structure at C-3 and C-7 based on the HMBC correlations from H-5 to C-3 and C-7; and from CH₃-14 to C-3 and C-5. The proposed structure of **5** is consistent with the full HMBC data. Additionally, the proposed structure was also corroborated by the NOESY data, which showed the following key correlations: H-6/H-9, H-2/CH₃-14 and H-5/CH₃-14 (**Figure 2.18**).

A search in the database (Reaxys) indicated that the isolation of structure **5** from nature has not been previously reported in the literature and therefore represents a new naturally-occurring pyrroloquinoline alkaloid. However, the structure of **5** was previously synthesized to determine the constitution of calycanthine through alkaloid degradation method (Eiter and Nagy, 1949).

In addition, there was a regioisomeric alkaloid named marinoquinoline A (**1a**) that was previously reported from the gliding bacterium *Ohtaekwangia kribbensis* (Okanya et al., 2011). The structures of **1** and **1a** are identical except for the location of the methyl group. While in **1** the methyl group is attached to the pyrrole nitrogen atom, in marinoquinoline A (**1a**) the methyl group is attached to C-2 (**Figure 2.19**). Furthermore, the ¹H and ¹³C NMR data for both the compounds are largely in good agreement with the largest deviation in chemical shifts involved C-2 and N-Me/NH (**Table 2.3**).

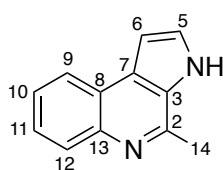


Figure 2.19 Structure of marinoquinoline A (**1a**)

Table 2. ³ NMR Spectroscopic Data of PML-1 (1)^a and marinoquinoline A (1a)^b (Okanya et al., 2011).

Position	PML-1 (1) ^a		Marinoquinoline A (1a) ^b	
	δ_{H} (ppm, <i>J</i> in Hz)	δ_{C} (ppm)	δ_{H} (ppm, <i>J</i> in Hz)	δ_{C} (ppm)
2	9.04, s, 1H	136.05	-	146.92
3	-	128.93	-	129.89
4 (NH)	-	-	11.12, br s	-
5	7.27, d (2, 9), 1H	130.76	7.57, d (2, 8), 1H	127.11
6	7.00, d (2, 9), 1H	100.18	7.12, d (2, 8), 1H	102.04
7	-	129.79	-	128.41
8	-	123.49	-	124.26
9	8.20, dd (7, 2), 1H	122.98	8.22, dd (7.7, 2.0), 1H	123.77
10	7.58, td (7, 2), 1H	125.94	7.48, td (7, 8.2), 1H	125.71
11	7.60, td (7, 2), 1H	126.06	7.51, td (7, 8.2), 1H	126.11
12	8.18, dd (7, 2), 1H	129.61	7.99, dd (7.7, 2.0), 1H	129.98
13	-	142.43	-	143.89
14	4.04, s, 3H	33.50	2.83, s	21.34

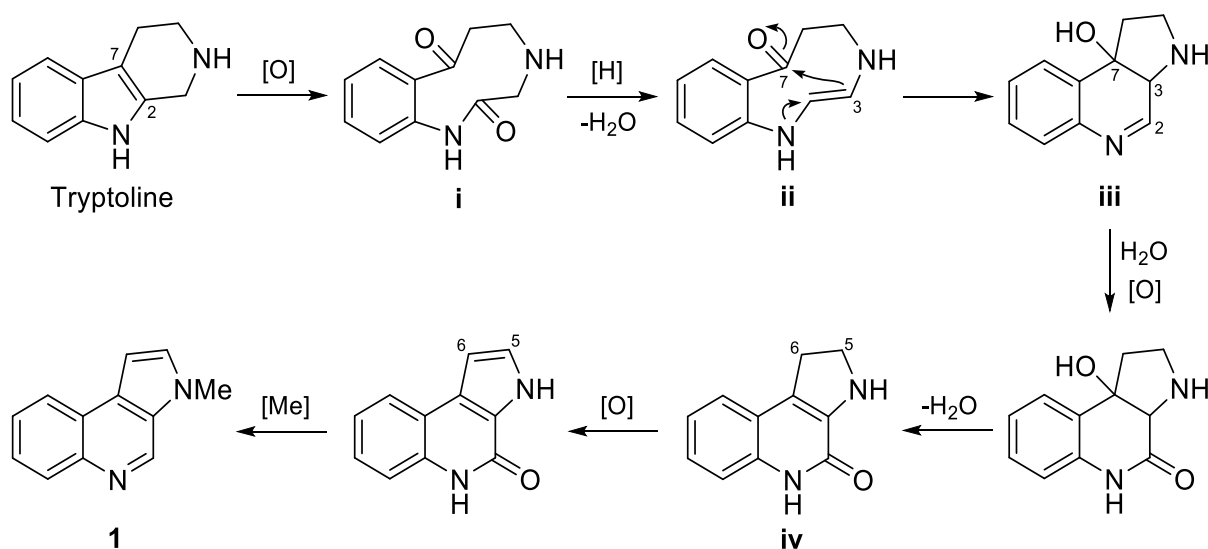
^aMeasured in CDCl₃, ¹H/¹³C 600/150 MHz

^bMeasured in acetone-d₆, ¹H/¹³C 600/150 MHz

Biosynthetic pathway to Eumatricine (5)

Since the genus *Palicourea*, a relative of *Eumachia*, also producers of β -carboline alkaloids (e.g. correantoside from *Palicourea correae*), eumatricine (5) is therefore assumed to be derived from a β -carboline precursor (Achenbach et al., 1995a, Klein-Júnior et al., 2020b). It is also known that a β -carboline alkaloid (pyridoindole, 6-5-6 ring system) can undergo a ring expansion rearrangement to a pyrroloquinoline alkaloid (6-6-5 ring system) (Dewick, 2009b). A plausible biosynthetic pathway to 5 starting from the β -carboline alkaloid tryptoline was proposed as demonstrated in Scheme 2.2. Firstly, oxidative cleavage of the C-2–C-7 double bond gives the dicarbonyl intermediate i, which following an amide reduction-dehydration step gives the enamine intermediate ii. Nucleophilic enamine addition onto the ketone at C-7 then gives the 6-6-5 tricyclic intermediate iii. The imine function at C-2 is then converted to an amide group, while the hydroxyl group at C-7 is dehydrated to form a tetrasubstituted double

bond at C-3 and C-7 giving rise to the intermediate iv. Finally, oxidative dehydrogenation at C-5 and C-6 followed by methylation of the pyrrole N atom furnish the structure of eumatricine (5).



Scheme 2.2 Plausible biosynthetic pathway to Eumatricine (5)

In this study, the isolation and characterisation of cyclotryptamine and β -carboline alkaloids from members of the Rubiaceae family (*Eumachia montana*) provide significant insights into their chemical diversity and potential pharmacological applications.

Oligocyclotryptamine alkaloids represent a distinctive subclass of pyrroloindoline natural products, characterized by their intricate oligomeric architectures. These structures arise from the C–C linkage of multiple *cis*-pyrrolidino[2,3-*b*]indoline (cyclotryptamine) units, forming higher-order oligomers through benzylic carbon–carbon bonds or by linking the benzylic carbon of one fragment to the peri C7 carbon of another. As oligomerization progresses, additional *cis*-pyrrolidino[2,3-*b*]indoline units are appended at the benzylic carbon (C3a) to the aromatic carbon (C7) of the preceding structure. This results in highly complex polycyclic frameworks that often incorporate the dimeric 3a–3a'-bispyrrolidino[2,3-*b*]indoline core, multiple C3a quaternary stereocenters, and numerous basic nitrogen centers. Notably, some members of this family exhibit up to seven C3a–C7' linkages, further contributing to their structural diversity and stereochemical intricacy (Steven and Overman, 2007).

2.3 Conclusion

From the leaves of *Eumachia montana*, a series of oligocyclotryptamine alkaloids were isolated and characterized, including the hexameric (+)-oleoidine (**2**), the heptameric (+)-caledonine (**3**), and new octameric (+)-eumatanine (**4**). In addition, the known dimer (–)-calycanthine (**1**) and a new tricyclic pyrroloquinoline alkaloid, eumatricine (**5**), were also obtained.

The present study highlights the chemical diversity and biological potential of cyclotryptamine and β -carboline alkaloids isolated from the Rubiaceae family. Their cytotoxic, antimicrobial, and analgesic properties underscore their relevance in NPDD. Further research are necessary to explore their mechanisms of action in greater detail. Investigating their interactions with specific molecular targets, such as DNA, topoisomerases, or neurotransmitter receptors, will provide deeper insights into their mode of action. Moreover, structural optimization through synthetic modifications could enhance potency and selectivity, making them more suitable candidates for drug development (Qazzaz et al., 2016).

Chapter 3 Anticancer evaluation of oleoidine (2), caledonine (3) and eumatanine (4)

3.1 Introduction

Cancer, a complex group of diseases with features of unrestricted cell proliferation, inhibited apoptosis, and resistance to therapies, remains a leading cause of mortality worldwide and therefore prompts ongoing research into novel anticancer agents or therapeutic strategies that are capable of selectively inducing cell death in cancerous tissues while minimizing cytotoxicity toward normal tissues. Natural products are secondary metabolites derived from plants, marine organisms, or microorganisms, which have been drug discovery sources for decades due to their various potent biological activities, especially anticancer activity. For instance, clinical anticancer drugs paclitaxel (Taxol®), vincristine (VCR), and vinblastine (VBL) are antimicrotubule agents derived from plants, namely from *Taxus brevifolia* (the Pacific yew) and *Catharanthus roseus* (L.) G. Don (Madagascar periwinkle), respectively (Gidding et al., 1999, Donehower, 1996). These compounds act as chemotherapy agents exert potent therapeutic efficacy in multiple cancers by evoking cellular pathways including apoptosis, the cell cycle, ROS generation, etc., namely, vincristine and vinblastine disrupt microtubule formation, preventing cell division and promoting apoptosis, while paclitaxel stabilises microtubules and prevents their depolymerisation, resulting in G2/M phase cell cycle arrest (Gidding et al., 1999, Donehower, 1996, Cragg and Pezzuto, 2016). Apoptosis, also known as programmed cell death, plays a pivot role in the process of dismantling and eliminating cancer cells, which is regulated by various factors, including caspases (e.g. 3 and 7), ROS, DNA damage and the cell cycle. It is crucial to understand the interplay among these factors and apoptosis for developing anticancer strategies.

VCR and VBL are characterized as alkaloids, which are a class of naturally occurring organic compounds that have exhibited a variety of bioactivities, including anticancer properties (Gidding et al., 1999, Cragg and Pezzuto, 2016). Other examples include naturally occurring oligocyclotryptamine alkaloids, which have exhibited diverse bioactivities, for instance,

cytotoxicity (quadrigemine H, quadrigemine C, psychotridine, isopsychotridine C from *Eumachia forsteriana*), analgesic ((+)-chimonanthine, hodgkinsine, quadrigemine C, psychotridine from *Palicourea colorata*), antimicrobial (psychotrimine from *Eumachia rostrata*) and antithrombotic (Psm2 from *Selaginella moellendorffii*) effects, (Roth et al., 1986, Nascimento et al., 2015, Saad et al., 1995, Adjibadé et al., 1990, Amador et al., 2001, Elisabetsky et al., 1995, Amador et al., 2000, Schallenberger et al., 2010, Shi et al., 2012, Su et al., 2016). The cytotoxicity of cyclotryptamine isolated from *Eumachia forsteriana* has been reported to be higher than vincristine against rat hepatoma cells (HTC line), from where a cellular mortality of 100% was obtained within 24h of incubation at concentrations of 2.5, 5, 5 and 10µM for alkaloids psychotridine, isopsychotridine, quadrigemine B and C, respectively (Roth et al., 1986). Thus, these data evidence excellent anticancer potential, and support anticancer evaluation of oligocyclotryptamine alkaloids, namely (+)-oleoidine (**2**), (+)-caledonine (**3**) and (+)-eumatanine (**4**) isolated from *Eumachia montana*.

In this study, anticancer activities of newly discovered oligocyclotryptamine alkaloids (compounds **2**, **3**, **4**) from leaves of *Eumachia montana* were assessed in terms of cytotoxicity against human-derived carcinoma cell lines (breast, colorectal, brain, and lung carcinoma) by conducting MTT, cell count and clonogenic assays. Furthermore, the cellular mechanisms of action underlying these three compounds' activities were investigated via cell cycle analysis, ROS-generation, apoptosis, caspase 3/7 assays and γH2AX detection.

3.2 Results and discussion

3.2.1 Preliminary screening of oleoidine (**2**), caledonine (**3**) and eumatanine (**4**)

(+)-Caledonine (**3**), as the most abundant compound from extract fractions in the first stage, has received the most thorough evaluation in preliminary screening (including MTT, cell count and clonogenic assays). Its activity was assessed against 8 different human-derived cell lines MCF-7, MDA-MB-468 (breast), HCT-116, HT-29 (colon), U373 (GBM, vector control), U373M (GBM, MGMT-transfected), A549 (non-small cell lung cancer) and non-transformed lung fibroblasts MRC-5, which enables a comprehensive understanding of the growth inhibitory and cytotoxic activity of **3**. Additionally, both oleoidine (**2**) and eumatanine (**4**) were

assessed against MCF-7 and HCT-116, and MRC-5, while the former was also evaluated against A549.

3.2.1.1 MTT assay

Triple or more (except the cell line A549) independent repeats (n=6 internal replicates) were conducted for each MTT assay to ensure robust data, and concentration parameters GI₅₀ (the concentration that causes 50% growth inhibition), TGI (Total Growth Inhibition, the concentration that causes total growth inhibition) and LC₅₀ (the concentration that causes 50% cell death) were produced to measure the growth inhibitory effect, cytostatic and cytotoxic effects of test agents, namely compounds **2-4**. At the same time, MTT assays using the compound vehicle DMSO at the same dilutions were carried out as a vehicle control test for each cell line.

The results of MTT assays in **Table 3.1** present the mean GI₅₀ values of compounds **2-4** against the 8 human-derived cell lines, including carcinoma cell lines MCF-7, MDA-MB-468 (breast), HCT-116, HT-29 (colon), U373 (GBM, vector control), U373M (GBM, MGMT-transfected), A549 (non-small cell lung cancer) and non-transformed lung fibroblasts MRC-5. It is shown that compound **3** elicits potent broad-spectrum growth inhibition against breast, colon, lung, and brain carcinoma cell lines with GI₅₀ values ranging from 0.1 to 2.7 μ M, while compounds **2** and **4** also presented potent activity against all test carcinoma cell lines with GI₅₀ values ranging from 0.5 to 1.2 μ M. The clinical anticancer drug vincristine sulfate (C₄₆H₅₆N₄O₁₀ · H₂O₄S) was used as the positive control and estimated GI₅₀ values were calculated for MCF-7 and HCT-116 cell lines. Vincristine exhibited significantly more potent growth inhibitory effects than compounds **2-4** with GI₅₀ values ranging between 0.4 -1.2E-03 μ M (**Table 3.4, Figure 3.3**). In the MTT linear dose–response plots, 0 on the x-axis represents the control group (0 concentration of the compound). As the dose–response relationship is only defined for non-zero concentrations, the x-axis does not need to begin at 0.

3 possesses the most potent growth inhibitory ability in MCF-7 and HCT-116 cell lines compared to **2** and **4**, and the mean GI₅₀ values of **3** were between 0.26 and 0.59 μ M for MCF-7, HCT-116 and MDA-MB-468. U373V and U373M cells exhibited the greatest sensitivity to **3** with the GI₅₀ values ~0.137 and 0.117 μ M. In comparison, HT-29 showed the greatest

resistance to **3** with a mean GI₅₀ value of 2.707 μM. However, the mean GI₅₀ value of **3** against MRC-5 is 0.877 μM, which is slightly higher than HCT-116 (~0.585 μM) and A549 (0.622 μM), suggesting that **3** may possess similar cytotoxic effects against normal human-derived cell lines, and thereby **3** may not be cancer-selective towards colon and non-small lung cancers. Nevertheless, the mean GI₅₀ value of **3** against MRC-5 is ≥2.9-fold higher than GI₅₀ in MCF-7 (~0.300 μM), MDA-MB-468 (~0.257 μM), U373V (~0.137 μM) and U373M (~0.117 μM), which implies that **3** may be cancer-selective towards BC and GBM (**Table 3.1**).

Compound **2** exhibited the least potent growth inhibitory effects against cell lines MCF-7 and HCT-116 compared to **3** and **4** with GI₅₀ values >0.9 μM. **4** showed similar growth inhibitory effects as **3** against HCT-116 with a GI₅₀ value ~0.6 μM, while less potency was recorded against MCF-7 (GI₅₀ value ~0.7 μM). Unfortunately, **2** and **4** presented no cancer selectivity, as similar growth inhibitory effects were observed in MRC-5 and all the other test cancer cell lines with GI₅₀ values of ~0.9 μM for **2** and ~0.6 μM for **4**. **Figures 3.1** and **3.2** include representative dose-response curves of compounds **2-4** against cell lines MCF-7 and HCT-116 produced by the 72h MTT assay.

Tables 3.2 and **3.3** exhibit the mean TGI and LC₅₀ values of compounds **2-4** against MCF-7, HCT-116, and MRC-5 cell lines. **3** exerts the most potent cytostatic effects on MCF-7 cells with a TGI value of ~0.7 μM, which is much lower than **3** against HCT-116 (~1.5 μM) and MRC-5 (~1.2 μM). Thus, the cancer selectivity of **3** on BC cell line MCF-7 is ascertained, which also corroborates the conclusion drawn from the GI₅₀ value of **3**. TGI values of **2** and **4** against these three cell lines were between 1.3-1.7 μM and 0.8-0.9 μM, respectively, suggesting potent cytostatic effects were produced by **2** or **4** on breast and colon cancer cell lines without any cancer selectivity. Interestingly, **4** produced the most cytotoxic effects on HCT-116 with an LC₅₀ value of ~0.6 μM, followed by **2** against HCT-116 (~0.9 μM) and **3** against MCF-7 (~1.1 μM). **2** and **4** induce higher levels of cytotoxic effects on colon cancer cell line HCT-116 than that of BC cell line MCF-7 and normal lung cell line MRC-5, while **3** exerts similar cytotoxic effects on all three cell lines (**Table 3.3**). Additionally, the comparison between 24h and 72h exposure of cells (MCF-7; HCT-116) to **3** inferred rapid onset of growth inhibitory activity and cytotoxicity (**Figure 3.4**). Differing exposure periods during the same overall experimental time (i.e. 24h treatment followed by 48h test agent-free vs 72h continuous

exposure of cells to test agent; Figure 3.4), revealed that **3** exerts almost identical growth inhibitory activity after 24h or 72h treatment; the slightly higher potency at 72h treatment at concentrations \sim GI₅₀ value is not significant ($p>0.05$).

Table 3.1 Mean GI₅₀ values of compounds **2**, **3**, **4** against various human-derived cell lines

Origin	Cell lines	Compounds GI ₅₀ mean \pm SEM (μ M)		
		Oleoidine (2)	Caledonine (3)	Eumatanine (4)
Breast carcinoma	MCF-7	1.204 \pm 0.148	0.300 \pm 0.044	0.706 \pm 0.105
	MDA-MB-468*	-	0.257 \pm 0.023	-
Colon carcinoma	HCT-116	0.950 \pm 0.022	0.585 \pm 0.032	0.618 \pm 0.102
	HT-29*	-	2.707 \pm 0.508	-
Brain carcinoma	U373V*	-	0.137 \pm 0.045	-
	U373M*	-	0.117 \pm 0.040	-
Lung carcinoma	A549*	-	0.622	0.531 \pm 0.081
Non-transformed lung fibroblast	MRC-5	0.943 \pm 0.006	0.877 \pm 0.191	0.630 \pm 0.058

MTT assays, following 72h exposure of cells to compounds **2**, **3** and **4**; mean \pm SEM GI₅₀ values (μ M) are values from ≥ 3 independent trials where $n=6$ internal repeats; except that of A549, only 1 independent trial was performed on **3** and **2** on **4**, where $n=6$; SI=GI₅₀ MRC-5 divided by GI₅₀ specific cancer cell lines; *experiments conducted by undergraduate students under Y. Shuai's supervision.

Table 3.2 Mean TGI values of compounds **2**, **3**, **4** against various human-derived cell lines

Cell lines	Compounds TGI mean \pm SEM (μ M)		
	Oleoidine (2)	Caledonine (3)	Eumatanine (4)
MCF-7	1.757 \pm 0.225	0.734 \pm 0.235	0.943 \pm 0.149
HCT-116	1.328 \pm 0.046	1.515 \pm 0.174	0.816 \pm 0.118
MRC-5	1.773 \pm 0.152	1.256 \pm 0.289	0.985 \pm 0.185

MTT assays, following 72h exposure of cells to compounds **2**, **3**, **4**; mean \pm SEM TGI values (μ M) are values from ≥ 3 independent trials where $n=6$ internal repeats

Table 3.3 Mean LC_{50} values of compounds **2**, **3**, **4** against various human-derived cell lines

Cell lines	Compounds LC_{50} mean \pm SEM (μ M)		
	Oleoidine (2)	Caledonine (3)	Eumatanine (4)
MCF-7	2.176 \pm 0.073	1.087 \pm 0.338	1.197 \pm 0.199
HCT-116	0.950 \pm 0.022	1.865 \pm 0.088	0.618 \pm 0.102
MRC-5	2.191 \pm 0.055	1.873 \pm 0.111	1.358 \pm 0.160

MTT assays, following 72h exposure of cells to compounds **2**, **3**, **4**; mean \pm SEM LC_{50} values (μ M) are values from ≥ 3 independent trials where $n=6$ internal repeats

Table 3.4 Effects of vincristine on MCF-7 and HCT-116.

Cell line	GI_{50} values (Vincristine (VCR), μ M)
MCF-7	1.1672E-03 \pm 8.2479E-04
HCT-116	4.1667E-04 \pm 1.2482E-04

MTT assays, following 72h exposure of cells to vincristine; mean \pm SEM GI_{50} values (μ M) are values from ≥ 3 independent trials where $n=6$ internal repeats

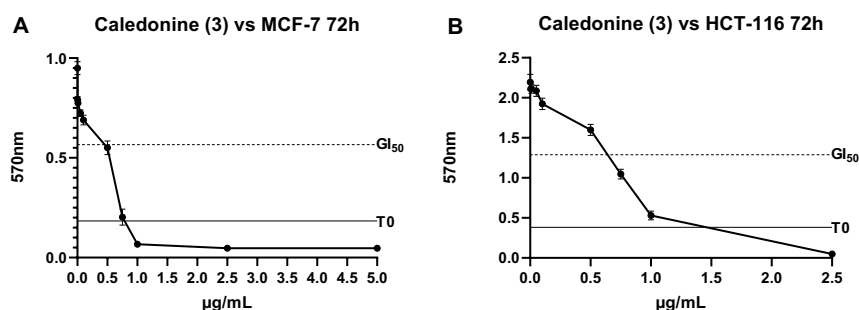


Figure 3.1 Growth inhibitory effect of caledonine (**3**) on MCF-7 (A) and HCT-116 (B) cell lines. Cells were seeded on 96-well plates and incubated for 72h ($n=6$ internal repeats, ≥ 3 independent trials). The line of T0 represents the number of cells treated, while GI_{50} helps allocate the concentration of test agents that could inhibit the growth of cells by 50%. The 0 on the x-axis represents the control group (0 concentration of the compound). The axis does not need to start at 0, as the dose-response curve is defined only for non-zero concentrations. All subsequent MTT assay graphs are presented in the same format.

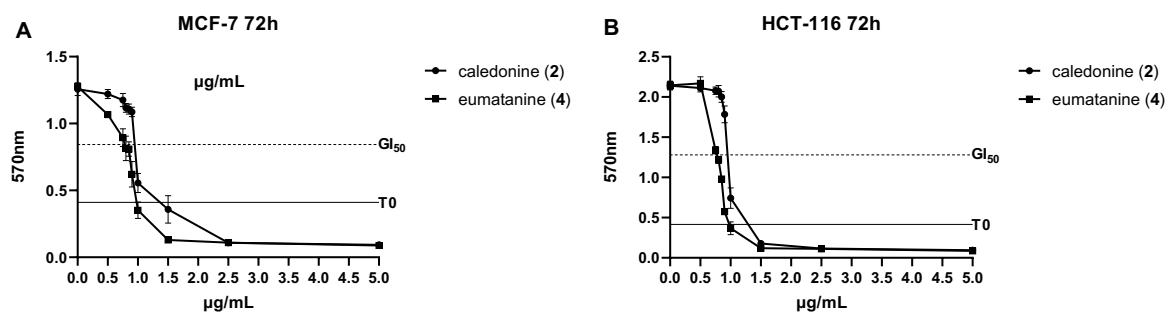


Figure 3.2 Growth inhibitory effects of oleoidine (2) and eumatanine (4) on MCF-7 (A), HCT-116 (B) cell lines. Cells were seeded on 96-well plates and incubated for 72h ($n=6$ internal repeats, ≥ 3 independent trials). The line of T0 represents the number of cells treated, while GI₅₀ helps allocate the concentration of test agents that could inhibit the growth of cells by 50%.

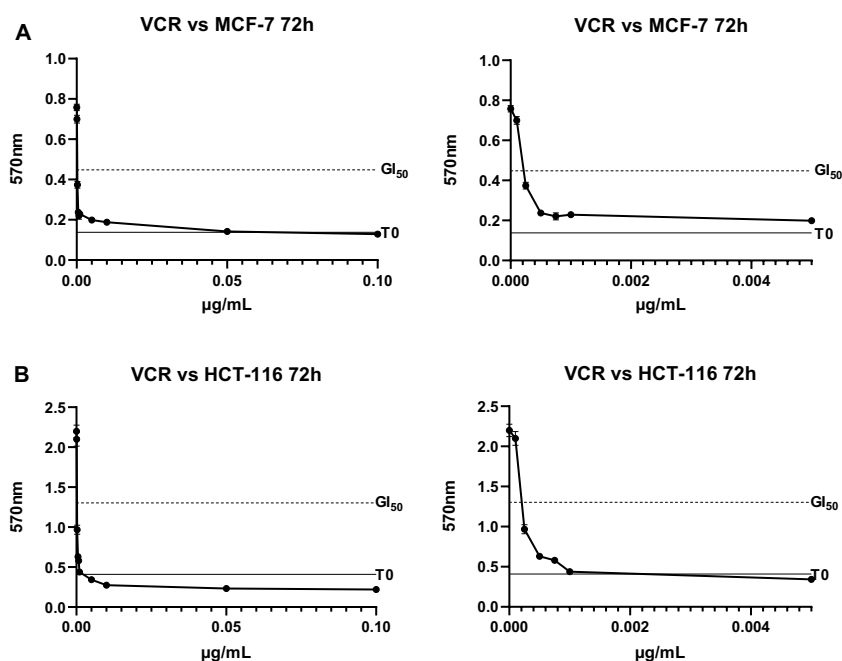


Figure 3.3 Growth inhibitory effects of vincristine on MCF-7 (A), HCT-116 (B) cell lines. Cells were seeded on 96-well plates and incubated for 72h ($n=6$ internal repeats, ≥ 3 independent trials). The line of T0 represents the number of cells treated, while GI₅₀ helps allocate the concentration of test agents that could inhibit the growth of cells by 50%. The adjacent panels provide zoom-in views of the low-concentration region.

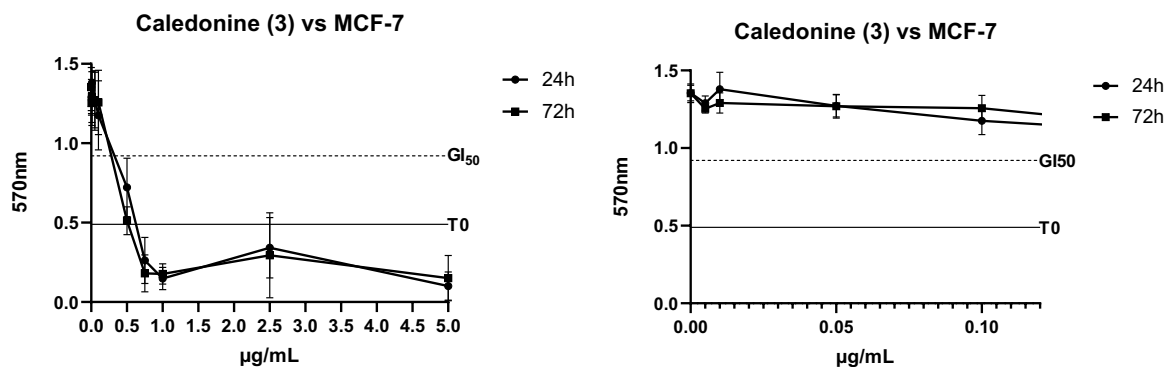


Figure 3.4 The comparison of growth inhibitory effect of caledonine (**3**) on MCF-7 following 24 and 72h's exposure; mean \pm SEM from ≥ 3 independent trials where $n=6$. The adjacent panels provide zoom-in views of the low-concentration region.

It is indicated in **Table 3.1** that the GBM cell lines are most sensitive to **3** among all cancer cell lines and the potency of **3** against U373V and U373M is almost the same, which may imply that the cytotoxicity of **3** is not influenced by MGMT gene expression. The DNA repair enzyme MGMT is capable of reversing *O*6-methyl guanine (*O*6MG) damage caused by alkylating agents (such as TMZ, the drug of choice for GBM treatment in the clinic) via a one-step transalkylation reaction, which is one of the major chemoresistance mechanisms of TMZ (Arora and Somasundaram, 2019). However, the ability of MGMT to reverse *O*6MG damage relies on continuous MGMT expression and multiple methods are available for the regulation of MGMT, including promoter methylation, altered expression, histone modifications, post-transcriptional modifications, and miRNA regulation of transcription levels (Kaina et al., 2007, Wick et al., 2014). Potentially, **3** caused cytotoxicity via pathways other than inducing the lesion of *O*6MG or **3** is a MGMT regulator. For example, the inhibition of wnt/ β -catenin pathway decreases MGMT gene expression, therefore preventing chemoresistance in response to TMZ as well as increasing drug sensitivity (Wickström et al., 2015). This may be especially advantageous in specific clinical conditions, as the overexpression of MGMT in cancer is currently a major obstacle to successful treatment and good prognoses for patients with GBM.

Although compounds **2**, **3** and **4** have shown potent activity towards various cancer cell lines, the GI_{50} values against non-transformed lung fibroblasts MRC-5 cells may suggest that **2** and **4** are not cancer-selective, only **3** indicated some cancer-selectivity (in certain cell lines). The possible techniques to circumvent potential cytotoxicity of natural product anticancer agents towards normal cells include nanoparticle formulations and antibody-drug conjugates (ACDs).

For instance, pegylated liposomal doxorubicin (Doxil®), the first FDA-approved nano-drug (1995) that encapsulated the anticancer agent doxorubicin in nanoparticles (liposomes in this case) for drug delivery, has shown great therapeutical benefit over free doxorubicin due to favourable bio-distribution, pharmacokinetic properties, and potentially enhanced permeation and retention (EPR) within the tumour microenvironment (Barenholz, 2012). Doxorubicin, a natural product (anthracycline antibiotic) originally isolated from microorganisms (*Streptomyces peucetius*), possesses potent broad-spectrum anticancer activity and has been used clinically for decades, but is plagued by cardiotoxicity as its major side effect (Speth et al., 1988, Jain, 2000, Octavia et al., 2012). Due to the use of PEGylated nano-liposomes and the remote liposomal drug-loading system, plus the EPR effects of the nanoparticles, nano-drug Doxil® displayed multiple advantages over conventional doxorubicin, including prolonged drug circulation time, reticuloendothelial system (RES) evasion, and enhanced cancer-selectivity (Barenholz, 2012). In addition, EPR effects may also allow a lower dose administration and thus minimise systemic-toxicity, reducing adverse side effects, significantly, doxorubicin-induced cardiotoxicity, which is dose-dependent, cumulative and irreversible (Jain, 2000). Nab paclitaxel, also known as Abraxane, is another example of nano-drugs that is clinically used to treat BC and pancreatic cancer, which combines the chemotherapy drug paclitaxel with protein albumin (UK). Paclitaxel has low solubility in water but provides potent anticancer efficacy by suppressing microtubule dynamic to block the progression of mitosis and prevent cell division, while vehicle albumin enables paclitaxel delivery with a higher administration dose compared to conventional, solvent-based formulation (Cremophor®) and thus exert significantly better therapeutic efficacy (Gradishar, 2006, Manfredi and Horwitz, 1984).

ADCs are another new class of therapeutic formulations that enable cytotoxic agents the targeting abilities by combining with cancer-specific monoclonal antibodies (mAbs) (Hamilton, 2015). To date, thirteen ADCs (such as Mylotarg, Adcetris, Kadcyla, and Trodelvy) have been approved by the FDA and all of them are used to treat cancer, suggesting tremendous promise for the ADCs in targeted cancer therapies. Take Kadcyla for example, which consists of the humanised monoclonal antibody trastuzumab (Herceptin) and the natural-originated cytotoxic agent DM1 (a derivative of plant natural product and microtubule disrupting agent maytansine), it has been used clinically to treat HER2+ BC while superior activity over Herceptin have been observed (Lewis Phillips et al., 2008). Trastuzumab enables the delivery of DM1 to tumour

cells as it is capable of selectively binding to the HER2 receptor (in HER2-overexpressing tumour cells), meanwhile, trastuzumab itself retains the ability to inhibit HER2-mediated signal transduction and activating antibody-dependent cell-mediated cytotoxicity (Junttila et al., 2011, Lewis Phillips et al., 2008). Maytansine is a potent antimicrotubule agent first isolated from the Ethiopian shrub *Maytenus serrata*, and DM1 is 25- to 270-fold more cytotoxic than paclitaxel and 180- to 4,000-fold more cytotoxic than doxorubicin (Martínez et al., 2016, Kupchan et al., 1977, Junttila et al., 2011). Apoferritin (AFt) represents a promising ADC delivery vehicle with distinct advantages in overcoming mechanisms of drug resistance mediated by ATP-binding cassette protein pumps, such as P-glycoprotein (Pgp) (Abuzaid et al., 2022). These pumps, which have co-evolved to mitigate damage from toxic natural products, are key contributors to multidrug resistance (MDR). For instance, encapsulation of the toxic alkaloid jerantinine A within AFt demonstrated significantly enhanced anticancer activity and improved cancer selectivity in a panel of BC cell lines (Qazzaz et al., 2016, Abuzaid et al., 2022).

3.2.1.2 Cell count assay

The cell count assays were conducted to corroborate the results of MTT assays since MTT assay measures the mitochondrial function of cells but does not directly measure cell number or viability. Cell counts were performed following 72h exposure of cells to test compounds. Triple or more independent repeats (n=2 internal repeats) were performed on **3** against MCF-7, HCT116, two independent repeats were performed on **2** and **4** against MCF-7, HCT116, while only one independent repeat (n=2 internal repeats) was performed on **3** against HT-29, MDA-MB-468, U373V, U373M and A549. GI₅₀ values for compounds **2**, **3** and **4** generated from MTT assays guided compound concentrations adopted in cell count assays. Concentrations of $1 \times \text{GI}_{50}$ applied were 0.25 µg/mL **3** (~0.207 µM) for MDA-MB-468, U373V, U373M, 0.5 µg/mL **3** (~0.414 µM) for MCF-7, HCT-116, 0.5 µg/mL **4** (~0.362 µM) for A549, 1.0 µg/mL **2** (~0.966 µM) and **4** (~0.725 µM) for MCF-7, HCT-116 or A549, 2.5 µg/mL **3** (~2.070 µM) for HT-29.

The representative graphs of individual cell count assays are shown in **Figure 3.5** and the combined results are presented in **Figure 3.6**, which reveal that compounds **2** and **4** at the concentration of $\sim 1 \times \text{GI}_{50}$ caused net cytotoxicity in MCF-7 and HCT-116, as fewer cells were

recorded than were initially seeded. It is noteworthy that **3** at the concentration of $1 \times \text{GI}_{50}$ inhibited the cells' growth $>50\%$ in HCT-116, while **3** caused cytotoxicity in MCF-7 at $2 \times \text{GI}_{50}$ (**Figure 3.5**). However, this may be due to MCF-7 is more sensitive to **3** when compared to HCT-116 and the applied concentration $1 \times \text{GI}_{50}$ was $\sim 0.414 \mu\text{M}$ **3**, which is slightly higher than the exact GI_{50} concentration of **3** against MCF-7 (determined by MTT assays: $0.300 \mu\text{M}$) but lower than that of **3** against HCT-116 ($0.585 \mu\text{M}$). And this hypothesis may be possibly confirmed by the cell count results of **2** and **4**, that the applied $1 \times \text{GI}_{50}$ concentrations of them caused cytotoxicity in both MCF-7 and HCT-116 cell lines and the applied concentrations of **2** and **4** are slightly higher all the exact $1 \times \text{GI}_{50}$ concentrations, except for **2** against MCF-7 (**Figure 3.6**).

To summarize, **3** at $\sim 1 \times \text{GI}_{50}$ appears to induce cytotoxicity in MCF-7, MDA-MB-468, U373V, U373M cell lines, and inhibited growth of HCT 116 and HT-29 cells by $>50\%$. **4** at $\sim 1 \times \text{GI}_{50}$ induced cytotoxicity in MCF-7 and HCT-116 and caused $>50\%$ A549 growth inhibition. The concentration of $\sim 2 \times \text{GI}_{50}$ **3** and **4** appeared to cause significant cytotoxicity against all tested cell lines, while **2** induced significant cytotoxicity against all tested cell lines at the concentration of $\sim 1 \times \text{GI}_{50}$.

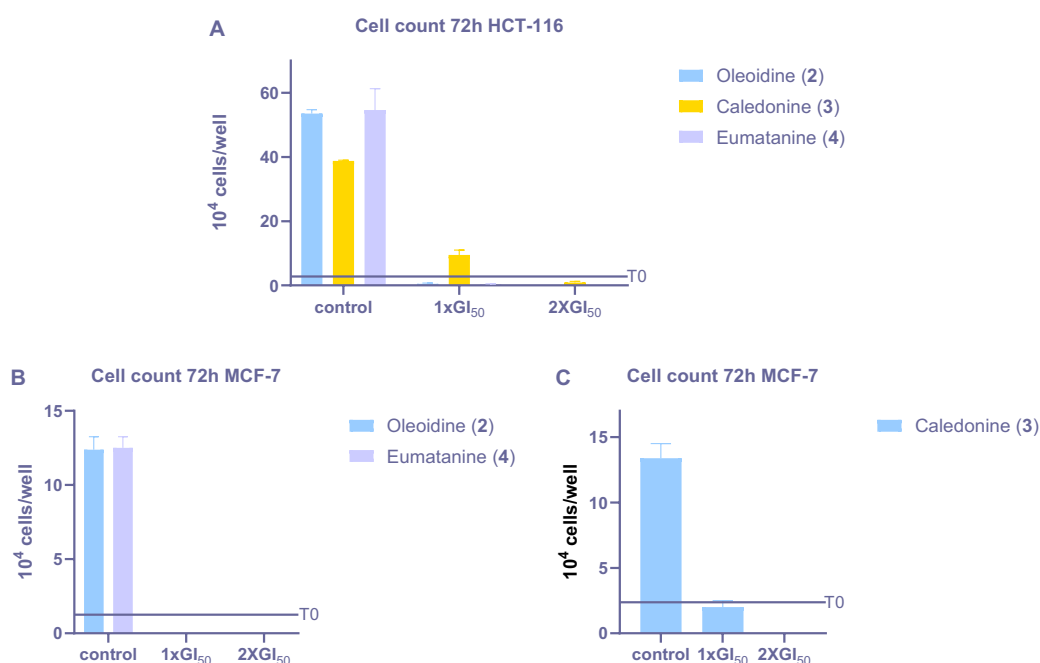


*Figure 3.5 Representative results of growth inhibitory effects of compounds **2**, **3** and **4** on HCT-116 (A), **2**, **4** (B) and **3** (C) on MCF-7 cell lines ($n=2$ internal repeats, 3 external repeats), the Y-axis reveals the cell numbers (equal to cell count $\times 10^4$) per mL. Cells were seeded at a density of 2×10^4 cells/well and incubated overnight before treating with **3** at 0, 1 \times , and 2 $\times \text{GI}_{50}$ (72h). Cells were harvested and counted by haemocytometer or cell counter.*

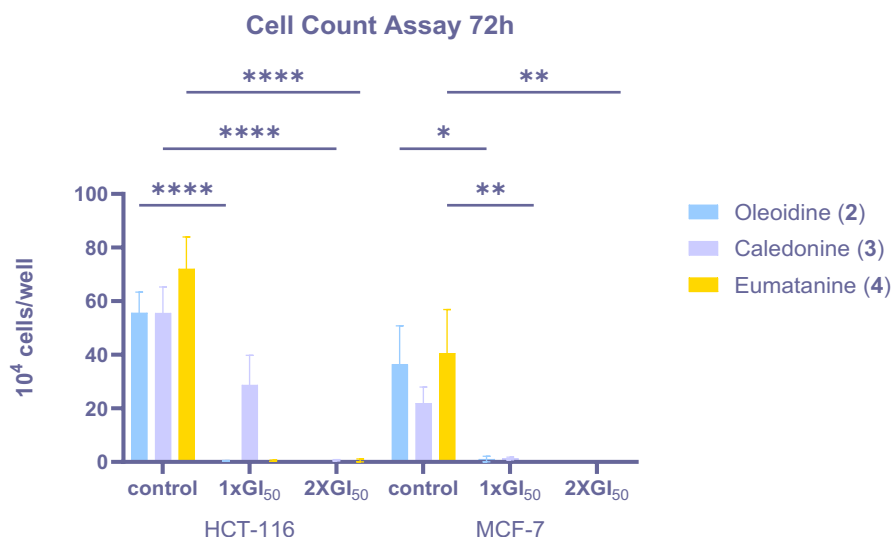


Figure 3.6 Effect of compounds **2**, **3** and **4** on cell growth (72h); mean \pm SEM from ≥ 2 independent trials where $n=2$; the Y-axis reveals the cell numbers (equal to cell count $\times 10^4$) per mL. Cells were seeded at a density of 2×10^4 cells/well and incubated overnight before treating with compounds **2**, **3** and **4** at 0, 1 \times , and 2 \times GI₅₀ (72h). Cells were harvested and counted by haemocytometer or cell counter.

3.2.1.3 Clonogenic assay

Clonogenic assays were conducted to examine the ability of test agent to kill cells and/or prevent progeny colony formation following a brief challenge (e.g. 24h) with test agent. This assay can reveal if the test agent is cytotoxic (in which situation fewer colonies than cells seeded will be observed) or cytostatic (in which situation similar colony numbers to cells seeded will be observed but with smaller size or fewer rounds of proliferation). Triple or more independent assays were performed on compound **3** against MCF-7, HCT116, U373V, and U373M, two independent assays were performed on compounds **2** and **4** against MCF-7, HCT116, while only one independent assay was performed on all the other experiments. Similar to the cell count assay, estimated GI₅₀ of compounds **2**, **3** and **4** values calculated from MTT assays were used as reference guides: while concentrations of 1 \times GI₅₀ applied were 0.25 μ g/mL **3** ($\sim 0.207 \mu$ M) for MDA-MB-468, U373V, U373M, 0.5 μ g/mL **3** ($\sim 0.414 \mu$ M) for MCF-7, HCT-116, 0.5 μ g/mL **4** ($\sim 0.362 \mu$ M) for A549, 1.0 μ g/mL **2** ($\sim 0.966 \mu$ M) and **4** ($\sim 0.725 \mu$ M) for MCF-7, HCT-116 or A549, 2.5 μ g/mL **3** ($\sim 2.070 \mu$ M) for HT-29.

The representative results of MCF-7 and HCT-116 colony counts following 24h exposure of cells to compounds **2**, **3** and **4** are shown in **Figures 3.7** and **3.8**, clearly demonstrating that all three compounds are cytotoxic agents. At concentrations equivalent to 1 \times GI₅₀, **2** and **4** induced

almost 100% colony growth inhibitory effects in MCF-7 and HCT-116 cells, while **3** exhibited an unstable colony growth inhibitory effect, i.e. colony formation was inhibited ranging from 100% to ~30% in MCF-7 and from 100% to ~80% in HCT-116 cells. **Figure 3.8** shows examples of MCF-7 and HCT-116 colonies formed in 6-well plates following initial seeding at 250cells/well exposure of cells (24h) to compounds **2**, **3**, **4** and the subsequent incubation (8-10 days). It is noteworthy that almost no colonies were observed in wells that treated with $1 \times GI_{50}$ compounds **2**, **3** or **4** against all tested cell lines (**2**: MCF-7, HCT-116; **3**: MCF-7, HCT-116, A549; **4**: MCF-7, HCT-116, HT-29, MDA-MB-468, U373V, and U373M), except for **3** against MCF-7 where $2 \times GI_{50}$ induced absolute colony growth inhibitory effect (**Figure 3.7**). Interestingly, **3** caused cytotoxicity in MCF-7 at $\sim 1 \times GI_{50}$ but in HCT-116 at $\sim 2 \times GI_{50}$ according to the cell count assay, while in clonogenic assays **3** caused absolute colony growth in HCT-116 at $\sim 1 \times GI_{50}$ but in MCF-7 at $\sim 2 \times GI_{50}$, suggesting that although MCF-7 is most sensitive to **3** (according to the result of MTT assays) and the applied $1 \times GI_{50}$ concentration of **3** is slightly higher than the exact $1 \times GI_{50}$ concentration against MCF-7, the ability of **3** preventing MCF-7 colony formation is somewhat inferior compared to **3** against other cell lines.

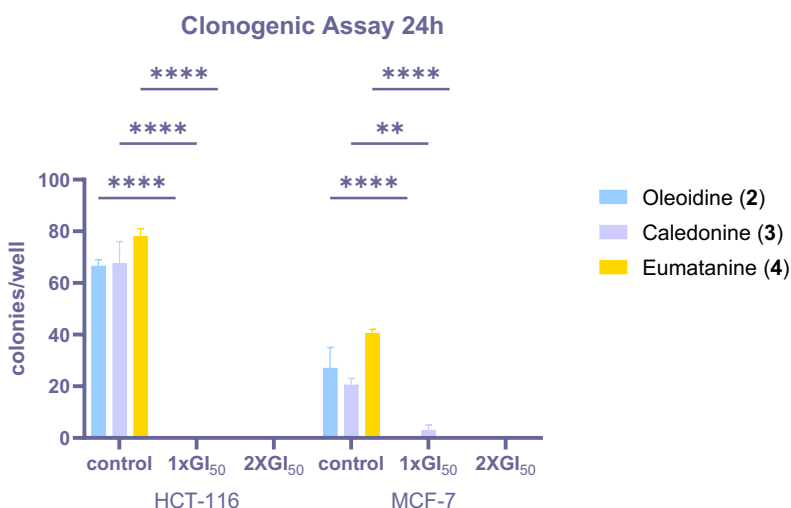


*Figure 3.7 Effects of compounds **2**, **3** and **4** on colony formation against cell lines MCF-7 and HCT-116 (n=2 internal repeats, assays shown in this graph were performed at the same period using the same passage of cells). Compounds **2**, **3** and **4** exhibited significant inhibition of colony formation at concentrations of $\sim 1 \times$ and $2 \times GI_{50}$ values respectively, as determined by MTT assay.*

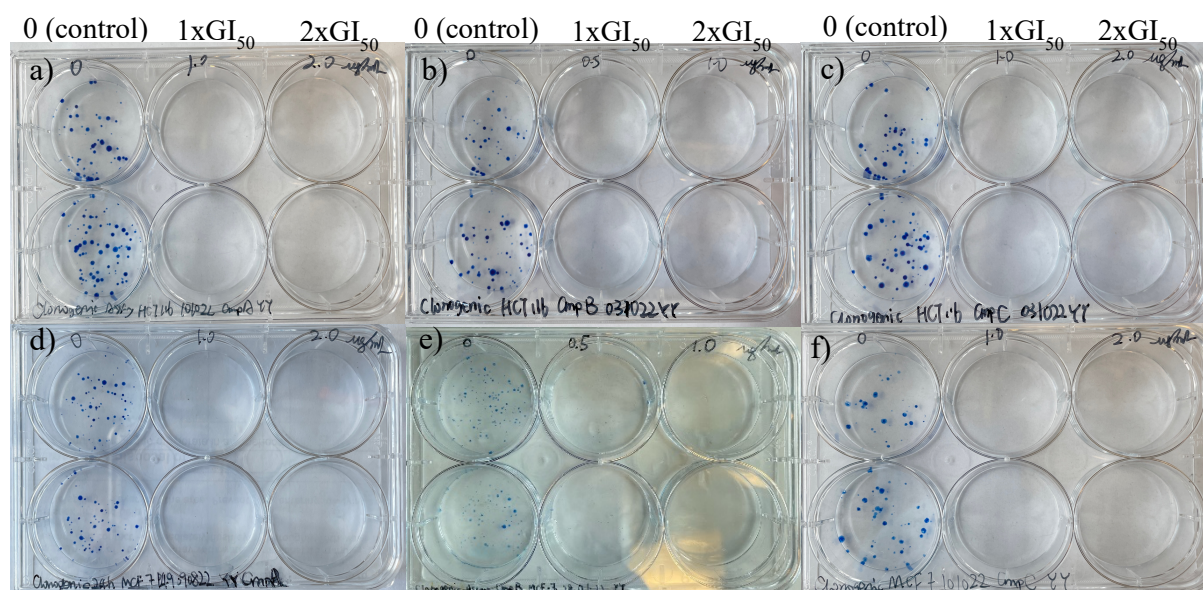


Figure 3.8 Representative photograph showing the effect of compounds **2**, **3** and **4** on HCT-116 (a, b, c) and MCF-7 (d, e, f) colony formation at 0, 1 × GI₅₀ and 2 × GI₅₀.

3.2.2 Cellular Mechanism of caledonine (**3**) and eumatanine (**4**)

3.2.2.1 Caledonine and eumatanine induced phase-independent apoptotic cell death

Annexin V-FITC/PI assays

After confirming that compounds **3** and **4** possess the ability to inhibit cancer cell proliferation and colony formation, their activity was further evaluated in terms of proapoptosis in MCF-7 and HCT-116. The apoptosis assay in this study combined the FITC annexin V and PI, which enables the identification of early apoptotic cells (PI negative, FITC Annexin V positive), late stage apoptotic cells (PI positive, FITC Annexin V positive), as well as viable cells (PI negative, FITC Annexin V negative)(Vermes et al., 1995).

Apoptosis assays were first conducted on compound **3** against MCF-7 and HCT-116, and representative results (**3** following in 24h and 72h exposure on MCF-7) exhibited in **Figure 3.9** shows that a special cluster of events (circled in red) appeared in the late stage apoptotic cell death area (PI+FITC+), suggesting that **3** at 2 × GI₅₀ (1.0 μg/mL; ~0.828 μM) induced apoptosis in MCF-7 and HCT-116 cells. Interestingly, although the dot graphs of both 24h and 72h exposure of **3** shows the induction of late stage apoptosis (**Figure 3.9ab**), according to the summary in **Figure 3.9c**, the increase of late stage apoptotic cell death was only recorded after

72h exposure of **3** on MCF-7, and the differences between control and treated groups are not significant ($p>0.5$) for both cell lines after 24h or 72h exposure. However, the method was further optimised after the evaluation of compound **3**, as it is obvious from **Figure 3.9** that the control groups possess a large number of apoptotic events in PI+FITC+ area, which means a great number of cells were undergoing apoptosis even without the drug addition. In this case, the way of collecting cells after trypsinisation was optimised, and all procedures thereafter were performed on ice to prevent cell death.

For the detection of apoptosis induced by **4** in HCT-116 and MCF-7, clear late-stage apoptotic cell death (PI+FITC+) was recorded in both cell lines after exposing to **4** at $2 \times \text{GI}_{50}$ ($2.0\mu\text{g/mL}$, $\sim 1.449\mu\text{M}$) for 24h ($p\leq 0.0002$), and at $1 \times \text{GI}_{50}$ ($1.0\mu\text{g/mL}$, $\sim 0.725\mu\text{M}$) for 72h ($p\leq 0.0001$). Interestingly, there was no significant early-stage apoptotic death (PI-FITC+) recorded for both cell lines after 24h and 72h exposure to **4** at the same concentrations. Although **4** at concentration of $1 \times \text{GI}_{50}$ caused no significant late-stage apoptosis in both cell lines following a 24-h exposure, it is obvious in **Figure 3.10b** that more late-stage apoptosis were induced in MCF-7 (ns, $p=0.2220$) when compared to HCT-116 (ns, $p=0.9889$). However, the data for HCT-116 cells treated with **4** for 24h ($n=2$) and for MCF-7 cells treated with **4** at $2 \times \text{GI}_{50}$ are based on one individual trial. The representative results of **4** against HCT-116 and MCF-7 are presented in **Figure 3.10**, where an increasing number of events showed a trend to travel to late stage apoptotic cell death (PI+FITC+) associated with the elevated concentration of **4**, and as a result of method optimization only a small number of events appeared in PI+FITC+ area for control groups. It is note worthy that the ability of **4** at $2 \times \text{GI}_{50}$ to induce late stage apoptotic cell death after 72h exposure is even higher than that of $5 \times \text{GI}_{50}$ vincristine (positive control) in both cell lines (**Figure 3.10**).

To sum up, **4** at concentration of $1 \times \text{GI}_{50}$ caused significant late stage apoptosis ($p<0.0001$) in HCT-116 and MCF-7 after 72h exposure, and following 72h exposure, $2 \times \text{GI}_{50}$ **4** induced higher levels of apoptosis in both cell lines when compared to $5 \times \text{GI}_{50}$ vincristine. Enhanced apoptosis in cancer cells may indicate that the apoptotic signalling pathways have been re-established and NP **4** have potential to eradicate cancer cells. Additionally, **3** slightly induced apoptotic cell death, but further reapeats are required after optimization of the method. Possible reasons for not detecting early-stage apoptosis should be considered, such as the extent of

DNA damage being catastrophic enough to trigger immediate cell death, or cell death may not only be caused by apoptosis but also a consequence of non-apoptotic cell death modes (e.g. senescence, paraptosis or autophagic cell death).

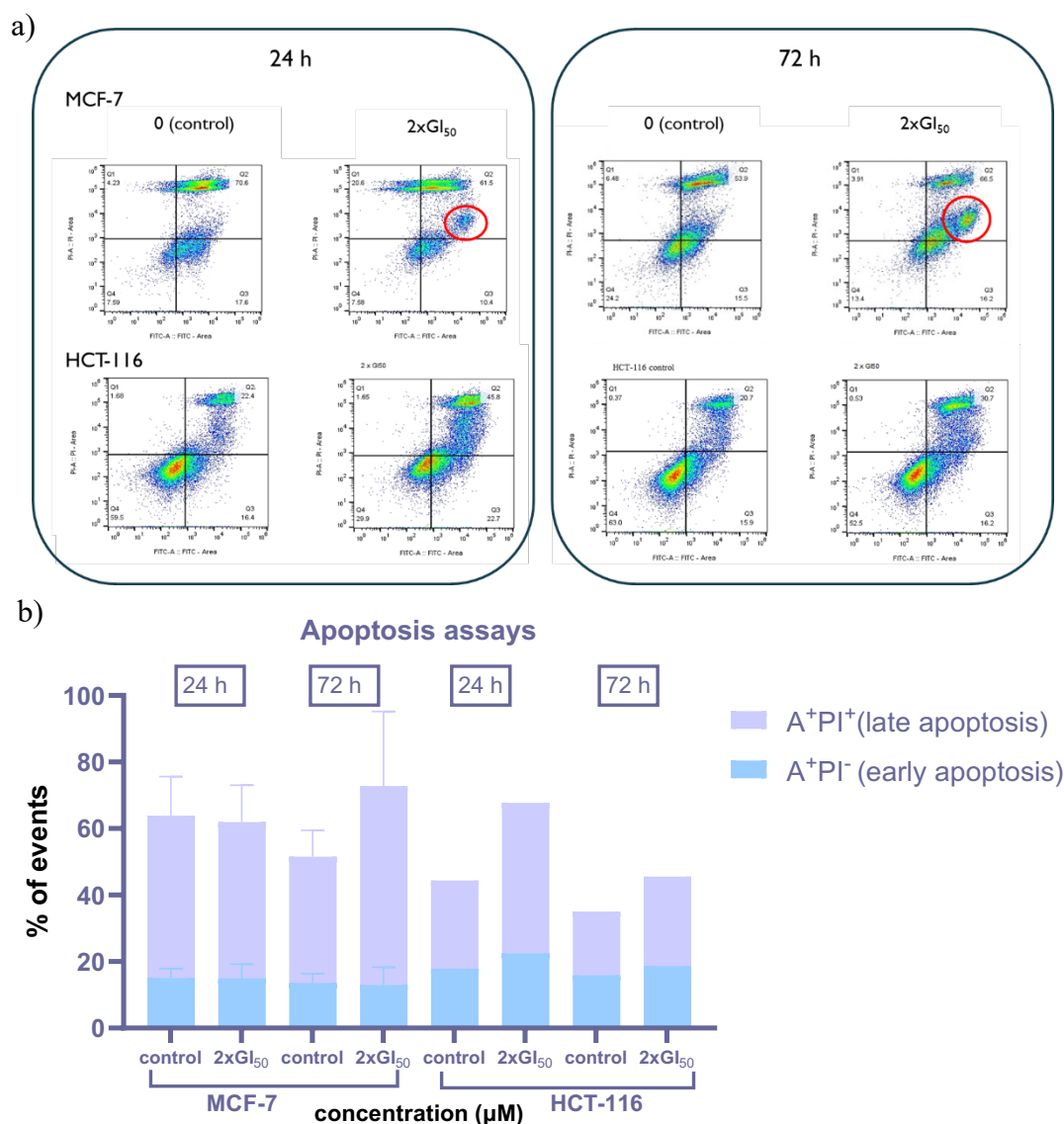


Figure 3.9 (a) Effect of $\sim 0.828 \mu\text{M}$ caledonine (**3**) (24 and 72h) on MCF-7 and HCT-116 apoptosis; X-axis is FITC, Y-axis is PI; ≥ 3 independent trials performed where $n=2$ on MCF-7, only one independent trial performed on HCT-116 ($n=2$); $>10,000$ events recorded per sample; (b) summary of the effect of $\sim 0.828 \mu\text{M}$ caledonine (**3**) (24h and 72h) on MCF-7 and HCT-116 apoptosis.

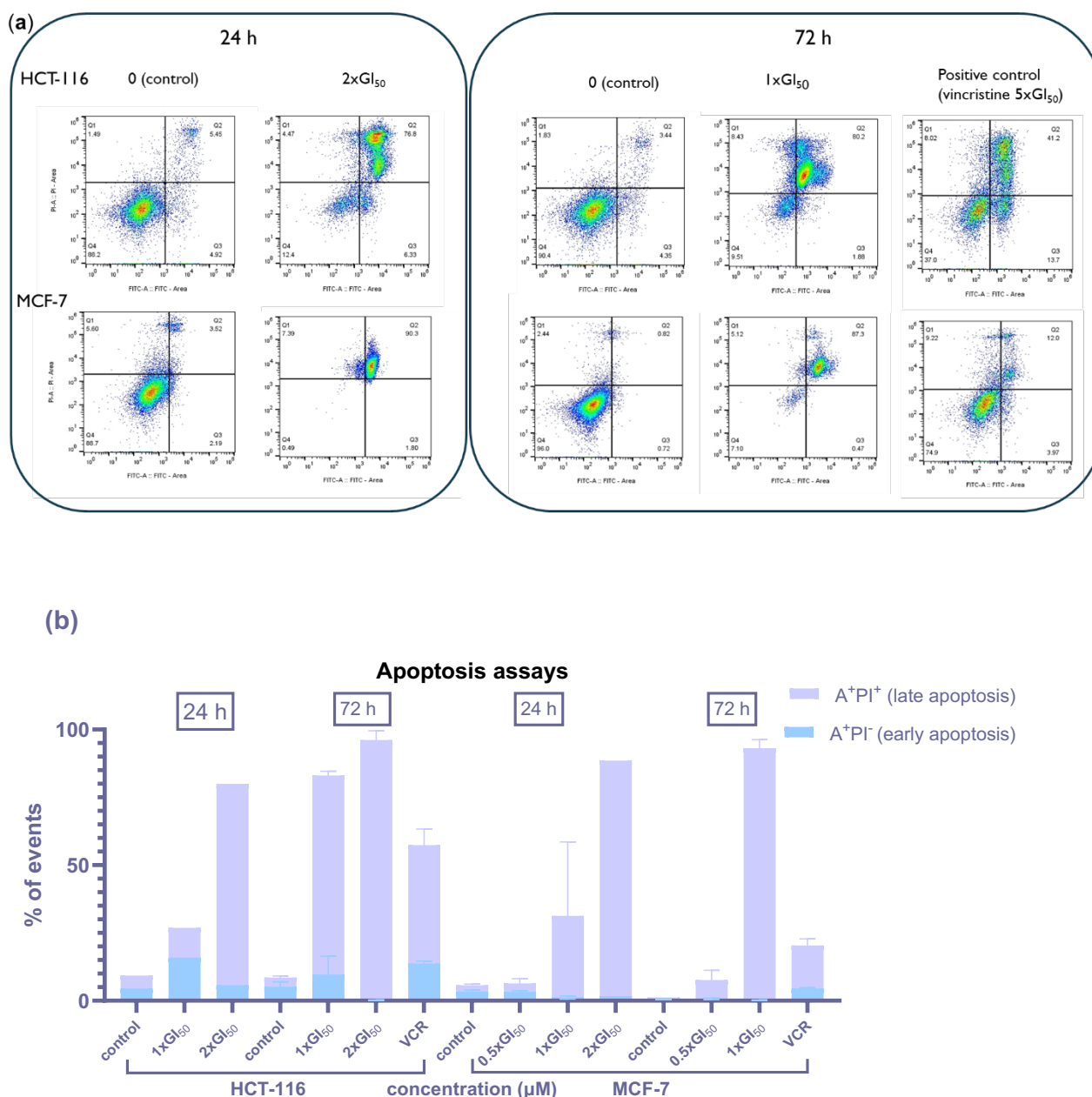


Figure 3.10 (a) Effect of ~ 0.363 , ~ 0.725 and $\sim 1.449 \mu\text{M}$ eumatanine (**4**) (24 and 72h) on HCT-116 and MCF-7 apoptosis; X-axis is FITC, Y-axis is PI; ≥ 3 independent trials performed where $n = 2$, except one trial for HCT-116 vs **4** - 24h and MCF-7 vs **4** - 24h at $2 \times \text{GI}_{50}$, two trial for MCF-7 vs **4** - 24h at $0.5 \times \text{GI}_{50}$; $> 10,000$ events recorded per sample; (b) summary of the effect of ~ 0.363 , ~ 0.725 and $\sim 1.449 \mu\text{M}$ eumatanine (**4**) (24h and 72h) on HCT-116 and MCF-7 apoptosis.

Evading apoptosis or apoptosis-resistance is a hallmark of cancer (Hanahan and Weinberg, 2000). Imbalance between pro-apoptotic signals (e.g. cytochrome-c, AIF, and death receptors TNFR1, FAS) and anti-apoptotic signals (e.g. BCL2 (group I), c-FLIP, IAP) is a vital mechanism for malignant cells to evade apoptosis (MA and R, 2008). Other mechanisms include decreased caspases' activity and blocked death receptor signalling (Fink Susan and

Cookson Brad, 2005, Lavrik et al., 2005). Apoptosis-evasion contributes to carcinogenesis, and apoptosis-induction is a valid strategy to treat cancer. Therapies capable of re-establishing apoptotic signaling pathways, enhancing apoptosis, or inducing alternative mechanisms of cancer cell death hold significant potential for effective cancer therapy.

Principally, apoptosis follows either intrinsic pathways (mitochondrial pathway and endoplasmic reticulum (ER) pathway) or extrinsic pathways (death receptor pathway), triggered by cellular stress, DNA damage, hypoxia, and immune surveillance mechanisms (Carneiro and El-Deiry, 2020). The intrinsic mitochondrial pathway, as the most common mechanism of apoptosis in vertebrates, can be positively regulated by proapoptotic BCL-2 family members such as BAX, BAK, BIM, BID, PUMA and negatively regulated by the anti-apoptotic BCL-2 family members such as BCL-XL, BCL2, A1 and MCL1 (Breckenridge and Xue, 2004). On the other hand, BCL-2 family proteins modulate mitochondrial outer membrane permeabilization (MOMP), and normally BAX and BAK trigger MOMP with the release of cytochrome c into the cytoplasm, which can engage caspase-9 and activate caspases-3 and 7, ultimately leading to apoptosis (Green and Llambi, 2015, Breckenridge and Xue, 2004, Garrido et al., 2006). Simultaneously with the release of cytochrome c, two other proapoptotic proteins are released from mitochondria, namely Smac and Omi, which can engage caspase inhibitor X-linked inhibitor of apoptosis (XIAP; **Figure 3.11**) (Eckelman et al., 2006).

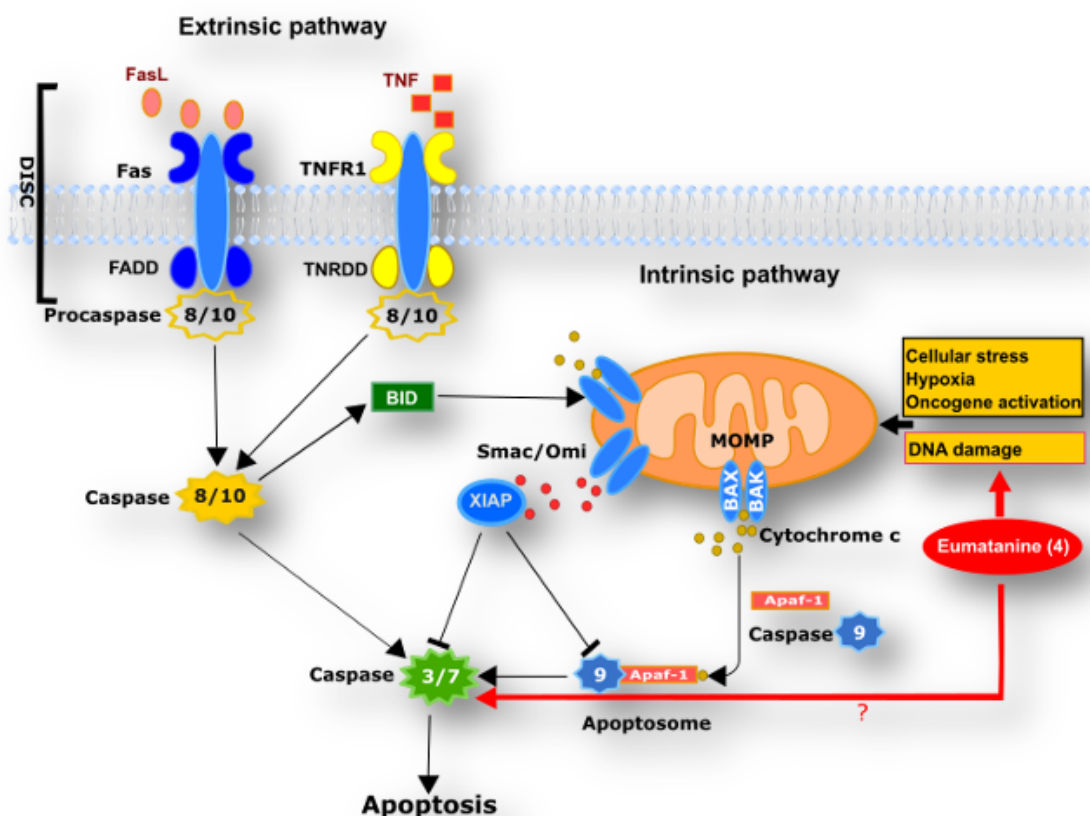


Figure 3.11 The extrinsic and intrinsic apoptotic pathways. The extrinsic pathway is activated through the binding of death receptors, such as FAS and TNFR1, to their corresponding ligands, including FasL and TNF. This interaction recruits the adaptor protein FAS-associated death domain (FADD) and the initiator procaspases-8 and -10, culminating in the formation of the death-inducing signaling complex (DISC). The assembly of DISC facilitates the dimerization and subsequent autoactivation of the initiator caspases. These activated caspases then cleave and activate the executioner caspases-3 and -7, driving the apoptotic process unless inhibited by X-linked inhibitor of apoptosis protein (XIAP). The intrinsic pathway is initiated in response to various intracellular stress signals that influence interactions among BCL-2 family proteins, ultimately regulating the activation of the BCL-2 effector proteins BAX and BAK. Once activated, BAX and BAK induce mitochondrial outer membrane permeabilization (MOMP), resulting in the release of proapoptotic proteins from the intermembrane space. Among these, cytochrome c (Cyt c) binds to APAF1, promoting its oligomerization and leading to the formation of the apoptosome. This complex recruits and activates initiator caspase-9, which subsequently cleaves and activates the executioner caspases-3 and -7. Concurrently, Smac/DIABLO is released from the mitochondrial intermembrane space along with Cyt c and acts to inhibit the X-linked inhibitor of apoptosis protein (XIAP), thereby promoting apoptosis. The intrinsic and extrinsic pathways are interconnected, as caspase-8 from the extrinsic pathway can cleave the BH3-only protein BID, producing its active form, which subsequently activates BAX and BAK, leading to intrinsic apoptosis. Eumatanine (4) has been shown to activate caspases-3/7 and induce DNA damage, as reported in this study. However, the specific cell death pathway involved remains unclear.

The extrinsic pathway initiates apoptosis by the ligation of death receptors (including proapoptotic death receptors TNFR1, FAS and TRAIL-DR4 and -DR5) and corresponding ligands at the cell membrane, followed by the recruitment of adaptor proteins such as FAS-associated death domain protein (FADD) and the activation of apoptosis-initiating protease caspases -8 and -9 (**Figure 3.11**) (Gonzalvez and Ashkenazi, 2010, Wilson et al., 2009,

Ashkenazi and Dixit, 1998). In this pathway, caspase-8 or 10 can then either cause the cleavage of the BH3-only protein BID and thereby drive the mitochondrial intrinsic pathway via BAX and BAK (mainly), or engage apoptosis by activating the executioner caspases -3 and -7 (minorly) (**Figure 3.11**) (Carneiro and El-Deiry, 2020, Ashkenazi and Salvesen, 2014). The p53 tumour suppressor can induce cell death (including cell cycle arrest, apoptosis and senescence) via both the extrinsic and intrinsic cell death pathways by regulating death receptors (such as FAS, DR5) in response to DNA damage, hypoxia, viral infection, or oncogene activation, and therefore the stabilized p53 protein is an important target of cancer therapy (el-Deiry, 1998). Additionally, the extrinsic pathway can be triggered by immune mechanisms (e.g. the expression of TRAIL (induced by interferon action) and cell death ligands (e.g. PD-L1) on natural killer (NK) cells and thereby lead to cell death (Sato et al., 2001, Pimentel et al., 2023). Various other cellular processes such as autophagy, anoikis, ferroptosis and regulated necrosis, can crosstalk with apoptotic signalling pathways in response to cancer therapeutics (e.g. proapoptotic agents) (Carneiro and El-Deiry, 2020).

Cell cycle analysis

The cell cycle consists of four distinct phases: G1 (gap 1), S (DNA synthesis), G2 (gap 2), and M (mitosis), which is responsible for cell division and regulated by cyclin-dependent kinases (CDKs) and their corresponding cyclins (Almalki, 2023). The G1/S and G2/M are two important checkpoints in cell cycle for the detection of DNA status, i.e. to ensure damaged DNA is repaired before it is passed on to daughter cells, otherwise cells with DNA damage that remain impaired may undergo apoptosis to prevent the propagation of mutation (Smith et al., 2020, De et al., 2020). Cell cycle regulation is critical for maintaining genomic stability and the dysregulation in cell cycle is tightly related to uncontrolled cell proliferation as well as the evasion of apoptosis, which are hallmarks of the development and progression of cancer. On the other hand, the induction of apoptosis in response to DNA damage can lead to cell cycle arrest, which eliminates damaged cells. Additionally, the activation of caspases in the context of DNA damage causes cell cycle arrest at G1 and pre-G1 phase accumulation in most cases.

Given that it is determined from the apoptosis assays above that compounds **3** and **4** caused apoptosis in HCT-116 and MCF-7, the cell cycle analysis is conducted to detect if they perturb cell cycle distribution by using a DNA intercalating stain (PI) and the flow cytometry technique.

PI is able to intercalate and bind strongly to cellular DNA and can be detected following the excitation of the argon-ion laser (blue light, 488nm), thus revealing the amount of DNA per cell/event and indicating the percentage of cells in each cell cycle phase. Flow cytometry is a sensitive technique, that is capable of analysing each cell and requires a relatively large number of cells when compared to the above assays (e.g. MTT, cell count, and clonogenic assays). Therefore, it is important to optimize the protocol of cell cycle analysis in terms of test agent concentrations (compounds **3** and **4**) and the seeding density of cells (MCF-7 and HCT-116), so as to capture cells in logarithmic cell growth.

The effects of compounds **3** and **4** on cell cycle progression were evaluated in MCF-7 and HCT-116 cells. For carcinoma cell line HCT-116, the treatment of **3** at concentrations of 0, $2 \times GI_{50}$ ($1.0 \mu\text{g/mL}$; $\sim 0.828 \mu\text{M}$), $3 \times GI_{50}$, and $4 \times GI_{50}$ resulted in similar cell cycle distributions, as the ratio of G1 and G2 peaks for all samples did not achieve significant differences, while the pre-G1 peak area gradually increased with increasing concentrations of **3** (**Figure 3.12a, b**).

As shown in **Figures 3.13** and **3.14**, similar results were observed for **3** and **4** in MCF-7 and HCT-116 cells, i.e. neither **3** nor **4** influenced the distribution of cells obviously in phases G1, S or G2 at majority of the concentrations tested at either 24h or 72h. However, as shown in the summary data (**Figure 3.15**), **4** caused no cell cycle phase arrest in G1, S or G2 phases in HCT-116 after 24h or 72h exposure and MCF-7 after 72h exposure, while significant ($p < 0.05$) cell cycle arrest in G1 phase was observed in MCF-7 after exposing to **4** for 24h, meanwhile just a slight increase was observed in the pre-G1 events (ns, $p = 0.9825$) (**Figure 3.15c**). In contrast, events in the pre-G1 phase increased gradually as **4** concentrations increased in either HCT-116 cells under all conditions or MCF-7 cells when the treatment time is 72h, for instance, $2 \times GI_{50}$ **4** caused almost 100% apoptotic cell death in MCF-7 following 72h exposure when there was only $\sim 3\%$ apoptotic cell death in control groups (**Figure 3.15ef**). And thus, subsequent cell cycle analysis of **4** against MCF-7 applied $0.5 \times$ and $1 \times GI_{50}$ experimental concentrations. Notably, **4** even induced a significant increase ($p < 0.0001$) in pre-G1 events at a concentration of $\sim 1 \times GI_{50}$ after 72h exposure in MCF-7 cells (**Figure 3.15d**).

Vincristine (VCR), an anti-cancer alkaloid derived from *Catharanthus roseus* (L.) G. Don (Madagascar periwinkle), was adopted as positive control causing significant G2 phase arrest in accordance with its microtubule-disruptive mechanism of action; **Figures 3.12 and 3.13** (Gidding et al., 1999). Notably, pre-G1 phase accumulation (<2N-DNA) and sustained G1-phase arrest were also observed in HCT-116 and MCF-7 cells by the addition of conofolidine, a bisindole alkaloid from the Malayan plant *Tabernaemontana corymbosa*, along with caspase activation, ROS generation, DNA damage. Interestingly, induction of apoptosis or senescence was observed in multiple carcinoma cell lines (including breast, colon and lung cancer) (Al-Hayali et al., 2024). This demonstrates that NPs may induce distinct cell fates; similarly, eumatanine (**4**) may trigger multiple cellular mechanisms resulting in cell death.

To summarize, cell cycle analyses revealed that **3** and **4** increased pre-G1 events dose- and time-dependently without perturbing cell cycle distribution in both cell lines for 72h treatment and in HCT-116 for 24h treatment. Interestingly, instead of causing an accumulation of pre-G1 phase events like in HCT-116 cells, $1 \times \text{GI}_{50}$ **4** significantly increased the G1 events ($p < 0.05$) and just slightly increased the pre-G1 events in MCF-7 cells after 24h exposure (ns, $p = 0.9825$) (**Figure 3.15c**), which may be due to greater initial seeding density for 24h exposure (2×10^5 for 24h assays, 1×10^5 for 72h assays), and thereby compounds added to give the same final concentration may exert a lower level of cytotoxicity on cells. Given that the same experimental conditions were applied, compound **4** likely exerts cytotoxic effects in HCT-116 and MCF-7 cells through distinct cell death mechanisms, potentially due to MCF-7 cells being caspase-3 null, which may prevent rapid apoptosis and instead trigger alternative pathways such as paraptosis or autophagy in response to oxidative stress and DNA damage (Jänicke, 2009). Similar results were obtained for 24h and 72h exposure to **4** against HCT-116, in which a significant increase was recorded in pre-G1 events ($p < 0.0001$) when treated with $\sim 2 \times \text{GI}_{50}$ (**Figure 3.15**). In this case, other reasons for not detecting cell cycle arrest should be considered, for example, the compound may not be cell cycle specific, or cell death may not be caused by apoptosis but may be a consequence of non-apoptotic cell death modes for example senescence, paraptosis or autophagic cell death. A pre-G1 population usually represents cells undergoing apoptotic cell death, and therefore further confirm the induction of apoptosis by compound **4**, corroborating the results of Annexin V-FITC/PI assays.

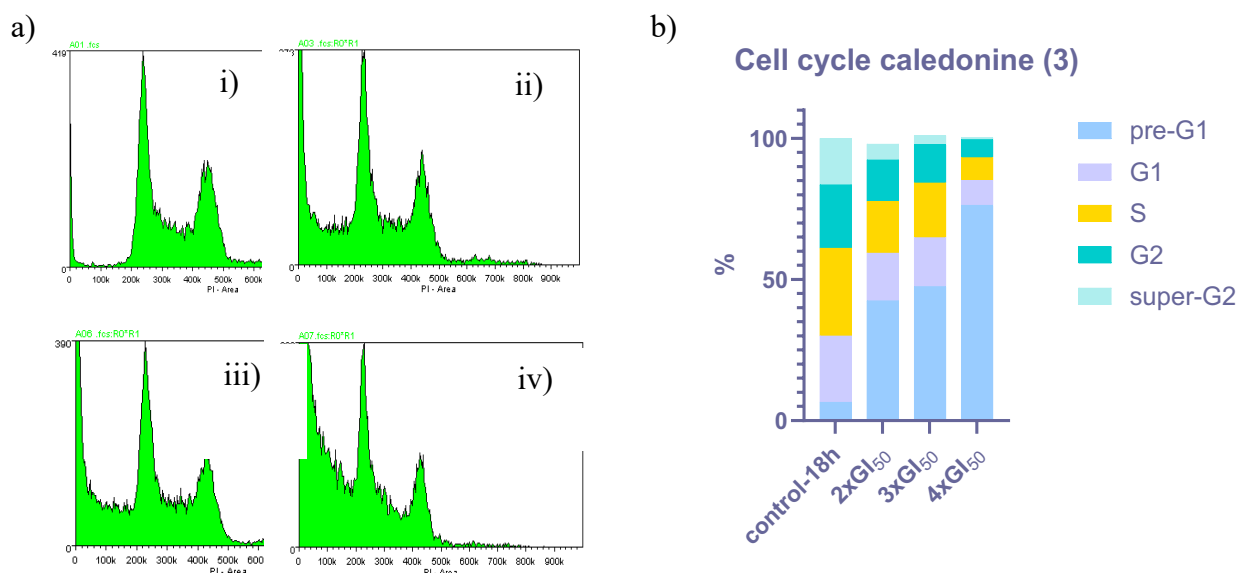


Figure 3.12 Effects of 0 (i), $2 \times GI_{50}$ ($1.0\mu\text{g/mL}$, ii), $3 \times GI_{50}$ ($1.5\mu\text{g/mL}$, iii), $4 \times GI_{50}$ ($2.0\mu\text{g/mL}$, iv) caledonine (3) following 18h exposure on HCT-116. Cells were seeded at the density of 1×10^6 cells/well using six-well-plates (control dishes were treated with blank media; $n=2$ internal repeats, 1 independent trial; 10,000 – 50,000 cells/events were analysed per sample).

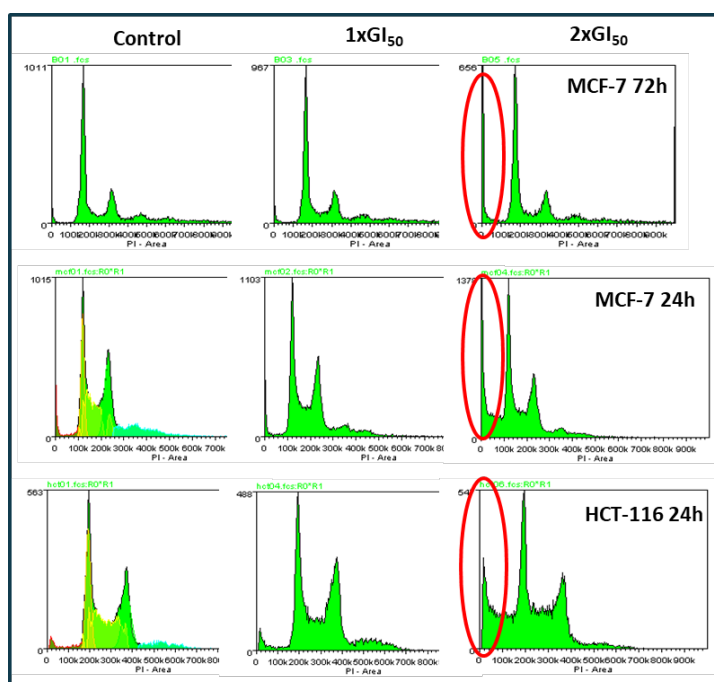


Figure 3.13 Effects of 0, $1 \times GI_{50}$ ($0.5\mu\text{g/mL}$), $2 \times GI_{50}$ ($1.0\mu\text{g/mL}$) caledonine (3) following 24h or 72h exposure on MCF-7 and HCT-116. Cells were seeded at the density of 1×10^6 cells/well using six-well-plates (control dishes were treated with blank media; $n=2$ internal repeats, ≥ 3 independent trials; 10,000 – 50,000 cells/events were analysed per sample)

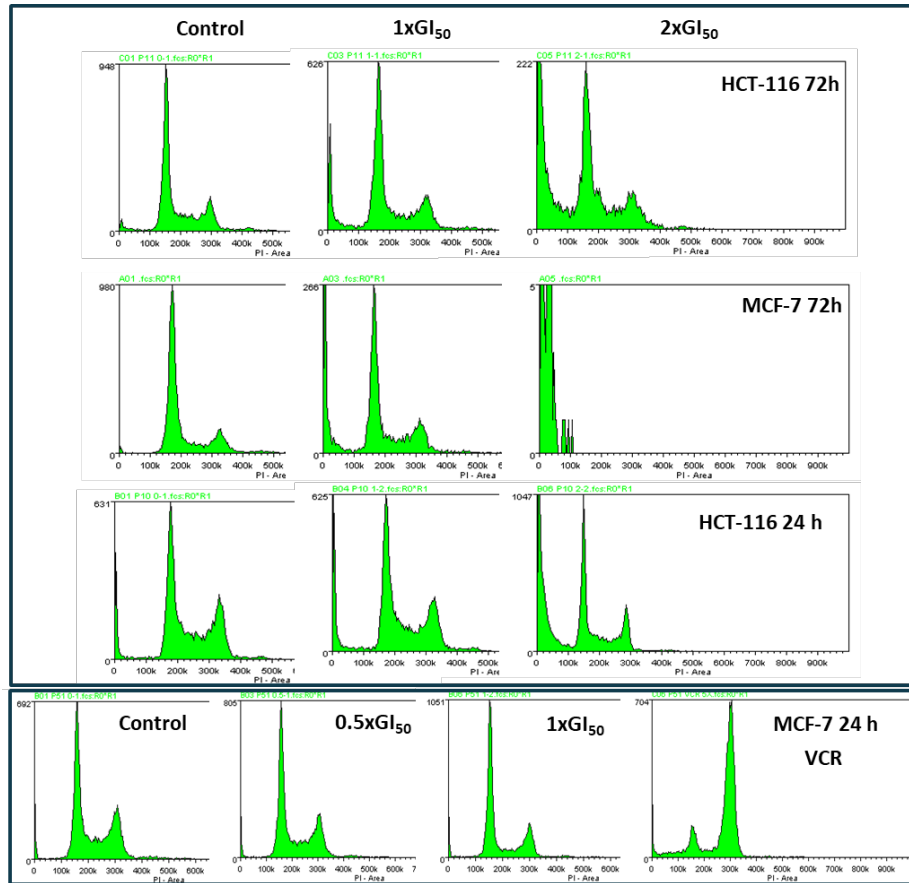
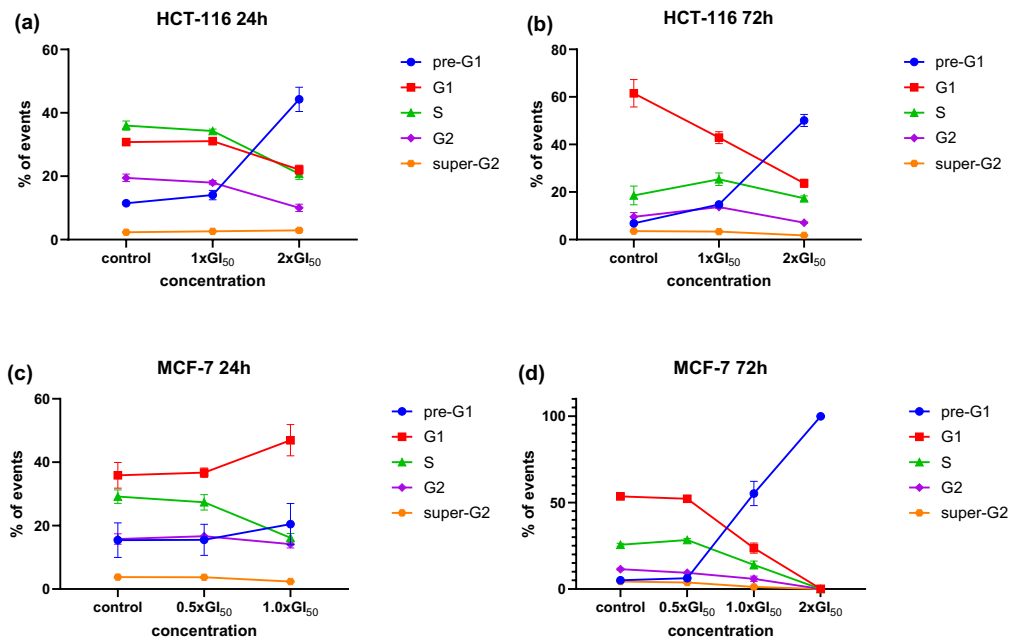


Figure 3.14 Effect of $1 \times$ and $2 \times$ GI_{50} compound eumatanine (**4**) (24 and 72h) on HCT-116 and $0.5 \times$, $1 \times$ and $2 \times$ GI_{50} eumatanine (**4**) (24 and 72h) on MCF-7 cell cycle; cells were seeded at the density of $1-2 \times 10^5$ cells/well using six-well-plates (control dishes were treated with blank media); mean \pm SEM from 3 independent trials where $n=2$; 10,000 – 50,000 cells/events were analysed per sample.



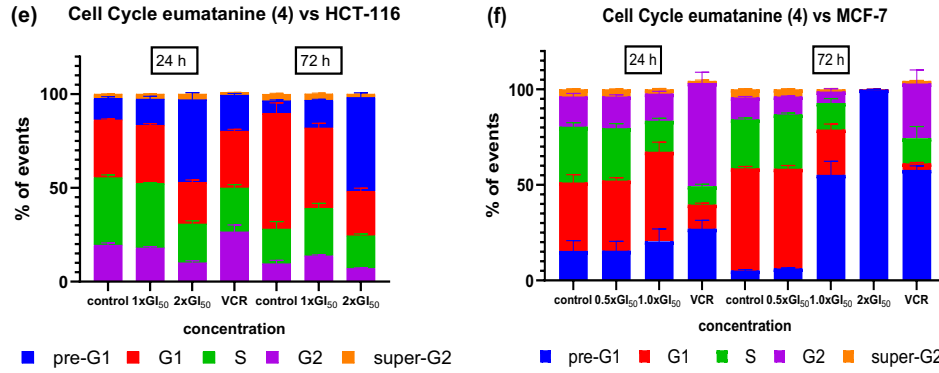


Figure 3.15 Summary of the effect of $1 \times$ and $2 \times$ GI₅₀ eumatanine (4) (24 and 72h) on HCT-116 and $0.5 \times$, $1 \times$ and $2 \times$ GI₅₀ 4 (24 and 72h) on MCF-7 cell cycle; cells were seeded at the density of $1-2 \times 10^5$ cells/well using six-well-plates (control dishes were treated with blank media); mean \pm SEM from 3 independent trials where $n=2$; 10,000 – 50,000 cells/events were analysed per sample.

G1/S and G2/M are two important checkpoints in the cell cycle that police DNA integrity, ensuring that damaged DNA is either repaired or cells with irreparable DNA damage are instructed to undergo programmed cell death (e.g. apoptosis). Upon detection of DNA damage, cell cycle arrest ensues, to stabilize the genome and prevent uncontrolled proliferation (Smith et al., 2020, De et al., 2020). Additionally, the G1/S checkpoint also ensures that the cell has adequate nutrients and growth factors for subsequent cell growth and division (Smith et al., 2020). The retinoblastoma (RB) protein (e.g. pRb, p107 (*RBL1*) and p130 (*RBL2*)) and transcription factor p53, are known as central tumour suppressors, both play an important role in the induction of apoptosis, senescence and the regulation of cell cycle, particularly in the G1 phase (Henley and Dick, 2012, Engeland, 2022). They crosstalk with cyclin-dependent kinase inhibitor p21/CDKN1A and manipulate transcription of genes that are involved in a variety of cell functions (e.g. MAP kinase MAP3K5/ASK-1 for cell division, the topoisomerase-binding protein TOPBP1 for DNA replication and repair) via p53-p21-RB signaling (Engeland, 2022).

Retinoblastoma (RB) modulates DNA replication and G1/S transition during the cell cycle by negatively regulating two positive regulators of cell cycle entry, namely CDKs and transcription factors E2F, while the interaction with E2F to form RB-E2F complexes is essential for repressing G1/S cell cycle genes (e.g. *CDK1*), DNA polymerase α (*POLA1*), cyclin A (*CCNA2*), thymidine kinase (*TK1*), *DHFR*, and *minichromosome maintenance complex component 3 and 5* (*MCM3/5*, DNA replication licensing factors) that are responsible for DNA synthesis, DNA replication and DNA repair (Henley and Dick, 2012, Helin et al., 1993). It is

notable that loss of RB function is observed in many tumors by various mechanisms (e.g. *RB1* mutation, RB proteolysis, loss of RB-E2F interaction), which gives rise to induction of cell division, defects in cell cycle exit, impaired ability to eliminate DNA damage and enter senescence, as well as positive regulation of cell-cycle-checkpoint control, particular at the G1/S transition, ultimately leading to cell cycle dysregulation and malignant proliferation (Engeland, 2022, Dyson, 2016).

p53, a widely studied tumour suppressor capable of inducing cell cycle arrest, and contributing to DNA repair, metabolic pathways' regulation, senescence- and apoptosis- induction, with the underlying mechanisms of transcriptional regulation of cell cycle genes (e.g. the apoptosis inducers *BAX*, *PUMA/BBC3*) (Miyashita and Reed, 1995, Nakano and Vousden, 2001). Similar to RB, p53 regulates the G1/S transition by repressing genes (e.g. p21), and p53 function is lost in > 50% of tumours, either consequence of p53 mutations, or disruption of the p53 pathway, for example the proteolysis of p53 induced by viral oncoproteins or *MDM2* overexpression (Engeland, 2022, Brugarolas et al., 1995). In the MTT assay, compound **3** exhibited potent cytotoxicity across all cell lines, with GI₅₀ values being slightly higher in wild-type p53-expressing cell lines (HCT-116, MCF-7, A549; range from 0.4 - 0.6μM) compared to mutant p53-expressing cell lines (MDA-MB-468, U373; range from 0.1 - 0.3μM), suggesting that the activity of **3** is independent of p53 status (Al-Hayali et al., 2024, Wasielewski et al., 2006, GUNTUR et al., 2010, Kaeser et al., 2004).

NP honokiol, a biphenolic compound isolated from *Magnolia* exerts anticancer activity by inducing apoptosis and autophagy in various cancer cell lines (e.g. ovarian cancer cells, human osteosarcoma cells, pancreatic cancer cells and B-cell chronic lymphocytic leukemia (B-CLL) cells) without causing cell cycle arrest in G1, S or G2/M phases (Huang et al., 2018, Battle et al., 2005, Arora et al., 2011, Lee et al., 2019). Instead, honokiol causes an accumulation in pre-G1 cell cycle phase and induce apoptosis via a variety of mechanisms, including modulating the adenosine monophosphate-activated protein kinase (AMPK), the ROS/ERK1/2 and the NF-κB signalling pathways, along with the activation of caspase-3, -7, and -9 and cleavage of PARP, as well as the generation of ROS (Arora et al., 2011, Lee et al., 2019, Huang et al., 2018, Battle et al., 2005).

3.2.2.2 Eumatanine (4) activated caspase 3/7 in MCF-7 and HCT-116

To further confirm the ability of **4** to induce apoptosis in MCF-7 and HCT-116, caspase3/7 assays were conducted to detect if caspase -3 or -7 is activated while **4** exerting cytotoxicity. Members of the caspase family of cysteine-aspartic acid-specific proteases play a key role in execution of apoptotic cell death. Caspases include the upstream initiators caspase-8, caspase-9, and caspase-10 in humans, as well as the downstream effectors caspase-3, caspase-6, and caspase-7 (Walsh et al., 2008). It has been reported that >400 substrates are proteolysed by apoptosis-associated caspases, among which are caspase-3 and caspase-7 major executioner caspases (Lüthi and Martin, 2007). The result of the caspases3/7 assay illustrated that the activities of caspases3/7 were significantly ($p<0.01$) induced by **4** at $1 \times \text{GI}_{50}$ ($\sim 0.725\mu\text{M}$) in MCF-7 and HCT-116 cells after 48 h exposure, further confirming that **4** caused apoptotic cell death in both MCF-7 and HCT-116 cells (**Figure 3.16**). Many anticancer drugs that derived from natural products induce apoptotic cell death by activating caspases. For example, doxorubicin and cisplatin are known to induce apoptosis via ROS generation and subsequent caspase activation (Octavia et al., 2012, García-Berrocal et al., 2007). Interestingly, although MCF-7 cells are deficient in caspase-3, a significant increase in the activity of casapase-3/7 was observed in these cells; similarly the styrylpyrone derivative (SPD) induced apoptotic cell death in MCF-7 cells through a caspase-7-dependent pathway (Lee et al., 2003, Jänicke, 2009).

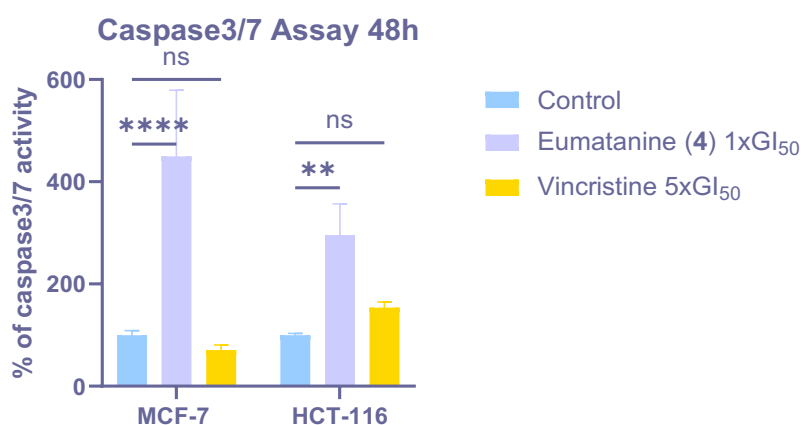


Figure 3.16 Effect of $1 \times \text{GI}_{50}$ eumatanine (**4**) (48h) on HCT-116 caspase activity; mean \pm SEM from ≥ 3 independent trials where $n=3$ (ns $p>0.05$, * $p<0.05$, ** $p<0.01$, *** $p<0.001$, **** $p<0.0001$ vs the control group.).

3.2.2.3 Eumatanine (4) induced ROS generation and DNA DSBs in MCF-7 and HCT-116

ROS, such as superoxide anion (O_2^-), hydrogen peroxide (H_2O_2), singlet oxygen, hydroxyl radical, and peroxy radical, arise from intracellular metabolic processes or external insult, mediating cell proliferation, differentiation, and migration, while playing a beneficial role in regulating normal cellular processes (i.e., redox signaling) and being implicated in physiological processes such as glucose homeostasis, inflammation, cellular lifespan, and the progression of diseases like carcinogenesis, cardiovascular disease, and neurodegeneration. (Tonelli et al., 2018, Rhee, 2006, Zhang et al., 2016, Rajendran et al., 2011). The role of excess ROS such as H_2O_2 has been connected to genomic (in)stability, regulation of transcription, and signal transduction, which may contribute to both tumour progression and cancer cell death (Alfadda and Sallam, 2012). H_2O_2 as the most stable ROS generated in cultured cells, has been utilised as a sensible biomarker to detect the ROS levels within cells and thus to evaluate how intracellular oxidative stress been affected by tested compounds or certain specific conditions (Newsholme et al., 2012).

Production of ROS was measured in HCT-116 and MCF-7 cell lines following the exposure to either 4 or vincristine. Significantly ($p < 0.01$) enhanced ROS were generated by 4 in treated HCT-116 (140%) and MCF-7 (174%) cells after 24h exposure at $1 \times GI_{50}$ ($\sim 0.725 \mu M$) (**Figure 3.17**). ROS are regarded as an important biomarker in cancer development that contribute not only to oncogenesis by the mediation of oxidative DNA damage, but also serving as targets for promising therapeutic strategies, such as modulating cellular redox status to manage cancer when ROS levels become excessive (Montero and Jassem, 2011). The toxic level of ROS contributes to the induction of apoptosis and DNA damage. The mechanism of ROS inducing apoptosis is engaging the intrinsic apoptotic pathway by causing mitochondrial dysfunction and the release of pro-apoptotic factors (e.g. cytochrome c), and then leading to caspase activation.

A significant number of natural anticancer agents generate ROS, an obligate facet of their mechanisms of action, and induce apoptosis in cancer cells, including etoposide, doxorubicin, taxanes (microtubule-stabilizing agents), cisplatin (an alkylating agent), and jerantinine B, with etoposide and doxorubicin being FDA-approved topoisomerase II inhibitors that cause DNA damage and evoke G2/M cell cycle arrest (Oh et al., 2007, Alexandre et al., 2006, Velma et al.,

2016, Choi et al., 2015, Schonn et al., 2010, Ehrlichová et al., 2012, Octavia et al., 2012, Qazzaz et al., 2016, Hande, 2008). Interestingly, doxorubicin caused both G1/S and G2/M arrest in MCF-7, NP 4 induced G1 phase arrest only after short-term exposure (24h) in MCF-7 cells, but caused no cell cycle arrest in HCT-116 cells, suggesting that doxorubicin and 4 may trigger similar mechanisms in MCF-7 cells, and also suggesting that NP 4 may trigger different mechanisms in distinct cell lines – according to their molecular machinery (Bar-On et al., 2007). Bar-on et al. reported that doxorubicin behaves differently in different BC cell lines, causing both G1/S and G2/M phase arrest in MCF-7, while inducing only G2/M phase arrest in MDA-MB-231. Additionally, in MCF-7, Skp2 was upregulated, p27 levels slightly reduced, and p53 and p21 levels increased, whereas in MDA-MB-231, p27 levels remained unchanged and cyclin B levels significantly increased, with the differential Skp2 expression attributed to arrest in different checkpoints of the cell cycle (Bar-On et al., 2007).

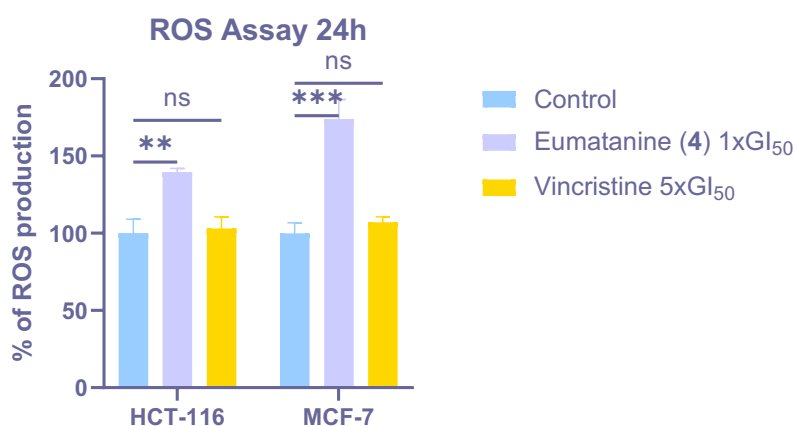


Figure 3.17 Effect of $1 \times GI_{50}$ eumatanine (4) (24h) on HCT-116 and MCF-7 ROS; mean \pm SEM from ≥ 3 independent trials where $n=2$ (ns $p>0.05$, * $p<0.05$, ** $p<0.01$, *** $p<0.001$, **** $p<0.0001$ vs the control group.).

Given that ROS induction is typically associated with DNA damage, as seen with doxorubicin and etoposide, it is important to determine if compound 4 causes DNA damage. Doxorubicin induces DNA damage either by inhibiting topoisomerase IIb or by intercalating with the strands, the latter typically occurring in regions rich in G-C base pairs (Yang et al., 2014, Chaires et al., 1987, Chaires et al., 1990). The formation of doxorubicin-DNA adducts has been shown to activate DNA damage responses and induce non-topoisomerase II cell death (Swift et al., 2006). Detection of DNA DSBs is a valuable diagnostic tool for identifying precancerous and cancerous cells and assessing cancer progression and therapeutic efficacy in carcinoma cells

(Hande, 2008). The DNA DSB is a serious DNA lesion that can be caused by exogenous or endogenous factors, such as cytotoxic agents, ROS, metabolic processes, deficient repair, telomere erosion and programmed biological processes, ultimately leading to cell death (e.g. apoptosis) through disturbance of genomic stability (Bonner et al., 2008). To detect and quantify DNA DSB in cells, a primary antibody against γ H2AX and a fluorescent secondary antibody were used, incorporated with flow cytometry, which is a sensitive method to allow the active distinction of cells based on a cell's particle density and fluorescence (Kuo and Yang, 2008). H2AX, regarded as a tumour suppressor, is a member of the H2A histone family and a key component in DNA repair (Bassing et al., 2003). Serine C-4 phosphorylation of H2AX (γ H2AX) forms in response to DNA double-strand break (DSB) damage, γ H2AX (phosphorylated H2AX) accumulates, surrounding the break sites, enabling the detection of individual DSBs by use of a γ H2AX antibody (Bonner et al., 2008, Kuo and Yang, 2008).

Figure 3.18 shows that **4** at $2 \times \text{GI}_{50}$ ($2.0\mu\text{g/mL}$, $\sim 1.449\mu\text{M}$) caused an obvious cluster of γ H2AX+ve HCT-116 and MCF-7 events increasing in number following 24h and 72h exposure, respectively. After 72h compound **4** treatment at $2 \times \text{GI}_{50}$, an extremely low level of events (~ 1500) was observed in HCT-116, and almost all events were apoptotic cells (**Figure 3.18**). Possible reasons for this include most cells being dead or undergoing apoptosis by then since only several small cell clusters remained attached to the bottom of plates after 72h treatment, according to microscopic observation. A similar phenomenon was observed in MCF-7 cells after exposure to $2 \times \text{GI}_{50}$ **4** for 24h, where fewer events were recorded compared to control groups, and in the positive group treated with vincristine, almost no events were observed (**Figure 3.18**). Selected data of γ H2AX detection is summarized in **Figure 3.19** ($2 \times \text{GI}_{50}$ **4**; HCT-116 (24h) and MCF-7 (72h) cells), which demonstrates that **4** at $2 \times \text{GI}_{50}$ triggered a significant increase of γ H2AX+ events in HCT-116 (24h) and a slight increase in MCF-7 (72h), suggesting **4** triggered DNA DSB to varying degrees in different cell lines, and caused cell death by perturbing DNA integrity.

HCT-116
24 h

HCT-116
72 h

MCF-7
24 h

MCF-7
72 h

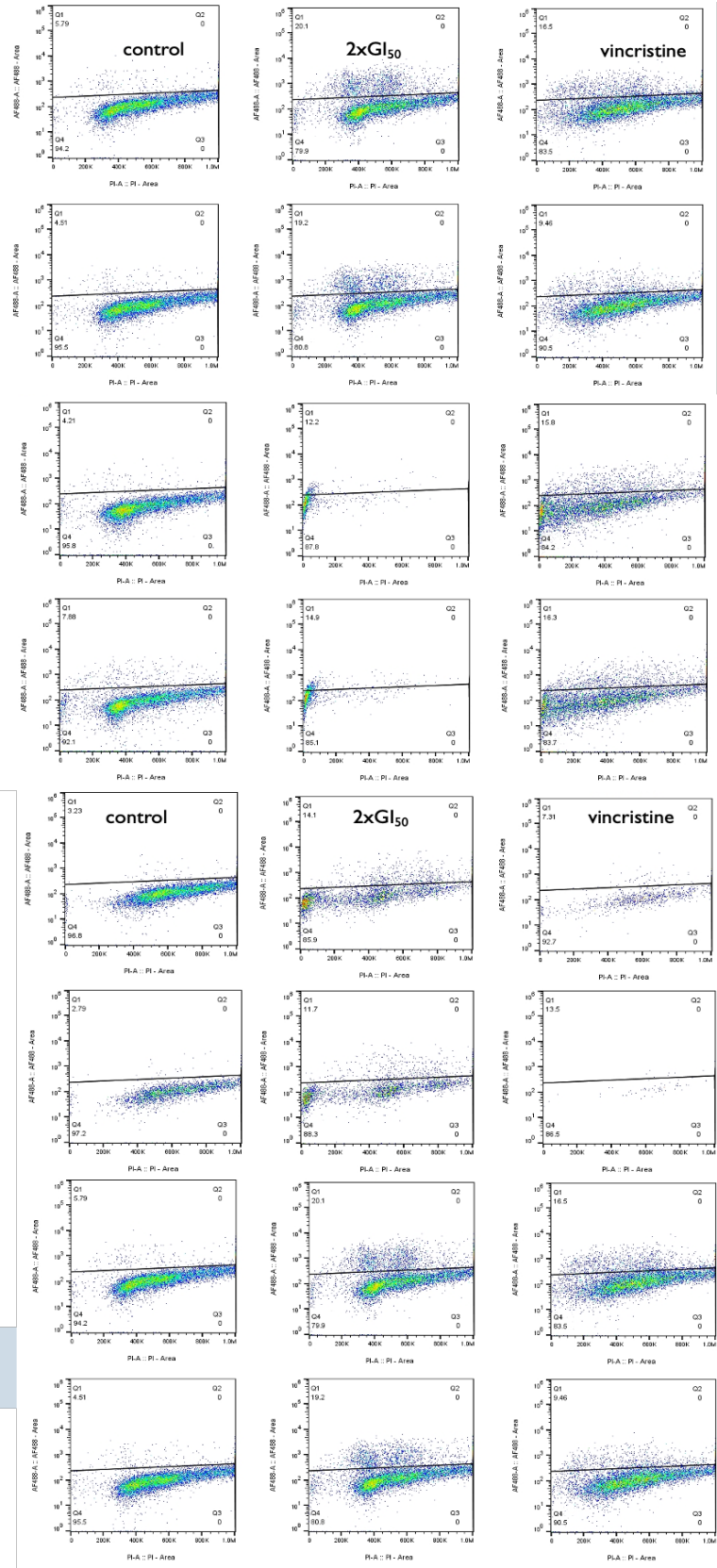


Figure 3.18 yH2AX detection of $2 \times GI_{50}$ eumatinine (**4**) ($2.0\mu\text{g/mL}$, $\sim 1.44\mu\text{M}$) on HCT-116 and MCF-7 following 24h and 72h exposure; X-axis is PI, Y-axis is yH2AX/AF488, the diagonal line indicates the gating threshold used to distinguish yH2AX-positive from yH2AX-negative cell populations; ≥ 3 independent trials performed where $n=2$, $>10,000$ events recorded per sample.

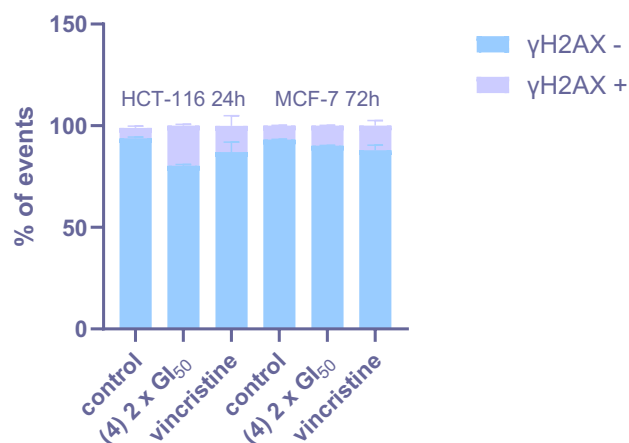


Figure 3.19 Summary of γ H2AX detection of $2 \times GI_{50}$ eumatanine (**4**) on HCT-116(24h) and MCF-7 (72h) cells, ≥ 2 independent trials performed where $n=2$.

To summarize, a series of assays were performed to investigate the cellular mechanism of action of compound **4** in MCF-7 and HCT-116 cells. Annexin V-FITC/PI staining (**Figures 3.9 and 3.10**) demonstrated that treatment with **4** induced significant late-stage apoptosis in both cell lines. Consistent with this, cell cycle analysis revealed pre-G1 phase arrest in both cell lines, with additional G1 phase arrest observed in MCF-7 cells (**Figures 3.12–3.15**). Furthermore, **4** significantly increased caspase-3/7 activity (**Figure 3.16**) and enhanced the generation of ROS (**Figure 3.17**). DNA damage was also evident, as indicated by a marked increase in γ H2AX levels in HCT-116 cells and a slight increase in MCF-7 cells (**Figures 3.18 and 3.19**). Collectively, these findings highlight the ability of **4** to induce apoptosis, disrupt the cell cycle, enhance oxidative stress, and promote DNA damage in cancer cells.

3.2.2.4 Fluorescence microscopy

Although cell cycle analysis, apoptosis assays, and caspase 3/7 assays suggest that compound **4** induces DNA fragmentation and caspase 3/7 activation - characteristics of apoptosis - the nomenclature committee on cell death (NCCD) emphasizes that these biochemical markers should not be solely used to detect apoptosis, as morphological changes are more reliable indicators (Galluzzi et al., 2007). Programmed cell death, indeed, apoptosis is not always caspase-dependent and can occur without oligonucleosomal DNA fragmentation, for instance staurosporine induces both caspase-dependent and caspase-independent apoptosis (Belmokhtar et al., 2001).

To observe morphological changes in MCF-7 and HCT-116 cells caused by **4**, fluorescence microscopy was conducted. The cytoskeleton of cells was dyed with phalloidin (presented as green), and nuclei were dyed with DRAQ5 (far-red DNA stain, presented as violet). Morphological phenomena observed include membrane blebbing, nuclear condensation, cytoplasmic swelling and cytoplasmic vacuolization (**Figure 3.20**). Membrane blebbing and nuclear condensation may suggest that cell death is associated with apoptosis, which corroborates the results obtained from the apoptosis assay and cell cycle analysis (Coleman et al., 2001, Sperandio et al., 2004, Kerr et al., 1972). Even though it is confirmed that **4** induced apoptotic cell death in MCF-7, the morphological features of apoptosis such as membrane blebbing and cell shrinkage are missing (**Figure 3.20**), which may be attributed to the fact that MCF-7 cells lack caspase-3 and the cell death ensues independently of caspase-3 (e.g. caspase-7-engagement) (Jänicke, 2009).

Cytoplasmic vacuolization observed in $1 \times \text{GI}_{50}$ **4** treated MCF-7 cells may imply autophagy or paraptosis (**Figure 3.20**) (Sperandio et al., 2004, Levine and Yuan, 2005). Classical apoptosis typically begins with the collapse of cytoskeletal elements while organelles are preserved until the later stages, whereas autophagy starts with the degradation of organelles, with cytoskeletal elements remaining intact until the later stages (Levine and Yuan, 2005). Autophagy, a regulated lysosomal degradation pathway, has been identified as the primary regulated mechanism for degrading long-lived proteins and the exclusive pathway for organelle degradation. Morphologically, autophagy is characterized by double-membraned vacuoles, which are formed to sequester cytoplasmic organelles such as mitochondria and ER (Levine and Yuan, 2005). Paraptosis is a non-apoptotic form of programmed cell death mediated by mitogen-activated protein kinases (MAPKs) and does not activate caspases, with AIP-1/Alix identified as a specific inhibitor of this process (Sperandio et al., 2004). Cini et al. reported cytoplasmic vacuolization in MDA-MB-468 and HCT-116 cells following treatment with a titanium complex and attributed it to paraptosis, a caspase-independent programmed cell death route (Cini et al., 2016).

Cytoplasmic swelling is an important morphological phenomenon of necrosis (Denecker et al., 2001, Galluzzi et al., 2007). Indeed, swelling in cytoplasm of both MCF-7 and HCT-116 cells was observed after these cell lines were exposed to **4** at the concentration of $0.5 \times \text{GI}_{50}$,

indicating the induction of necrotic cell death occurred when exposed to low concentration ($\sim 0.363 \mu\text{M}$) of **4** (**Figure 3.20**). Necrotic cell death, an alternative pathway when the classical caspase-dependent apoptotic pathway is inhibited and sharing the same stimuli as apoptosis, is typically caused by mitochondrial oxidative phosphorylation, reactive oxygen species production, and non-caspase proteolytic cascades involving serine proteases, calpains, or cathepsins (Denecker et al., 2001, Wyllie et al., 1980). Compared to the morphological features of apoptosis, such as cell shrinkage, extensive nuclear fragmentation, and intact plasma membrane until the later stages, necrosis is characterized by cytoplasmic swelling, rapid plasma membrane rupture, and organelle breakdown, with remarkably few changes in nuclear contents (Kerr et al., 1972, Wyllie et al., 1980).

Given that recent studies have shown autophagic cell death frequently occurs in diseased tissues and tumour cells in response to chemotherapy (Zhang et al., 2014), it is understandable that combinations of morphological features of autophagic and apoptotic, or autophagic and necrotic, have been observed within the same cell; for instance, honokiol triggered both apoptosis and autophagy in human osteosarcoma cells (Levine and Yuan, 2005, Huang et al., 2018). Morphological observations from **4** - treated carcinoma cells in this study, support engagement of multiple death pathways, demonstrating that features of autophagic/paraptotic cell death (cytoplasmic vacuolization) and necrotic cell death (cytoplasmic swelling) were observed in MCF-7 cells. On the other hand, morphological features of both apoptotic and necrotic cell death were observed in compound **4**-treated HCT-116 cells, further supporting the conclusion drawn from cell cycle analysis that different mechanisms of action are involved in MCF-7 and HCT-116 cells.

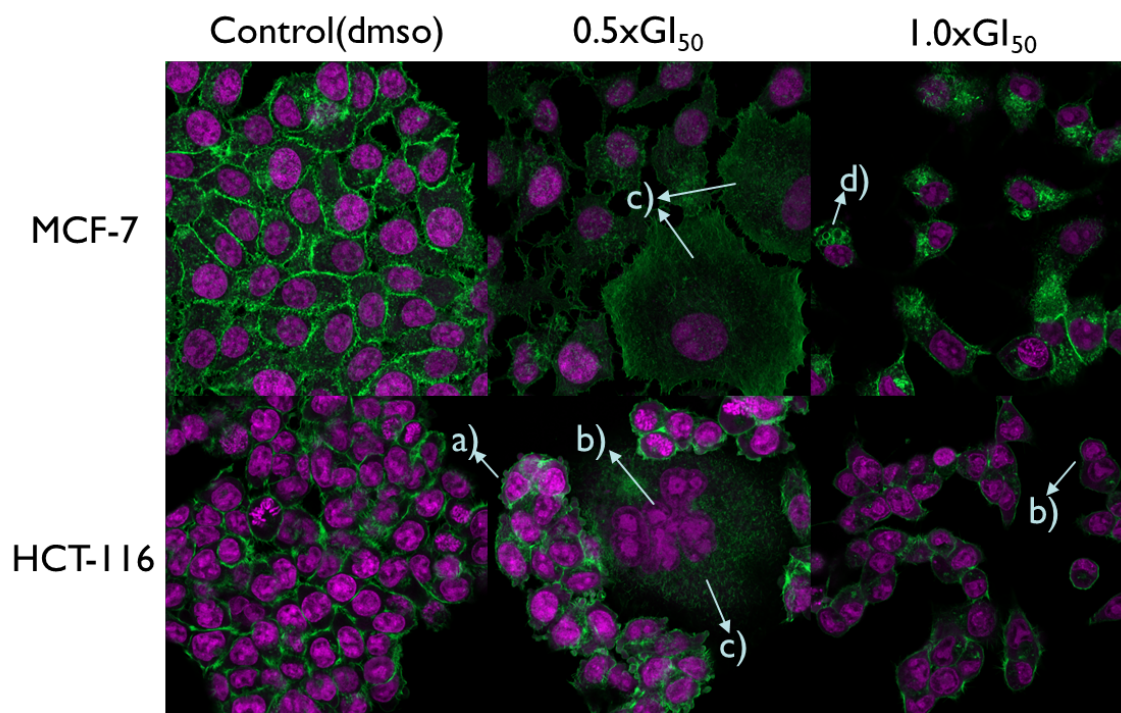


Figure 3.20 Effect of ~ 0.363 and $\sim 0.725 \mu\text{M}$ eumatanine (**4**) (24h exposure) on MCF-7 and HCT-116 cell morphology; a) membrane blebbing; b) nuclear condensation; c) cytoplasmic swelling; d) cytoplasmic vacuolization; ≥ 3 independent trials performed where $n=2$; green dye represents cytoskeleton, violet dye represents nuclear contents, $20 \times 1 \times \text{Airy Scan}$.

3.3 Conclusion

Oligocyclotryptamine alkaloids **2**, **3** and **4** from the leaves of *Pychotria montana* were characterized as oleiodin, caledonine, and a new octameric alkaloid, respectively. Preliminary assays suggested that compounds **2-4** exert potent broad-spectrum growth inhibitory and cytotoxic activity against carcinoma cell lines. Cell cycle analysis and apoptosis assays indicated that compounds **2** and **3** cause rapid, cell cycle phase-independent apoptotic cell death, possibly involving ROS generation. Results obtained from the detection of γH2AX foci suggest that **4** causes cell death by evoking lethal DNA DSBs. Finally, morphological changes including membrane blebbing and nuclear condensation in MCF-7 and HCT-116 cells were observed by fluorescence microscopy, which further corroborate apoptosis induction by **4**. However, this may not be the only cell death mechanism triggered, as cytoplasmic vacuolisation is a marker of paraptosis.

The broad-spectrum and potent cytotoxicity of these newly-identified oligocyclotryptamines argue for further preclinical evaluation as experimental and putative antitumour agents;

however, its potentially non-cancer selectivity should be acknowledged and nano-formulations considered to minimise adverse toxicities. It is hoped that this research will initiate further studies, not only on the investigation of the mechanism(s) of action and molecular targets, but also in potential drug delivery systems with the purpose of more cancer-targeted therapy.

Chapter 4 Metabolomics Studies

4.1 Introduction

Cancer is a complex disease characteristic by uncontrolled cell proliferation, metabolic reprogramming, and resistance to apoptosis. NPs have historically served as a cornerstone for anticancer drugs discovery and these compounds such as paclitaxel (Taxol®) and vincristine (VCR) have also been involved in promising clinically cancer therapies with diverse mechanisms of action (e.g. the induction of apoptosis, cell cycle arrest, inhibition of angiogenesis, epigenetic modulation, and metabolic reprogramming) (Donehower, 1996, Gidding et al., 1999). Among these mechanisms, metabolic reprogramming is a hallmark of cancer, which is characterized by alterations in cellular metabolic patterns, encompassing cancer cell glycolysis, glucose uptake, OXPHOS, and lipid metabolism (Wang et al., 2021a). Despite their significant contributions on the discovery of anticancer drugs, elucidating the molecular mechanisms of action underlying their anticancer activities and their specific impacts on cancer metabolism remains a formidable challenge. This difficulty arises from the chemical complexity of naturally derived compounds and the dynamic nature of cancer metabolic networks. These factors hinder both the identification of active constituents and the characterisation of their specific biological effects.

In this context, metabolomics provides a transformative tool for addressing these challenges. By integrating high-performance analytical platforms (primarily MS and NMR) with computational tools (e.g. Compound Discover), metabolomics enable a comprehensive study of small molecules (<1500 Da) in biological systems (Johnson and Gonzalez, 2012). It captures the profile of the end products of gene expression or cellular activity, providing a snapshot of the metabolic changes that result from biotic (e.g. disease onset and progression) or biotic perturbation (e.g. drug treatment, and xenobiotic exposure). By analysing intracellular and extracellular metabolites, metabolomics can uncover metabolic pathways affected by NPs, identify biomarkers associated with anticancer responses, and shed light on metabolic drivers that may expose cancer vulnerabilities. Thereby, metabolomics has become an invaluable tool for elucidating pathological mechanisms, discovering diagnostic and therapeutic biomarkers, and evaluating drug efficacy (Clish, 2015, Johnson et al., 2012, Johnson et al., 2016).

Several examples highlight the utility of metabolomics in elucidating NP mechanisms of action. Berberine, a plant-derived alkaloid, demonstrates anticancer activity by inducing cell cycle arrest, inhibiting cancer cell proliferation, as well as disrupting glycolysis and OXPHOS (Fan et al., 2013). Another example is the paclitaxel, which is an microtubule-stabilising agent, inducing cell cycle arrest and apoptosis while also disrupting cancer cell lipid metabolism by depressing CPT18 and FAO expression level in BC cells (McGrogan et al., 2008, Wang et al., 2018). Additionally, metabolomics can aid in the identification of predictive biomarkers of therapeutic responses (e.g. patient-specific benefits and markers of drug resistance), facilitating the stratification of patients most likely to benefit from specific anticancer treatments (Danzi et al., 2023). For example, resveratrol treatment alters glucose and amino acid metabolism in BC cells, with serotonin, kynurenine, and spermidine levels increasing up to 61-fold in MCF-7 and MDA-MB-231 cells, highlighting potential biomarkers of response (Zambrano et al., 2019, Jäger et al., 2011).

In addition to identifying therapeutic mechanisms and biomarkers, metabolomics is also a valuable tool for exploring cancer-specific metabolic vulnerabilities. A notable example is the Warburg effect, a characteristic metabolic feature of cancer in which cells preferentially convert glucose to lactate under aerobic conditions to support the increased energy and biosynthetic demands of rapid tumour growth and proliferation (Hosios and Manning, 2021). Through the application of metabolomics, it has been demonstrated that noscapine, an opium alkaloid, and FUZI alkaloidal extracts, a TCM, target the Warburg effect via the PI3K/mTOR signalling pathway in colon cancer cells and NSCLC cells, respectively, thereby providing a framework for precision medicine (Tian et al., 2020, Zhang et al., 2024).

MS is one of the most widely applied technologies in metabolomics, capable of simultaneously detecting and identifying thousands of metabolites with high precision by generating ions, separating ions based on their mass-to-charge (m/z) ratios, and detecting the resulting ion signals. Coupling MS with chromatographic techniques such as GC, LC, or capillary electrophoresis (CE) further enhances sensitivity, speed, and selectivity, significantly improving the accuracy of compound identification, detection, and quantification (Silva et al., 2019). However, these platforms are inherently destructive, require extensive sample

preparation, and are associated with high operational costs, which represent major limitations for routine and large-scale metabolomic analyses.

GC-MS-based metabolomics is widely used for the separation and analysis of volatile and thermally stable compounds, with advantages of efficiency, selectivity and reproducibility (Scalbert et al., 2009, Silva et al., 2019). However, its application is limited to compounds that are inherently volatile and thermally stable, such as aldehydes, ketones, alkanes, and organic acids. Although some non-volatile or thermolabile metabolites (e.g., amino acids, sugars, and lipids) can be analysed via GC-MS after chemical derivatization, particularly those containing polar functional groups (e.g., hydroxyl, carboxyl, or amino groups) (Fiehn et al., 2000), certain compounds, such as ATP, NADPH or arginine, often remain impossible to measure by GC-MS due to their instability or limited volatility (Scalbert et al., 2009, Bamji-Stocke et al., 2018). In this case, LC-MS-based metabolomics offers the advantage of analysing polar and high molecular weight metabolites without the need for derivatization, enabling rapid analysis from small sample volumes. A variety of mass detectors are compatible with LC-MS, including ultra-high-resolution systems such as Fourier transform ion cyclotron resonance (FT-ICR) and Orbitrap, high-resolution time-of-flight (TOF), low-resolution ion traps, triple quadrupoles, and more recently, ion mobility TOF-MS systems (Dwivedi et al., 2008). However, a key limitation of LC-MS, particularly with electrospray ionisation (ESI), is ion suppression caused by matrix compound, which can reduce ionisation efficiency. This can be alleviated through improved chromatographic separation or the use of nanospray ionisation (Scalbert et al., 2009). Additionally, the choice of ionisation method should be aligned with the physicochemical properties of the analytes; for example, non-polar metabolites such as cholesterol are poorly ionised by ESI and are better suited to atmospheric pressure chemical ionization (APCI) (Bamji-Stocke et al., 2018).

Another widely used analytical platform in metabolomics is NMR spectroscopy. Although it is less sensitive than mass spectrometry, it offers highly reproducible, non-destructive analysis and valuable structural information, enabling comprehensive profiling and identification of bioactive metabolites from natural sources (e.g. plants, fungi, and marine organisms) (Noreldeen et al., 2020).

For data analysis following the collection of raw data, multivariate statistical methods (e.g., PCA and PLS-DA) and pathway analysis tools (e.g., MetaboAnalyst) were employed to differentiate metabolic profiles and identify key metabolites and impacted metabolic pathways (Pang et al., 2021, Pang et al., 2022). To achieve a comprehensive understanding of how NPs exert their cytotoxic effects on cancer cells, metabolomics can be seamlessly integrated with other omics approaches, such as proteomics, genomics, and transcriptomics, providing valuable insights into complex biological systems.

To summarize, metabolomics remains uniquely positioned to transform NP research by uncovering new therapeutic targets, enabling biomarker discovery, and accelerating the development of effective anticancer agents. It represents a novel and indispensable approach for studying NPs, not only providing powerful tools to uncover their molecular mechanisms of action against cancer and thereafter elucidating their impact on cancer metabolism but also establishing a foundation for developing novel therapies and improving existing treatments, which integrates with other omics approaches and computational tool accelerates the discovery of effective anticancer agents from natural sources.

In this study, to perform a comprehensive study of metabolites in BC cell cultures (MCF-7) and interpret metabolic response to test compounds (caledonine (**3**) and eumatanine (**4**)), LC-HRMS was utilised, which enables global metabolic profiling (also known as an untargeted metabolomics approach) and identification of key metabolites (Gertsman and Barshop, 2018, Zubarev and Makarov, 2013).

4.2 Results and discussion

The extracts of cell cultures were collected from the BC cell line MCF-7 after a 24-h exposure to caledonine (**3**) and eumatanine (**4**) at the concentration of $2.5 \times \text{GI}_{50}$ (1.25 and 2.5 $\mu\text{g/mL}$ respectively).

Similar to flow cytometry, LC-HRMS-based metabolomics analysis requires a relatively large number of cells compared to assays such as MTT, cell counting, and clonogenic assays. Optimizing the protocol for this analysis is crucial, particularly in determining the appropriate concentrations of the tested agents and the seeding density of MCF-7 cells. To meet the requirements of metabolomics assays, specifically ensuring a similar number of cells ($\pm 10\%$ variation) between treated and control groups, the concentration of compounds was optimized through preliminary examinations. The use of $2.5 \times \text{GI}_{50}$ ensured that sufficient cell numbers remained for metabolic analysis without significant cytotoxicity. The applied concentrations of compounds **3** and **4** are as high as 2.5 times GI_{50} value (the GI_{50} value is from corresponding MTT assays), which is due to more cells (2×10^6 cells per 10cm petri dish/T-25cm² flask) being seeded for metabolomics assays and thereby compounds added to exert the same level of cytotoxicity on cells require a higher concentration.

The pooled QC (quality control) samples, standard (268 standards) mixtures and all intracellular samples were processed to the same analytical run on LC-HRMS for metabolites identification and quantification, while QC samples were inserted throughout the analysis to check instrument performance.

4.2.1 LC-HRMS-based data processing and metabolite identification

The results of LC-MS-based metabolite profiling of MCF-7 cells treated with compounds **3** and **4** revealed the detection of 1247 ions in total, among which 360 ions were annotated. Sixty-four L1 and L2 metabolites were putatively annotated based on m/z , RT and/or, MS/MS referring to public/commercial spectral libraries and authentic reference standards (**Figure 4.1**).

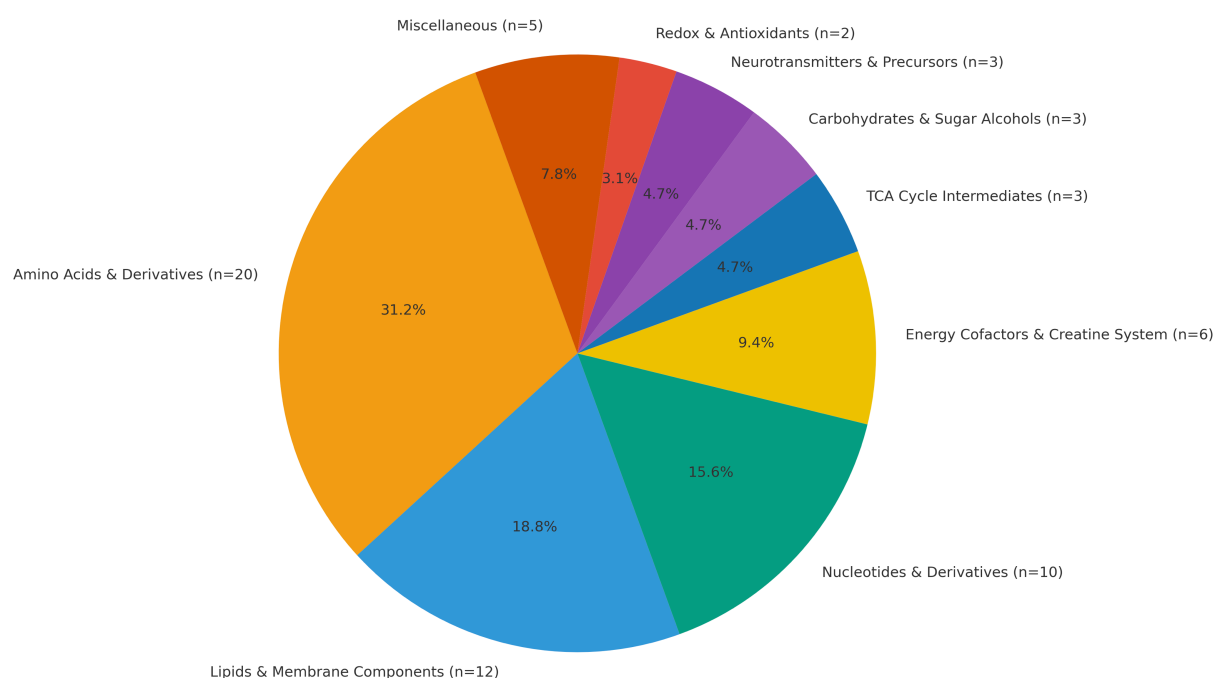


Figure 4.1 Classification of metabolites identified in MCF-7 cell extracts according to their biological role.

The largest class of metabolites identified was amino acids & derivatives, representing 31.2% (20 metabolites) of the total metabolites, including ornithine, citrulline, and N-acetylglutamine. These metabolites are critical in protein synthesis and nitrogen metabolism. For instance, ornithine and citrulline play pivotal roles in the urea cycle, which acts as the primary defence against ammonia toxicity in mammalian enterocytes (Wu, 2009).

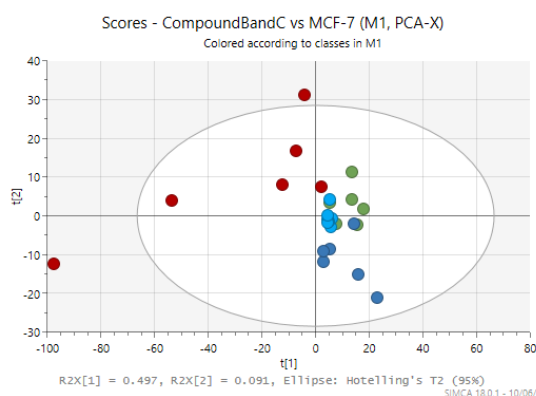
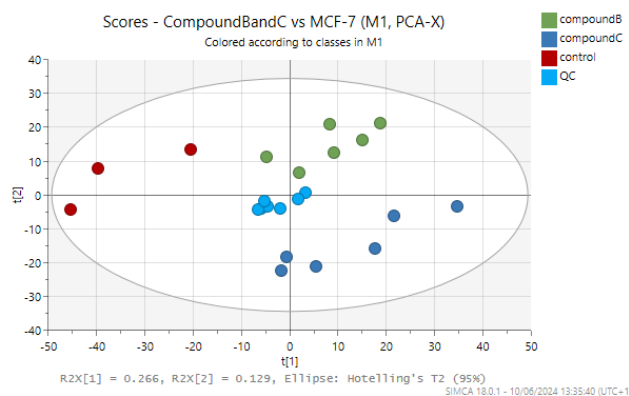
The lipids & membrane components group, representing 18.8% (12 metabolites), including specific examples such as SM(d18:1/16:0) (sphingomyelin), phosphodimethylethanolamine, glycerophosphocholine (GPC), glycerol 3-phosphate (G3P) and phospholipids like PC (16:0/18:2(9Z,12Z)). This category encompasses a wide variety of lipid species, which are essential for maintaining cellular membrane integrity, energy storage, and signalling (van Meer et al., 2008). Lipids such as phospholipids, sphingolipids, and glycerolipids play integral roles in cell structure and intercellular communication. Phospholipids, such as GPC and G3P, are critical for membrane dynamics and glycerolipid metabolism (Karanjia et al., 2016). The nucleotides and derivatives follow closely, contributing 15.6% (10 metabolites). Nucleotides

are indispensable for genetic information storage and transfer, as well as for their roles in redox reactions (e.g., NADPH) and supporting anabolic demands (Patra and Hay, 2014).

Smaller categories, such as Energy cofactors & creatine system (6 metabolites), TCA cycle intermediates (5 metabolites), carbohydrates & sugar alcohols (3 metabolites), neurotransmitters and precursors (3 metabolites), redox & antioxidants (3 metabolites), and miscellaneous (5 metabolites), represent metabolites with specialized roles. For example, Maleic acid, which is critical for the TCA, contributing to cellular respiration and energy production (Skorokhodova et al., 2022, Akram, 2014). Neurotransmitters and their precursors, such as acetylcholine (ACh), are not only essential for synaptic signaling but also play a central role in mediating autocrine stimulation, which contributes to the proliferation of carcinoma cells (Xie and Raufman, 2016, Whitteridge, 1948, Cheng et al., 2008). Antioxidants such as glutathione is vital for regulates cell proliferation, apoptosis, and immune function (Lu, 2013). The miscellaneous category includes metabolites not clearly fitting above classes (e.g. 6-oxohexanoic acid).

4.2.2 The analytical performance of LC-HRMS and Multivariate Analysis

As the quality assessment of metabolomics data, PCA, which is an unsupervised multivariate analysis, has been widely applied for interpreting large datasets due to its advantages of reducing the dimensionality of the many variables, and increasing interpretability while minimising information loss (Jolliffe and Cadima, 2016). Two control samples appeared as outliers in the initial PCA analysis (**Figure 4.2A**), likely due to partial sample loss caused by spillage during preparation. However, whether these outliers were included or excluded, the PCA scores plot (**Figure 4.2B**) consistently demonstrated tight clustering of pooled QC samples, confirming the stability and reproducibility of the LC-HRMS system. This consistency validates the analytical performance of the LC-HRMS platform for untargeted metabolomics. Nonetheless, the initial PCA analysis did not reveal clear separation between the control, QC, and treated groups (**Figure 4.2A**).

A**B**

*Figure 4.2 PCA scores plot of the metabolic profiles of the cell extracts from MCF-7 after treating with caledonine (**3**) and eumatanine (**4**), and the untreated control group. For clarity, compound B denotes caledonine (**3**) and compound C denotes eumatanine (**4**); this nomenclature is used throughout subsequent figures. Pooled quality-control (QC) samples (light blue) cluster near the centre of the plot, indicating analytical stability. Group colours are: control (red), caledonine (**3**) (green), and eumatanine (**4**) (blue). Each point represents one biological replicate ($n = 6$ per group).*

Although PCA is a useful technique to evaluate similarities and differences among all samples or groups, and to assess the robustness of generated models, it is not comprehensive to effectively visualize distinct group differences. PCA provides an unbiased overview of dataset structure and reveals global trends, but clear separation emerges only when between-group variance exceeds within-group (including technical) variance, so subtle effects may be obscured (Broeckling et al., 2023, Worley and Powers, 2013). Consequently, exploratory analyses should begin with PCA to verify data structure and analytical stability before any supervised modelling, with subsequent comparative analysis employing OPLS-DA to maximise class-related covariance while filtering orthogonal (non-discriminatory) variation and thereby enhance interpretability of group differences (Worley and Powers, 2013, Al-natour et al., 2022). As supervision can yield spurious separation, OPLS-DA must be guided by the PCA structure and subjected to rigorous validation (e.g., cross-validation and permutation testing) to ensure biological relevance. In this study, subtoxic dosing (to avoid >10–15% viability loss) likely reduced effect sizes, accounting for weak clustering in PCA. Accordingly, PCA was used solely as an unbiased quality/structure check (QC clustering) (Al-natour et al., 2022, González-Domínguez et al., 2024).

Subsequently, the peak list data was further analysed on orthogonal partial least squares – discriminant analysis (OPLS-DA) models using SIMCA-P v16 (Umetrics, Sweden) for

comparative class analysis to identify the differences between samples (e.g. the control and compound treated group). Clear clustering and separation were observed between the metabolic profile of the control and compound treated groups in OPLS-DA score plots (**Figure 4.3**). The metabolic profiles of compounds **3** and **4** treated groups were compared individually to that of the control group for OPLS-DA, as shown in **Figure 4.3**. Clear separations were observed for both comparisons: the control and **3** treated groups, as well as the control and **4** treated groups. Additionally, to evaluate the robustness of the generated models, cross-validations (leave-one-out-method, 1 out of 7 in this study) were used, in which the parameters include (R^2Y) for OPLS-DA and predictive ability (Q^2) are monitored, while models with values over 0.5 are considered robust (L. Eriksson, 2013). The permutation results of all OPLS-DA models are shown in the supplementary information, which exhibited good fitness and well-predictive ability of all models (**Figure S20, S21**).

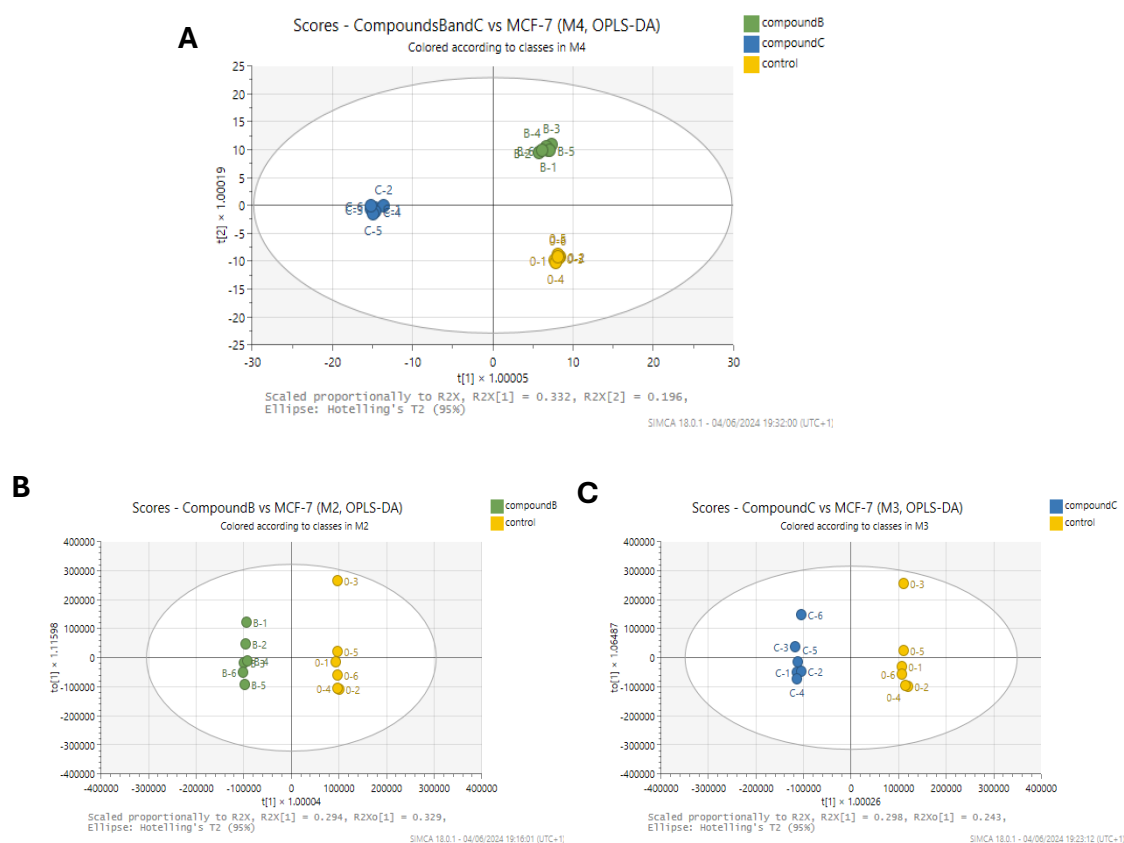


Figure 4.3 OPLS-DA score plot of the cell extracts of MCF-7 after treated with caledonine (**3**) and eumatanine (**4**), and the untreated control. **A** compound **3**- and **4**- treated MCF-7 cells and the control. **B** Two-way orthogonal comparison between control and **3** treated cells ($R^2Y=0.999$ and $Q^2=0.94$). **C** Two-way orthogonal comparison between control and **4** treated cells ($R^2Y=0.998$ and $Q^2=0.931$). The control (yellow circle), **3**-treated cells (green circle), and **4**-treated cells (blue circle). $n=6$

4.2.3 Metabolite Comparison

Variable importance in the projection (VIP), which was used to extract differential metabolites between two classes, is capable of generating scores to estimate the importance of each variable used in the OPLS-DA model, in which only scores more than 1 are regarded as important (Galindo-Prieto et al., 2015). Therefore, metabolites with adjusted $p < 0.05$ and $VIP > 1$ are considered to be potential significant metabolites of the comparison of two classes. The lists of significant metabolites generated from the cell extracts of MCF-7 being exposed to compounds **3** and **4** are presented in **Tables 4.2** and **4.3** with their accurate masses (m/z), retention time (RT), and Log₂ fold changes (Log₂ FC). It is exhibited that the Log₂ FC value of all significant metabolites from either **3** vs control or **4** vs control were above 0, suggesting that all metabolites were increased. These significant metabolites may provide insight into developing therapeutic targets in BC or as biomarkers for BC treatment. In addition, the comparison of **4** vs control (24 significant metabolites) possesses more significant metabolites than that of **3** vs control (8 significant metabolites), while six of them are shared by these two comparisons (**Table 4.2**).

Table 4.2 Significant metabolites from caledonine (3) vs MCF-7 (Log₂ FC: caledonine (3) / Control; adjusted p value < 0.05 , VIP value > 1 .)

Name	Formula	m/z	RT [min]	HMDB ID	Log ₂ FC	ID confidence
Nervonic acid	C ₂₄ H ₄₆ O ₂	365.3423	3.259	HMDB0002368	3.58	3
Cer(d18:1/22:1(13Z))	C ₄₀ H ₇₇ NO ₃	620.5966	3.561	HMDB0011775	2.04	-
Pregnanetriol	C ₂₁ H ₃₆ O ₃	337.273	3.184	HMDB0006070	1.61	-
7-ketodeoxycholic acid	C ₂₄ H ₃₈ O ₅	407.2784	3.721	HMDB0000391	1.54	3
Creatinine	C ₄ H ₇ N ₃ O	112.0516	10.728	HMDB0000562	1.32	2
Ceramide (d18:1/16:0)	C ₃₄ H ₆₇ NO ₃	538.5187	4.668	HMDB0004949	1.26	-
Stearoylethanolamide	C ₂₀ H ₄₁ NO ₂	328.3205	7.314	HMDB0013078	1.11	-
Pregabalin	C ₈ H ₁₇ NO ₂	158.1186	8.469	HMDB0014375	0.95	-

Table 4.3 Significant metabolites from eumatanine (4) vs MCF-7 (Log₂ FC: eumatanine (4) / Control; adjusted p value < 0.05 , VIP value > 1 .)

Name	Formula	m/z	RT [min]	HMDB ID	Log ₂ FC	ID confidence
Nervonic acid	C ₂₄ H ₄₆ O ₂	365.3423	3.259	HMDB0002368	3.33	3
Cer(d18:1/22:1(13Z))	C ₄₀ H ₇₇ NO ₃	620.5966	3.561	HMDB0011775	2.41	-
S-3-oxodecanoyl cysteamine	C ₁₂ H ₂₃ NO ₂ S	246.1519	3.343	HMDB0059773	2.08	2
Norepinephrine sulfate	C ₈ H ₁₁ NO ₆ S	248.0234	11.631	HMDB0002062	1.85	-

7-ketodeoxycholic acid	C24H38O5	407.2784	3.721	HMDB0000391	1.62	3
Ceramide (d18:1/16:0)	C34H67NO3	538.5187	4.668	HMDB0004949	1.55	-
Creatinine	C4H7N3O	112.0516	10.728	HMDB0000562	1.37	2
trans-2-Dodecenoylcarnitine	C19H35NO4	342.2633	4.604	HMDB0013326	1.36	3
Thioprolin	C4 H7NO2S	132.0124	7.32	HMDB0062164	1.29	-
Cer(d18:1/24:1)	C42H81NO3	646.6147	3.861	HMDB0004953	1.25	-
Acetylcysteine	C5H9NO3S	162.023	4.635	HMDB0001890	1.24	3
N-Acetyl-D-glucosamine	C8H15NO6	222.0969	9.133	HMDB0000215	1.2	2
N-Gluconyl ethanolamine phosphate	C8H18NO10P	318.0595	9.574	HMDB0032294	1.18	3
Ribose 5-phosphate	C5H11O8P	289.033	10.254	HMDB0001548	1.18	1
Pregabalin	C8H17NO2	158.1186	8.469	HMDB0014375	1.1	-
Ceramide (d18:1/16:0)	C8H17NO2	538.5186	3.752	HMDB0004949	1.08	-
Adenine	C5H5N5	134.0472	9.571	HMDB0000034	1.08	2
sn-Glycerol 3-phosphate	C3H9O6P	171.0063	9.554	HMDB0000126	1.07	1
Hypotaurine	C2H7NO2S	110.0269	10.858	HMDB0000965	1.01	2
Acetylcarnitine	C9H17NO4	204.1228	6.593	HMDB0000201	1	1
L-Hexanoylcarnitine	C13H25NO4	260.1852	4.636	HMDB0000756	0.98	3
trans-Hexadec-2-enoyl carnitine	C23H43NO4	398.3258	4.345	HMDB0006317	0.96	3
(S)C(S)S-S-Methylcysteine sulfoxide	C4H9NO3S	134.0268	4.659	HMDB0029432	0.92	-
DL-Carnitine	C7H15NO3	160.0978	8.46	HMDB0000062	0.92	1

4.2.4 Pathway Analysis

Based on the results of multivariate analysis (PCA-X and OPLS-DA), it is ascertained that compounds **3** and **4** both induced metabolic differences on MCF-7 cells when compared to the non-treated control group. After excluding putative non-human metabolites, the identified metabolites (64 L1 and L2 metabolites) were processed on MetaboAnalyst 6.0 for metabolic pathway analysis, as an attempt to elaborate how **3** and **4** perturb metabolism in MCF-7 cells regarding the metabolic pathway (Pang et al., 2021, Pang et al., 2022). Metabolite abundances were log-transformed and Pareto-scaled prior to analysis.

MetaboAnalyst is an easy-to-use online platform widely used to support LC-HRMS-based global metabolomic data analysis, interpretation, and integration with other omics data. MetaboAnalyst has gradually developed into a powerful tool to resolve the demands of

complex bioinformatic and statistical from global metabolomics data (e.g. raw spectra processing, functional analysis, and integration with other omics data) since v4.0 (Pang et al., 2022, Pang et al., 2021). Log transformation and Pareto scaling are widely regarded as stable preprocessing methods in metabolomics. Log transformation reduces skew and heteroscedasticity and renders multiplicative effects approximately additive, but perfectly stabilises variance only when relative SD is constant (Kvalheim et al., 1994, van den Berg et al., 2006). Pareto scaling (mean-centring and division by the square root of its standard deviation) down-weights high-variance features while preserving magnitude information, improving interpretability without forcing unit variance (Eriksson, 1999, van den Berg et al., 2006). Accordingly, log transformation followed by Pareto scaling was adopted in this study.

By comparing the control group to the compound treated groups, metabolic differences were observed in 28 metabolic pathways for both compounds (**3** and **4**). Eight of these were significant for the **3** treated group by applying the criteria of adjusted $p < 0.05$ and impact > 0.1 , whereas only four metabolic pathways were significant for **4** treated group (**Figure 4.4; Table 4.4**). Notably, Glycerophospholipid Metabolism, Arginine and Proline Metabolism, and Amino Sugar and Nucleotide Sugar Metabolism were significantly affected in either 3- or 4-treated MCF-7 cells. (**Figure 4.5; Table 4.5**). In the metabolomics pathway analysis, a significant metabolite that is successfully mapped to a pathway in the reference database (e.g. KEGG) is defined as a hit. The majority of hit metabolites in these three pathways were upregulated in response to treatment, except for phosphocreatine in arginine and proline metabolism (**Figures 4.6, 4.7 and 4.8**).

- Glycerophospholipid Metabolism: Compounds 3 and 4 induced an increase in GPC and ACh, disrupting membrane integrity and stimulating cell proliferation (Karanjia et al., 2016, Cheng et al., 2008).
- Arginine and Proline Metabolism: Increase of L-ornithine and creatine highlighted disruptions in energy buffering and tumour proliferation pathways (Satriano, 2004, Zhang et al., 2021, Zhang and Bu, 2022).
- Amino Sugar Metabolism: Elevated levels of uridine-5'-diphospho-N-acetylglucosamine (UDP-GlcNAc) and D-fructose-6-phosphate (F6P) suggested enhanced glycosylation, a hallmark of cancer proliferation (Paneque et al., 2023, Hosios and Manning, 2021).

In this project - evaluating the anticancer activity of isolated compounds against MCF-7 cells - glycerophospholipid metabolism exemplifies pathway relevance. Compounds **3** and **4** increased GPC and ACh, consistent with perturbed choline–phospholipid turnover that can influence membrane integrity and proliferative signalling (Karanjia et al., 2016, Cheng et al., 2008). This axis is pharmacologically tractable: the licensed alkylphosphocholine miltefosine perturbs phosphatidylcholine/sphingolipid metabolism, and licensed cholinergic agents (e.g., donepezil, ipratropium) modulate ACh signalling (Jiménez-López et al., 2010, Zulueta Díaz et al., 2020, Kumar A, Naji A, Gross, 1988). These examples are cited as proof-of-concept for druggability of nodes centred on GPC/GPE/ACh, underscoring this pathway’s relevance in cancers with dysregulated choline metabolism (Sonkar et al., 2019).

Similar pathway analysis results were observed in MCF-7 cells treated with the anticancer agent annonaceous acetogenins (ACGs), identifying five affected metabolomic pathways: arginine and proline metabolism, glycerophospholipid metabolism, taurine and hypotaurine metabolism, alanine, aspartate and glutamate metabolism, and D-glutamine and D-glutamate metabolism (Ma et al., 2018). Among these, the first three pathways were also found to be affected in MCF-7 cells following treatment with **3** or **4** in this study (**Figures 4.4 and 4.5; Tables 4.4. and 4.5**).

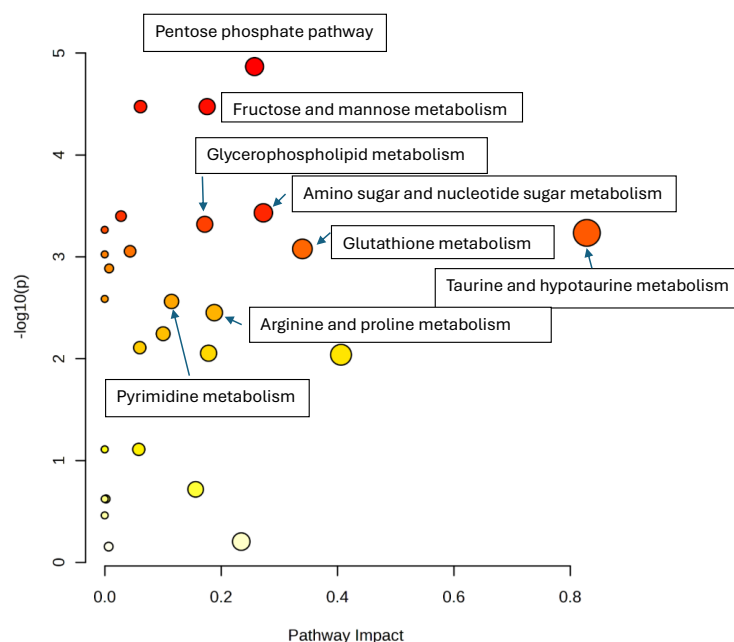


Figure 4.4 Summary of Pathway Analysis from caledonine (**3**) against MCF-7 (The size of the bubble represents the number of compounds mapped on the pathway; the color represents the degree of significant; the impact factor represents the importance of identified pathway on the whole metabolic network.)

Table 4.4 Result from Pathway Analysis of caledonine (**3**) vs MCF-7 (adjusted $p < 0.05$ and impact > 0.1). In particular, the Total is the total number of compounds in the pathway; the Hits is the actually matched number of significant metabolites from the dataset that overlap with a known pathway; the Raw p is the original p value calculated from the enrichment analysis; the Holm p is the p value adjusted by Holm-Bonferroni method; the Impact is the pathway impact value calculated from pathway topology analysis.

Pathway name	Total Compound	Hits	Raw p	Holm adjust p	Impact
Pentose phosphate pathway	23	2	1.36E-05	3.80E-04	0.26
Fructose and mannose metabolism	20	1	3.36E-05	9.06E-04	0.18
Amino sugar and nucleotide sugar metabolism	42	4	3.70E-04	9.26E-03	0.27
Glycerophospholipid metabolism	36	4	4.79E-04	1.10E-02	0.17
Taurine and hypotaurine metabolism	8	3	5.82E-04	1.22E-02	0.83
Glutathione metabolism	28	4	8.36E-04	1.67E-02	0.34
Pyrimidine metabolism	39	2	2.74E-03	4.14E-02	0.11
Arginine and proline metabolism	36	4	3.53E-03	4.95E-02	0.19

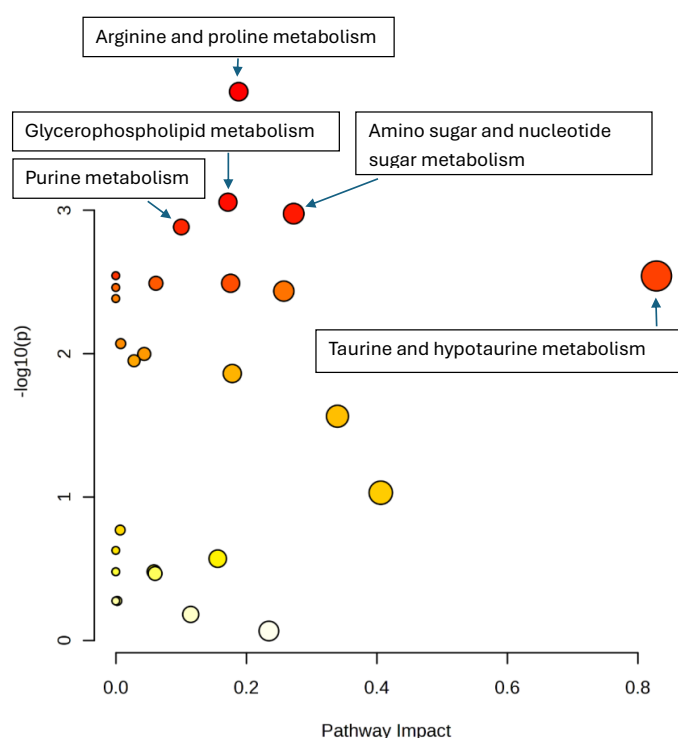


Figure 4.5 Summary of Pathway Analysis from eumatanine (**4**) against MCF-7 (The size of the bubble represents the number of compounds mapped on the pathway; the color represents the degree of significant; the impact factor represents the importance of identified pathway on the whole metabolic network.)

Table 4.5 Result from Pathway Analysis of eumatanine (**4**) against MCF-7 (adjusted $p < 0.05$ and impact > 0.1). In particular, the Total is the total number of compounds in the pathway; the Hits is the actually matched number of significant metabolites from the dataset that overlap with a known pathway; the Raw p is the original p value calculated from the enrichment analysis; the Holm p is the p value adjusted by Holm-Bonferroni method; the Impact is the pathway impact value calculated from pathway topology analysis.

Pathway name	Total Compound	Hits	Raw p	Holm adjust p	Impact
Arginine and proline metabolism	36	4	1.49E-04	4.18E-03	0.19
Glycerophospholipid metabolism	36	4	8.79E-04	2.37E-02	0.17
Amino sugar and nucleotide sugar metabolism	42	4	1.06E-03	2.75E-02	0.27
Purine metabolism	70	5	1.31E-03	3.27E-02	0.10

In this study, fructose 6-phosphate (F6P) and ribose 5-phosphate (R5P) were observed in MCF-7 cells and exhibited an increasing trend in response to the addition of **3** through the pentose phosphate pathway (PPP). R5P is one of the final products of the oxidative branch of the PPP from the oxidative decarboxylation of 6-phosphogluconate, where NADPH is irreversibly

generated. Subsequently, R5P serves as a precursor for ribonucleotide synthesis through the formation of phosphoribosyl pyrophosphate (**Figure 4.6**) (Patra and Hay, 2014, Horecker, 2002, Ge et al., 2020). R5P and NADPH are essential for cancer cell division and defence against ROS-induced damage, and consequently, alterations in PPP are often observed during cancer development and progression (Riganti et al., 2012). F6P, on the other hand, serves as an additional glycolytic intermediate that can be converted into glucose 6-phosphate, which can subsequently be recycled as the starting substrate in the oxidative branch of the PPP (Kruger and von Schaewen, 2003).

The upregulation of the pentose phosphate pathway (PPP) has been observed in various cancer types, including human clear cell-renal cell carcinoma (ccRCC), papillary thyroid carcinoma, CRC, and prostate cancer (Lucarelli et al., 2015, Chen et al., 2015, Cohen et al., 1968, Zampella et al., 1982). Notably, decreased cancer cell (clear cell-renal cell carcinoma) survival along with decreased level of NADPH has been reported upon the inhibition of PPP-derived metabolites, namely glucose 6-phosphate dehydrogenase (G6PDH), highlighting the critical role of the PPP as a novel target in cancer therapy (Lucarelli et al., 2015). The increase of PPP reactions was also reported to be attributed to long-term exposure to doxorubicin in yeast cells (*Saccharomyces cerevisiae*), while doxorubicin and **4** induced multiple similar cellular process in MCF-7 cells, including the induction of apoptosis, cell cycle G1/S phase arrest, and ROS generation (Taymaz-Nikerel et al., 2018). The PPP, as a key contributor to ribonucleotide synthesis and the major source of NADPH (essential for biological processes such as fatty acid synthesis and ROS scavenging), plays a pivotal role in cancer cells survival by supporting anabolic demands and maintaining redox homeostasis (Patra and Hay, 2014).

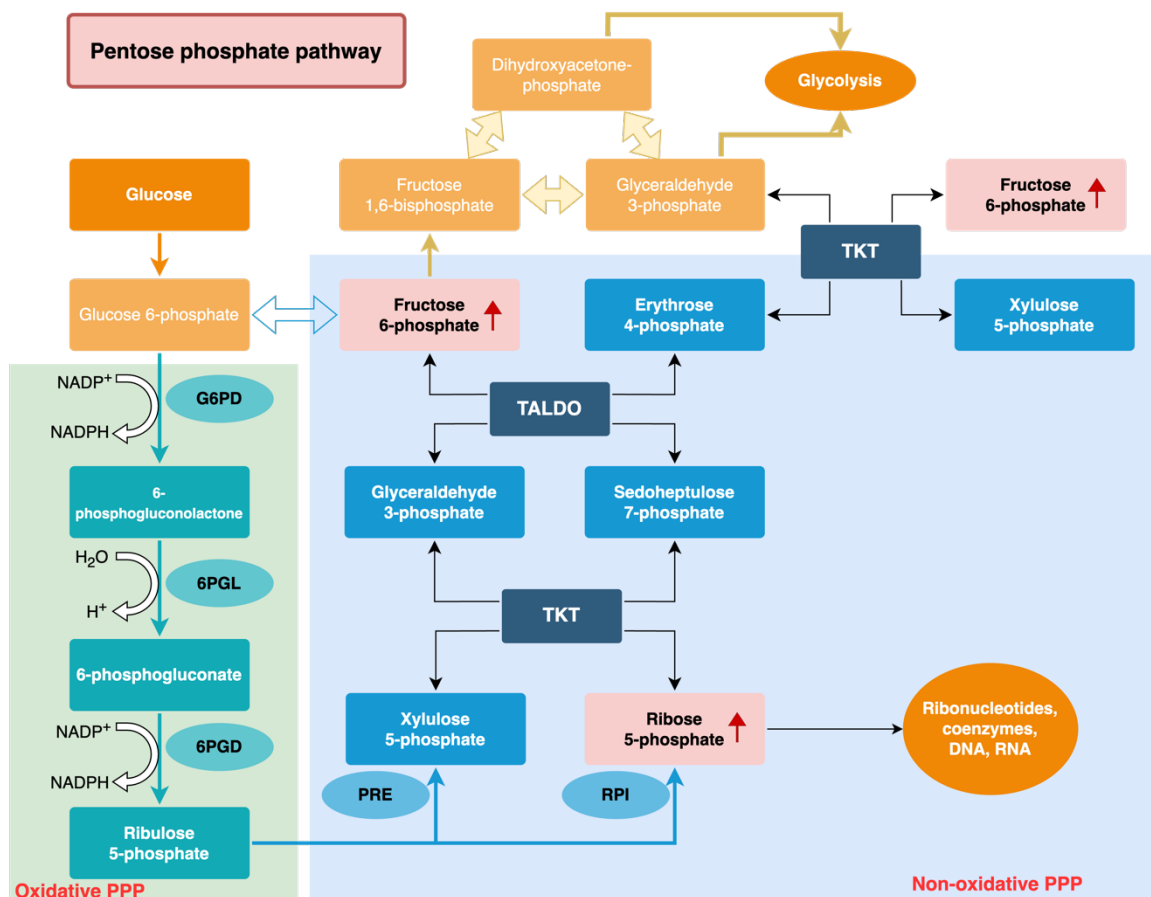


Figure 4.6 The pentose phosphate pathway (PPP) consists of two branches: oxidative and nonoxidative. The oxidative branch begins with the conversion of glucose to glucose-6-phosphate (G6P) by hexokinases, followed by the oxidation of G6P by glucose-6-phosphate dehydrogenase (G6PDH), resulting in the production of 6-phosphogluconolactone and NADPH. Hydrolysis of 6-phosphogluconolactone by 6-phosphogluconolactonase (6PGL) generates 6-phosphogluconate (6PG), which is subsequently oxidized by 6-phosphogluconate dehydrogenase (6PGDH) to form ribulose-5-phosphate (Ru5P) and a second NADPH molecule. The NADPH produced is essential for lipid biosynthesis and detoxification of reactive oxygen species (ROS) via reduced glutathione (GSH). Ru5P undergoes further processing either through isomerization by Ru5P isomerase (RPI) to produce ribose-5-phosphate (R5P) or via epimerization by Ru5P epimerase (RPE) to generate xylulose-5-phosphate (Xu5P). R5P serves as a precursor for ribonucleotide synthesis, which is crucial for DNA replication and DNA damage repair. The nonoxidative branch of the PPP utilizes R5P and Xu5P to produce glycolytic intermediates. Transketolase (TKT) transfers two-carbon units from Xu5P to R5P, resulting in sedoheptulose-7-phosphate (S7P) and glyceraldehyde-3-phosphate (G3P). Transaldolase (TALDO) then transfers three-carbon units from S7P to G3P, forming erythrose-4-phosphate (E4P) and fructose-6-phosphate (F6P). A second TKT reaction transfers two-carbon units from Xu5P to E4P, producing additional F6P and G3P. F6P can either enter glycolysis or regenerate G6P to support the oxidative branch, while G3P is channeled into glycolysis based on cellular requirements. The oxidative (highlighted in green background) and nonoxidative (highlighted in blue background) branches of the PPP work synergistically to meet the biosynthetic and metabolic needs of the cell. In this study, substrates R5P and F6P, highlighted with a red background, were observed in MCF-7 cell extracts.

Glycerophospholipid metabolism

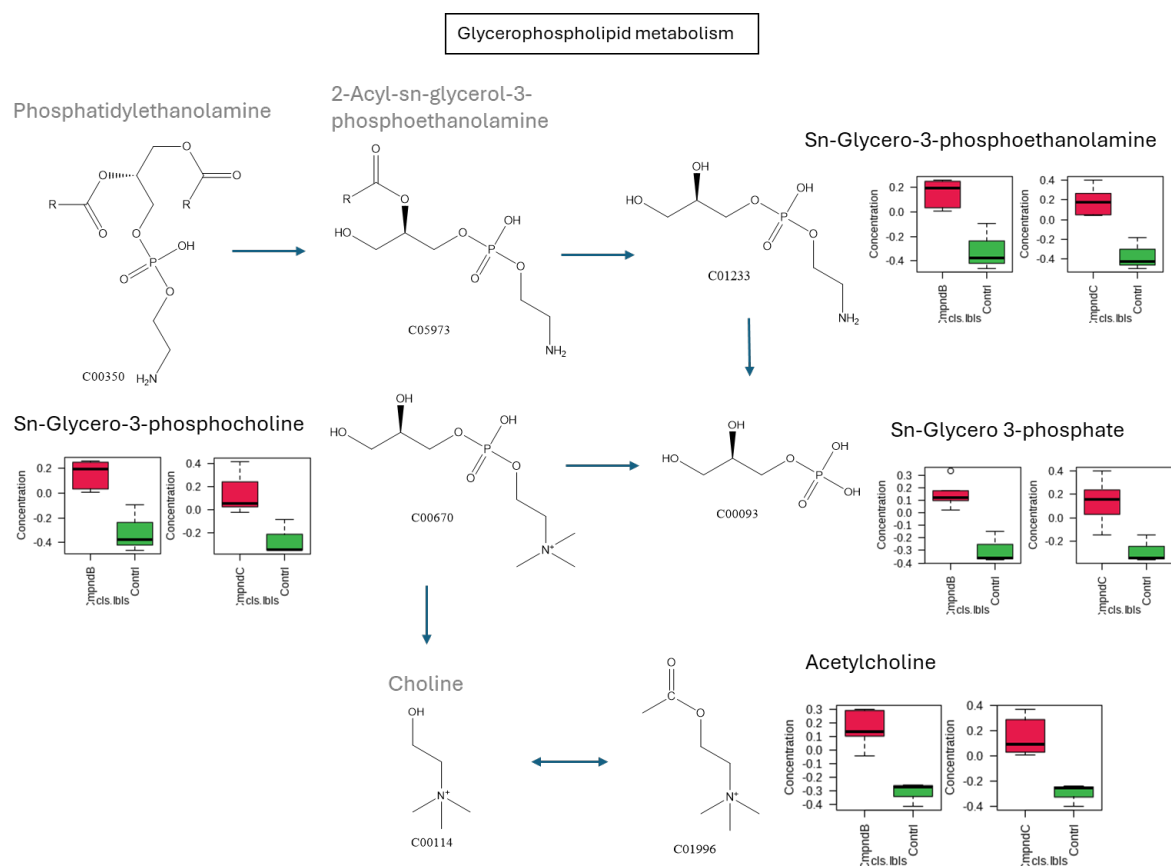


Figure 4.7 glycerophospholipid metabolism affected by caledonine (3) and eumatanine (4) in MCF-7 cells; analysed via MetaboAnalyst 6.0, data transformation: Log, data scaling: pareto; names in black are hit metabolites.

The reprogramming of glycerophospholipid metabolism is considered a cancer-specific feature, as its dysregulation has been observed in multiple cancers, including breast cancer (Brantley et al., 2022), pharyngolaryngeal cancer (Jee et al., 2016), esophageal squamous cell carcinoma (ESCC) (Yang et al., 2022), lung cancer (e.g. Lewis lung carcinoma (LLC), NSCLC) (Wu et al., 2020a, Shi et al., 2019), prostate cancer (Lima et al., 2022), hepatocellular carcinoma (HCC) (Bi et al., 2024), cholangiocarcinoma (CCA), gastric cancer (GC) (Wang et al., 2021c), retinoblastoma (Rb) (Gulati et al., 2023), CRC (Wang et al., 2021b), ovarian cancer (Lu et al., 2022), and skin squamous cell carcinoma (SCC) (Mei et al., 2024). Glycerophospholipid metabolism has shown great potential as a novel target for cancer therapy. For instance, significant alterations in glycerophospholipid metabolism have been observed during ESCC progression, with 16 out of 77 related genes displaying differential mRNA expression. Among these, Phosphatidylserine Synthase 1 (PTDSS1) and Lysophosphatidylcholine Acyltransferase 1 (LPCAT1) demonstrated strong diagnostic potential when compared between ESCC and

normal controls (Yang et al., 2022). Additionally, Compound Kushen Injection (CKI), a TCM formulation with over 15 years of established clinical use in the management of NSCLC and recognised antitumour efficacy, has also been reported to exert therapeutic effects on LLC through an association with glycerophospholipid metabolism by modulating the abnormal biosynthetic pathway of 1-acyl-sn-glycero-3-phosphoinositol (Wu et al., 2020a). However, alterations in glycerophospholipid metabolism may also be associated with drug resistance. For instance, significant changes in glycerophospholipid metabolism-derived metabolites (e.g. Lysophosphatidylcholine (lyso PC), sn-glycero-3-phosphocholine) have been observed in cisplatin-resistant NSCLC cells (A549), multidrug-resistant CRC cells (SW620/Ad300) and paclitaxel-resistant ovarian cancer cells (Shi et al., 2019, Wang et al., 2021b).

Glycerophospholipids, not only are amphipathic molecules that asymmetrically distributed between the two bilayers of all cellular membranes, but also important components of the membrane that are capable of offering a suitable environment, fluidity, and ion permeability. Additionally, it is pointed out that neural membranes glycerophospholipids are involved in apoptosis, generation of second messengers, (e.g. arachidonic acid, eicosanoids), regulation of enzyme activities (e.g. phospholipases A1, A2, C and D), membrane anchor, antioxidant and membrane fusion, elaborating its possible role in acute neural trauma and chronic neurological diseases (Farooqui et al., 2000). It is suggested that phospholipase A2 inhibitors may exert neuroprotective and anti-apoptotic effects in neural cells, and thus it may play an important role in the development of treatments of neurologic disorders such as stroke, Alzheimer disease, Parkinson disease, and head and spinal cord injuries (Farooqui et al., 2007). Since the characterisation of apoptosis includes the loss of intact membrane and the externalisation of phosphatidylserine (PS), the detection of apoptotic cells can be realised by detecting the PS on the cell surface by using a fluorescent conjugated annexin V (as described in section 6.2.5.2 Apoptosis assay). The increased abundance of metabolites in glycerophospholipid metabolism also corroborated the positive results of the apoptosis assay in section 3.2.2 of this study.

In MetaboAnalyst, intensities are first normalised (e.g., to sample sum/median), then log-transformed—so values <1 become negative—and finally Pareto-scaled (mean-centred and divided by the square root of standard deviation), meaning values below the across-sample grand mean plot negative. Accordingly, negative y-axis values do not indicate negative

concentrations but measurements below the reference/mean on the transformed scale. For example, **Figure 4.7** shows four differential metabolites—sn-glycero-3-phosphoethanolamine (GPE), sn-glycero-3-phosphocholine (also known as glycerophosphocholine, GPC), sn-glycero-3-phosphate (G3P) and acetylcholine (ACh)—that map to the glycerophospholipid pathway. On the normalised, log-transformed, Pareto-scaled scale, these metabolites are negative in the control and positive in the treated groups, indicating higher abundance after exposure to either 3 or 4 and suggesting that both compounds may induce glycerophospholipid metabolism.

Among these four metabolites, GPE and GPC are widely recognised as indicators of disruptions in the formation and maintenance of cellular membranes (Karanjia et al., 2016). They also serve as precursors in choline biosynthesis, the dysregulation of which is acknowledged as a metabolic hallmark of oncogenesis (Grinde et al., 2014, Glunde et al., 2011). For instance, GPE and GPC demonstrated a significant inverse association with the risk of ER+ BC at distant timepoints, although these associations were weaker and not statistically significant at proximate timepoints (Brantley et al., 2022).

GPC has exhibited various patterns of dysregulation across different cancer types. It was significantly downregulated in patients with RB, and a decrease in GPC, along with GTP, hypoxanthine, and niacinamide, was observed in MDA-MB-231 cells (Gulati et al., 2023, Gallo et al., 2023). Conversely, elevated levels of GPC, along with myoinositol, taurine, and creatine, were found in senescent H-Ras cell extracts, where cellular senescence, characterised by stable cell cycle arrest, often promotes tumour progression through a senescence-associated secretory phenotype (SASP) (Knopf et al., 2024). This characteristic was also observed in compound **3/4**-treated MCF-7 cells in this study. Furthermore, GPC has been identified as the preferred substrate of the glycerophosphodiesterase endometrial differential 3 (EDI3), which produces G3P, an enzyme that has been positively associated with metastasis in endometrial carcinoma (Marchan et al., 2012).

Similarly, GPE has shown significant dysregulation in various cancers. It was downregulated in advanced neuroendocrine tumours (NETs), upregulated in SCC, and altered in CRC,

highlighting its potential as a diagnostic biomarker for these cancers (Soldevilla et al., 2021, Mei et al., 2024, Liu et al., 2020b).

ACh, a key product of phospholipid biosynthesis, was also identified as a dynamic metabolic biomarker in locally advanced rectal cancer (LARC) patients undergoing neoadjuvant chemoradiation therapy (NCRT) (Lv et al., 2022). ACh levels demonstrated a decreasing trend throughout treatment, with elevated levels specifically observed in NCRT-sensitive patients, underscoring its potential role in predicting treatment response (Lv et al., 2022). ACh acts as an autocrine growth factor in CRC, promoting tumour proliferation and progression through nicotinic acetylcholine receptor signaling pathways (Xie and Raufman, 2016, Cheng et al., 2008). These findings highlight the critical role of ACh in tumour metabolism and its potential as a biomarker for therapeutic sensitivity in LARC.

These metabolites also play critical roles in drug resistance mechanisms. For example, the upregulation of GPC levels observed in paclitaxel-resistant ovarian cancer have been linked to the reprogramming of glycerophospholipid metabolism, contributing to drug resistance (Lu et al., 2022). Similarly, ACh was identified as a key metabolite in drug-tolerant persister (DTP) cells in EGFR-mutant NSCLC, where its accumulation was observed following EGFR-TKI treatment (Yao et al., 2023, Nie et al., 2022). This treatment also increased choline acetyltransferase (ChAT), the rate-limiting enzyme in ACh biosynthesis, through YAP-mediated signaling, highlighting ACh's critical role in drug resistance (Nie et al., 2022).

To summarize, the dysregulation of glycerophospholipid metabolism is a hallmark of cancer progression, therapeutic resistance, and other diseases. Metabolites such as GPE, GPC, and ACh are closely linked to membrane integrity, oncogenic signaling, and metabolic reprogramming. In this study, compounds **3** and **4** demonstrated a significant ability to modulate glycerophospholipid metabolism, evidenced by the upregulation of key metabolites such as GPE, GPC, and ACh in treated MCF-7 cells. These alterations reflect the compounds' ability to disrupt cancer cell membrane dynamics, induce apoptosis, and modulate metabolic pathways critical for tumour proliferation and survival (Karanjia et al., 2016, Cheng et al., 2008, Xie and Raufman, 2016).

Arginine and proline metabolism

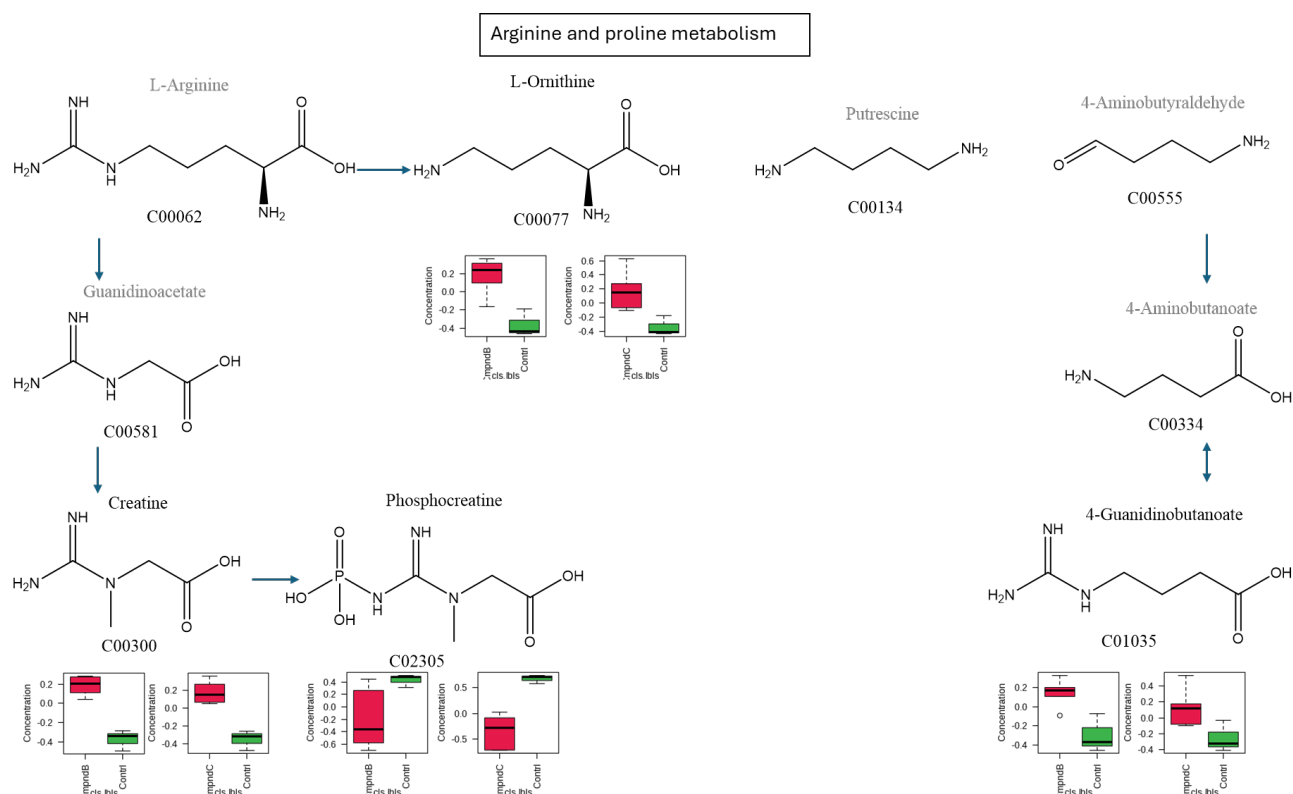


Figure 4.8 Arginine and proline metabolism affected by caledonine (**3**) and eumatanine (**4**) in MCF-7 cells; analysed via MetaboAnalyst 6.0, data transformation: Log, data scaling: pareto; names in black are hit metabolites.

Arginine and proline metabolism is the pathway to biosynthesising the amino acids arginine and proline from glutamate, which plays a critical role in the regulation of various cellular process. The metabolic pathway analysis highlights significant dysregulation in arginine and proline metabolism in response to the treatment of compound **3** and **4**, with specific upregulation of L-ornithine, creatine, and 4-guanidinobutanoate, and downregulation of phosphocreatine. These four metabolites were identified and showed the same regulation patterns in both **3** vs control and **4** vs control comparisons (**Figure 4.8**). These consistent regulatory patterns across both compounds highlight the pathway's involvement in cancer cell metabolic adaptations and cytotoxic responses.

The arginine and proline metabolism pathway has been identified as a consistently altered pathway at both transcriptional and metabolic levels when comparing the androgen-dependent prostate cancer cell line LNCaP with its androgen-independent derivative (Dai et al., 2023).

These findings underscore the significant involvement of the arginine and proline metabolism pathway in castration-resistant prostate cancer (CRPC), highlighting the importance of developing therapeutic strategies that target dysregulated metabolites and differentially expressed genes for effective clinical management of the disease. Besides, it has been reported that increased proline catabolism is associated with metastasis formation in BC, while inhibition of this pathway results in decreased lung metastasis formations in vivo (Elia et al., 2017).

L-Ornithine, an essential intermediate in the arginine and proline metabolic pathway, plays a dual role in tumour biology by driving both polyamine and proline synthesis. The upregulation of L-ornithine by compounds **3** and **4** may reflect their influence on arginase activity, which converts L-arginine to L-ornithine (Wu and Morris, 1998). This upregulation is particularly significant because elevated L-ornithine levels enhance the production of polyamines, such as putrescine, spermidine, and spermine, through the enzymatic action of ornithine decarboxylase (ODC), while polyamines are critical for DNA stabilization, cell proliferation, and tumour progression (Lange et al., 2004, Satriano, 2004).

By modulating L-ornithine metabolism, compounds **3** and **4** may interfere with polyamine biosynthesis, while increased polyamine levels have been proposed as promising biomarkers for cancer diagnosis and treatment response, including in lung, liver, ovarian, colon, and pancreatic cancers (Liu et al., 2017b, Xu et al., 2016, Niemi et al., 2017, Liu et al., 2018, Asai et al., 2018). Previous studies have demonstrated that inhibitors of ODC, such as difluoromethylornithine (DFMO), exhibit potent anti-proliferative effects by depleting polyamine levels in cancers such as neuroblastoma, colon cancer, and hepatocellular carcinoma (Koomoa et al., 2013, Raul, 2007, Arisan et al., 2012, Liu et al., 2021). Similarly, compounds **3** and **4** may exploit this pathway to reduce polyamine production, thereby impairing MCF-7 cancer cell proliferation and survival. Furthermore, as L-ornithine can also be converted into proline via ornithine aminotransferase (OAT), compounds **3** and **4** may influence collagen synthesis and extracellular matrix remodelling, processes that are essential for tumour invasion and metastasis (Durante et al., 2007). Additionally, elevated ODC activity has been observed in hepatocellular carcinoma cells, while the inhibition of ODC expression contributing to reduced cell proliferation, impaired colony formation, and induced cell cycle arrest (Ye et al.,

2019). Furthermore, L-ornithine acts as a potent feedback inhibitor of arginase, underscoring its critical role in regulating arginase activity and associated metabolic pathways (e.g. arginine and proline metabolism) (Hunter and Downs, 1945). The ability of these compounds to disrupt both polyamine and proline production positions them as promising pharmacological agents for highly aggressive and metastatic cancers.

Creatine (Cr) is a key metabolite involved in cellular energy buffering and transport, with its upregulation following treatment with compounds **3** and **4** potentially suggests an adaptive response by MCF-7 cancer cells to meet their elevated energy demands (Zhang and Bu, 2022). Cr, a nitrogenous organic acid, is synthesized endogenously in the kidney and liver from arginine and glycine through the enzymes L-arginine:glycine amidinotransferase (AGAT/GATM) and guanidinoacetate N-methyltransferase (GAMT) (Li and Yang, 2021). Once synthesized, Cr enters circulation and is taken up by Cr transporter (CrT/SLC6A8)-expressing cells, where it is phosphorylated by creatine kinase (CK) using ATP to form phosphocreatine (PCr), a high-energy phosphate reservoir (Wyss and Kaddurah-Daouk, 2000). Cancer cells rely heavily on this pathway to sustain rapid proliferation and survival.

Compounds **3** and **4** appear to disrupt the creatine-phosphocreatine shuttle by simultaneously upregulating Cr and downregulating PCr levels. This suggests that these compounds may inhibit CK, an enzyme that catalyzes the reversible transfer of phosphate between Cr and ATP. CK inhibitors (CKi), such as those targeting the active cysteine residue of CK isoforms to suppress the production of PCr, have been shown to disrupt tumour energy homeostasis and induce apoptosis in acute myeloid leukaemia (AML) (Darabedian et al., 2023). Besides, in prostate cancer (PC3 cells), PCr depletion has been associated with suppressed cell proliferation and impaired cell invasion (Patel et al., 2022). The downregulation of phosphocreatine reflects the disrupted energy dynamics in cancer cells, with the PCr-CK circuit serving as a potential target to impair cancer cell energy homeostasis (Darabedian et al., 2023). By interfering with CK activity and reduce PCr level, **3** and **4** could reduce ATP buffering capacity, leading to energy depletion and subsequent cell death. This mechanism highlights the pharmacological potential of targeting CK and Cr metabolism in energy-demanding cancers such as glioblastoma, CRC, BC, AML and prostate cancer (Pirzkall et al., 2009, Zhang et al., 2021, Darabedian et al., 2023, Patel et al., 2022).

Additionally, CK contributes to the growth of various tumours and exists in isoforms localized within both the cytoplasm and mitochondria. In the cytoplasm, three isoenzymes have been identified: muscle-type (CKMM), brain-type (CKBB), and heart-type (CKMB) (Wallimann et al., 1992). Among these isoenzymes, CKBB and CKMB serve as poor prognostic markers in lung cancer and are significantly associated with metastasis in lung, prostate, and ovarian cancers (Forman, 1979, Liu et al., 2017a, Ng et al., 1987, Pan et al., 2013, Pedersen et al., 1985). In the mitochondria, two isoenzymes—ubiquitous-type (CKMT1) and sarcomeric-type (CKMT2)—are transcriptionally upregulated in multiple cancers, including breast invasive carcinoma, bladder urothelial carcinoma, lung adenocarcinoma and small cell carcinoma, stomach adenocarcinoma, and ovarian cancer, as revealed by TCGA and GEO datasets (Schlattner et al., 2006, Kurmi et al., 2018).

Furthermore, the upregulation of Cr by these compounds may have context-dependent pharmacological implications. While elevated Cr levels are associated with tumour progression in certain cancers (hepatocellular carcinoma, BC, and glioblastoma), Cr supplementation has demonstrated anti-tumour effects in CRC, sarcoma, and neuroblastoma, suggesting that Cr metabolism is highly cancer-specific (Ladep et al., 2014, Lécuyer et al., 2018, Pirzkall et al., 2009, Maguire et al., 2021, Zhang et al., 2021, Kristensen et al., 1999, Miller et al., 1993). These contradictory findings highlight the complex role of Cr metabolism in different cancers and the effect of compounds **3** and **4** on Cr metabolism is warrant further investigation.

4-Guanidinobutanoate, an intermediate in the catabolism of arginine, has received less attention in cancer research. However, its accumulation following the treatment of **3** or **4** could indicate enhanced arginine degradation, which might contribute to the production of energy intermediates or signalling molecules promoting tumour survival. By upregulating 4-guanidinobutanoate, **3** and **4** may promote the depletion of arginine, which is critical for immune cell activation, thereby potentially impairing cancer cell survival (Lind, 2004). For example, in hepatocellular carcinoma and melanomas, enhanced arginine degradation through the use of the arginine-degrading enzyme arginine deiminase (ADI) has been shown to contribute to the inhibition of tumour growth (Ensor et al., 2002).

To sum up, compounds **3** and **4** demonstrate significant potential by targeting key aspects of the arginine and proline metabolism pathway. They modulate critical metabolites, including L-

ornithine, Cr, 4-guanidinobutanoate, and PCr, disrupting processes such as polyamine and proline biosynthesis, as well as energy buffering. L-ornithine plays a central role, driving tumour growth and metastasis, while Cr and PCr disruption impair energy homeostasis, inducing cytotoxic effects (Caldwell et al., 2018, Murray-Stewart et al., 2016, Kristensen et al., 1999, Miller et al., 1993, Darabedian et al., 2023). Their ability to inhibit key enzymes such as ornithine ODC and CK highlights their potential to suppress cancer cell proliferation and survival (Ye et al., 2019, Darabedian et al., 2023).

These findings highlight the pharmacological relevance of targeting the arginine and proline metabolism pathway in various cancer, including CRPC, and metastasis in breast and lung cancers (Dai et al., 2023, Elia et al., 2017). Further research into the cytotoxic mechanisms of compounds **3** and **4**, along with their impact on these dysregulated metabolites, could provide valuable insights for developing more effective cancer treatments.

Amino sugar and nucleotide sugar metabolism (ANM)

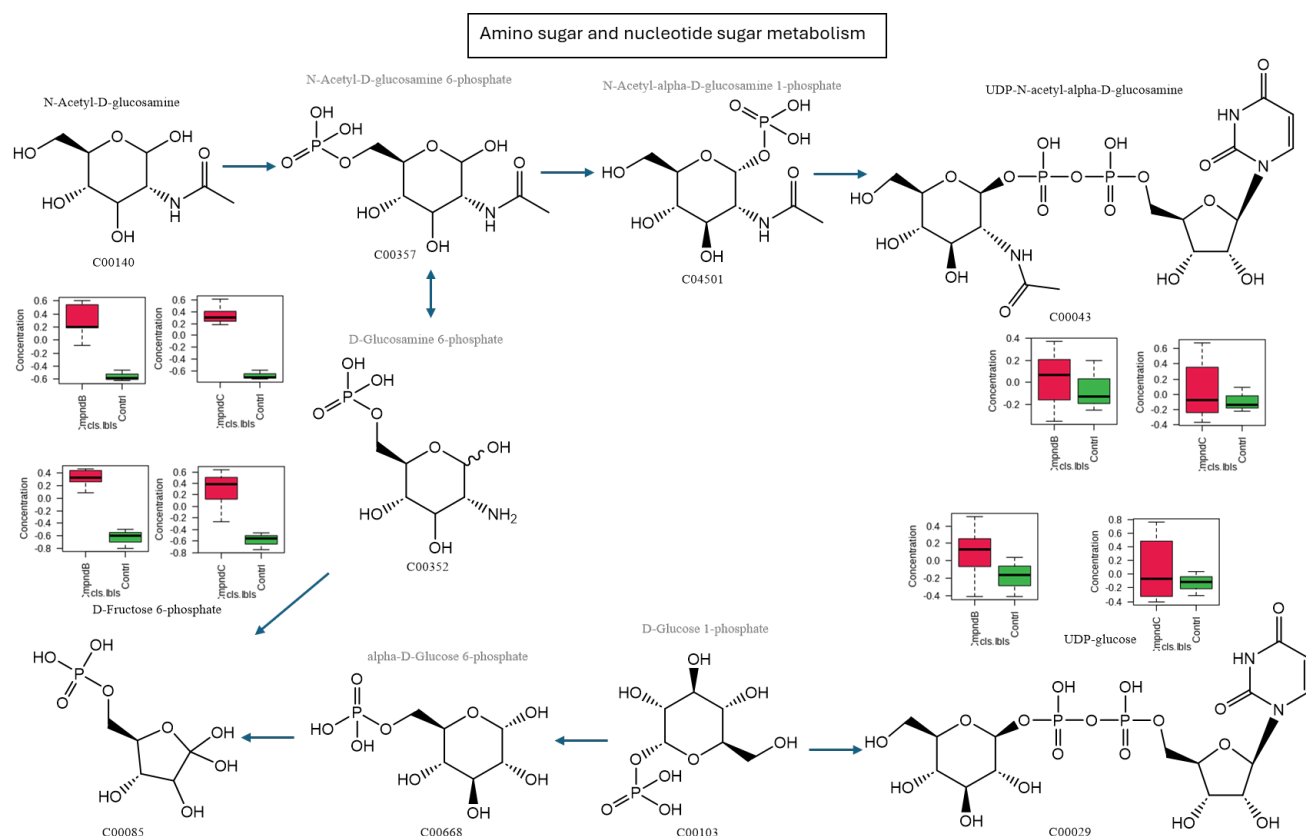


Figure 4.9 Amino sugar and nucleotide sugar metabolism affected by caledonine (**3**) and eumatanine (**4**) in MCF-7 cells; analysed via MetaboAnalyst 6.0, data transformation: Log, data scaling: pareto; names in black are hit metabolites.

Amino sugars are sugar derivatives in which a hydroxyl group is replaced by an amine group, with glucosamine, galactosamine, and neuraminic acid being prominent examples. In contrast, nucleotide sugars are activated monosaccharides that serve as glycosyl donors in glycosylation reactions catalyzed by glycosyltransferases. Both amino sugars and nucleotide sugars play critical roles in regulating protein function.

Amino sugar metabolism begins with the phosphorylation of D-fructose, producing β -D-fructose 6-phosphate, which serves as a key intermediate for three metabolic pathways, namely, hexosamine biosynthetic pathway (HBP), mannose pathway, and HBP-glucose and galactose pathway. These pathways are central to the consumption of glucose and glutamine, and the production of nucleotide sugars, which act as glycosyl donors in glycosylation processes, supporting vital biological functions (Mikkola, 2020). For example, the HBP is a critical metabolic pathway that produces uridine-5'-diphospho-N-acetylglucosamine (UDP-GlcNAc), a key metabolite used in N-linked glycosylation of secretory and cell-surface proteins and O-GlcNAcylation of intracellular proteins at serine/threonine residues (Paneque et al., 2023). The high consumption of glucose is commonly in tumour cells and alterations in glycosylation are often observed in cancers, including gastric and colon cancers, hepatocellular carcinomas, as well as pancreatic, breast, lung, prostate, cervical and ovarian cancers, reflecting the metabolic reprogramming required to sustain rapid proliferation, invasion, and metastasis (Brockhausen, 1999, Kudelka et al., 2015, Corfield, 2015, Dhanisha et al., 2018, Nikitovic et al., 2018). The observed upregulation of N-acetyl-D-glucosamine (GlcNAc), UDP-N-acetyl-alpha-D-glucosamine (UDP-GlcNAc), D-fructose 6-phosphate (D-F6P), and UDP-glucose in response to both **3** and **4** treatment highlights the profound impact of these compounds on cancer cell metabolism.

GlcNAc and its nucleotide derivative UDP-GlcNAc are central components of the HBP, which channels glucose and glutamine metabolism toward glycosylation (Paneque et al., 2023). The upregulation of these metabolites by both **3** and **4** suggests that they enhance HBP activity, thereby influencing glycosylation-dependent processes in cancer cells. Glycosylation of proteins (N-glycosylation), such as EGFR and programmed death ligand 1(PD-L1), plays a critical role in tumour proliferation, metastasis, and immune evasion (Dhanisha et al., 2018, Chen et al., 2021, Dragic et al., 2022). However, this enhanced glycosylation could also be

triggered therapeutically, as elevated levels of UDP-GlcNAc have been observed in cisplatin-treated tumour cells, where its accumulation is associated with the induction of apoptosis, suggesting a potential role in mediating cancer cell death (Pan et al., 2011).

UDP-GlcNAc plays a vital role in protein glycosylation, influencing protein folding, stability, and function, while GlcNAc contributes exclusively to UDP-GlcNAc in cultured mammalian cells (Ryczko et al., 2016, Wellen et al., 2010). In N-glycosylation, it facilitates glycoprotein maturation and branching in the Golgi, which is essential for membrane protein stability and cell signaling. Defects in N-glycosylation lead to misfolded proteins, ER stress, and altered cell fate (Denzel and Antebi, 2015, Vasseur and Manié, 2015). Similarly, O-GlcNAcylation, which modifies signaling proteins, transcription factors, and metabolic regulators, impacts cell signaling, metabolism, and immune surveillance (Akella et al., 2019, Swamy et al., 2016). Notably, activated immune T cells exhibit elevated concentrations of UDP-GlcNAc and enhanced intracellular protein O-GlcNAcylation (Swamy et al., 2016). Besides, the availability of UDP-GlcNAc is tightly regulated by nutrient flux and key enzymes, particularly glutamine: fructose-6-phosphate amidotransferase (GFAT), the rate-limiting enzyme of the de novo HBP. Elevated UDP-GlcNAc level and GFAT overexpression have been linked to aggressive cancers, including NSCLC, pancreatic ductal adenocarcinoma (PDAC) and colon cancer (Kim et al., 2020, Campbell et al., 2021, Vasconcelos-dos-Santos et al., 2017). This suggests that GFAT could serve as a promising pharmacological target for inhibiting tumour growth, as studies have demonstrated a reduction in tumour size, growth, and metastasis following GFAT deficiency in colon cancer models (Vasconcelos-dos-Santos et al., 2017).

D-Fructose-6-phosphate (D-F6P) is a central metabolite in both the pentose phosphate pathway (PPP) and amino sugar and nucleotide sugar metabolism (ANM), where the two pathways diverge after sharing the initial two steps. Differential levels of D-F6P were observed in MCF-7 cells following treatment with compounds **3** or **4**. Pathway analysis revealed that both the PPP and amino ANM were annotated in response to treatment with compound **3**, whereas only ANM was annotated for cells treated with compound **4**. The upregulation of D-F6P by **3** or **4** indicates increased glycolytic flux and improved metabolic demand, hallmarks of the Warburg effect in cancer cells (Hosios and Manning, 2021). By enhancing the levels of D-F6P, compound **3** or **4** may be driving tumour cells to rely heavily on glycolysis and the HBP for

energy production and biosynthesis, supporting their rapid proliferation and survival (Akella et al., 2019).

UDP-glucose, a nucleotide sugar involved in glycogen biosynthesis and glycosylation, is also upregulated in response to the treatment of **3** and **4**. The observed increase may indicate enhanced N-linked glycosylation, with UDP-glucose acting as a key donor substrate, facilitating the glycosylation of cancer cells to promote the binding of growth factors (e.g., EGFR) and cytokines, thereby driving proliferation and metastasis through multiple signalling cascades (Wolfe et al., 2021, Dhanisha et al., 2018). Additionally, given that UDP-glucose serves as the direct precursor in glycogen biosynthesis, elevated UDP-glucose levels may indicate increased glycogen biosynthesis, which is a strategy employed by cancer cells to buffer energy fluctuations, withstand metabolic stress, and subsequently sustain proliferation (Wolfe et al., 2021, Favaro et al., 2012, Zois et al., 2014).

However, the upregulation of UDP-glucose has also been associated with impaired tumour metastasis in lung cancer through the regulation of UDP-glucose 6-dehydrogenase (UGDH) and SNAI1 (Wang et al., 2019). UGDH, a key enzyme in the uronic acid pathway, catalyzes the conversion of UDP-glucose to UDP-glucuronic acid, stabilizing SNAI1, a critical regulator of epithelial–mesenchymal transition (EMT), thereby promoting tumour cell migration and metastasis (Spicer et al., 1998).

To summarize, the simultaneous upregulation of GlcNAc, UDP-GlcNAc, D-F6P, and UDP-glucose in response to the treatment of **3** or **4** in MCF-7 cells highlights its profound impact on amino sugar and nucleotide sugar metabolism. These alterations reflect enhanced glycosylation, glycolysis, and glycogen biosynthesis in MCF-7 cells, which are cellular processes essential for their survival and proliferation. Additionally, the ability of **3** and **4** to upregulate metabolites like UDP-GlcNAc and UDP-glucose may have implications for tumour glycosylation and immune evasion. Aberrant glycosylation is a hallmark of aggressive cancers, and targeting glycosylation pathways could impair tumour growth and metastasis while enhancing immune recognition (Swamy et al., 2016, Pan et al., 2011). Further research is warranted to elucidate the precise mechanisms underlying these metabolic changes and their impact on tumour progression.

4.3 Conclusion and future work

The metabolomics study within this project aims to discover the metabolic effects caused by caledonine (**3**) and eumatanine (**4**) on BC phenotypes' metabolomes MCF-7 and thus attempt to identify potential biomarkers and metabolic pathways related to its mechanisms of action in terms of anticancer activity. Multiple analyses were conducted to achieve this, including the multivariate analysis, significant metabolites analysis and metabolic pathway analysis. The OPLS-DA models indicated obvious metabolic differences between the drug treated and control group, while more significant metabolites were obtained for the comparison of **4** vs control group than **3** vs control group.

There are three key metabolic pathways were simultaneously affected by **3** and **4** in MCF-7, namely, glycerophospholipid metabolism, arginine and proline metabolism, and amino sugar and nucleotide sugar metabolism. Notably, the majority of metabolites within these pathways were increased. This metabolomics study highlights that treatment with **3** or **4** led to significant changes in the metabolomic phenotype of MCF-7 cells compared to the non-treated control group. Both compounds demonstrated considerable pharmacological potential by targeting critical metabolic pathways essential for cancer progression and survival.

In MCF-7 cells, **3** and **4** modulated glycerophospholipid metabolism, increasing key metabolites such as GPE, GPC, and ACh. These changes disrupted membrane integrity, induced apoptosis, and exploited metabolic vulnerabilities. Additionally, **3** and **4** disrupted arginine and proline metabolism by targeting metabolites such as L-ornithine, Cr, and PCr, impairing energy buffering and tumour proliferation. These compounds may suppressed cancer growth and metastasis by influencing enzymes like ODC and CK. Their treatment also upregulated key metabolites such as GlcNAc, UDP-GlcNAc, D-F6P, and UDP-glucose, indicating enhanced glycosylation, glycolysis, and glycogen biosynthesis, which are processes essential for cancer cell proliferation. These findings suggest potential implications for tumour glycosylation and immune evasion, offering a potential strategy to impair tumour growth and metastasis.

To further advance the understanding of the pharmacological potential of **3** and **4**, metabolomics-driven research could be expanded to explore broader metabolic changes across different cancer types and stages. Metabolomics can help elucidate the precise mechanisms underlying the metabolic shifts induced by these compounds, providing a systems-level understanding of how cancer cells adapt their metabolism to sustain survival under stress conditions. This approach would also allow the identification of additional biomarkers for drug response, which could facilitate understanding the underlying cellular mechanisms of **3** and **4**. Additionally, future work should investigate the primary molecular targets of compounds **3** and **4**, in which advanced target identification techniques, such as CRISPR/Cas9-based gene editing, thermal proteome profiling, or chemical proteomics can be employed. Validating these targets through knockdown or overexpression studies will clarify how these compounds disrupt cellular processes.

In the light of anticancer drug discovery, these findings reveal the importance of targeting specific metabolic pathways as a strategy to combat drug resistance and improve pharmacological outcomes. The development of derivatives or analogues of **3** and **4** with improved pharmacokinetics and lower toxicity profiles could enhance their clinical potential. To validate the broad-spectrum cytotoxicity of **3** and **4**, their effects should be tested across diverse cancer cell lines and patient-derived tumour models. By comparing their impact on cancer versus normal cells, their cancer selectivity and minimize off-target effects can be assessed. Furthermore, investigating their activity in drug-resistant cancer models could provide insights into overcoming drug resistance.

Given the significant role of glycosylation and lipid metabolism in cancer metastasis and immune evasion, further research should explore the potential of **3** and **4** in modulating tumour-stromal interactions and immune cell function within the tumour microenvironment. The integration of metabolomics with proteomics and transcriptomics would provide a multi-dimensional understanding of the molecular changes induced by these compounds, offering a robust platform for the discovery of next-generation anticancer therapies.

Despite its advantages, metabolomics faces challenges in studying NPs due to the inherent complexity of NP mixtures, low reproducibility across different cell lines, models, and analytical platforms arising from variability in experimental design, and the limited availability of comprehensive spectral libraries for NPs, which further complicates identification. To address these challenges, future research should integrate metabolomics with multiomics approaches (e.g., genomics, transcriptomics, and proteomics) to provide holistic insights into the mechanisms of NP action. Additionally, the application of AI and machine learning holds the potential to enhance metabolite identification and pathway prediction. Precision medicine is another promising avenue, where metabolomics-guided NP research can facilitate personalized anticancer therapies by targeting specific metabolic vulnerabilities in tumours.

Chapter 5 General Conclusion

This study has significantly contributed to the understanding of *Eumachia montana* as a novel source of bioactive oligocyclotryptamine alkaloids, expanding the chemical and biological knowledge of this underexplored genus. A series of structurally related alkaloids, including the hexameric (+)-oleoidine (**2**), the heptameric (+)-caledonine (**3**), and new octameric (+)-eumatanine (**4**), were successfully isolated and characterized, alongside the known dimer (–)-calycanthine (**1**) and a newly identified tricyclic pyrroloquinoline alkaloid eumatricine (**5**). The structural elucidation of these compounds underscores the remarkable chemical diversity within the Rubiaceae family and highlights their potential for further pharmaceutical development.

The biological evaluation of these alkaloids revealed potent cytotoxicity, broad-spectrum growth inhibition, and apoptosis induction in carcinoma cell lines, reinforcing their relevance in NPDD. Compounds **2** and **3** exhibited cell cycle-independent apoptotic activity, likely mediated by ROS generation, while compound **4** triggered DNA DSBs and apoptosis, as indicated by γ H2AX foci detection and fluorescence microscopy analyses. Additionally, cytoplasmic vacuolization observed in treated cells suggests the possible involvement of alternative cell death pathways, such as paraptosis. The observed antitumour effects highlight the potential of these alkaloids as lead compounds for cancer therapy, although their non-cancer selectivity and potential toxicity warrant further study, and investigation of the potential for nanoparticle formation or delivery.

Metabolomic profiling of BC cells treated with **3** and **4** revealed profound alterations in key metabolic pathways, particularly glycerophospholipid metabolism, arginine and proline metabolism, and amino sugar and nucleotide sugar metabolism. These metabolic disruptions suggest that the anticancer activity of these compounds is, at least in part, mediated by their ability to interfere with essential metabolic processes that support tumour growth and survival. The increase of metabolites such as GPE, GPC, and ACh suggests a role in disrupting membrane integrity and inducing apoptosis, while the modulation of arginine and proline metabolism, targeting metabolites such as L-ornithine and creatine, implicates their influence on energy buffering and tumour proliferation. Additionally, enhanced glycosylation, glycolysis,

and glycogen biosynthesis highlight a potential impact on tumour glycosylation and immune evasion, providing novel therapeutic insights.

While these findings emphasize the promising anticancer potential of *E. montana*-derived alkaloids, several critical aspects require further investigation. Expanding metabolomics-driven research to different cancer types and stages would provide a broader understanding of the metabolic vulnerabilities targeted by these compounds. The integration of metabolomics with advanced proteomics and transcriptomics could offer a systems-level perspective on their mode of action, facilitating the identification of molecular targets. Future research should also explore the use of CRISPR/Cas9-based gene editing, thermal proteome profiling, or chemical proteomics to elucidate the precise mechanisms by which these alkaloids disrupt cellular processes. Furthermore, validation of these targets through genetic knockdown or overexpression studies will be crucial in confirming their role in mediating cytotoxicity.

From a drug development perspective, optimizing the pharmacokinetic and toxicity profiles of these alkaloids through structural modifications or nano-formulation strategies may enhance their potency and minimize adverse effects. Investigating their cytotoxicity in drug-resistant cancer models could provide insights into overcoming drug resistance. Moreover, given the significant role of glycosylation and lipid metabolism in cancer metastasis and immune evasion, further studies should explore the impact of 3 and 4 on tumour-stromal interactions and immune cell function within the tumour microenvironment.

In conclusion, this research underscores the importance of natural product-based drug discovery and highlights *E. montana* as a promising source of structurally unique and biologically potent alkaloids. By bridging the gap between metabolomics, structural biology, and pharmacological evaluation, this study provides a foundation for future investigations into the therapeutic potential of these compounds. The continued exploration of oligocyclotryptamine alkaloids may lead to the development of next-generation anticancer therapies with improved potency and specificity.

Chapter 6 Materials and Methods

6.1 Isolation and Characterisation of Alkaloids

6.1.1 Plant Source and Authentication

The leaves of *E. montana* (Blume) I.M.Turner (syn. *Psychotria montana*) were collected in July 2019 from Hulu Langat, Selangor, Malaysia (3.05792° N, 101.87036° E) and the plant identity was determined by Dr K. T. Yong from Institute of Biological Sciences, Universiti Malaya, Malaysia. A voucher specimen (KLU50139) was deposited at the Herbarium, Universiti Malaya. Although Malaysia had enacted the Access to Biological Resources and Benefit Sharing Act 2017 [Act 795], the Act only came into force on 18 December 2020. At the time of collection, there was no functional system or enforcement mechanism in place for obtaining access and benefit-sharing (ABS) permits. As such, no formal approval was sought. The collection was conducted solely for academic research and without any commercial intent.

6.1.2 General Experimental Procedures

Optical rotation values were measured on a JASCO P-1020 automatic digital polarimeter. 1D and 2D NMR spectra were recorded in CDCl₃ using tetramethylsilane as an internal standard on a Bruker Avance III 600 MHz NMR spectrometer. HRESIMS data were measured on a Thermo Scientific™ Q Exactive™ Plus Hybrid Quadrupole-Orbitrap™ Mass Spectrometer that linked to Dionex HPLC systems (compounds **2-4**), and on a Bruker Daltonics micrOTOF-Q III mass spectrometer (compounds **1** and **5**). Semipreparative HPLC was conducted on a Waters Acquity Arc Ultra High Performance Liquid Chromatography (UHPLC) System equipped with a Waters 2998 photodiode array (PDA) detector and a Waters Fraction Collector III. X-ray diffraction analysis was carried out on a Rigaku Oxford (formerly Agilent Technologies) SuperNova Dual diffractometer with Cu K α (λ = 1.54184 Å) radiation at rt.

6.1.3 Chromatography Techniques

To fractionate and isolate pure alkaloids from the crude alkaloidal extracts, multiple chromatographic methods were employed, including TLC, CTLC, CC and HPLC.

6.1.3.1 Thin Layer Chromatography

TLC was used as a detective chromatography technique in this project. TLC was employed as a pre-examination step before CTLC, CC and HPLC were performed to determine the separation profile of the sample to be separated in order to establish the optimum starting solvent system. Additionally, TLC was also used to monitor the separation and purity of the fractions collected following CTCL, CC and HPLC separations.

In this experiment, TLC was performed on a sheet of aluminium foil coated with a thin layer of silica gel 60 F254. Different samples were applied in a row of spots the same distance from the bottom edge, each of which will develop on the plate according to their chemical characteristics under the effect of saturated solvent systems in a tank. Once the solvent front was 1 cm away from the top edge of the plate, it was removed from the tank and the plate was allowed to dry in a fume hood. The plate was then examined under UV light (254nm). Compounds with a chromophore were visualised as dark spots against a green background. A Dragendorff's reagent spray was used to indicate the presence of alkaloid spots on the TLC plate. Upon spraying, spots containing alkaloids will react with the reagent and turn orange.

To reduce the 'tailing' effect of the TLC spots approximately 0.1% of concentrated ammonia was added to the solvent system. The 'tailing' effect on the TLC was due to protonation of the basic nitrogen in the alkaloids by the acidic silica stationary phase.

6.1.3.2 Column Chromatography

CC was used to fractionate the crude alkaloid mixture and semi-purified fractions that were more than 800 mg. Silica gel 60 (Merck 9385, 230-400 mesh) was used at approximately 50:1 ratio of silica gel to sample, by weight. The silica gel was made into a suspension and packed into the column with repeated solvent refills until the silica bed reached its minimum height.

To further compact the column of silica gel, the column was gently tapped as freshly prepared solvent was eluted under gravity initially (two-column volume) and under vacuum suction eventually (two-column volume). The solvent level in the column was always maintained above the silica bed to prevent air from getting into the silica gel. The sample to be separated was dissolved in a minimum amount of solvent before being transferred to the top of the silica bed by using a long pipette. To protect the layer of sample that was evenly spread on the silica bed during the subsequent addition of solvents, fine sodium sulfate anhydrous (Na_2SO_4) salt was added to the top of the silica bed (approximately 2cm height). The sample was then eluted using solvent of increasing polarity, which started with 100% chloroform, and increasing the polarity with gradual increase of methanol composition. The collected fractions were monitored by TLC, where fractions with similar profiles were combined and then subjected to further separation either by centrifugal TLC or further column chromatography.

6.1.3.3 Centrifugal Thin Layer Chromatography

CTLC is a chromatography technique used to separate fractions with weights below 1 g, which in this case are the majority of fractions collected from the column chromatography. CTLC employs similar principles to TLC, therefore TLC was carried out with every fraction prior to CTLC and then a suitable mobile phase for this fraction was determined. The major difference between TLC and CTLC is that the latter incorporates centrifugal force for elution and UV imaging during separation. CTLC was carried out using a silica-coated circular glass plate that has a diameter of 24cm and a UV transparent lid that enables the visualisation of UV-active bands during the separation process.

The silica-coated plate was prepared by securing the edge of the plate using cellophane tape to form a mould. Silica gel (Kieselgel 60 PF256, Merck 7749) suspension was prepared by adding cold distilled water to the silica gel powder. The suspension was shaken vigorously and was then quickly poured onto the previously prepared mould. To evenly distribute the suspension, the circular glass plate was rotated manually while the gel was being poured, and then the plate with silica gel was tapped a few times before it was left to air-dry for 1 hour. Chromatographic plates with different thickness (1mm, 2mm or 4mm) were made based on the weight of the fraction to be separated. The volume of cold distilled water and amount of silica gel powder

used to make a plate are dependent on the desired thickness of the silica layer and these recipes are shown in **Table 6.1**.

After 1 hour of air-drying, the plate was placed in an oven at 80°C overnight. The silica plate was activated at 100°C for 1 hour prior to use. After activation, the plate was cooled to room temperature and was then shaved to the desirable thickness (1mm, 2mm or 4mm) before being mounted onto the Chromatotron to be used. The chromatotron was cleaned with acetone before use.

Table 6. 1 Recipes for making the silica-coated CTLC glass plate.

Silica layer thickness (mm)	Weight of fraction (mg)	Silica gel (g)	Cold distilled water (mL)
1	<400	40	90
2	400-800	60	110
4	800-1500	110	250

The sample to be separated was dissolved in minimum volume (approximately 0.5 – 2mL) of chloroform and then was loaded to the centre of the plate while the silica-coated glass plate was spinning to form a thin band of sample. This thin band was eluted with the appropriate solvent system, which is usually a system with an increasing polarity gradient. Fractions were collected, concentrated on a rotary evaporator, and were examined by TLC. Fractions with similar TLC profiles were appropriately combined.

6.1.3.4 High-Performance Liquid Chromatography

HPLC was used to separate the alkaloidal fractions that failed to be separated by CTLC after several attempts. Firstly, to develop a method of separation using a semi-preparative HPLC, the sample was dissolved in ethanol, and thus several gradient injections were performed. The solvent system used was H₂O:ACN (0.1%NH₃) or H₂O:MeOH (0.1%NH₃), eluted under a gradient from a ratio of 90:10 to 30:70 in the HPLC system. The H₂O:MeOH 15:85 (0.1%NH₃) solvent system provided the best peak resolution based on the HPLC chromatogram. Thus,

H₂O:MeOH 15:85 (0.1%NH₃) was utilised for the separation of all fractions using a semi-preparative reverse-phase HPLC column (Waters XBridge BEH C18 Prep Column; 5µm, 10 X 100mm). Additionally, a Waters ACQUITY Arc SYSTEM UHPLC equipped with a Waters 2998 PDA detector was used and the separated fractions were collected automatically using a Waters Fraction Collector III. Detailed information summarising the method of HPLC is outlined in **Table 6.2**.

Table 6. 2 HPLC parameters used for semi-preparative separation.

Concentration of sample	~ 10 - 50 mg/mL
Injection volume	10 - 40 µL
Flow rate	4 mL/min
Column Temperature	40 °C
Elution time	30 - 45 min
Mobile phase	H ₂ O:MeOH 15:85 (0.1% NH ₃)

6.1.4 Spray Reagent (Dragendorff's reagent)

To detect the presence of alkaloids on a developed TLC plate, Dragendorff's reagent was used, which was prepared as described by the following steps:

- Solution A: 0.85g bismuth nitrate was added to 40mL distilled water and 10 mL acetic acid.
- Solution B: 8g potassium indole was added to 20mL distilled water.
- The stock solution was prepared by mixing solutions A and B in a ratio of 1:1.
- 100mL of Dragendorff's reagent was prepared by mixing 10mL stock solution, 20mL acetic acid and 70mL distilled water.

The Dragendorff's reagent was eventually poured into a spray bottle to be used as a staining reagent for alkaloid detection.

6.1.5 Extraction of alkaloids

The ground leaf material of *E. montana* (980g) was extracted with 95% ethanol overnight. The extracts were then filtered using a Büchner funnel and the ethanolic filtrate was concentrated using a rotary evaporator to furnish the crude ethanolic extract. This procedure was repeated six times.

Acid-base Extraction

The classical approach to isolate crude alkaloid mixture from a plant extract is the acid-base extraction method, which manipulates the different ionisation state of alkaloids and non-alkaloid substances, thus affecting their solubility in water and an organic solvent (e.g., ether, ethyl acetate and dichloromethane). The approach assumes that most organic compounds are soluble in water-immiscible organic solvents. Alkaloidal compounds are organic weak bases that could be made water-soluble by reacting with acid (e.g., tartaric acid), which converts the alkaloidal compounds into a positively charged quaternary ionic species. By using solvent-solvent partitioning, alkaloid salts which are water soluble, would be separated from non-alkaloidal compounds that are only mainly soluble in the organic solvent (water-immiscible) layer. Subsequently, the free alkaloids can be retrieved by basifying the aqueous layer with a base (e.g., concentrated ammonia).

Firstly, the crude ethanolic extracts were suspended in 3% tartaric acid solution (300mL) with vigorous stirring (10minutes). The suspension was then allowed to settle, and the supernatant was decanted into a 500mL separating funnel. The acidic solution was washed with ethyl acetate three times (300mL, 200mL, and 200mL) to remove the non-alkaloidal organic substances from the acidic aqueous solution. This acidic solution was then filtered through a patch of kieselguhr to remove the precipitations, which were also non-alkaloidal substances. To basify the filtered acidic solution (to convert the alkaloid salts to free bases), concentrated ammonia solution (NH_3) was added until pH 10 was achieved. The basic solution was then extracted with 5% methanol in chloroform 3 times (200mL). The bottom organic layer was kept, later washed with distilled water, dried over anhydrous Na_2SO_4 , and concentrated on a rotary evaporator to produce the basic crude alkaloidal mixture (15.2g).

6.1.6 Isolation of alkaloids

To fractionate the basic crude alkaloidal mixtures (15.2g) obtained from the leaves of *E. montana*, column chromatography was employed to give a series of alkaloid fractions based on polarity differences. The elution started with 100% chloroform, and then the solvent system polarity was gradually increased by adding methanol. A total of 42 fractions were collected from the column chromatography and they were inspected using TLC. The fractions with similar TLC profiles were combined to eventually furnish a total of nine combined fractions, namely, PML-A to PML-I (**Figure 3.6**). Of these, only fraction PML-B showed insignificant presence of alkaloids according to the TLC profiles.

Fraction PML-A (69.2mg) was subjected to CTLC (1mm plate). The elution was started with ethyl acetate:hexane 1:1 (1% NH₃), and only one combined fraction (PML-A-F45) showed significant presence of alkaloids. The fraction PML-A-F45 was re-chromatographed on a 1 mm CTLC plate using CHCl₃:hexane 1:1 (1% NH₃) as the starting solvent, which resulted in one pure alkaloid being obtained, namely PML-1 (**5**) (2.0mg).

Fraction PML-C (364.8mg) was subjected to CTLC (2mm plate). The elution was performed with CHCl₃: hexane 1:1 (1% NH₃), followed by 100% CHCl₃ (1% NH₃), and finally CHCl₃:MeOH (1% NH₃) with a gradual increase of MeOH proportion. A total of 9 fractions were collected, of which the flasks that contained fractions F3, F4, and F5 showed presence of crystalline solid when the solvent within them was evaporated. Fractions F3 and F4 were combined since they have similar TLC profiles, which revealed a single alkaloid spot on TLC, suggesting a pure alkaloid sample was obtained and was given the code PML-2 (**1**) (134.7mg).

The masses of both fractions PML-D (4.4285g) and PML-E (4.9569g) were >4g, and therefore PML-D was separated by a second column chromatography. The starting solvent used for the elution was 5% MeOH in ethyl acetate (2% diethylamine), and then the percentage of methanol was increased gradually to adjust the polarity of the solvent system. A total of 21 fractions were collected from this column chromatography, which eventually based on TLC profiles provided 9 combined fractions, namely, PML-D-A to PML-D-I (**Figure 6.1**).

Fractions PML-D-A, PML-D-B, PML-D-C and PML-D-G were repeatedly subjected to chromatography using CTLC but failed to give any pure alkaloids. All the single alkaloid spots observed on TLC were not actually due to a single alkaloid based on ^1H NMR assessment. Therefore, these fractions that cannot be separated by CTLC were subjected to HPLC for further separation, which resulted in the acquisition of compounds **2-4**. The chemical structure of compounds **2-4** were confirmed by NMR under varied conditions (acquired spectra include: ^1H , ^{13}C , HSQC, HMBC, COSY and NOSEY; temperatures applied include -30°C , 25°C and 55°C ; solvents applied include CDCl_3 and CD_3OH), and HRESIMS analysis.

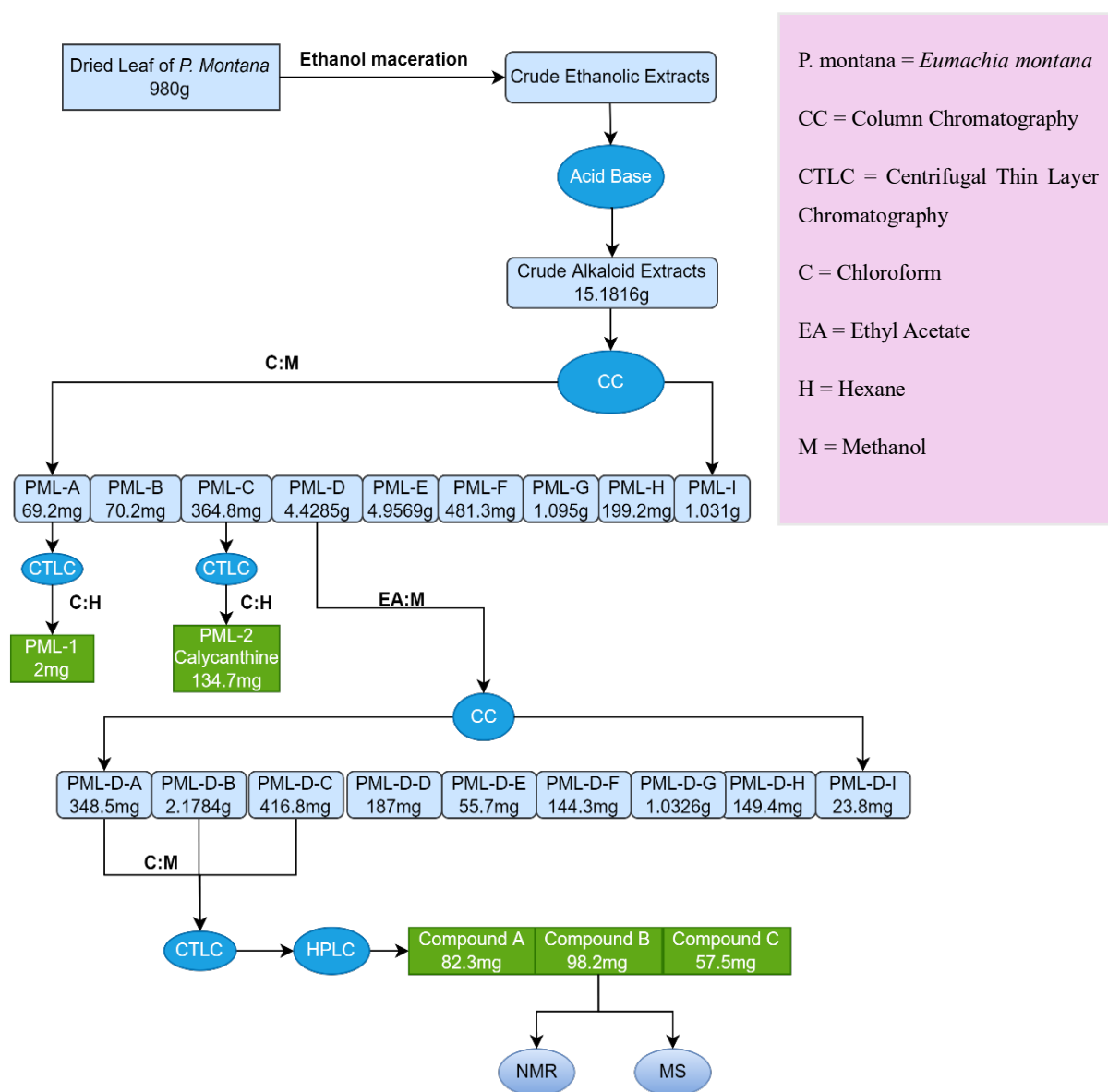


Figure 6. 1 Isolation of alkaloids from the leaves of *Eumachia montana*. For clarity, compound A denotes oleoidine (2), compound B denotes caledonine (3) and compound C denotes eumatanine (4); this nomenclature is used throughout subsequent figures.

6.1.7 Compound Data

Variable-temperature NMR spectroscopy was performed on compounds **2–4** at room temperature (25°C), high temperature (55°C), and extreme low temperature (-32°C) to obtain detailed NMR spectra. HRESIMS analysis of compounds **2–5** determined their molecular weights and chemical formulae. ECD measurements for compounds **2–4** provided additional structural confirmation. The structure of compound **1** was determined by X-ray diffraction and ¹H NMR spectroscopy, while compound **5** was characterized through HRESIMS and a comprehensive set of NMR experiments, including ¹³C, ¹H, HMBC, COSY, and NOESY.

(-)-Calycanthine (1). Light yellowish crystals; [α]_D +106 (*c* 0.43, EtOH); ¹H NMR data (CDCl₃, 600 MHz) δ 7.00 (dd, *J* = 7.8, 1.5 Hz, 2H), 6.81 (td, *J* = 7.6 Hz, 2H), 6.53 (td, *J* = 7.5, 1.2 Hz, 1H), 6.26 (dd, *J* = 8.0, 1.2 Hz, 2H), 4.57 (s, 2H), 4.30 (s, 2H), 3.11 (td, *J* = 13.2, 5.5 Hz, 2H), 2.61 (ddd, *J* = 11.5, 5.5, 1.6 Hz, 2H), 2.40 (s, 6H), 2.25 (ddd, *J* = 13.1, 11.6, 4.1 Hz, 2H), 1.28 (ddd, *J* = 13.2, 4.1, 1.6 Hz, 2H); HRESIMS: *m/z* 347.2250 [M + H]⁺ (calcd for C₂₂H₂₆N₄ + H⁺, 347.2230).

Oleoidine (2). Light yellowish powder; [α]_D +106 (*c* 0.43, EtOH); ¹³C NMR data (CD₃OD, 150 MHz, 328 K) δ 150.75, 150.68, 148.08, 147.69, 133.20, 132.89, 132.29, 131.42, 128.15, 127.60, 125.36, 125.25, 124.80, 124.52, 124.46, 124.37, 123.87, 122.71, 122.32, 121.94, 121.76, 119.11, 118.29, 118.17, 117.22, 108.27, 108.10, 86.33, 86.29, 85.21, 84.20, 82.58, 81.89, 62.61, 62.31, 61.04, 60.53, 60.37, 59.88, 59.62, 52.49, 51.99, 51.87, 51.72, 50.95, 50.89, 48.43, 38.13, 37.86, 37.36, 37.19, 35.19, 35.05, 34.99, 34.74, and 34.31; HRESIMS: *m/z* 1035.6217 [M + H]⁺ (calcd for C₆₆H₇₄N₁₂ + H⁺, 1035.6232).

Caledonine (3). Light yellowish powder; [α]_D +139 (*c* 0.80, EtOH); ¹³C NMR data (CD₃OD, 150 MHz, 328 K) δ 150.18, 149.84, 147.62, 147.46, 147.02, 132.57, 132.11, 131.38, 130.75, 127.40, 127.32, 124.57, 124.38, 124.09, 123.74, 123.14, 122.42, 121.86, 121.67, 121.04, 117.72, 117.37, 107.34, 107.07, 85.58, 85.22, 84.31, 83.45, 61.79, 59.82, 59.68, 59.23, 59.16, 59.05, 58.94, 51.58, 51.15, 50.81, 50.66, 50.17, 47.73, 37.88, 37.56, 37.19, 36.93, 36.74, 34.46,

34.36, 34.29, 34.14, and 34.01; HRESIMS: m/z 1207.7219 $[M + H]^+$ (calcd for $C_{77}H_{86}N_{14} + H^+$, 1207.7233).

Eumatanine (4). Colourless oil; $[\alpha]_D^{+122}$ (c 0.33, EtOH); ^{13}C NMR data (CD_3OD , 150 MHz, 328 K) δ 150.87, 150.67, 148.62, 148.18, 147.88, 133.33, 133.29, 132.91, 132.16, 131.52, 128.12, 127.79, 125.32, 125.30, 124.95, 124.84, 124.63, 124.49, 124.44, 123.83, 123.58, 123.31, 122.66, 122.32, 121.93, 121.76, 119.08, 118.18, 118.12, 118.08, 117.68, 108.13, 108.07, 86.34, 86.27, 85.72, 85.12, 84.19, 82.57, 81.83, 62.61, 60.57, 59.90, 59.81, 59.66, 52.44, 51.88, 51.49, 50.91, 48.45, 38.63, 38.25, 38.03, 37.48, 37.41, 35.10, 35.05, 34.86, 34.77, 34.75; HRESIMS: m/z 1379.8215 $[M + H]^+$ (calcd for $C_{88}H_{98}N_{16} + H^+$, 1379.8233).

Eumatricine (5). Light yellowish powder; 1H NMR ($CDCl_3$, 600 MHz) and ^{13}C NMR ($CDCl_3$, 150 MHz) data, see Table 1; HRESIMS: m/z 183.0932 $[M + H]^+$ (calcd for $C_{12}H_{10}N_2 + H^+$, 183.0917).

6.2 Cell Culture Assays

6.2.1 General Cell Culture

T-25 cm^2 Tissue culture flasks (Corning, Product Code (PC) - 3056), cryopreservation vials (Thermo Scientific, PC – 10440613), RPMI-1640 medium stored at 4 °C (Sigma-Aldrich, PC-R8758), minimum essential medium (MEM) stored at 4°C (Sigma-Aldrich UK, Catalogue No.:M2279), non-essential amino acids (Sigma-Aldrich UK, Catalogue No.: M71 45), HEPES (Sigma-Aldrich UK, Catalogue No. H0887), L-glutamine (Sigma-Aldrich UK, Catalogue No.: G7513), penicillin-streptomycin (Sigma-Aldrich UK, Catalogue No.: P4333), heat-inactivated foetal bovine serum (FBS), trypsin-ethylenediaminetetraacetic acid (EDTA) stored at -20°C (Sigma-Aldrich, PC – F9665), freezing medium stored at 4°C (95% FBS and 5% dimethyl sulfoxide (DMSO)), phosphate-buffered saline (PBS) stored at room temperature (Sigma-Aldrich, PC – P4417; 1 tablet was dissolved in 200 mL of dH_2O).

The cell lines used in this study include 6 human epithelial cancer (carcinoma) cell lines (HCT-116, MCF-7, MDA-MB-468, HT-29, U373V, and U373M) and one non-transformed foetal lung fibroblast line (MRC-5), among which, U373V (vector control) and U373M (methylguanine DNA-methyltransferase (MGMT)-transfected) isogenic cell lines were a gift from Schering Plough corporation. All others were originally purchased from the European Collection of Cell Culture (supplied via Sigma-Aldrich) and American Type Tissue Culture Collection (ATCC). All cell lines were stored in liquid nitrogen (-196°C). After reviving frozen cells, each cell line was passaged for ~4 months before being discarded, which was adopted to minimise genotypic shift as a result of continual passage.

Reviving frozen cells

The vials of cells were taken from liquid nitrogen storage after checking the specific location in cell bank and were defrosted rapidly in a water bath at 37°C after sterilising by spraying with 70% industrial methylated spirit (IMS) in dH₂O. Subsequently, the thawed cells were resuspended directly in a T-25cm² culture flask containing 7-8mL pre-warmed complete growth medium. The medium of cell lines MCF-7, HCT-116, and HT-29 was RPMI-1640 supplemented with 10% v/v FBS. For MRC-5 fibroblast medium comprised MEM supplemented with 1% 0.1mM non-essential amino acids (NEAA), 1% 1M N-2-hydroxyethylpiperazine-N'-2-ethanesulfonic acid (HEPES), 1% 200 mM L-glutamine, and 1% penicillin-streptomycin and 10% v/v FBS. For MDA-MB-468 medium comprised MEM supplemented with 1% 200mM L-glutamine and 1% penicillin-streptomycin, as well as 10% v/v FBS. U373V and U373M were subcultured in RPMI 1640 medium, to which 1% mM NEAA, 1% gentamicin (50µg/mL), 1% G418 sulphate (400µg/mL), 1% 200mM L-glutamine, and 10% v/v FBS were added. FBS had previously been inactivated by heating at 56°C for 60min to denature complement proteins which would otherwise evoke a cellular immune response. Cells were allowed to attach overnight in a LEEC incubator at 37°C and 5% CO₂. The following day, cells were inspected under the microscope to monitor their attachment, viability, morphology and growth. The medium was thereafter replaced to remove DMSO and any dead cells. Cells were passaged when ~70-80% confluency was reached and were subcultured at least once to establish normal growth before being used for experiments.

Cell culture

All cell lines were serially subcultured in 25cm² tissue culture flasks once or twice weekly, depending on the cell type, incubating at 37°C in a humidified atmosphere of 95% air and 5% CO₂ in a LEEC incubator. To maintain normal logarithmic cell growth, cells were 70%-80% confluent at the time of sub culturing or setting up experiments.

All cell work prior to fixation or lysis was carried out in a BioMat2 MDH Class II microbiological safety cabinet using aseptic techniques. The first step was to decontaminate the cabinet by spraying and wiping it with 70% IMS. Thereafter, the consumed culture medium was aspirated, and cells were washed with 1-2mL sterilised PBS, as any trace of medium will minimise the ability of trypsin to detach cells from the flask. The flask was then incubated for 3-5min after adding 0.5-1mL of trypsin -EDTA 1 × solution to detach the cells from the bottom of the flask. Afterwards, cells were inspected under light microscope and when the majority of cells had disassociated, cells were resuspended in 7mL fresh complete medium to neutralise the effect of trypsin-EDTA 1 × solution. After that, the appropriate amount of cell suspension was added to new pre-labelled flasks (labelled with the username, name of the cell line, date and passage number) containing 8mL fresh growth medium and flasks were placed in the incubator.

Freezing and storing cells

For long-term storage in the liquid nitrogen cell bank, cells were cryopreserved. The growth medium was aspirated when cell confluency reached ~70-80%, and thereafter 1-2mL of pre-warmed PBS was added to wash the cells and remove the dead cells. Subsequently, PBS was removed and 1 mL trypsin-EDTA 1 × solution was added to the flask to detach the viable cells. The flask was gently agitated so that the trypsin completely covered all the cells in the flasks, before the trypsin solution was removed and the flask was replaced in the incubator at 37°C for enough time (~2-5minutes) to allow residual trypsin-EDTA 1 × solution to disassociate the majority of cells from the bottom of flask. After disassociation, 1mL of freezing medium (95% FBS, 5%DMSO) was added to the flasks to resuspend the cells and the contents were mixed by pipetting up and down. As the last step, ~1mL of the cell suspension was transferred to sterile cryogenic vials labelled with the username, full name of the cell line, date, and passage number. The cryovials were stored at -20°C overnight, and -80°C for 1-14 days before being placed in the liquid nitrogen.

Cancer cell lines used

MCF-7 is the abbreviation of a foundation in Detroit called the Michigan Cancer Foundation-7 (Soule et al., 1973). MCF-7 is a cell line with adherent epithelial morphology isolated in 1970 from a 69-year-old woman who had metastatic BC (Levenson and Jordan, 1997, Sutherland et al., 1983). The cell line has a doubling time of ~24h. MCF-7 is used as an excellent *in vitro* model for studying the mechanism of hormonal antitumour therapy due to the detection of ER in MCF-7 cells (Levenson and Jordan, 1997). The MCF-7 BC cell line has wild-type *KRAS* and *TP53* genes, indicating functional RAS and p53 proteins (von Lintig et al., 2000, Scott et al., 2009). Additionally, MCF-7 cells are proficient in MMR mechanisms (Scott et al., 2009).

HCT-116 is an epithelial adherent colorectal cell line with a short doubling time of ~21h. The HCT-116 cell line was isolated from the colon of an adult male, colon cancer patient (Brattain et al., 1981). HCT-116 cells possess a codon 13 mutation in the *KRAS* proto-oncogene, exhibit MMR deficiency, and maintain wild-type *TP53* expression (ATCC, Vernole et al., 2006).

HT-29 is a cell line with epithelial morphology isolated from a primary tumour of a 44-year-old white, female patient with colorectal adenocarcinoma (ATCC). HT-29 cells are MMR-proficient, p53-deficient, and possess oncogenic *KRAS* mutations (Oliver et al., 2020, Ravizza et al., 2004, Nakata et al., 1998).

MDA-MB-468 a cell line with epithelial morphology isolated from a pleural effusion of a 51-year-old Black female patient with metastatic adenocarcinoma of the breast (Wojtowicz et al., 2020, Cailleau et al., 1978). It is a TNBC cell line with high expression of EGFR, and therefore MDA-MB-468 is widely used as a model for TNBC (Filmus et al., 1985). MDA-MB-468 cells are MMR-proficient, harbour a mutation in p53 gene, and possess wild-type RAS (Rasti and Azimi, 2015, Eckert et al., 2004, Lee et al., 2020).

U373 (Uppsala) is a patient-derived GBM, grade IV astrocytoma cell line. At Schering Plough Corporation, the isogenic cell line pair U373M and U373V were developed (Zhang et al., 2010).

U373M displays resistance to the chemotherapeutic alkylating agent TMZ due to its expression of DNA direct repair protein MGMT (Zhang et al., 2010).

The U373 glioblastoma cell line has been widely utilized as a model system for studying GBM pathophysiology and drug responses. These cells are particularly useful for evaluating the cytotoxic effects of novel natural compounds. Studies using U373 cells have demonstrated the potency of resveratrol and curcumin in inhibiting GBM proliferation and inducing apoptosis or autophagy (Yamamoto et al., 2010, Abdullah Thani et al., 2012)

The A549 cell line, derived from the alveolar basal epithelium, was established in 1972 by Giard et al. using carcinoma tissue from a 58-year-old male patient (Smith et al., 1986). These cancer cells are known to produce lecithin enriched with highly desaturated fatty acids via the cytidine diphosphocholine pathway, which plays a crucial role in maintaining the integrity of the phospholipid bilayer of the cell membrane (Shi et al., 2009). A549 cells grow adherently as a monolayer and have a population doubling time of ~22h (ATCC).

The A549 cell line is one of the most extensively used in lung cancer research. Established in 1972 from a lung adenocarcinoma patient, A549 cells exhibit epithelial morphology and retain characteristics of alveolar type II pneumocytes. This cell line has been instrumental in drug screening, allowing researchers to evaluate the efficacy and toxicity of chemotherapeutic agents, targeted therapies, and natural compounds (Zhukova et al., 2007). A549 cells are also widely employed in molecular studies to investigate signalling pathways involved in lung cancer progression, including EGFR and *KRAS*-driven oncogenesis (Jiang et al., 2016). A549 cells are MMR-proficient (express hMLH1 and hMSH2 proteins), and harbour a mutant RAS while retaining wild-type p53 (Jiang et al., 2016, Zhang et al., 2009b, Taverna et al., 2000). Due to its adaptability in both 2D and 3D cultures, A549 remains a cornerstone of lung cancer research, contributing to significant advancements in drug discovery and mechanistic understanding.

The MRC-5 (Medical Research Council strain 5) cell line, a human fibroblast line established in 1966 by J.P. Jacobs et al., was derived from the lung tissue of a 14-week-old foetus following an elective termination of pregnancy by a 27-year-old woman (ATCC). MRC-5 fibroblasts exhibit a population doubling time ranging from 42 to 84h (ATCC).

6.2.2 MTT cell viability assay

The 3-(4,5-dimethylthiazol-2-yl)-2,5 diphenyltetrazolium bromide (MTT) cell viability assay (Mosmann, 1983) is a quantitative colourimetric assay, as the aqueous tetrazolium salt is reduced by the enzymes (mitochondrial dehydrogenases) of viable cells. The product of the reduction is purple formazan crystals that need to be dissolved in organic solvents (e.g. DMSO) into a coloured solution. The absorbance of the coloured solution can be quantified by measuring at a certain wavelength (e.g. 570nm) by a spectrophotometer. The deeper the purple colour, thus the higher the absorbance equates to larger viable cell numbers. This rapid, reproducible and robust *in vitro* method is applied widely to measure the cytotoxicity and growth inhibitory activity of test agents and proliferation of mammalian cells.

Materials

The MTT solution is prepared by dissolving MTT powder (stored at 4°C; Sigma-Aldrich, PC-M2128-10g) in sterile PBS to obtain the 2mg/mL MTT solution. DMSO (Sigma-Aldrich, PC-154938-500mL) is stored at room temperature. Cells were seeded in 96-well plates (Nunc; VWR, PC - 734-2097). Cell suspensions were prepared in 10cm Petri dishes.

Method

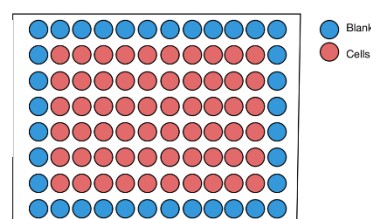
Time zero (T0) plates were set for each cell line for every independent trial to determine the absorbance values (i.e., initial optical density (OD)) at the time of test agent addition. For treated plates, the blank fresh complete medium was added to the first and the last row, as well as the first and the last column, while cells were seeded all the other wells (10 × 6wells) at the desired density (**Table 6.2.2**). For T0 plates, only three columns of wells (3 × 6wells) were seeded with the cell suspension, and similar to the treated plates, the blank fresh medium was added to wells surrounding cell-seeded wells (**Figure 6.2**). Medium alone-containing wells surrounding cell suspensions serves to minimise the ‘edge effect’, i.e., avoiding volume loss

caused by evaporation of the medium, which is inevitable in a 37°C incubator and may affect cell growth and compound concentration.

Table 6. 3 72h MTT assay seeding densities.

Cell Line	Cells/well
HCT-116	3000
MCF-7	4000
HT-29	2500
MDA-MB-468	5000
U373V	3000
U373M	3000
MRC-5	2500

Experimental
treatment



T0

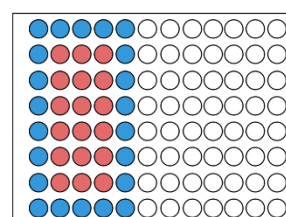


Figure 6. 2 Seeding of MTT assay in 96-well plate.

Flasks of cells were inspected under the microscope and cells were trypsinized when the confluency reached 70-80%. Cells were harvested and then resuspended in ~7mL complete medium. To dislodge cells from clusters, cells were gently pumped 2-3 times using a 10mL pipette pump. Thereafter, 10µL of cell suspension was pipetted for cell counting on a haemocytometer; cells in 0.1µL cell suspension (volume in the haemocytometer well counting chamber) were counted. Therefore, the final cell concentration of the suspension equals to the counted cell number $\times 10^4$ cells/mL. Sufficient cell suspension with desirable density was prepared in a petri dish for all wells required in advance. The seeding density is influenced by the doubling time of the cells and the length of treatment in 180µL complete medium (**Table 6.3**). The ideal consequence is that the cells in control wells are 70-80% confluent at the day of plate reading. The cell suspension was pipetted up and down multiple times using a multichannel pipette before to each cell seeding well was added 180µL of cell suspension. Both experimental treatment plate and T0 plate were seeded with cell suspensions. The T0 plate was set up to measure the absorbance of cells at the time of tested compounds' introduction, and the T0 plates were set up with the same manner for absorbance measurement. The cells in treated plate were allowed to grow overnight in incubator at 37°C before the tested compounds at desired concentrations were introduced. The top stock (7mg/mL and 10mg/mL) of test compounds was prepared by dissolving the compound in DMSO, while the concentration of DMSO was kept <1%. A volume of 20µL of each dilution was added to wells to make a final

volume of 200 μ L, and therefore the concentration of tested compounds was prepared at ten times the final required concentration in complete medium. Control wells, located in the first column of each cell-seeded plate, were treated with 20 μ L of blank complete medium. The tested compounds were applied at the following final concentrations:

- Compounds **2** and **4** against HCT-116, MCF-7 and A549: 0.005, 0.01, 0.05, 0.1, 0.5, 0.75, 1.0, 2.5, 5.0 μ g/mL.
- Compound **3** against HCT-116, MCF-7 and MDA-MB-468: 0.005, 0.01, 0.05, 0.1, 0.5, 0.75, 1.0, 2.5, 5.0 μ g/mL.
- Compound **3** against HT-29: 0.01, 0.05, 0.1, 0.5, 1.0, 2.5, 3.5, 5.0 μ g/mL.
- Compound **3** against U373V and U373M: 0.005, 0.010, 0.05, 0.1, 0.2, 0.4, 0.5, 0.75, 1.00 μ g/mL.

Experimental treatment plates were incubated at 37°C for 72h following the introduction of test compounds. Following 72h exposure to test compounds (and at the time of test agent addition for T0 plates), to each well (excluding the blanks) was added 50 μ L of MTT solution (400 μ g/mL). Plates were then incubated at 37°C for 3-4h. The liquid well contents (including the blanks; medium and unmetabolised MTT) were aspirated gently following the incubation, and thereafter 150 μ L of DMSO was added per well to dissolve the formazan product. As the last step, plates were shaken using an orbital plate shaker (Amersham) for 10min to assist formazan dissolution before the absorbance was measured (a surrogate marker for number of viable cells)) at 570nm using a PerkinElmer Envision plate reader. Data were collected and analysed using Wallac Envision Manager 1.12 software.

A separate DMSO control trial was performed using DMSO diluted in medium to contain the same % DMSO as in compound dilutions, and therefore eliminating the possibility that DMSO as the drug vehicle may influence cell viability or growth. The control trials were treated and measured in the same manner as the drug treatment trials.

Data Analysis

Means and standard deviations (SDs) of repeats (n=6) were calculated and the OD₅₇₀ for estimated GI₅₀ values were calculated using the following formula:

$$\frac{(\text{Control OD}_{570} - \text{Initial OD}_{570}) + \text{Initial OD}_{570}}{2} = \text{OD}_{570} \text{ at GI}_{50}$$

The GI₅₀ was then estimated by interpolation. Independent MTT assays for each trial were repeated at least 3 times and mean \pm SEM GI₅₀ values were calculated.

6.2.3 Cell counting assay

The MTT assay is a widely used method used to measure cell viability and cell proliferation, while its shortfall lies in the mechanism of the MTT assay; instead of directly quantifying the viable cells, it measures the number of functioning mitochondria, which can reduce the tetrazolium salt to a coloured insoluble formazan. Therefore, if tested compounds are capable of disrupting mitochondrial function or the cells have a low metabolism such as thymocytes and splenocytes who reduce very little tetrazole, the MTT assay may cause false positive results.

For the purpose of validating the results from MTT assay, cell counting assays were conducted as this assay directly counts the number of viable cells. Flasks of cells were trypsinised, harvested and counted before being prepared to desired density (to dispense 2×10^4 cells/well) of cell suspensions. Cells were seeded at 6-well-plates with 2mL medium per well and a separate T0 plate was seeded for each cell line. The T0 plates had 2-3 repeats, which were trypsinised and counted at the same day of treatment. For experimental treatment plates, following overnight incubation, 1mL of medium was added to wells containing compound **3** to yield final concentrations equivalent to $1 \times \text{GI}_{50}$ and $2 \times \text{GI}_{50}$ compound **3**. Control wells received complete medium alone; each experimental condition had two repeats. Thereafter, plates were incubated at 37°C for 72h before cells were counted. At the day of counting (for both T0 plates and treated plates), well contents were aspirated before the addition of 500 μ L/well trypsin-EDTA 1 \times solution. A volume of 500 μ L of fresh complete medium was added per well when the majority of cells were disassociated, and thereafter the well contents were pipetted up and down to disperse the cells from clusters. As the last step, 10 μ L of cell suspensions were transferred from each well and counted on a haemocytometer respectively.

6.2.4 Clonogenic assay

In this study, the clonogenic assay together with MTT assay were conducted as an initial screening of the tested compound. The clonogenic assay is able to detect the capability of a single cell to survive and retain proliferative ability following a brief exposure (e.g., 24h) to test compounds (Qazzaz et al., 2016).

Materials

Methylene blue (0.05%) in a 1:1 solution of dH₂O: MeOH stored at 4°C.

Method

Flasks of cells were trypsinized, harvested and counted using a haemocytometer. Subsequently, sufficient cell suspension with a density of 250cells/well were prepared. Cells were seeded in 6-well plate with 2mL medium per well. Cells were then allowed to attach overnight in an incubator at 37°C before being treated with test compounds. The test compounds at concentrations of $1 \times \text{GI}_{50}$ and $2 \times \text{GI}_{50}$ were prepared in complete medium and added in a volume of 1mL per well. The first column of plates was controls and was treated with 1mL blank complete medium. After 24h exposure of cells to tested compounds, the well contents with compounds were removed gently by aspiration, and then wells were washed with 1mL PBS twice. Thereafter, 3mL fresh complete medium was introduced per well and cells were allowed to develop colonies in an incubator at 37°C for 7-14 days. The colonies were counted when colonies in control wells contain ≥ 50 cells. At the day of counting, as the first step, aqueous well contents were removed gently by aspiration and colonies were washed with 1mL cold PBS twice. Thereafter, the cells were fixed in 1 mL 100% MeOH for ~10min before 0.5mL 0.05% methylene blue were introduced per well to stain colonies. Following ~10min staining, colonies were rinsed with 1mL dH₂O three times, air dried, photographed and counted.

Data Analysis

The plating efficiency (PE) and survival fraction (SF) were calculated following the formulae:

$$\text{PE} = \text{Number of colonies counted} / \text{Number of cells plated} \times 100\%$$

$$\text{SF} = \text{PE of treated sample} / \text{PE of control} \times 100\%$$

6.2.5 Flow cytometry studies

An ID7000 Sony flow cytometer was used for sample analysis and 10,000 - 50,000 events were recorded for each sample (depending on the cell pellets size / number of cells present in the sample). The acquired data were analysed using Flowjo or Weasel software.

6.2.5.1 Cell cycle analysis

In this study, the cell cycle is analysed by flow cytometry and the DNA intercalating stain PI is used to bind cellular DNA (Nicoletti et al., 1991). The PI fluoresces strongly when it is activated by an argon ion laser (blue light, 488nm), and the emitted fluorescence is proportional to the amount of DNA content in each cell/event recorded. Thus, by using flow cytometry techniques, the DNA content in each cell/event can be determined and the percentage of cells in each cell phase (pre-G1, G1, S, and G2) can be revealed. Therefore, how tested compounds perturb cell cycle distribution can be evaluated. Since PI is unable to penetrate intact cell membranes, hypotonic solution was used to permeabilise the cells and hence enable PI's entry. PI is also able to bind the RNA contents in cells, and therefore the ribonuclease A is applied to remove double-stranded RNA. During analysis of the data acquired from flow cytometry, the pre-G1 peak can be used as an indicator of the cell population that are undergoing apoptosis.

Materials

Hypotonic fluorochrome solution prepared in PBS to contain: 50 µg/mL PI (Sigma-Aldrich PC - 81845) stored at 4 °C; 0.1mg/mL RNA (Sigma-Aldrich PC- R4642) stored at -20°C; 0.1v/v Triton X - 100 (Sigma-Aldrich PC-x100) stored at RT; 0.1w/v sodium citrate (Sigma-Aldrich PC - 1613859) stored at RT.

Method

Cells were trypsinised, harvested and counted on a haemocytometer, before preparation of cell suspensions containing the required cell densities. Cells were seeded in 6-well plates (2mL medium) or 10cm petri dishes (10mL medium). Cells were incubated for 24h at 37°C for growth and attachment before introduction of test compounds. Cells were exposed to test compound for 24h and 72h, and thereafter the consumed medium was aspirated and transferred to pre-labelled glass vials (vials were always on ice). Cold PBS (0.5-1.0mL) was used to wash

the wells/dishes before cells were detached by adding 0.5-1.0mL trypsin-EDTA 1 × solution. Subsequently, cells were harvested and transferred into corresponding pre-labelled glass vials (vials were always on ice). Glass vials with cell suspension were centrifuged (1350rpm, 4°C, 7min), and thereafter the medium of each vial was aspirated gently. A volume of 1 mL cold PBS was added per vial to wash the cell pellets and then vials were centrifuged again (1350 rpm, 4°C, 7min). As the last step, hypotonic fluorochrome solution (300-500µL) was added per vial, and vials were vortexed before being stored at 4°C for 1h in the dark. Vials were vortexed again to obtain single cell suspensions before being analysed using flow cytometry.

6.2.5.2 Apoptosis assay

Apoptosis, also known as programmed cell death, is characterized by the loss of membrane phospholipid asymmetry, chromatin condensation, and internucleosomal cleavage of DNA (Koopman et al., 1994, Wyllie, 1980). The loss of membrane asymmetry is one of the morphological features of early apoptotic cells, resulting in the exposure of phosphatidylserine (PS) at the cell surface. Expression of PS at the cell surface enables the detection of apoptosis by utilising the binding of PS to fluorochromes-labelled (e.g. FITC) annexin V, which is a 35-36kDa Ca²⁺ dependent phospholipid-binding protein that has high affinity to the PS at the cell surface, but not to intracellular membranes (Koopman et al., 1994, Casciola-Rosen et al., 1996).

In this study, the FITC annexin V is used in conjugation with propidium iodide (PI), which is a DNA binding dye that permeate the membranes of dead or damaged cells, but not viable cells with intact membranes. Thus, this method allows the identification of early apoptotic cells (PI negative, FITC Annexin V positive), late stage apoptotic cells (PI positive, FITC Annexin V positive), as well as viable cells (PI negative, FITC Annexin V negative)(Vermes et al., 1995).

Materials

FITC Annexin V Apoptosis Detection Kit I (BD Pharmingen™, 556547), including 10 × Annexin V Binding Buffer (51-66121E, 50ml), FITC Annexin V (51-65874X, 0.5mL), and Propidium Iodide Staining Solution (51-66211E, 2.0mL); store at 4°C and protected from prolonged exposure to light.

Method

Flasks of cells were trypsinised, harvested and counted on a cell counter (DeNovix, Cell Drop BF), before being prepared at the appropriate density for the required cell suspensions. Cells were seeded in 6-well plates ($1-2 \times 10^5$ cells/well, 2mL medium). Cells were incubated for 24h at 37°C to allow attachment (and cell cycle entry) before introduction of test compounds. Cells were exposed to tested compound for 24h and 72h, and thereafter the consumed medium was aspirated and transferred to pre-labelled glass vials (vials were always on ice). Cold PBS (0.5-1.0mL) was used to wash the wells/dishes before cells were detached by adding 0.5-1.0mL trypsin-EDTA $1 \times$ solution. Subsequently, cells were harvested and transferred into corresponding pre-labelled glass vials (vials were always on ice). Glass vials with cell suspension were centrifuged (1350rpm, 4°C, 7min), and thereafter the medium of each vial was aspirated gently. A volume of 1mL cold PBS was added per vial to wash the cell pellets and then vials were centrifuged again (1350rpm, 4°C, 7min). Subsequently, Annexin-V-FITC (5µL) plus 100µL $1 \times$ annexin-V buffer were added to cells, incubating for 15min in the dark on ice. PI (10µL; 50µg/mL in PBS) plus 400µL annexin-V buffer were then added to cells, incubating on ice for at least 10min in the dark before being proceeded to flow cytometry analysis.

6.2.5.3 γ H2AX assay

H2AX, regarded as a tumour suppressor, is a member of the H2A histone family and a key component in DNA repair (Bassing et al., 2003). Serine c-4 phosphorylation of H2AX (γ H2AX) forms in response to DNA DSB damage, γ H2AX (phosphorylated H2AX) accumulates, surrounding the break sites, enabling the detection of individual DSBs by use of a γ H2AX antibody (Bonner et al., 2008, Kuo and Yang, 2008). The DNA DSB is a serious DNA lesion that can be caused by exogenous or endogenous factors, such as cytotoxic agents, ROS, metabolic processes, deficient repair, telomere erosion and programmed biological processes, ultimately leading to cell death (apoptosis) by disturbing the genomic stability (Bonner et al., 2008). The detection of DSBs is a useful tool for the diagnosis of precancerous and cancerous cells, while in carcinoma cells it is also effective to detect cancer progression and therapy.

To detect and quantify DNA DSB in cells, a primary antibody against γ H2AX and a fluorescent secondary antibody are used, incorporated with the flow cytometry, which is a sensitive method

to allow the active distinction of cells based on a cell's particle density and fluorescence colour (Kuo and Yang, 2008).

Materials and reagent preparation

- 1% methanol-free formaldehyde in PBS: 1mL 16% methanol-free formaldehyde (Thermo-Scientific UK, Catalogue No.:28906) was added to 15mL PBS. Stored at 4°C.
- 0.4% Triton X-100 in PBS: 80 µL Triton (TM) X100 (Sigma-Aldrich, product no.: X100) was added to 20 mL PBS. Stored at 4 °C.
- 1% FBS in PBS: 0.5mL FBS was dissolved in 49.5mL PBS.
- Primary antibody: anti-γ-H2AX antibody (Millipore, product no.:05-636) was diluted 1:3333 in 1% FBS in PBS.
- Secondary antibody: anti-mouse Alexa Fluor 488 (Invitrogen, product no.: A21200) was diluted 1:1750 in 1% FBS in PBS.
- PI (50µg/mL and RNase 100µg/mL in PBS): 2.5mL PI (Sigma-Aldrich, product no.: P4864), 0.125-0.25mL RNA (Sigma-Aldrich, product no.: P4642) was dissolved in 50mL PBS.

Method

Flasks of cells were trypsinised, harvested and counted on a cell counter (DeNovix, Cell Drop BF), before being prepared to the appropriate density of cell suspensions. Cells were seeded in 6-well plates ($1-2 \times 10^5$ cells/well, 2mL medium) or 10cm petri dishes (1×10^6 cells/well, 10mL medium). Cells were incubated for 24h at 37°C for growth and attachment before introduction of test compounds. Cells were exposed to tested compound for 24h and 72h, and thereafter the consumed medium was aspirated and transferred to pre-labelled FACS tubes (12×75 mm, Falcon, product no.: 352052) (vials were always on ice). Cold PBS (0.5-1.0mL) was used to wash the wells/dishes before cells were detached by adding 0.5-1.0mL trypsin-EDTA $1 \times$ solution. Subsequently, cells were harvested and transferred into corresponding pre-labelled FACS tubes (vials were always on ice). FACS tubes with cell suspension were centrifuged (1250rpm, 10min, room temperature), and thereafter the medium of each vial was aspirated gently. A volume of 1mL PBS was added per vial to wash the cell pellets and then vials were centrifuged again (1250rpm, 10min, room temperature). The supernatant was aspirated, and the cell pellets were retained.

Cell pellets were fixed in a vented class II cabinet by adding 500 μ L of 1% methanol-free formaldehyde in PBS into each tube and pipetted up and down several times to ensure a single cell suspension. After 5 min incubation at room temperature, cells were permeabilised by adding 500 μ L of (Triton X-100 in PBS) into each tube and then mixed gently. Cells were allowed to settle at room temperature for 1 min and then were centrifuged again (1250rpm, 10min, RT). The supernatant was aspirated, and the cell pellets were retained.

Cell pellets were re-suspended in 1 mL of 1% FBS in PBS, gently mixed, and then incubated either at room temperature for 30min (same day analysis) or at 4°C for later analysis (maximum of one week). Subsequently, cells were then centrifuged again (1250rpm, 10min, RT), following by the supernatant aspiration (the cell pellets were retained). A volume of 200 μ L of diluted antibody was added to each FACS tube, then samples mixed gently, and allowed to incubate for 1.5h at RT. After incubation, an additional 1mL of 1% FBS in PBS was added to each sample, which was followed by the centrifuge (1250rpm, 10min, RT) of cells and supernatant aspiration (the cell pellets were retained). A volume of 200 μ L diluted antibody was added to each FACS tube, samples mixed gently and incubated for 1h at RT in the dark. Following the addition of 1 mL of 1% FBS in PBS, a final centrifuge (1250rpm, 10min, RT) was performed and the supernatant was aspirated. For concurrent cell cycle analysis, cells were re-suspended in 300mL PI (50 μ g/mL and RNase 100 μ g/mL in PBS) solution and incubated for >10 min at room temperature prior to analysis on a flow cytometer.

6.2.6 Fluorescent microscopy

To detect the morphological changes during treatment of carcinoma cells with compound **4** (at concentrations of $0.5 \times$ and $1 \times \text{GI}_{50}$) and further confirm the results obtained from the apoptosis assay, fluorescent microscopy was performed. By using multiple fluorescence antibodies that could be excited by different wavelengths' laser, the target parts (such as the cytoskeleton, the nuclear area and membrane) of cells can be visualised (a different colour could represent different wavelength) under a microscope and thus their morphological changes upon compound **4** can be analysed individually or together (overlayed).

Materials

Alexa Fluor™ 488 phalloidin (Invitrogen, catalog no.: A12379), DRAQ5™ Fluorescent Probe Solution (5mM) (Thermo-Scientific, catalog no.: 62254), Bovine serum albumin (BSA).

Method

Cells (3000-5000 cells/well) were seeded into glass 96-Well Glass-Bottom CELLview Microplates (Greiner, product no.: 655891) in 180uL growth medium. Cells were allowed to attach overnight in incubator at 37°C. Cells were then treated with 0.5 × and 1 × GI₅₀ compound **4** (20μL) for an additional 24h or 72h. Growth medium was then aspirated and cells were washed with PBS.

Thereafter, cells were fixed with 3.7% formaldehyde in PBS for 15mins at RT (50-100μL/well). 3.7% Formaldehyde was removed before 100μl of PBT (0.1% Triton X-100 in PBS) was added per well and incubated for 2mins at room temperature to increase cell membrane permeability. Subsequently, cells were blocked for 1h at RT to prevent any nonspecific binding of antibodies using PBT + 1% BSA (50-100μL/well).

Cells were then incubated for 45min at RT with 1:160000 diluted phalloidin. Cells were washed with PBT twice before incubating with DRAQ5 (a cell membrane permeable DNA binding dye, excited by the 633nm red laser) (1:1000 dilution) for 2-5mins in the dark at 37°C (cell incubator). Cells were washed with PBT and then were kept in the fridge in PBS (200μL/well) before being observed under an automated microscope (ZEISS, Celldiscoverer 7 (LSM900, confocal)).

6.2.7 Caspase 3/7 assay

Members of the caspase family of aspartic acid-specific proteases play a key role in execution of apoptotic cell death. Caspases include the upstream initiators caspase-8, caspase-9, and caspase-10 in humans, as well as the downstream effectors caspase-3, caspase-6, and caspase-7 (Walsh et al., 2008). It has been reported that >400 substrates are proteolysed by apoptosis-

associated caspases, among which, caspase-3 and caspase-7 are the major executioner caspases (Lüthi and Martin, 2007).

To detect caspase 3/7 activity in carcinoma cell lines that have been exposed to test agents, the Caspase-Glo® 3/7 Assay kit optimised for caspase 3/7 activity, luciferase activity and cell lysis was applied. In response to caspase 3/7 activities presented, the assay provides a luminogenic caspase 3/7 substrate that can trigger luciferase reaction subsequent to caspase cleavage, and result in the generation of luminescent signals, while the luminescence detected is proportional to the amount of caspase activity in the cells (**Figure 6.3**).

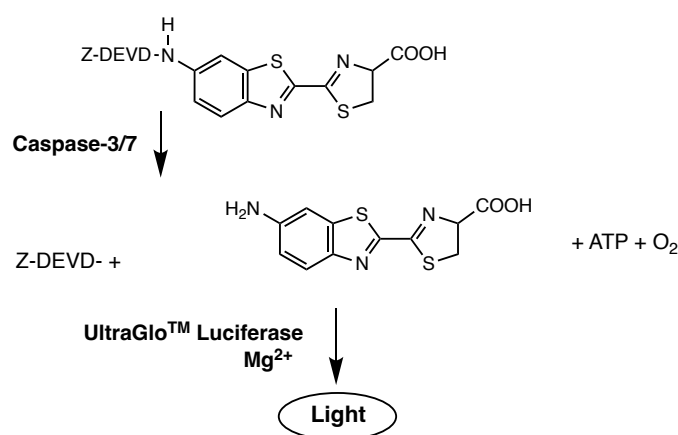


Figure 6. 3 Schematic Diagram of the Caspase-Glo® 3/7 Assay Technology. Following caspase cleavage of the pro-luciferin DEVD substrate, a substrate for luciferase (aminoluciferin) is released and, in the presence of luciferase and ATP, results in the luciferase reaction and the production of light.

Materials

The Caspase-Glo® 3/7 Assay (Promega, Catalog no.: G8091), components include Caspase-Glo® 3/7 substrate (1 bottle, lyophilized) and Caspase-Glo® 3/7 buffer (1 × 10mL).

Method

The Caspase-Glo® 3/7 Assay was used to detect caspase 3/7 activity of tested cells. Cells were seeded in 96-well opaque white culture plates (3-5 × 10³ cells/well) and incubated for 24h at 37°C before introducing test compounds. Following 48 h exposure, Caspase-Glo® 3/7 reagent

(Caspase-Glo® 3/7 buffer + Caspase-Glo® 3/7 substrate) was added to each well, and plates shaken ≥ 30 secs). Well luminescence was recorded using a PerkinElmer Envision plate reader.

6.2.8 Reactive oxygen species assay

ROS such as superoxide anion, hydrogen peroxide, singlet oxygen, hydroxy radical, and peroxy radical, arising from intracellular metabolic processes or the insult of exogenous agents, have been widely noted contributing to various physiological processes such as glucose homeostasis, inflammation, cellular lifespan, and multiple aging-related diseases including cancer (Rajendran et al., 2011). The role of the excess ROS such as H_2O_2 in cell cultures has been connected to genomic (in)stability, regulation of transcription, and signal transduction, which may ultimately lead to cell death (Alfadda and Sallam, 2012). H_2O_2 as the most stable ROS generated in cultured cells, has been utilised as a sensible biomarker to detect the ROS levels within cells and thus to evaluate how intracellular oxidative stress been affected by tested compounds or certain specific conditions (Newsholme et al., 2012).

The ROS-Glo™ assay measures the levels of H_2O_2 by a direct reaction of H_2O_2 to generate a luciferin precursor, which is subsequently converted to luciferin by the addition of ROS-Glo™ detection reagent that contains Ultra-Glo™ recombinant luciferase and d-cysteine (**Figure 6.4**). Ultimately, the luminescent signal is generated by the reaction of luciferin and Ultra-Glo™ recombinant luciferase, and the signal is proportional to H_2O_2 concentration (**Figure 6.4**).

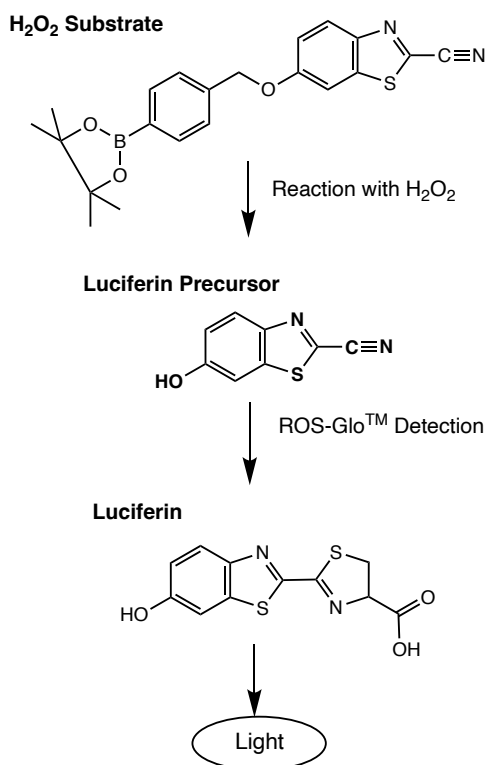


Figure 6. 4 ROS-Glo™ H₂O₂ Assay chemistry.

Materials

ROS-Glo™ H₂O₂ Assay, 10 mL (Promega, catalog no.: G8820), components are as follows:

- 40μL H₂O₂ Substrate, 10mM
- 100μL Signal enhancer solution
- 100μL D-cysteine, 100X
- 2mL H₂O₂ Substrate dilution buffer
- 1 Vial luciferin detection reagent
- 10mL Reconstitution buffer

Method

The ROS-Glo™ H₂O₂ Assay was used to determine ROS production. Cells were seeded in 96-well opaque white culture plates (3-5 × 10³ cells/well) and incubated for 24h at 37°C before introduction of test compounds. Following 24h exposure, H₂O₂ substrate (25μM, H₂O₂ Substrate was diluted in H₂O₂ Substrate Dilution Buffer) was added and incubated for up to 6h in a cell incubator (37°C CO₂). Subsequently, ROS-Glo™ detection solution (luciferin

detection reagent (prepared by adding 10mL reconstitution buffer to the vial of luciferin detection reagent, D-cysteine: signal enhancer solution, 100:1:1) was introduced, and plates incubated for 20min at room temperature. Well luminescence was recorded using a PerkinElmer Envision plate reader.

6.2.9 Metabolomics study

Metabolomics is defined as the comprehensive analysis of metabolites in a biological specimen. Metabolites are the final downstream products of genomic, transcriptomic, and/or proteomic and biological changes affecting the specimen (cells). The detailed analysis of these metabolites can detect precise biological changes in the host (e.g. cell cultures) due to the addition of test compounds, thereby enabling discovery of novel therapeutic targets or biomarkers of disease diagnosis/therapy.

Materials

Cell culture Petri dishes 10cm/T-25cm² flasks; Cell scraper 25cm; HPLC vial (2mL); Methanol (LC-MS grade); PBS; dry ice.

Method

MCF-7 cells were seeded at a density of 2×10^6 in 10cm Petri dishes/T-25cm² flasks with appropriate medium and incubated overnight.

Cells were treated with test agent or appropriate medium alone for 72h (n=7 dishes per treatment). Cell-free medium dishes were also incubated under the same conditions as an additional control (n=6). Following 24h /72h exposure, 1mL growth medium/floating cells were collected for all treated conditions (n=6), frozen down promptly by putting on ice, and stored at -80°C for further extracellular samples' preparation. The cell number of the seventh dish of each treatment condition was counted using a haemocytometer / cell counter (DeNovix, Cell Drop BF).

For intracellular samples' preparation:

Medium was removed from 6 dishes/flasks and cells were washed with PBS (3mL). Cells were quenched with pre-cooled (dry ice) methanol (1 mL, $\leq -48^{\circ}\text{C}$), scraped, and then transferred into pre-cooled tubes (performing on dry ice). The cell extracts were vigorously vortexed for 1 h (on a temperature-controlled shaker with set temperature at 4°C), and then centrifuged at 13300rpm for 10min at 4°C . The supernatants were transferred to pre-cooled tubes, and completely dried under nitrogen.

The samples were reconstituted with methanol (70 μL) (at this point, a little bit of sonication or warming up may be required if undissolved precipitation appeared) and centrifuged (13300rpm for 10min at 4°C) again. Subsequently, the supernatants were transferred into pre-labelled auto-sampler vials and stored at -80°C before analysis using LC-HRMS (Thermo-Scientific, Q Exactive™ Plus Hybrid Quadrupole-Orbitrap™ Mass Spectrometer). Five mixed authentic-standard solutions, comprising a total of 268 standards, were diluted in methanol and injected under identical conditions.

Quality control sample preparation

QC samples are material-matched references used to monitor and correct technical variation across an analytical batch. They can be prepared either as pooled QC, by combining small aliquots of study samples, or as commercial biofluids when pooling is impractical; in this study, pooled QC was used to minimise information loss. QC samples were run to condition and equilibrate the platform at the start of analysis, to quantify technical precision and remove features showing excessive drift in signal, retention time, or m/z , and to support QC-based signal-drift correction with QC injections bracketing approximately three to five study samples (Dunn et al., 2011). Tight QC clustering in PCA confirmed analytical stability, after which QC data were excluded from biological modelling.

Vial up supernatant once evaporated and re-dissolved - at least 30 μL of supernatant was taken into an individual HPLC vial; and then 10 μL was transferred into a pooled HPLC vial (called

QC) where 10 μ L of every sample was put together (excluding the blank), then the vial was vortexed at the end. It is important that it is the same volume from every sample in the QC. It is also important that there is at least 100 μ l +10 μ l for every 8 samples in the vial.

LC-HRMS separation and detection

Metabolite separation was performed on a ZIC-pHILIC column (5 μ m, 4.6 \times 150mm; Merck SeQuant, Watford, UK) with a guard column, using a Dionex Ultimate 3000 HPLC system (Thermo Fisher Scientific, UK). The mobile phase comprised 20mM ammonium carbonate (A) and acetonitrile (B), delivered via a linear gradient: 0–15min, 20–95% A; 15–17min, 95–20% A; 17–24min, 20% A. The flow rate was 300 μ L/min, injection volume 10 μ L, with autosampler and column temperatures maintained at 4°C and 45°C, respectively.

Detection was carried out on a Q Exactive™ Plus Hybrid Quadrupole-Orbitrap™ Mass Spectrometer (Thermo Fisher Scientific, UK) equipped with a HESI source, operating in fast polarity switching mode (+4.5 kV/–3.5 kV). Key parameters included: capillary temperature, 275°C; sheath gas, 40; auxiliary gas, 5; sweep gas, 1 (all in arbitrary units); S-lens RF level, 55%. Full-scan MS was acquired at 70,000 resolution over an m/z range of 70-1050, with an AGC target of 3×10^6 . Data-dependent MS/MS (Top 10) was performed on QC samples at 17,500 resolution, with an AGC target of 1×10^5 and stepped NCE of 20, 30, and 40. Total ion chromatograms from LC-MS, including those from experimental, QC, and blank samples, were visualised and inspected using Xcalibur software.

LC-HRMS-based data processing and metabolite identification

Raw data acquired from liquid chromatography-high resolution mass spectrometry (LC-HRMS) was processed on Compound Discoverer 3.3 (Thermo Fisher Scientific, Hemel Hempstead, UK) using a tailored untargeted metabolomics workflow with retention time range 0.5 - 23.5min, peak rating results (>5), aligned window (within m/z 5ppm) for precursor and fragment ions. After normalising peaks to cell count, specific steps within the workflow, including untargeted peak-picking, peak alignment and annotation of related peaks were

conducted, resulting in a peak list of identified metabolites. To improve the confidence in metabolite identification, the BioCyc Human Database, retention times of 268 authentic standards and the ddMS/MS mzCloud fragmentation database (Thermo Fisher Scientific, Hemel Hempstead, UK), the Human Metabolites Database (HMDB), and KEGG) were referenced when matching metabolites with accurate masses of the detected peaks. According to the Metabolomics Standards Initiative (MSI), the confidence of metabolite identification was ranked from level 1 to 4 (L1-4), in which level 1 (L1) means metabolites identification was based on m/z, RT and/or, MS/MS of authentic reference standards, level 2 (L2) means metabolites were putatively annotated using m/z, RT and/or, MS/MS referring to public/commercial spectral libraries, level 3 (L3) are metabolites that were putatively characterized, while level 4 representing unknown metabolites (Sumner et al., 2014, Sumner et al., 2007). In this study, metabolite identification was conducted based on L1 and L2 in most cases.

Statistical analysis

Unless otherwise stated, independent repeat experiments were performed $\geq 3 \times$ where internal replicated ≥ 2 (with representative experiments illustrated). One-way and two-way analyses of variance (ANOVAs) were used to determine statistical significance. Dunnett's multiple comparison tests were used to determine the minimal level of significance ($p < 0.05$).

References

- DOXOrubicin* [Online]. Available: <https://www.drugs.com/monograph/doxorubicin.html> [Accessed 3006 2022].
- Psychotria rubra* (Lour.) Poir. [Online]. Scientific Database of China Plant Species (DCP). Available: <http://db.kib.ac.cn/CNFlora/SearchResult.aspx?id=45982> [Accessed].
- Psychotria serpens* Linn. [Online]. Scientific Database of China Plant Species (DCP). Available: <https://db.kib.ac.cn/YNFlora/SearchResult.aspx?id=3560> [Accessed].
1989. Chemotaxonomic Studies On *Psychotria Rostrata* And *Alseodaphne Perakensis*.
2015. Chapter 2 - Alkaloids Derived from Tryptophan. In: FUNAYAMA, S. & CORDELL, G. A. (eds.) *Alkaloids*. Boston: Academic Press.
- ABDULLAH THANI, N. A., SALLIS, B., NUTTALL, R., SCHUBERT, F. R., AHSAN, M., DAVIES, D., PUREWAL, S., COOPER, A. & ROOPRAI, H. K. 2012. Induction of apoptosis and reduction of MMP gene expression in the U373 cell line by polyphenolics in *Aronia melanocarpa* and by curcumin. *Oncol Rep*, 28, 1435-1442.
- ABIZOV, E. & TOLKACHEV, O. 2012. Dynamics of accumulation and distribution of β -carboline alkaloids in *Elaeagnus* species cultivated in Moscow Region. *Pharmaceutical Chemistry Journal*, 45, 632-635.
- ABUZOID, H., ABDELRAZIG, S., FERREIRA, L., COLLINS, H. M., KIM, D.-H., LIM, K.-H., KAM, T.-S., TURYANSKA, L. & BRADSHAW, T. D. 2022. Apoferritin-Encapsulated Jerantinine A for Transferrin Receptor Targeting and Enhanced Selectivity in Breast Cancer Therapy. *ACS Omega*, 7, 21473-21482.
- ACHENBACH, H., LOTTES, M., WAIBEL, R., KARIKAS, G., CORREA, M. & GUPTA, M. 1995a. Alkaloids and other compounds from *Psychotria correae*. *Phytochemistry*, 38, 1537-1545.
- ACHENBACH, H., LOTTES, M., WAIBEL, R., KARIKAS, G. A., CORREA, M. D. & GUPTA, M. P. 1995b. Alkaloids and other compounds from *Psychotria correae*. *Phytochemistry*, 38, 1537-1545.
- ADAMCZYK, A., GRELA-WOJEWODA, A., DOMAGAŁA-HADUCH, M., AMBICKA, A., HARAZIN-LECHOWSKA, A., JANECKA, A., CEDRYCH, I., MAJCHRZYK, K.,

- KRUCZAK, A., RYŚ, J. & NIEMIEC, J. 2017. Proteins Involved in HER2 Signalling Pathway, Their Relations and Influence on Metastasis-Free Survival in HER2-Positive Breast Cancer Patients Treated with Trastuzumab in Adjuvant Setting. *J Cancer*, 8, 131-139.
- ADJIBADÉ, Y., SAAD, H., KUBALLA, B., BECK, J. P., SÉVENET, T., CABALION, P. & ANTON, R. 1990. In vitro cytotoxicity of polyindolenine alkaloids on rat hepatoma cell lines. structure activity relationships. *Journal of Ethnopharmacology*, 29, 127-136.
- ADJIBADE, Y., WENIGER, B., QUIRION, J. C., KUBALLA, B., CABALION, P. & ANTON, R. 1992. Dimeric alkaloids from *Psychotria forsteriana*. *Phytochemistry*, 31, 317-319.
- AKELLA, N. M., CIRAKU, L. & REGINATO, M. J. 2019. Fueling the fire: emerging role of the hexosamine biosynthetic pathway in cancer. *BMC Biology*, 17, 52.
- AKRAM, M. 2014. Citric Acid Cycle and Role of its Intermediates in Metabolism. *Cell Biochemistry and Biophysics*, 68, 475-478.
- AL-HAYALI, M. Z., NGE, C.-E., LIM, K. H., COLLINS, H. M., KAM, T.-S. & BRADSHAW, T. D. 2024. Conofolidine: A Natural Plant Alkaloid That Causes Apoptosis and Senescence in Cancer Cells. *Molecules* [Online], 29.
- AL-NATOUR, M. A., ABDELRAZIG, S., GHAEMMAGHAMI, A. M., ALEXANDER, C. & KIM, D.-H. 2022. Metabolic Signatures of Surface-Modified Poly(lactic-co-glycolic acid) Nanoparticles in Differentiated THP-1 Cells Derived with Liquid Chromatography-Mass Spectrometry-based Metabolomics. *ACS Omega*, 7, 28806-28819.
- ALEXANDRE, J., BATTEUX, F., NICCO, C., CHÉREAU, C., LAURENT, A., GUILLEVIN, L., WEILL, B. & GOLDWASSER, F. 2006. Accumulation of hydrogen peroxide is an early and crucial step for paclitaxel-induced cancer cell death both in vitro and in vivo. *Int J Cancer*, 119, 41-8.
- ALFADDA, A. A. & SALLAM, R. M. 2012. Reactive oxygen species in health and disease. *J Biomed Biotechnol*, 2012, 936486.
- ALMALKI, S. G. 2023. The pathophysiology of the cell cycle in cancer and treatment strategies using various cell cycle checkpoint inhibitors. *Pathology - Research and Practice*, 251, 154854.
- AMADOR, T. A., VEROTTA, L., NUNES, D. S. & ELISABETSKY, E. 2000. Antinociceptive Profile of Hodgkinsine. *Planta Med*, 66, 770-772.

AMADOR, T. A., VEROTTA, L., NUNES, D. S. & ELISABETSKY, E. 2001. Involvement of NMDA receptors in the analgesic properties of psychotridine. *Phytomedicine*, 8, 202-6.

ANET, E., HUGHES, G. & RITCHIE, E. 1961. Hodgkinsine, the alkaloid of *Hodgkinsonia frutescens* F. Muell. *Australian Journal of Chemistry*, 14, 173-174.

ARİSAN, E. D., ÇOKER, A. & PALAVAN-ÜNSAL, N. 2012. Polyamine depletion enhances the roscovitine-induced apoptosis through the activation of mitochondria in HCT116 colon carcinoma cells. *Amino Acids*, 42, 655-665.

ARORA, A. & SOMASUNDARAM, K. 2019. Glioblastoma vs temozolomide: can the red queen race be won? *Cancer Biology & Therapy*, 20, 1083-1090.

ARORA, S., BHARDWAJ, A., SRIVASTAVA, S. K., SINGH, S., MCCLELLAN, S., WANG, B. & SINGH, A. P. 2011. Honokiol arrests cell cycle, induces apoptosis, and potentiates the cytotoxic effect of gemcitabine in human pancreatic cancer cells. *PLoS One*, 6, e21573.

ASAI, Y., ITOI, T., SUGIMOTO, M., SOFUNI, A., TSUCHIYA, T., TANAKA, R., TONOZUKA, R., HONJO, M., MUKAI, S., FUJITA, M., YAMAMOTO, K., MATSUNAMI, Y., KUROSAWA, T., NAGAKAWA, Y., KANEKO, M., OTA, S., KAWACHI, S., SHIMAZU, M., SOGA, T., TOMITA, M. & SUNAMURA, M. 2018. Elevated Polyamines in Saliva of Pancreatic Cancer. *Cancers*, 10, 43.

ASHKENAZI, A. & DIXIT, V. M. 1998. Death Receptors: Signaling and Modulation. *Science*, 281, 1305-1308.

ASHKENAZI, A. & SALVESEN, G. 2014. Regulated cell death: signaling and mechanisms. *Annu Rev Cell Dev Biol*, 30, 337-56.

ASHTON-RICKARDT, P. G., DUNLOP, M. G., NAKAMURA, Y., MORRIS, R. G., PURDIE, C. A., STEEL, C. M., EVANS, H. J., BIRD, C. C. & WYLLIE, A. H. 1989. High frequency of APC loss in sporadic colorectal carcinoma due to breaks clustered in 5q21-22. *Oncogene*, 4, 1169-74.

ATANASOV, A. G., ZOTCHEV, S. B., DIRSCH, V. M., ORHAN, I. E., BANACH, M., ROLLINGER, J. M., BARRECA, D., WECKWERTH, W., BAUER, R., BAYER, E. A., MAJEED, M., BISHAYEE, A., BOCHKOV, V., BONN, G. K., BRAIDY, N., BUCAR, F., CIFUENTES, A., D'ONOFRIO, G., BODKIN, M., DIEDERICH, M., DINKOVA-KOSTOVA, A. T., EFFERTH, T., EL BAIRI, K., ARKELLS, N., FAN, T.-P., FIEBICH, B. L.,

FREISSMUTH, M., GEORGIEV, M. I., GIBBONS, S., GODFREY, K. M., GRUBER, C. W., HEER, J., HUBER, L. A., IBANEZ, E., KIJJOA, A., KISS, A. K., LU, A., MACIAS, F. A., MILLER, M. J. S., MOCAN, A., MÜLLER, R., NICOLETTI, F., PERRY, G., PITTALÀ, V., RASTRELLI, L., RISTOW, M., RUSSO, G. L., SILVA, A. S., SCHUSTER, D., SHERIDAN, H., SKALICKA-WOŹNIAK, K., SKALTSOUNIS, L., SOBARZO-SÁNCHEZ, E., BREDT, D. S., STUPPNER, H., SUREDA, A., TZVETKOV, N. T., VACCA, R. A., AGGARWAL, B. B., BATTINO, M., GIAMPIERI, F., WINK, M., WOLFENDER, J.-L., XIAO, J., YEUNG, A. W. K., LIZARD, G., POPP, M. A., HEINRICH, M., BERINDAN-NEAGOE, I., STADLER, M., DAGLIA, M., VERPOORTE, R., SUPURAN, C. T. & THE INTERNATIONAL NATURAL PRODUCT SCIENCES, T. 2021. Natural products in drug discovery: advances and opportunities. *Nature Reviews Drug Discovery*, 20, 200-216.

ATCC. *A549 CCL-185* TM [Online]. Available: <https://www.atcc.org/products/ccl-185> [Accessed].

ATCC. *HCT 116*

CCL-247 TM [Online]. Available: <https://www.atcc.org/products/ccl-247> [Accessed].

ATCC. *HT-29 HTB-38* TM [Online]. Available: <https://www.atcc.org/products/htb-38> [Accessed].

ATCC KB

CRL-3596 TM.

ATCC. *MRC-5 CCL-171* TM [Online]. Available: <https://www.atcc.org/products/ccl-171> [Accessed].

BAMJI-STOCKE, S., VAN BERKEL, V., MILLER, D. M. & FRIEBOES, H. B. 2018. A review of metabolism-associated biomarkers in lung cancer diagnosis and treatment. *Metabolomics*, 14, 81.

BAR-ON, O., SHAPIRA, M. A. & HERSHKO, D. D. 2007. Differential effects of doxorubicin treatment on cell cycle arrest and Skp2 expression in breast cancer cells. *Anti-Cancer Drugs*, 18.

BARDOU, V.-J., ARPINO, G., ELLEDGE, R. M., OSBORNE, C. K. & CLARK, G. M. 2003. Progesterone Receptor Status Significantly Improves Outcome Prediction Over Estrogen

Receptor Status Alone for Adjuvant Endocrine Therapy in Two Large Breast Cancer Databases. *Journal of Clinical Oncology*, 21, 1973-1979.

BARENHOLZ, Y. 2012. Doxil® — The first FDA-approved nano-drug: Lessons learned. *Journal of Controlled Release*, 160, 117-134.

BASSING, C. H., SUH, H., FERGUSON, D. O., CHUA, K. F., MANIS, J., ECKERSDORFF, M., GLEASON, M., BRONSON, R., LEE, C. & ALT, F. W. 2003. Histone H2AX: A Dosage-Dependent Suppressor of Oncogenic Translocations and Tumors. *Cell*, 114, 359-370.

BATTLE, T. E., ARBISER, J. & FRANK, D. A. 2005. The natural product honokiol induces caspase-dependent apoptosis in B-cell chronic lymphocytic leukemia (B-CLL) cells. *Blood*, 106, 690-697.

BELL, D. W., GORE, I., OKIMOTO, R. A., GODIN-HEYMAN, N., SORDELLA, R., MULLOY, R., SHARMA, S. V., BRANNIGAN, B. W., MOHAPATRA, G. & SETTLEMAN, J. 2005. Inherited susceptibility to lung cancer may be associated with the T790M drug resistance mutation in EGFR. *Nature genetics*, 37, 1315-1316.

BELMOKHTAR, C. A., HILLION, J. & SÉGAL-BENDIRDJIAN, E. 2001. Staurosporine induces apoptosis through both caspase-dependent and caspase-independent mechanisms. *Oncogene*, 20, 3354-3362.

BENDELL, J. C., DOMCHEK, S. M., BURSTEIN, H. J., HARRIS, L., YOUNGER, J., KUTER, I., BUNNELL, C., RUE, M., GELMAN, R. & WINER, E. 2003. Central nervous system metastases in women who receive trastuzumab-based therapy for metastatic breast carcinoma. *Cancer*, 97, 2972-2977.

BENTLEY, S. D., CHATER, K. F., CERDEÑO-TÁRRAGA, A. M., CHALLIS, G. L., THOMSON, N. R., JAMES, K. D., HARRIS, D. E., QUAIL, M. A., KIESER, H., HARPER, D., BATEMAN, A., BROWN, S., CHANDRA, G., CHEN, C. W., COLLINS, M., CRONIN, A., FRASER, A., GOBLE, A., HIDALGO, J., HORNSBY, T., HOWARTH, S., HUANG, C. H., KIESER, T., LARKE, L., MURPHY, L., OLIVER, K., O'NEIL, S., RABBINOWITSCH, E., RAJANDREAM, M. A., RUTHERFORD, K., RUTTER, S., SEEGER, K., SAUNDERS, D., SHARP, S., SQUARES, R., SQUARES, S., TAYLOR, K., WARREN, T., WIETZORREK, A., WOODWARD, J., BARRELL, B. G., PARKHILL, J. & HOPWOOD, D. A. 2002. Complete genome sequence of the model actinomycete *Streptomyces coelicolor* A3(2). *Nature*, 417, 141-147.

- BERGER, A., VALANT-VETSCHERA, K., SCHINNERL, J. & BRECKER, L. 2022. A revised classification of the sister tribes Palicoureeae and Psychotrieae (Rubiaceae) indicates genus-specific alkaloid accumulation. *Phytochemistry Reviews*, 21, 941-986.
- BI, Y., YING, X., CHEN, W., WU, J., KONG, C., HU, W., FANG, S., YU, J., ZHAI, M., JIANG, C., CHEN, M., SHEN, L., JI, J. & TU, J. 2024. Glycerophospholipid-driven lipid metabolic reprogramming as a common key mechanism in the progression of human primary hepatocellular carcinoma and cholangiocarcinoma. *Lipids in Health and Disease*, 23, 326.
- BLUEMLEIN, K., GRÜNING, N.-M., FEICHTINGER, R. G., LEHRACH, H., KOFLER, B. & RALSER, M. 2011. No evidence for a shift in pyruvate kinase PKM1 to PKM2 expression during tumorigenesis. *Oncotarget*, 2, 393.
- BONNER, W. M., REDON, C. E., DICKEY, J. S., NAKAMURA, A. J., SEDELNIKOVA, O. A., SOLIER, S. & POMMIER, Y. 2008. γ H2AX and cancer. *Nature Reviews Cancer*, 8, 957-967.
- BOOTH, S. C., WELJIE, A. M. & TURNER, R. J. 2013. Computational tools for the secondary analysis of metabolomics experiments. *Comput Struct Biotechnol J*, 4, e201301003.
- BRAND, G., HENRIQUES, A. T., PASSOS, C. D. S., BALDOQUI, D. C., DE OLIVEIRA SANTIN, S. M., FERREIRA DA COSTA, W. & SARRAGIOTTO, M. H. 2012. Pyrrolidinoindoline alkaloids from *Margaritopsis cymuligera* (Muell. Arg.) C.M. Taylor (Rubiaceae). *Biochemical Systematics and Ecology*, 45, 155-157.
- BRANDES, A. A., TOSONI, A., FRANCESCHI, E., RENI, M., GATTA, G. & VECHT, C. 2008. Glioblastoma in adults. *Critical Reviews in Oncology/Hematology*, 67, 139-152.
- BRANTLEY, K. D., ZELEZNIK, O. A., ROSNER, B., TAMIMI, R. M., AVILA-PACHECO, J., CLISH, C. B. & ELIASSEN, A. H. 2022. Plasma Metabolomics and Breast Cancer Risk over 20 Years of Follow-up among Postmenopausal Women in the Nurses' Health Study. *Cancer Epidemiology, Biomarkers & Prevention*, 31, 839-850.
- BRATTAIN, M. G., FINE, W. D., KHALED, F. M., THOMPSON, J. & BRATTAIN, D. E. 1981. Heterogeneity of malignant cells from a human colonic carcinoma. *Cancer Res*, 41, 1751-6.

BRECKENRIDGE, D. G. & XUE, D. 2004. Regulation of mitochondrial membrane permeabilization by BCL-2 family proteins and caspases. *Current Opinion in Cell Biology*, 16, 647-652.

BRENNAN, CAMERON W., VERHAAK, ROEL G. W., MCKENNA, A., CAMPOS, B., NOUSHMEHR, H., SALAMA, SOFIE R., ZHENG, S., CHAKRAVARTY, D., SANBORN, J. Z., BERMAN, SAMUEL H., BEROUKHIM, R., BERNARD, B., WU, C.-J., GENOVESE, G., SHMULEVICH, I., BARNHOLTZ-SLOAN, J., ZOU, L., VEGESNA, R., SHUKLA, SACHET A., CIRIELLO, G., YUNG, W. K., ZHANG, W., SOUGNEZ, C., MIKKELSEN, T., ALDAPE, K., BIGNER, DARELL D., VAN MEIR, ERWIN G., PRADOS, M., SLOAN, A., BLACK, KEITH L., ESCHBACHER, J., FINOCCHIARO, G., FRIEDMAN, W., ANDREWS, DAVID W., GUHA, A., IACOCCA, M., O'NEILL, BRIAN P., FOLTZ, G., MYERS, J., WEISENBERGER, DANIEL J., PENNY, R., KUCHERLAPATI, R., PEROU, CHARLES M., HAYES, D. N., GIBBS, R., MARRA, M., MILLS, GORDON B., LANDER, E., SPELLMAN, P., WILSON, R., SANDER, C., WEINSTEIN, J., MEYERSON, M., GABRIEL, S., LAIRD, PETER W., HAUSSLER, D., GETZ, G., CHIN, L., BENZ, C., BARNHOLTZ-SLOAN, J., BARRETT, W., OSTROM, Q., WOLINSKY, Y., BLACK, KEITH L., BOSE, B., BOULOS, PAUL T., BOULOS, M., BROWN, J., CZERINSKI, C., EPPLEY, M., IACOCCA, M., KEMPSTA, T., KITKO, T., KOYFMAN, Y., RABENO, B., RASTOGI, P., SUGARMAN, M., SWANSON, P., YALAMANCHII, K., OTEY, ILANA P., LIU, YINGCHUN S., XIAO, Y., AUMAN, J. T., CHEN, P.-C., HADJIPANAYIS, A., LEE, E., LEE, S., PARK, PETER J., SEIDMAN, J., YANG, L., KUCHERLAPATI, R., KALKANIS, S., MIKKELSEN, T., POISSON, LAILA M., RAGHUNATHAN, A., SCARPACE, L., BERNARD, B., BRESSLER, R., EAKIN, A., IYPE, L., et al. 2013. The Somatic Genomic Landscape of Glioblastoma. *Cell*, 155, 462-477.

BRISTY, T. A., BARUA, N., MONTAKIM TAREQ, A., SAKIB, S. A., ETU, S. T., CHOWDHURY, K. H., JYOTI, M. A., AZIZ, M. A. I., REZA, A. A. & CAIAZZO, E. 2020. Deciphering the pharmacological properties of methanol extract of *Psychotria calocarpa* leaves by in vivo, in vitro and in silico approaches. *Pharmaceuticals*, 13, 183.

BROCKHAUSEN, I. 1999. Pathways of O-glycan biosynthesis in cancer cells. *Biochimica et Biophysica Acta (BBA)-General Subjects*, 1473, 67-95.

BROECKLING, C. D., BEGER, R. D., CHENG, L. L., CUMERAS, R., CUTHBERTSON, D. J., DASARI, S., DAVIS, W. C., DUNN, W. B., EVANS, A. M., FERNÁNDEZ-OCHOA, A.,

GIKA, H., GOODACRE, R., GOODMAN, K. D., GOUVEIA, G. J., HSU, P.-C., KIRWAN, J. A., KODRA, D., KULIGOWSKI, J., LAN, R. S.-L., MONGE, M. E., MOUSSA, L. W., NAIR, S. G., REISDORPH, N., SHERROD, S. D., ULMER HOLLAND, C., VUCKOVIC, D., YU, L.-R., ZHANG, B., THEODORIDIS, G. & MOSLEY, J. D. 2023. Current Practices in LC-MS Untargeted Metabolomics: A Scoping Review on the Use of Pooled Quality Control Samples. *Analytical Chemistry*, 95, 18645-18654.

BRUGAROLAS, J., CHANDRASEKARAN, C., GORDON, J. I., BEACH, D., JACKS, T. & HANNON, G. J. 1995. Radiation-induced cell cycle arrest compromised by p21 deficiency. *Nature*, 377, 552-557.

BüLBüL, E. F., BODE, H. B., SCHMITT, S. & BOZHÜYÜK, K. A. J. 2025. Engineering the future of medicine: Natural products, synthetic biology and artificial intelligence for next-generation therapeutics. *Clinical and Translational Medicine*, 15, e70146.

CAILLEAU, R., OLIVÉ, M. & CRUCIGER, Q. V. 1978. Long-term human breast carcinoma cell lines of metastatic origin: preliminary characterization. *In Vitro*, 14, 911-5.

CALDWELL, R. W., RODRIGUEZ, P. C., TOQUE, H. A., NARAYANAN, S. P. & CALDWELL, R. B. 2018. Arginase: A Multifaceted Enzyme Important in Health and Disease. *Physiol Rev*, 98, 641-665.

CALIXTO, N. O., PINTO, M. E. F., RAMALHO, S. D., BURGER, M., BOBEY, A. F., YOUNG, M. C. M., BOLZANI, V. S. & PINTO, A. C. 2016. The genus *Psychotria*: phytochemistry, chemotaxonomy, ethnopharmacology and biological properties. *Journal of the Brazilian Chemical Society*, 27, 1355-1378.

CALLAWAY, J. C., BRITO, G. S. & NEVES, E. S. 2005. Phytochemical analyses of *Banisteriopsis caapi* and *Psychotria viridis*. *J Psychoactive Drugs*, 37, 145-50.

CAMPBELL, S., MESAROS, C., IZZO, L., AFFRONTI, H., NOJI, M., SCHAFFER, B. E., TSANG, T., SUN, K., TREFELY, S., KRUIJNING, S., BLENIS, J., BLAIR, I. A. & WELLEN, K. E. 2021. Glutamine deprivation triggers NAGK-dependent hexosamine salvage. *eLife*, 10, e62644.

CARNEIRO, B. A. & EL-DEIRY, W. S. 2020. Targeting apoptosis in cancer therapy. *Nat Rev Clin Oncol*, 17, 395-417.

- CASCIOLA-ROSEN, L., ROSEN, A., PETRI, M. & SCHLISSEL, M. 1996. Surface blebs on apoptotic cells are sites of enhanced procoagulant activity: implications for coagulation events and antigenic spread in systemic lupus erythematosus. *Proc Natl Acad Sci U S A*, 93, 1624-9.
- CAVALIERI, E., CHAKRAVARTI, D., GUTTENPLAN, J., HART, E., INGLE, J., JANKOWIAK, R., MUTI, P., ROGAN, E., RUSSO, J., SANTEN, R. & SUTTER, T. 2006. Catechol estrogen quinones as initiators of breast and other human cancers: implications for biomarkers of susceptibility and cancer prevention. *Biochim Biophys Acta*, 1766, 63-78.
- CHAIRES, J. B., FOX, K. R., HERRERA, J. E., BRITT, M. & WARING, M. J. 1987. Site and sequence specificity of the daunomycin-DNA interaction. *Biochemistry*, 26, 8227-8236.
- CHAIRES, J. B., HERRERA, J. E. & WARING, M. J. 1990. Preferential binding of daunomycin to 5'TACG and 5'TAGC sequences revealed by footprinting titration experiments. *Biochemistry*, 29, 6145-6153.
- CHEBIB, M., DUKE, R. K., DUKE, C. C., CONNOR, M., MEWETT, K. N. & JOHNSTON, G. A. 2003. Convulsant actions of calycanthine. *Toxicology and applied pharmacology*, 190, 58-64.
- CHEN, A. 2011. PARP inhibitors: its role in treatment of cancer. *Chin J Cancer*, 30, 463-71.
- CHEN, M., SHEN, M., LI, Y., LIU, C., ZHOU, K., HU, W., XU, B., XIA, Y. & TANG, W. 2015. GC-MS-based metabolomic analysis of human papillary thyroid carcinoma tissue. *Int J Mol Med*, 36, 1607-1614.
- CHEN, W., SAXTON, B., TESSEMA, M. & BELINSKY, S. A. 2021. Inhibition of GFAT1 in lung cancer cells destabilizes PD-L1 protein. *Carcinogenesis*, 42, 1171-1178.
- CHENG, K., SAMIMI, R., XIE, G., SHANT, J., DRACHENBERG, C., WADE, M., DAVIS, R. J., NOMIKOS, G. & RAUFMAN, J. P. 2008. Acetylcholine release by human colon cancer cells mediates autocrine stimulation of cell proliferation. *Am J Physiol Gastrointest Liver Physiol*, 295, G591-7.
- CHOI, Y.-M., KIM, H.-K., SHIM, W., ANWAR, M. A., KWON, J.-W., KWON, H.-K., KIM, H. J., JEONG, H., KIM, H. M., HWANG, D., KIM, H. S. & CHOI, S. 2015. Mechanism of Cisplatin-Induced Cytotoxicity Is Correlated to Impaired Metabolism Due to Mitochondrial ROS Generation. *PLOS ONE*, 10, e0135083.

CHRISTOFK, H. R., VANDER HEIDEN, M. G., HARRIS, M. H., RAMANATHAN, A., GERSZTEN, R. E., WEI, R., FLEMING, M. D., SCHREIBER, S. L. & CANTLEY, L. C. 2008. The M2 splice isoform of pyruvate kinase is important for cancer metabolism and tumour growth. *Nature*, 452, 230-233.

CINI, M., WILLIAMS, H., FAY, M. W., SEARLE, M. S., WOODWARD, S. & BRADSHAW, T. D. 2016. Correction: Enantiopure titanocene complexes – direct evidence for paraptosis in cancer cells. *Metallomics*, 8, 260-260.

CLISH, C. B. 2015. Metabolomics: an emerging but powerful tool for precision medicine. *Cold Spring Harb Mol Case Stud*, 1, a000588.

COELHO, R. G., DE CASTRO CALAÇA, I., DE MOURA CELESTRINI, D., CORREIA, A. H., COSTA, M. A. S. M. & SOLA-PENNA, M. 2011. Clotrimazole disrupts glycolysis in human breast cancer without affecting non-tumoral tissues. *Molecular genetics and metabolism*, 103, 394-398.

COHEN, H. J., ELIZALDE, A. & MILLER, S. P. 1968. Cytologic studies of glucose-6-phosphate dehydrogenase in malignancy. *Cancer*, 21, 1055-1060.

COLDWELL, K. E., CUTTS, S. M., OGNIBENE, T. J., HENDERSON, P. T. & PHILLIPS, D. R. 2008. Detection of Adriamycin–DNA adducts by accelerator mass spectrometry at clinically relevant Adriamycin concentrations. *Nucleic acids research*, 36, e100.

COLEMAN, M. L., SAHAI, E. A., YEO, M., BOSCH, M., DEWAR, A. & OLSON, M. F. 2001. Membrane blebbing during apoptosis results from caspase-mediated activation of ROCK I. *Nat Cell Biol*, 3, 339-45.

CORFIELD, A. P. 2015. Mucins: a biologically relevant glycan barrier in mucosal protection. *Biochimica et Biophysica Acta (BBA)-General Subjects*, 1850, 236-252.

COSTA, E. V., PINHEIRO, M. L., DE SOUZA, A. D., BARISON, A., CAMPOS, F. R., VALDEZ, R. H., UEDA-NAKAMURA, T., FILHO, B. P. & NAKAMURA, C. V. 2011. Trypanocidal activity of oxoaporphine and pyrimidine- β -carboline alkaloids from the branches of *Annona foetida* Mart. (Annonaceae). *Molecules*, 16, 9714-20.

CRAGG, G. M. & PEZZUTO, J. M. 2016. Natural Products as a Vital Source for the Discovery of Cancer Chemotherapeutic and Chemopreventive Agents. *Med Princ Pract*, 25 Suppl 2, 41-59.

- CUI, X., SCHIFF, R., ARPINO, G., OSBORNE, C. K. & LEE, A. V. 2005. Biology of Progesterone Receptor Loss in Breast Cancer and Its Implications for Endocrine Therapy. *Journal of Clinical Oncology*, 23, 7721-7735.
- CUSTODIO, A. & FELIU, J. 2013. Prognostic and predictive biomarkers for epidermal growth factor receptor-targeted therapy in colorectal cancer: beyond KRAS mutations. *Critical reviews in oncology/hematology*, 85, 45-81.
- D'ARPA, P. & LIU, L. F. 1989. Topoisomerase-targeting antitumor drugs. *Biochimica et Biophysica Acta (BBA) - Reviews on Cancer*, 989, 163-177.
- DAI, X., SHI, X., LUO, M., LI, P. & GAO, Y. 2023. Integrative analysis of transcriptomic and metabolomic profiles reveals enhanced arginine metabolism in androgen-independent prostate cancer cells. *BMC Cancer*, 23, 1241.
- DANZI, F., PACCHIANA, R., MAFFICINI, A., SCUPOLI, M. T., SCARPA, A., DONADELLI, M. & FIORE, A. 2023. To metabolomics and beyond: a technological portfolio to investigate cancer metabolism. *Signal Transduction and Targeted Therapy*, 8, 137.
- DARABEDIAN, N., JI, W., FAN, M., LIN, S., SEO, H.-S., VINOGRADOVA, E. V., YARON, T. M., MILLS, E. L., XIAO, H., SENKANE, K., HUNTSMAN, E. M., JOHNSON, J. L., CHE, J., CANTLEY, L. C., CRAVATT, B. F., DHE-PAGANON, S., STEGMAIER, K., ZHANG, T., GRAY, N. S. & CHOUGHANI, E. T. 2023. Depletion of creatine phosphagen energetics with a covalent creatine kinase inhibitor. *Nature Chemical Biology*, 19, 815-824.
- DAVIS, R. A., CARROLL, A. R. & QUINN, R. J. 1998. Eudistomin V, a New β -Carboline from the Australian Ascidian *Pseudodistoma aureum*. *Journal of Natural Products*, 61, 959-960.
- DE CARVALHO, A. R., DE CARVALHO, M. G., BRAZ-FILHO, R. & VIEIRA, I. J. C. 2016. Chapter 7 - Psychotria Genus: Chemical Constituents, Biological Activities, and Synthetic Studies. In: ATTA UR, R. (ed.) *Studies in Natural Products Chemistry*. Elsevier.
- DE OLIVEIRA, A. M., LEMOS, R. P. L. & CONSERVA, L. M. 2013. b-Carboline alkaloids from *Psychotria barbiflora* DC.(Rubiaceae). *Biochem Syst Ecol*, 50, 339-341.
- DE OLIVEIRA FIGUEIREDO, P., PERDOMO, R. T., GARCEZ, F. R., MATOS, M. D. F. C., DE CARVALHO, J. E. & GARCEZ, W. S. 2014. Further constituents of *Galianthe thalictroides*

(Rubiaceae) and inhibition of DNA topoisomerases I and II α by its cytotoxic β -carboline alkaloids. *Bioorganic & Medicinal Chemistry Letters*, 24, 1358-1361.

DE, S., CAMPBELL, C., VENKITARAMAN, A. R. & ESPOSITO, A. 2020. Pulsatile MAPK Signaling Modulates p53 Activity to Control Cell Fate Decisions at the G2 Checkpoint for DNA Damage. *Cell Reports*, 30, 2083-2093.e5.

DEBERARDINIS, R. J., MANCUSO, A., DAIKHIN, E., NISSIM, I., YUDKOFF, M., WEHRLI, S. & THOMPSON, C. B. 2007. Beyond aerobic glycolysis: Transformed cells can engage in glutamine metabolism that exceeds the requirement for protein and nucleotide synthesis. *Proceedings of the National Academy of Sciences*, 104, 19345-19350.

DENECKER, G., VERCAMMEN, D., DECLERCQ, W. & VANDENABEELE, P. 2001. Apoptotic and necrotic cell death induced by death domain receptors. *Cell Mol Life Sci*, 58, 356-70.

DENZEL, M. S. & ANTEBI, A. 2015. Hexosamine pathway and (ER) protein quality control. *Current Opinion in Cell Biology*, 33, 14-18.

DERRY, W. B., WILSON, L. & JORDAN, M. A. 1995. Substoichiometric binding of taxol suppresses microtubule dynamics. *Biochemistry*, 34, 2203-2211.

DEWICK, P. M. 2009a. *Medicinal Natural Products: A Biosynthetic Approach*, Wiley.

DEWICK, P. M. 2009b. *Medicinal Natural Products: A Biosynthetic Approach*, Wiley.

DHANISHA, S. S., GURUVAYOORAPPAN, C., DRISHYA, S. & ABEESH, P. 2018. Mucins: Structural diversity, biosynthesis, its role in pathogenesis and as possible therapeutic targets. *Critical reviews in oncology/hematology*, 122, 98-122.

DO NASCIMENTO, C. A., GOMES, M. S., LIAO, L. M., DE OLIVEIRA, C. M., KATO, L., DA SILVA, C. C. & TANAKA, C. M. 2006. Alkaloids from *Palicourea coriacea* (Cham.) K. Schum. *Zeitschrift für Naturforschung B*, 61, 1443-1446.

DOGAN, S., SHEN, R., ANG, D. C., JOHNSON, M. L., D'ANGELO, S. P., PAIK, P. K., BRZOSTOWSKI, E. B., RIELY, G. J., KRIS, M. G. & ZAKOWSKI, M. F. 2012. Molecular epidemiology of EGFR and KRAS mutations in 3,026 lung adenocarcinomas: higher susceptibility of women to smoking-related KRAS-mutant cancers. *Clinical cancer research*, 18, 6169-6177.

DONEHOWER, R. C. 1996. The Clinical Development of Paclitaxel: A Successful Collaboration of Academia, Industry and the National Cancer Institute. *Stem Cells*, 14, 25-28.

DRAGIC, H., BARTHELAIX, A., DURET, C., LE GOUPIL, S., LAPRADE, H., MARTIN, S., BRUGIÈRE, S., COUTÉ, Y., MACHON, C., GUITTON, J., RUDEWICZ, J., HOFMAN, P., LEBECQUE, S., CHAVEROUX, C., FERRARO-PEYRET, C., RENNO, T. & MANIÉ, S. N. 2022. The hexosamine pathway and coat complex II promote malignant adaptation to nutrient scarcity. *Life Science Alliance*, 5, e202101334.

DRUGS.COM. *Methotrexate* [Online]. 4500 East-West Highway, Suite 900, Bethesda, Maryland 20814: The American Society of Health-System Pharmacists. Available: <https://www.drugs.com/monograph/methotrexate.html> [Accessed].

DUKE, R. K., ALLAN, R. D., JOHNSTON, G. A., MEWETT, K. N., MITROVIC, A. D., DUKE, C. C. & HAMBLEY, T. W. 1995. Idiospermuline, a trimeric pyrrolidinoindoline alkaloid from the seed of *Idiospermum australiense*. *Journal of natural products*, 58, 1200-1208.

DUNN, W. B., BROADHURST, D., BEGLEY, P., ZELEN, E., FRANCIS-MCINTYRE, S., ANDERSON, N., BROWN, M., KNOWLES, J. D., HALSALL, A., HASELDEN, J. N., NICHOLLS, A. W., WILSON, I. D., KELL, D. B., GOODACRE, R. & THE HUMAN SERUM METABOLOME, C. 2011. Procedures for large-scale metabolic profiling of serum and plasma using gas chromatography and liquid chromatography coupled to mass spectrometry. *Nature Protocols*, 6, 1060-1083.

DURANTE, W., JOHNSON, F. K. & JOHNSON, R. A. 2007. Arginase: a critical regulator of nitric oxide synthesis and vascular function. *Clin Exp Pharmacol Physiol*, 34, 906-11.

DWIVEDI, P., WU, P., KLOPSCH, S. J., PUZON, G. J., XUN, L. & HILL, H. H. 2008. Metabolic profiling by ion mobility mass spectrometry (IMMS). *Metabolomics*, 4, 63-80.

DYSON, N. J. 2016. RB1: a prototype tumor suppressor and an enigma. *Genes Dev*, 30, 1492-502.

ECKELMAN, B. P., SALVESEN, G. S. & SCOTT, F. L. 2006. Human inhibitor of apoptosis proteins: why XIAP is the black sheep of the family. *EMBO Rep*, 7, 988-94.

- ECKERT, L. B., REPASKY, G. A., ÜLKÜ, A. S., MCFALL, A., ZHOU, H., SARTOR, C. I. & DER, C. J. 2004. Involvement of Ras Activation in Human Breast Cancer Cell Signaling, Invasion, and Anoikis. *Cancer Research*, 64, 4585-4592.
- EHRLICHOVÁ, M., OJIMA, I., CHEN, J., VÁCLAVÍKOVÁ, R., NĚMCOVÁ-FÜRSTOVÁ, V., VOBOŘILOVÁ, J., ŠIMEK, P., HORSKÝ, S., SOUČEK, P., KOVÁŘ, J., BRABEC, M. & GUT, I. 2012. Transport, metabolism, cytotoxicity and effects of novel taxanes on the cell cycle in MDA-MB-435 and NCI/ADR-RES cells. *Naunyn-Schmiedeberg's Archives of Pharmacology*, 385, 1035-1048.
- EIBL, R., MEIER, P., STUTZ, I., SCHILDBERGER, D., HÜHN, T. & EIBL, D. 2018. Plant cell culture technology in the cosmetics and food industries: current state and future trends. *Appl Microbiol Biotechnol*, 102, 8661-8675.
- EITER, K. & NAGY, M. 1949. Zur Konstitution des Calycanthins. *Monatshefte für Chemie und verwandte Teile anderer Wissenschaften*, 80, 607-621.
- EL-DEIRY, W. S. 1998. Regulation of p53 downstream genes. *Semin Cancer Biol*, 8, 345-57.
- ELIA, I., BROEKAERT, D., CHRISTEN, S., BOON, R., RADAELLI, E., ORTH, M. F., VERFAILLIE, C., GRÜNEWALD, T. G. P. & FENDT, S. M. 2017. Proline metabolism supports metastasis formation and could be inhibited to selectively target metastasizing cancer cells. *Nat Commun*, 8, 15267.
- ELISABETSKY, E., AMADOR, T. A., ALBUQUERQUE, R. R., NUNES, D. S. & CARVALHO ADO, C. 1995. Analgesic activity of *Psychotria colorata* (Willd. ex R. & S.) Muell. Arg. alkaloids. *J Ethnopharmacol*, 48, 77-83.
- ENG, W., FAUCETTE, L., JOHNSON, R. K. & STERNGLANZ, R. 1988. Evidence that DNA topoisomerase I is necessary for the cytotoxic effects of camptothecin. *Molecular pharmacology*, 34, 755-760.
- ENGELAND, K. 2022. Cell cycle regulation: p53-p21-RB signaling. *Cell Death & Differentiation*, 29, 946-960.
- ENSOR, C. M., HOLTSBERG, F. W., BOMALASKI, J. S. & CLARK, M. A. 2002. Pegylated Arginine Deiminase (ADI-SS PEG20,000 mw) Inhibits Human Melanomas and Hepatocellular Carcinomas in Vitro and in Vivo. *Cancer Research*, 62, 5443-5450.

ERIKSSON, L. 1999. *Introduction to multi-and megavariable data analysis using projection methods (PCA & PLS)*, Umetrics AB.

FAN, L.-X., LIU, C.-M., GAO, A.-H., ZHOU, Y.-B. & LI, J. 2013. Berberine combined with 2-deoxy-d-glucose synergistically enhances cancer cell proliferation inhibition via energy depletion and unfolded protein response disruption. *Biochimica et Biophysica Acta (BBA) - General Subjects*, 1830, 5175-5183.

FAN, W.-H., WANG, F.-C., JIN, Z., ZHU, L. & ZHANG, J.-X. 2022. Curcumin Synergizes with Cisplatin to Inhibit Colon Cancer through Targeting the MicroRNA-137-Glutaminase Axis. *Current Medical Science*, 42, 108-117.

FAROOQUI, A. A., HORROCKS, L. A. & FAROOQUI, T. 2000. Glycerophospholipids in brain: their metabolism, incorporation into membranes, functions, and involvement in neurological disorders. *Chemistry and Physics of Lipids*, 106, 1-29.

FAROOQUI, A. A., HORROCKS, L. A. & FAROOQUI, T. 2007. Interactions between neural membrane glycerophospholipid and sphingolipid mediators: A recipe for neural cell survival or suicide. *Journal of Neuroscience Research*, 85, 1834-1850.

FAVARO, E., BENSAAD, K., CHONG, MEI G., TENNANT, DANIEL A., FERGUSON, DAVID J. P., SNELL, C., STEERS, G., TURLEY, H., LI, J.-L., GÜNTHER, ULRICH L., BUFFA, FRANCESCA M., MCINTYRE, A. & HARRIS, ADRIAN L. 2012. Glucose Utilization via Glycogen Phosphorylase Sustains Proliferation and Prevents Premature Senescence in Cancer Cells. *Cell Metabolism*, 16, 751-764.

FEARON, E. R. & VOGELSTEIN, B. 1990. A genetic model for colorectal tumorigenesis. *Cell*, 61, 759-767.

FIEHN, O. 2016. Metabolomics by Gas Chromatography-Mass Spectrometry: Combined Targeted and Untargeted Profiling. *Curr Protoc Mol Biol*, 114, 30.4.1-30.4.32.

FIEHN, O., KOPKA, J., DÖRMANN, P., ALTMANN, T., TRETHEWEY, R. N. & WILLMITZER, L. 2000. Metabolite profiling for plant functional genomics. *Nature Biotechnology*, 18, 1157-1161.

FILIPPI-CHIELA, E. C., THOMÉ, M. P., BUENO E SILVA, M. M., PELEGRINI, A. L., LEDUR, P. F., GARICOCHEA, B., ZAMIN, L. L. & LENZ, G. 2013. Resveratrol abrogates

the Temozolomide-induced G2 arrest leading to mitotic catastrophe and reinforces the Temozolomide-induced senescence in glioma cells. *BMC Cancer*, 13, 147.

FILMUS, J., POLLAK, M. N., CAILLEAU, R. & BUICK, R. N. 1985. MDA-468, a human breast cancer cell line with a high number of epidermal growth factor (EGF) receptors, has an amplified EGF receptor gene and is growth inhibited by EGF. *Biochemical and Biophysical Research Communications*, 128, 898-905.

FINK SUSAN, L. & COOKSON BRAD, T. 2005. Apoptosis, Pyroptosis, and Necrosis: Mechanistic Description of Dead and Dying Eukaryotic Cells. *Infection and Immunity*, 73, 1907-1916.

FLOSS, H. G. 1976. Biosynthesis of ergot alkaloids and related compounds. *Tetrahedron*, 32, 873-912.

FORMAN, D. T. 1979. The significance of creatine kinase (CKBB) in metastatic cancer of the prostate. *Annals of Clinical & Laboratory Science*, 9, 333-337.

FORREST, R. A., SWIFT, L. P., REPHAELI, A., NUDELMAN, A., KIMURA, K.-I., PHILLIPS, D. R. & CUTTS, S. M. 2012. Activation of DNA damage response pathways as a consequence of anthracycline-DNA adduct formation. *Biochemical pharmacology*, 83, 1602-1612.

FRIEDMAN, R. & CAFLISCH, A. 2009. Discovery of Plasmepsin Inhibitors by Fragment-Based Docking and Consensus Scoring. *ChemMedChem*, 4, 1317-1326.

FRISVAD, J. C., SMEDSGAARD, J., LARSEN, T. O. & SAMSON, R. A. 2004. Mycotoxins, drugs and other extrolites produced by species in *Penicillium* subgenus *Penicillium*. *Stud. Mycol*, 49, e41.

FRITZ KÖGL, A. J. H.-S. A. H. E. 1933. . Über ein Phytohormon der Zellstreckung. Reindarstellung des Auxins aus menschlichem Harn. 4. Mitteilung über pflanzliche Wachstumsstoffe. *Hoppe-Seyler's Zeitschrift für physiologische Chemie*, 214, 241-261.

FROELICH-AMMON, S. J. & OSHEROFF, N. 1995. Topoisomerase Poisons: Harnessing the Dark Side of Enzyme Mechanism (*). *Journal of Biological chemistry*, 270, 21429-21432.

FU, Y.-H., HUANG, L.-G., WANG, X.-C., LI, X.-B., LI, K.-K., WU, S.-L. & LIU, Y.-P. 2015. [Studies on chemical constituents from *Psychotria straminea*]. *Zhongguo Zhong yao za zhi* = *Zhongguo zhongyao zazhi* = *China journal of Chinese materia medica*, 40, 2138-2143.

FUKUMURA, D., XU, L., CHEN, Y., GOHONGI, T., SEED, B. & JAIN, R. K. 2001. Hypoxia and Acidosis Independently Up-Regulate Vascular Endothelial Growth Factor Transcription in Brain Tumors in Vivo. *Cancer Research*, 61, 6020-6024.

FUNAYAMA, S. & CORDELL, G. A. 2014. *Alkaloids: A Treasury of Poisons and Medicines*, Elsevier Science.

FURUTA, T., TAKEMURA, H., LIAO, Z. Y., AUNE, G. J., REDON, C., SEDELNIKOVA, O. A., PILCH, D. R., ROGAKOU, E. P., CELESTE, A., CHEN, H. T., NUSSENZWEIG, A., ALADJEM, M. I., BONNER, W. M. & POMMIER, Y. 2003. Phosphorylation of histone H2AX and activation of Mre11, Rad50, and Nbs1 in response to replication-dependent DNA double-strand breaks induced by mammalian DNA topoisomerase I cleavage complexes. *J Biol Chem*, 278, 20303-12.

GALINDO-PRIETO, B., ERIKSSON, L. & TRYGG, J. 2015. Variable influence on projection (VIP) for OPLS models and its applicability in multivariate time series analysis. *Chemometrics and Intelligent Laboratory Systems*, 146, 297-304.

GALLAGHER, F. A., KETTUNEN, M. I., DAY, S. E., LERCHE, M. & BRINDLE, K. M. 2008. ¹³C MR spectroscopy measurements of glutaminase activity in human hepatocellular carcinoma cells using hyperpolarized ¹³C-labeled glutamine. *Magnetic Resonance in Medicine: An Official Journal of the International Society for Magnetic Resonance in Medicine*, 60, 253-257.

GALLO, M., FERRARI, E., TERRAZZAN, A., BRUGNOLI, F., SPISNI, A., TACCIOLI, C., AGUIARI, G., TRENTINI, A., VOLINIA, S., KEILLOR, J. W., BERGAMINI, C. M., BIANCHI, N. & PERTINHEZ, T. A. 2023. Metabolic characterisation of transglutaminase 2 inhibitor effects in breast cancer cell lines. *The FEBS Journal*, 290, 5411-5433.

GALLUZZI, L., MAIURI, M. C., VITALE, I., ZISCHKA, H., CASTEDO, M., ZITVOGEL, L. & KROEMER, G. 2007. Cell death modalities: classification and pathophysiological implications. *Cell Death & Differentiation*, 14, 1237-1243.

GAMO, F.-J., SANZ, L. M., VIDAL, J., DE COZAR, C., ALVAREZ, E., LAVANDERA, J.-L., VANDERWALL, D. E., GREEN, D. V. S., KUMAR, V., HASAN, S., BROWN, J. R., PEISHOFF, C. E., CARDON, L. R. & GARCIA-BUSTOS, J. F. 2010. Thousands of chemical starting points for antimalarial lead identification. *Nature*, 465, 305-310.

GAO, P., TCHERNYSHYOV, I., CHANG, T.-C., LEE, Y.-S., KITA, K., OCHI, T., ZELLER, K. I., DE MARZO, A. M., VAN EYK, J. E., MENDELL, J. T. & DANG, C. V. 2009. c-Myc suppression of miR-23a/b enhances mitochondrial glutaminase expression and glutamine metabolism. *Nature*, 458, 762-765.

GARCÍA-BERROCAL, J. R., NEVADO, J., RAMÍREZ-CAMACHO, R., SANZ, R., GONZÁLEZ-GARCÍA, J. A., SÁNCHEZ-RODRÍGUEZ, C., CANTOS, B., ESPAÑA, P., VERDAGUER, J. M. & TRINIDAD CABEZAS, A. 2007. The anticancer drug cisplatin induces an intrinsic apoptotic pathway inside the inner ear. *British Journal of Pharmacology*, 152, 1012-1020.

GARRIDO, C., GALLUZZI, L., BRUNET, M., PUIG, P. E., DIDELOT, C. & KROEMER, G. 2006. Mechanisms of cytochrome c release from mitochondria. *Cell Death & Differentiation*, 13, 1423-1433.

GE, T., YANG, J., ZHOU, S., WANG, Y., LI, Y. & TONG, X. 2020. The Role of the Pentose Phosphate Pathway in Diabetes and Cancer. *Frontiers in Endocrinology*, 11.

GERTSMAN, I. & BARSHOP, B. A. 2018. Promises and pitfalls of untargeted metabolomics. *J Inherit Metab Dis*, 41, 355-366.

GIDDING, C. E. M., KELLIE, S. J., KAMPS, W. A. & DE GRAAF, S. S. N. 1999. Vincristine revisited. *Critical Reviews in Oncology/Hematology*, 29, 267-287.

GILLIAM, L. A. A., MOYLAN, J. S., PATTERSON, E. W., SMITH, J. D., WILSON, A. S., RABBANI, Z. & REID, M. B. 2012. Doxorubicin acts via mitochondrial ROS to stimulate catabolism in C2C12 myotubes. *American Journal of Physiology-Cell Physiology*, 302, C195-C202.

GLUNDE, K., BHUJWALLA, Z. M. & RONEN, S. M. 2011. Choline metabolism in malignant transformation. *Nature Reviews Cancer*, 11, 835-848.

GONZÁLEZ-DOMÍNGUEZ, Á., ESTANYOL-TORRES, N., BRUNIUS, C., LANDBERG, R. & GONZÁLEZ-DOMÍNGUEZ, R. 2024. QComics: Recommendations and Guidelines for Robust, Easily Implementable and Reportable Quality Control of Metabolomics Data. *Anal Chem*, 96, 1064-1072.

GONZALVEZ, F. & ASHKENAZI, A. 2010. New insights into apoptosis signaling by Apo2L/TRAIL. *Oncogene*, 29, 4752-65.

- GORDIN, H. 1905. ON THE CRYSTALLINE ALKALOID OF CALYCANTHUS GLAUCUS. *Journal of the American Chemical Society*, 27, 1418-1429.
- GRADISHAR, W. J. 2006. Albumin-bound paclitaxel: a next-generation taxane. *Expert Opinion on Pharmacotherapy*, 7, 1041-1053.
- GREEN, D. R. & LLAMBI, F. 2015. Cell Death Signaling. *Cold Spring Harb Perspect Biol*, 7.
- GRINDE, M. T., SKRBO, N., MOESTUE, S. A., RøDLAND, E. A., BORGAN, E., KRISTIAN, A., SITTER, B., BATHEN, T. F., BørRESEN-DALE, A.-L., MæLANDSMO, G. M., ENGBRAATEN, O., SørLIE, T., MARANGONI, E. & GRIBBESTAD, I. S. 2014. Interplay of choline metabolites and genes in patient-derived breast cancer xenografts. *Breast Cancer Research*, 16, R5.
- GROCHANS, S., CYBULSKA, A. M., SIMIŃSKA, D., KORBECKI, J., KOJDER, K., CHLUBEK, D. & BARANOWSKA-BOSIACKA, I. 2022. Epidemiology of Glioblastoma Multiforme—Literature Review. *Cancers*, 14, 2412.
- GROSS, N. J. 1988. Ipratropium bromide. *N Engl J Med*, 319, 486-94.
- GUÉRITTE-VOEGELEIN, F., SÉVENET, T., PUSSET, J., ADELIN, M.-T., GILLET, B., BELOEIL, J.-C., GUÉNARD, D., POTIER, P., RASOLONJANAHARY, R. & KORDON, C. 1992. Alkaloids from *Psychotria oleoides* with Activity on Growth Hormone Release. *Journal of Natural Products*, 55, 923-930.
- GULATI, K., MANUKONDA, R., KAIRAMKONDA, M., KALIKI, S. & POLURI, K. M. 2023. Serum Metabolomics of Retinoblastoma: Assessing the Differential Serum Metabolic Signatures of Unilateral and Bilateral Patients. *ACS Omega*, 8, 48233-48250.
- GUNTUR, V. P., WALDREP, J. C., GUO, J. J., SELTING, K. & DHAND, R. 2010. Increasing P53 Protein Sensitizes Non-Small Cell Lung Cancer to Paclitaxel and Cisplatin *In Vitro*. *Anticancer Research*, 30, 3557-3564.
- GUPTA, M. P., SOLÍS, P. N., CALDERÓN, A. I., GUINNEAU-SINCLAIR, F., CORREA, M., GALDAMES, C., GUERRA, C., ESPINOSA, A., ALVENDA, G. I., ROBLES, G. & OCAMPO, R. 2005. Medical Ethnobotany of the Teribes of Bocas del Toro, Panama. *Journal of Ethnopharmacology*, 96, 389-401.

- HADI, S., RAHMAWATI, K. P., ASNAWATI, D., ERSALENA, V. F. & AZWARI, A. 2014. Characterization Of Alkaloids From The Leaves Of Psychotria Malayana Jack Of Lombok Island On The Basis Of Gas Chromatography-Mass Spectroscopy. *2014*, 3, 6.
- HALLBERG, B. & PALMER, R. H. 2013. Mechanistic insight into ALK receptor tyrosine kinase in human cancer biology. *Nature Reviews Cancer*, 13, 685-700.
- HAMILTON, G. S. 2015. Antibody-drug conjugates for cancer therapy: The technological and regulatory challenges of developing drug-biologic hybrids. *Biologicals*, 43, 318-332.
- HANAHAN, D. & WEINBERG, R. A. 2000. The hallmarks of cancer. *Cell*, 100, 57-70.
- HANAHAN, D. & WEINBERG, R. A. 2017. Biological hallmarks of cancer. *Holland-Frei Cancer Medicine*, 1, 1-10.
- HANDE, K. R. 2008. Topoisomerase II inhibitors. *Update on Cancer Therapeutics*, 3, 13-26.
- HART, N., JOHNS, S., LAMBERTON, J. & SUMMONS, R. 1974. Psychotridine, a C₅₅H₆₂N₁₀ Alkaloid From *Psychotria beccarioides* (Rubiaceae). *Australian Journal of Chemistry*, 27, 639-646.
- HASAWI, N. A., ALKANDARI, M. F. & LUQMANI, Y. A. 2014. Phosphofructokinase: A mediator of glycolytic flux in cancer progression. *Critical Reviews in Oncology/Hematology*, 92, 312-321.
- HASLAM, S. Z. & WOODWARD, T. L. 2003. Host microenvironment in breast cancer development: epithelial-cell-stromal-cell interactions and steroid hormone action in normal and cancerous mammary gland. *Breast Cancer Res*, 5, 208-15.
- HAYASHI, T., SMITH, F. T. & LEE, K. H. 1987. Antitumor agents. 89. Psychorubrin, a new cytotoxic naphthoquinone from *Psychotria rubra* and its structure-activity relationships. *Journal of medicinal chemistry*, 30, 2005-2008.
- HEGI, M. E., DISERENS, A.-C., GORLIA, T., HAMOU, M.-F., TRIBOLET, N. D., WELLER, M., KROS, J. M., HAINFELLNER, J. A., MASON, W., MARIANI, L., BROMBERG, J. E. C., HAU, P., MIRIMANOFF, R. O., CAIRNCROSS, J. G., JANZER, R. C. & STUPP, R. 2005. *MGMT* Gene Silencing and Benefit from Temozolomide in Glioblastoma. *New England Journal of Medicine*, 352, 997-1003.

- HELIN, K., HARLOW, E. & FATTAEY, A. 1993. Inhibition of E2F-1 transactivation by direct binding of the retinoblastoma protein. *Mol Cell Biol*, 13, 6501-8.
- HEMMATEENEJAD, B., ABBASPOUR, A., MAGHAMI, H., MIRI, R. & PANJEHSHAHIN, M. R. 2006. Partial least squares-based multivariate spectral calibration method for simultaneous determination of beta-carboline derivatives in *Peganum harmala* seed extracts. *Analytica Chimica Acta*, 575, 290-299.
- HENLEY, S. A. & DICK, F. A. 2012. The retinoblastoma family of proteins and their regulatory functions in the mammalian cell division cycle. *Cell Div*, 7, 10.
- HESS, D. & IGAL, R. A. 2011. Genistein downregulates de novo lipid synthesis and impairs cell proliferation in human lung cancer cells. *Experimental Biology and Medicine*, 236, 707-713.
- HOOS, A. 2016. Development of immuno-oncology drugs—from CTLA4 to PD1 to the next generations. *Nature reviews Drug discovery*, 15, 235-247.
- HORECKER, B. L. 2002. The Pentose Phosphate Pathway. *Journal of Biological Chemistry*, 277, 47965-47971.
- HORWITZ, S. B. 1994. How to make taxol from scratch. *Nature*, 367.
- HOSIOS, A. M. & MANNING, B. D. 2021. Cancer Signaling Drives Cancer Metabolism: AKT and the Warburg Effect. *Cancer Research*, 81, 4896-4898.
- HSIANG, Y. H., HERTZBERG, R., HECHT, S. & LIU, L. F. 1985. Camptothecin induces protein-linked DNA breaks via mammalian DNA topoisomerase I. *Journal of Biological Chemistry*, 260, 14873-14878.
- HUANG, K., CHEN, Y., ZHANG, R., WU, Y., MA, Y., FANG, X. & SHEN, S. 2018. Honokiol induces apoptosis and autophagy via the ROS/ERK1/2 signaling pathway in human osteosarcoma cells in vitro and in vivo. *Cell Death Dis*, 9, 157.
- HUENNEKENS, F. M. 1994. The methotrexate story: A paradigm for development of cancer chemotherapeutic agents. *Advances in Enzyme Regulation*, 34, 397-419.
- HUNTER, A. & DOWNS, C. E. 1945. THE INHIBITION OF ARGINASE BY AMINO ACIDS. *Journal of Biological Chemistry*, 157, 427-446.

- HUTAN, P. P., WHITMORE, T. C., NG, F. S. P. & MALAYSIA, I. P. P. 1989. *Tree Flora of Malaya: A Manual for Foresters*, Longman.
- ISMAIL, N. I., OTHMAN, I., ABAS, F., H. LAJIS, N. & NAIDU, R. 2019. Mechanism of Apoptosis Induced by Curcumin in Colorectal Cancer. *International Journal of Molecular Sciences*, 20, 2454.
- IVANESCU, B., MIRON, A. & CORCIOVA, A. 2015. Sesquiterpene lactones from *Artemisia* genus: Biological activities and methods of analysis. *Journal of analytical methods in chemistry*, 2015, 247685.
- JÄGER, W., GRUBER, A., GIESSRIGL, B., KRUPITZA, G., SZEKERES, T. & SONNTAG, D. 2011. Metabolomic Analysis of Resveratrol-Induced Effects in the Human Breast Cancer Cell Lines MCF-7 and MDA-MB-231. *OMICS: A Journal of Integrative Biology*, 15, 9-14.
- JAIN, D. 2000. Cardiotoxicity of doxorubicin and other anthracycline derivatives. *Journal of Nuclear Cardiology*, 7, 53-62.
- JAIN, R. K., DI TOMASO, E., DUDA, D. G., LOEFFLER, J. S., SORENSEN, A. G. & BATCHELOR, T. T. 2007. Angiogenesis in brain tumours. *Nature Reviews Neuroscience*, 8, 610-622.
- JAMISON, C. R., BADILLO, J. J., LIPSHULTZ, J. M., COMITO, R. J. & MACMILLAN, D. W. 2017. Catalyst-controlled oligomerization for the collective synthesis of polypyrroloindoline natural products. *Nature chemistry*, 9, 1165-1169.
- JÄNICKE, R. U. 2009. MCF-7 breast carcinoma cells do not express caspase-3. *Breast Cancer Research and Treatment*, 117, 219-221.
- JANNIC, V., GUÉRITTE, F., LAPRÉVOTE, O., SERANI, L., MARTIN, M.-T., SÉVENET, T. & POTIER, P. 1999. Pyrrolidinoindoline Alkaloids from *Psychotria oleoides* and *Psychotria lyciiflora*. *Journal of Natural Products*, 62, 838-843.
- JARDÉ, T., PERRIER, S., VASSON, M. P. & CALDEFIE-CHÉZET, F. 2011. Molecular mechanisms of leptin and adiponectin in breast cancer. *Eur J Cancer*, 47, 33-43.
- JEE, S. H., KIM, M., KIM, M., KANG, M., SEO, Y. W., JUNG, K. J., LEE, S. J., HONG, S. & LEE, J. H. 2016. Clinical relevance of glycerophospholipid, sphingomyelin and glutathione metabolism in the pathogenesis of pharyngolaryngeal cancer in smokers: the Korean Cancer Prevention Study-II. *Metabolomics*, 12, 164.

- JENKINS, C. M., YANG, J., SIMS, H. F. & GROSS, R. W. 2011. Reversible high affinity inhibition of phosphofructokinase-1 by acyl-CoA: a mechanism integrating glycolytic flux with lipid metabolism. *Journal of Biological Chemistry*, 286, 11937-11950.
- JESUS, J.-B., FRANCISCO, A.-G. & JAMES, P. S. 2002. The Solid State, Solution and Tubulin-Bound Conformations of Agents that Promote Microtubule Stabilization. *Current Medicinal Chemistry - Anti-Cancer Agents*, 2, 91-122.
- JIANG, Z.-B., HUANG, J., XIE, C., LI, X., LIU, L., HE, J., PAN, H., HUANG, L., FAN, X.-X., YAO, X.-J., XIE, Y., LI, N., LIU, L., HE, J.-X. & LEUNG, E. L.-H. 2016. Combined use of PI3K and MEK inhibitors synergistically inhibits lung cancer with EGFR and KRAS mutations. *Oncol Rep*, 36, 365-375.
- JIMÉNEZ-LÓPEZ, J. M., RÍOS-MARCO, P., MARCO, C., SEGOVIA, J. L. & CARRASCO, M. P. 2010. Alterations in the homeostasis of phospholipids and cholesterol by antitumor alkylphospholipids. *Lipids in Health and Disease*, 9, 33.
- JOHANSSON, S., GOLDENBERG, D. M., GRIFFITHS, G. L., WAHREN, B. & HINKULA, J. 2006. Elimination of HIV-1 infection by treatment with a doxorubicin-conjugated anti-envelope antibody. *AIDS*, 20.
- JOHNSON, C. H. & GONZALEZ, F. J. 2012. Challenges and opportunities of metabolomics. *J Cell Physiol*, 227, 2975-81.
- JOHNSON, C. H., IVANISEVIC, J. & SIUZDAK, G. 2016. Metabolomics: beyond biomarkers and towards mechanisms. *Nat Rev Mol Cell Biol*, 17, 451-9.
- JOHNSON, C. H., PATTERSON, A. D., IDLE, J. R. & GONZALEZ, F. J. 2012. Xenobiotic metabolomics: major impact on the metabolome. *Annu Rev Pharmacol Toxicol*, 52, 37-56.
- JOHNSTON, J. B., PAUL, J. T., NEUFELD, N. J., HANEY, N., KROPP, D. M., HU, X., CHEANG, M. & GIBSON, S. B. 2004. Role of Myeloid Cell Factor-1 (Mcl-1) in Chronic Lymphocytic Leukemia. *Leukemia & Lymphoma*, 45, 2017-2027.
- JOLLIFFE, I. T. & CADIMA, J. 2016. Principal component analysis: a review and recent developments. *Philos Trans A Math Phys Eng Sci*, 374, 20150202.
- JOLY, L., GUERRA, S., SÉPTIMO, R., SOLÍS, P., CORREA, M., GUPTA, M., LEVY, S. & SANDBERG, F. 1987. Ethnobotanical inventory of medicinal plants used by the Guaymí Indians in Western Panama. Part I. *Journal of Ethnopharmacology*, 20, 145-171.

JORDAN, M. A. 2002. Mechanism of Action of Antitumor Drugs that Interact with Microtubules and Tubulin. *Current Medicinal Chemistry - Anti-Cancer Agents*, 2, 1-17.

JORDAN, M. A., MARGOLIS, R. L., HIMES, R. H. & WILSON, L. 1986. Identification of a distinct class of vinblastine binding sites on microtubules. *Journal of Molecular Biology*, 187, 61-73.

JORDAN, M. A., THROWER, D. & WILSON, L. 1991. Mechanism of Inhibition of Cell Proliferation by Vinca Alkaloids¹. *Cancer Research*, 51, 2212-2222.

JORDAN, M. A., TOSO, R. J., THROWER, D. & WILSON, L. 1993. Mechanism of mitotic block and inhibition of cell proliferation by taxol at low concentrations. *Proceedings of the National Academy of Sciences*, 90, 9552-9556.

JORDAN, M. A. & WILSON, L. 2004. Microtubules as a target for anticancer drugs. *Nature Reviews Cancer*, 4, 253-265.

JUNTILA, T. T., LI, G., PARSONS, K., PHILLIPS, G. L. & SLIWKOWSKI, M. X. 2011. Trastuzumab-DM1 (T-DM1) retains all the mechanisms of action of trastuzumab and efficiently inhibits growth of lapatinib insensitive breast cancer. *Breast Cancer Research and Treatment*, 128, 347-356.

KAESER, M. D., PEBERNARD, S. & IGGO, R. D. 2004. Regulation of p53 Stability and Function in HCT116 Colon Cancer Cells*. *Journal of Biological Chemistry*, 279, 7598-7605.

KAINA, B., CHRISTMANN, M., NAUMANN, S. & ROOS, W. P. 2007. MGMT: Key node in the battle against genotoxicity, carcinogenicity and apoptosis induced by alkylating agents. *DNA Repair*, 6, 1079-1099.

KANEKO, K. J., GELINAS, C. & GORSKI, J. 1993. Activation of the silent progesterone receptor gene by ectopic expression of estrogen receptors in a rat fibroblast cell line. *Biochemistry*, 32, 8348-8359.

KARANJIA, R. N., CROSSEY, M. M., COX, I. J., FYE, H. K., NJIE, R., GOLDIN, R. D. & TAYLOR-ROBINSON, S. D. 2016. Hepatic steatosis and fibrosis: Non-invasive assessment. *World J Gastroenterol*, 22, 9880-9897.

KCIUK, M., GIELECÍŃSKA, A., MUJWAR, S., KOŁAT, D., KAŁUZIŃSKA-KOŁAT, Ź., CELIK, I. & KONTEK, R. 2023. Doxorubicin—An Agent with Multiple Mechanisms of Anticancer Activity. *Cells*, 12, 659.

- KEATING, G. M. 2012. Pertuzumab. *Drugs*, 72, 353-360.
- KERBER, V. A., GREGIANINI, T. S., PARANHOS, J. T., SCHWAMBACH, J., FARIAS, F., FETT, J. P., FETT-NETO, A. G., ZUANAZZI, J. A. S., QUIRION, J.-C. & ELIZABETSKY, E. 2001. Brachycerine, a Novel Monoterpene Indole Alkaloid from *Psychotria brachyceras*. *Journal of Natural Products*, 64, 677-679.
- KERR, J. F., WYLLIE, A. H. & CURRIE, A. R. 1972. Apoptosis: a basic biological phenomenon with wide-ranging implications in tissue kinetics. *Br J Cancer*, 26, 239-57.
- KIM, J., LEE, H. M., CAI, F., KO, B., YANG, C., LIEU, E. L., MUHAMMAD, N., RHYNE, S., LI, K., HALOUL, M., GU, W., FAUBERT, B., KAUSHIK, A. K., CAI, L., KASIRI, S., MARRIAM, U., NHAM, K., GIRARD, L., WANG, H., SUN, X., KIM, J., MINNA, J. D., UNSAL-KACMAZ, K. & DEBERARDINIS, R. J. 2020. The hexosamine biosynthesis pathway is a targetable liability in KRAS/LKB1 mutant lung cancer. *Nature Metabolism*, 2, 1401-1412.
- KITAJIMA, M., MORI, I., ARAI, K., KOGURE, N. & TAKAYAMA, H. 2006. Two new tryptamine-derived alkaloids from *Chimonanthus praecox* f. *concolor*. *Tetrahedron Letters*, 47, 3199-3202.
- KLEIHUES, P., LOUIS, D. N., SCHEITHAUER, B. W., RORKE, L. B., REIFENBERGER, G., BURGER, P. C. & CAVENEE, W. K. 2002. The WHO Classification of Tumors of the Nervous System. *Journal of Neuropathology & Experimental Neurology*, 61, 215-225.
- KLEIN-Júnior, L. C., CRETTON, S., VANDER HEYDEN, Y., GASPER, A. L., NEJAD-EBRAHIMI, S., CHRISTEN, P. & HENRIQUES, A. T. 2020a. Bioactive azepine-indole alkaloids from *Psychotria nemorosa*. *Journal of natural products*, 83, 852-863.
- KLEIN-Júnior, L. C., CRETTON, S., VANDER HEYDEN, Y., GASPER, A. L., NEJAD-EBRAHIMI, S., CHRISTEN, P. & HENRIQUES, A. T. 2020b. Bioactive Azepine-Indole Alkaloids from *Psychotria nemorosa*. *J Nat Prod*, 83, 852-863.
- KNOPE, P., PACHECO-TORRES, J., ZIZMARE, L., MORI, N., WILDES, F., ZHOU, B., KRISHNAMACHARY, B., MIRONCHIK, Y., KNEILLING, M., TRAUTWEIN, C., PICHLER, B. J. & BHUJWALLA, Z. M. 2024. Metabolic fingerprinting by nuclear magnetic resonance of hepatocellular carcinoma cells during p53 reactivation-induced senescence. *NMR in Biomedicine*, 37, e5157.

KO, A. H. 2016. Nanomedicine developments in the treatment of metastatic pancreatic cancer: focus on nanoliposomal irinotecan. *International journal of nanomedicine*, 1225-1235.

KO, Y. H., SMITH, B. L., WANG, Y., POMPER, M. G., RINI, D. A., TORBENSON, M. S., HULLIHEN, J. & PEDERSEN, P. L. 2004. Advanced cancers: eradication in all cases using 3-bromopyruvate therapy to deplete ATP. *Biochemical and Biophysical Research Communications*, 324, 269-275.

KOOMOA, D. L., GEERTS, D., LANGE, I., KOSTER, J., PEGG, A. E., FEITH, D. J. & BACHMANN, A. S. 2013. DFMO/eflornithine inhibits migration and invasion downstream of MYCN and involves p27Kip1 activity in neuroblastoma. *Int J Oncol*, 42, 1219-28.

KOOPMAN, G., REUTELINGSPERGER, C., KUIJTEN, G., KEEHNEN, R. M. J., PALS, S. T. & OERS, M. H. J. 1994. Koopman G, Reutelinsperger CP, Kuijten GAM, Keehnen RMJ, Pals ST, van Oers MHJAnnexin V for flow cytometric detection of phosphatidylserine expression on B cell undergoing apoptosis. *Blood* 84: 1415-1420. *Blood*, 84, 1415-20.

KRISTENSEN, C. A., ASKENASY, N., JAIN, R. K. & KORETSKY, A. P. 1999. Creatine and cyclocreatine treatment of human colon adenocarcinoma xenografts: ³¹P and ¹H magnetic resonance spectroscopic studies. *British Journal of Cancer*, 79, 278-285.

KRUGER, N. J. & VON SCHAEWEN, A. 2003. The oxidative pentose phosphate pathway: structure and organisation. *Current Opinion in Plant Biology*, 6, 236-246.

KUDELKA, M. R., JU, T., HEIMBURG-MOLINARO, J. & CUMMINGS, R. D. 2015. Simple sugars to complex disease—mucin-type O-glycans in cancer. *Advances in cancer research*, 126, 53-135.

KUMAR A, G. V., SHARMA S. DONEPEZIL. *Donepezil* [Online]. In: StatPearls [Internet]. Treasure Island (FL): StatPearls Publishing. Available: <https://www.ncbi.nlm.nih.gov/books/NBK513257/> [Accessed 2025].

KUO, L. J. & YANG, L. X. 2008. Gamma-H2AX - a novel biomarker for DNA double-strand breaks. *In Vivo*, 22, 305-9.

KUPCHAN, S. M., KOMODA, Y., BRANFMAN, A. R., SNEDEN, A. T., COURT, W. A., THOMAS, G. J., HINTZ, H. P. J., SMITH, R. M. & KARIM, A. 1977. Tumor inhibitors. 122. The maytansinoids. Isolation, structural elucidation, and chemical interrelation of novel ansa macrolides. *The Journal of Organic Chemistry*, 42, 2349-2357.

- KURMI, K., HITOSUGI, S., YU, J., BOAKYE-AGYEMAN, F., WIESE, E. K., LARSON, T. R., DAI, Q., MACHIDA, Y. J., LOU, Z. & WANG, L. 2018. Tyrosine phosphorylation of mitochondrial creatine kinase 1 enhances a druggable tumor energy shuttle pathway. *Cell metabolism*, 28, 833-847. e8.
- KUZNETSOV, G., TOWLE, M. J., CHENG, H., KAWAMURA, T., TENDYKE, K., LIU, D., KISHI, Y., YU, M. J. & LITTLEFIELD, B. A. 2004. Induction of Morphological and Biochemical Apoptosis following Prolonged Mitotic Blockage by Halichondrin B Macrocyclic Ketone Analog E7389. *Cancer Research*, 64, 5760-5766.
- KVALHEIM, O. M., BRAKSTAD, F. & LIANG, Y. 1994. Preprocessing of analytical profiles in the presence of homoscedastic or heteroscedastic noise. *Analytical Chemistry*, 66, 43-51.
- KWIATKOWSKA, A., NANDHU, M. S., BEHERA, P., CHIOCCA, E. A. & VIAPIANO, M. S. 2013. Strategies in Gene Therapy for Glioblastoma. *Cancers*, 5, 1271-1305.
- L. ERIKSSON, T. B., E. JOHANSSON, J. TRYGG, C. VIKSTRÖM 2013. *Multi- and Megavariate Data Analysis Basic Principles and Applications, Volume I*, Umetrics Academy, 2013.
- LADEP, N. G., DONA, A. C., LEWIS, M. R., CROSSEY, M. M., LEMOINE, M., OKEKE, E., SHIMAKAWA, Y., DUGURU, M., NJAI, H. F. & FYE, H. K. 2014. Discovery and validation of urinary metabotypes for the diagnosis of hepatocellular carcinoma in West Africans. *Hepatology*, 60, 1291-1301.
- LAJIS, N. H., MAHMUD, Z. & TOIA, R. F. 1993. The Alkaloids of *Psychotria rostrata*. *Planta Med*, 59, 383-4.
- LANGE, P. S., LANGLEY, B., LU, P. & RATAN, R. R. 2004. Novel Roles for Arginase in Cell Survival, Regeneration, and Translation in the Central Nervous System. *The Journal of Nutrition*, 134, 2812S-2817S.
- LASTWIKA, K. J., WILSON III, W., LI, Q. K., NORRIS, J., XU, H., GHAZARIAN, S. R., KITAGAWA, H., KAWABATA, S., TAUBE, J. M. & YAO, S. 2016. Control of PD-L1 expression by oncogenic activation of the AKT–mTOR pathway in non–small cell lung cancer. *Cancer research*, 76, 227-238.
- LAVRIK, I., GOLKS, A. & KRAMMER, P. H. 2005. Death receptor signaling. *Journal of Cell Science*, 118, 265-267.

- LÉCUYER, L., VICTOR BALA, A., DESCHASAU, M., BOUCHEMAL, N., NAWFAL TRIBA, M., VASSON, M.-P., ROSSARY, A., DEMIDEM, A., GALAN, P., HERCBERG, S., PARTULA, V., LE MOYEC, L., SROUR, B., FIOLET, T., LATINO-MARTEL, P., KESSE-GUYOT, E., SAVARIN, P. & TOUVIER, M. 2018. NMR metabolomic signatures reveal predictive plasma metabolites associated with long-term risk of developing breast cancer. *International Journal of Epidemiology*, 47, 484-494.
- LEE, A. T. C., AZIMAHTOL, H. L. P. & TAN, A. N. 2003. Styrylpyrone Derivative (SPD) induces apoptosis in a caspase-7-dependent manner in the human breast cancer cell line MCF-7. *Cancer Cell International*, 3, 16.
- LEE, J. S., SUL, J. Y., PARK, J. B., LEE, M. S., CHA, E. Y. & KO, Y. B. 2019. Honokiol induces apoptosis and suppresses migration and invasion of ovarian carcinoma cells via AMPK/mTOR signaling pathway. *Int J Mol Med*, 43, 1969-1978.
- LEE, K. J., MANN, E., WRIGHT, G., PIETT, C. G., NAGEL, Z. D. & GASSMAN, N. R. 2020. Exploiting DNA repair defects in triple negative breast cancer to improve cell killing. *Therapeutic Advances in Medical Oncology*, 12, 1758835920958354.
- LEVENSON, A. S. & JORDAN, V. C. 1997. MCF-7: the first hormone-responsive breast cancer cell line. *Cancer Res*, 57, 3071-8.
- LEVINE, B. & YUAN, J. 2005. Autophagy in cell death: an innocent convict? *J Clin Invest*, 115, 2679-88.
- LEWIS PHILLIPS, G. D., LI, G., DUGGER, D. L., CROCKER, L. M., PARSONS, K. L., MAI, E., BLÄTTLER, W. A., LAMBERT, J. M., CHARI, R. V. J., LUTZ, R. J., WONG, W. L. T., JACOBSON, F. S., KOEPPEN, H., SCHWALL, R. H., KENKARE-MITRA, S. R., SPENCER, S. D. & SLIWKOWSKI, M. X. 2008. Targeting HER2-Positive Breast Cancer with Trastuzumab-DM1, an Antibody–Cytotoxic Drug Conjugate. *Cancer Research*, 68, 9280-9290.
- LI, B. & YANG, L. 2021. Creatine in T Cell Antitumor Immunity and Cancer Immunotherapy. *Nutrients*, 13, 1633.
- LI, S.-F., ZHANG, Y., LI, Y., LI, X.-R., KONG, L.-M., TAN, C.-J., LI, S.-L., DI, Y.-T., HE, H.-P. & HAO, X.-J. 2012. β -Carboline alkaloids from the leaves of *Trigonostemon liliifolius* YT Chang. *Bioorganic & medicinal chemistry letters*, 22, 2296-2299.

- LI, W., YUAN, H., LIU, Y., WANG, B., XU, X., XU, X., HUSSAIN, D., MA, L. & CHEN, D. 2024. Current analytical strategies for the determination of resveratrol in foods. *Food Chemistry*, 431, 137182.
- LI, X., WU, C., CHEN, N., GU, H., YEN, A., CAO, L., WANG, E. & WANG, L. 2016. PI3K/Akt/mTOR signaling pathway and targeted therapy for glioblastoma. *Oncotarget*, 7, 33440-50.
- LIBOT, F., MIET, C., KUNESCH, N., POISSON, J. E., PUSSET, J. & SéVENET, T. 1987. Rubiacées d'Océanie: Alcaloïdes de Psychotria oleoides de Nouvelle-Calédonie et de Calycodendron milnei du Vanuatu (Nouvelles-Hébrides). *Journal of Natural Products*, 50, 468-473.
- LIM, M., XIA, Y., BETTEGOWDA, C. & WELLER, M. 2018. Current state of immunotherapy for glioblastoma. *Nature Reviews Clinical Oncology*, 15, 422-442.
- LIMA, A. R., CARVALHO, M., AVEIRO, S. S., MELO, T., DOMINGUES, M. R., MACEDO-SILVA, C., COIMBRA, N., JERÓNIMO, C., HENRIQUE, R., BASTOS, M. D. L., GUEDES DE PINHO, P. & PINTO, J. 2022. Comprehensive Metabolomics and Lipidomics Profiling of Prostate Cancer Tissue Reveals Metabolic Dysregulations Associated with Disease Development. *Journal of Proteome Research*, 21, 727-739.
- LIND, D. S. 2004. Arginine and Cancer. *The Journal of Nutrition*, 134, 2837S-2841S.
- LIU, J., LUO, X., GUO, R., JING, W. & LU, H. 2020a. Cell Metabolomics Reveals Berberine-Inhibited Pancreatic Cancer Cell Viability and Metastasis by Regulating Citrate Metabolism. *Journal of Proteome Research*, 19, 3825-3836.
- LIU, L., HE, Y., GE, G., LI, L., ZHOU, P., ZHU, Y., TANG, H., HUANG, Y., LI, W. & ZHANG, L. 2017a. Lactate dehydrogenase and creatine kinase as poor prognostic factors in lung cancer: A retrospective observational study. *PLoS One*, 12, e0182168.
- LIU, R., LI, P., BI, C. W., MA, R., YIN, Y., BI, K. & LI, Q. 2017b. Plasma N-acetylputrescine, cadaverine and 1,3-diaminopropane: potential biomarkers of lung cancer used to evaluate the efficacy of anticancer drugs. *Oncotarget*, 8, 88575-88585.
- LIU, R., LIN, X., LI, Z., LI, Q. & BI, K. 2018. Quantitative metabolomics for investigating the value of polyamines in the early diagnosis and therapy of colorectal cancer. *Oncotarget*, 9, 4583-4592.

- LIU, R., ZHU, L.-L., YU, C.-Y., SHUAI, Y.-P., SUN, L.-L., BI, K.-S. & LI, Q. 2021. Quantitative Evaluation of the Compatibility Effects of Aidi Injection on the Treatment of Hepatocellular Carcinoma Using Targeted Metabolomics: A New Strategy on the Mechanism Study of an Anticancer Compound in Traditional Chinese Medicine. *World Journal of Traditional Chinese Medicine*, 7.
- LIU, T., TAN, Z., YU, J., PENG, F., GUO, J., MENG, W., CHEN, Y., RAO, T., LIU, Z. & PENG, J. 2020b. A conjunctive lipidomic approach reveals plasma ethanolamine plasmalogens and fatty acids as early diagnostic biomarkers for colorectal cancer patients. *Expert Review of Proteomics*, 17, 233-242.
- LOMOVSKAYA, N., OTTEN SHAREE, L., DOI-KATAYAMA, Y., FONSTEIN, L., LIU, X.-C., TAKATSU, T., INVENTI-SOLARI, A., FILIPPINI, S., TORTI, F., COLOMBO ANNA, L. & HUTCHINSON, C. R. 1999. Doxorubicin Overproduction in *Streptomyces peucetius*: Cloning and Characterization of the *dnrU* Ketoreductase and *dnrV* Genes and the *doxA* Cytochrome P-450 Hydroxylase Gene. *Journal of Bacteriology*, 181, 305-318.
- LOSMAN, J.-A. & KAE LIN, W. G. 2013. What a difference a hydroxyl makes: mutant IDH,(R)-2-hydroxyglutarate, and cancer. *Genes & development*, 27, 836-852.
- LOSMAN, J.-A., LOOPER, R. E., KOIVUNEN, P., LEE, S., SCHNEIDER, R. K., MCMAHON, C., COWLEY, G. S., ROOT, D. E., EBERT, B. L. & KAE LIN, W. G. 2013. (R)-2-Hydroxyglutarate Is Sufficient to Promote Leukemogenesis and Its Effects Are Reversible. *Science*, 339, 1621-1625.
- LOUIS, D. N., PERRY, A., WESSELING, P., BRAT, D. J., CREE, I. A., FIGARELLA-BRANGER, D., HAWKINS, C., NG, H. K., PFISTER, S. M., REIFENBERGER, G., SOFFIETTI, R., VON DEIMLING, A. & ELLISON, D. W. 2021. The 2021 WHO Classification of Tumors of the Central Nervous System: a summary. *Neuro-Oncology*, 23, 1231-1251.
- LU, J., LI, Y., LI, Y. A., WANG, L., ZENG, A. R., MA, X. L. & QIANG, J. W. 2022. In vivo detection of dysregulated choline metabolism in paclitaxel-resistant ovarian cancers with proton magnetic resonance spectroscopy. *Journal of Translational Medicine*, 20, 92.
- LU, S. C. 2013. Glutathione synthesis. *Biochimica et Biophysica Acta (BBA) - General Subjects*, 1830, 3143-3153.

- LUCARELLI, G., GALLEGGIANTE, V., RUTIGLIANO, M., SANGUEDOLCE, F., CAGIANO, S., BUFO, P., LASTILLA, G., MAIORANO, E., RIBATTI, D., GIGLIO, A., SERINO, G., VAVALLO, A., BETTOCCHI, C., SELVAGGI, F. P., BATTAGLIA, M. & DITONNO, P. 2015. Metabolomic profile of glycolysis and the pentose phosphate pathway identifies the central role of glucose-6-phosphate dehydrogenase in clear cell-renal cell carcinoma. *Oncotarget*, 6, 13371-86.
- LUCILIA, K., OLIVEIRA, C., FARIA, E. O., RIBEIRO, L. C., CARVALHO, B. G., SILVA, C. C. D., SCHUQUEL, I. T., SANTIN, S. M., NAKAMURA, C. V. & BRITTA, E. A. 2012. Antiprotozoal alkaloids from *Psychotria prunifolia* (Kunth) Steyerl. *Journal of the Brazilian Chemical Society*, 23, 355-360.
- LUENGO, A., LI, Z., GUI, D. Y., SULLIVAN, L. B., ZAGORULYA, M., DO, B. T., FERREIRA, R., NAAMATI, A., ALI, A., LEWIS, C. A., THOMAS, C. J., SPRANGER, S., MATHESON, N. J. & VANDER HEIDEN, M. G. 2021. Increased demand for NAD⁺ relative to ATP drives aerobic glycolysis. *Molecular Cell*, 81, 691-707.e6.
- LÜPERTZ, R., WÄTJEN, W., KAHL, R. & CHOVOLOU, Y. 2010. Dose- and time-dependent effects of doxorubicin on cytotoxicity, cell cycle and apoptotic cell death in human colon cancer cells. *Toxicology*, 271, 115-121.
- LÜTHI, A. U. & MARTIN, S. J. 2007. The CASBAH: a searchable database of caspase substrates. *Cell Death & Differentiation*, 14, 641-650.
- LV, J., JIA, H., MO, M., YUAN, J., WU, Z., ZHANG, S., ZHE, F., GU, B., FAN, B., LI, C., ZHANG, T. & ZHU, J. 2022. Changes of serum metabolites levels during neoadjuvant chemoradiation and prediction of the pathological response in locally advanced rectal cancer. *Metabolomics*, 18, 99.
- LYNCH, H. T. & LYNCH, J. F. Hereditary nonpolyposis colorectal cancer. *Seminars in Surgical Oncology*, 2000. Wiley Online Library, 305-313.
- MA, C., LI, Y., WU, H., JI, J., SUN, Q., SONG, Y., WANG, S., LI, X., CHEN, Y. & CHEN, J. 2018. Metabolomics analysis of the potential anticancer mechanism of annonaceous acetogenins on a multidrug resistant mammary adenocarcinoma cell. *Analytical Biochemistry*, 553, 1-6.

- MA, O. B. & R, K. 2008. - Apoptosis: A review of pro-apoptotic and anti-apoptotic pathways and. *J Vet Emerg Crit Care*, 18, 572-85.
- MACDONALD, B. T., TAMAI, K. & HE, X. 2009. Wnt/β-Catenin Signaling: Components, Mechanisms, and Diseases. *Developmental Cell*, 17, 9-26.
- MAGUIRE, O. A., ACKERMAN, S. E., SZWED, S. K., MAGANTI, A. V., MARCHILDON, F., HUANG, X., KRAMER, D. J., ROSAS-VILLEGAS, A., GELFER, R. G., TURNER, L. E., CEBALLOS, V., HEJAZI, A., SAMBORSKA, B., RAHBANI, J. F., DYKSTRA, C. B., ANNIS, M. G., LUO, J.-D., CARROLL, T. S., JIANG, C. S., DANNENBERG, A. J., SIEGEL, P. M., TERSEY, S. A., MIRMIRA, R. G., KAZAK, L. & COHEN, P. 2021. Creatine-mediated crosstalk between adipocytes and cancer cells regulates obesity-driven breast cancer. *Cell Metabolism*, 33, 499-512.e6.
- MAHMUD, Z. 1989. *CHEMOTAXONOMIC STUDIES ON PSYCHOTRIA ROSTRATA AND ALSEODAPHNE PERAKENSIS* master, Universiti Pertanian Malaysia.
- MAHMUD, Z., MUSA, M., ISMAIL, N. & LAJIS, N. H. 1993. Cytotoxic and bacteriocidal activities of Psychotria rostrata. *International journal of pharmacognosy*, 31, 142-146.
- MANFREDI, J. J. & HORWITZ, S. B. 1984. Taxol: an antimetabolic agent with a new mechanism of action. *Pharmacology & Therapeutics*, 25, 83-125.
- MARCHAN, R., LESJAK, M. S., STEWART, J. D., WINTER, R., SEELIGER, J. & HENGSTLER, J. G. 2012. Choline-releasing glycerophosphodiesterase EDI3 links the tumor metabolome to signaling network activities. *Cell Cycle*, 11, 4499-4506.
- MARKMAN, M. 2003. Managing taxane toxicities. *Supportive care in cancer*, 11, 144-147.
- MARTÍNEZ, M. T., PÉREZ-FIDALGO, J. A., MARTÍN-MARTORELL, P., CEJALVO, J. M., PONS, V., BERMEJO, B., MARTÍN, M., ALBANELL, J. & LLUCH, A. 2016. Treatment of HER2 positive advanced breast cancer with T-DM1: A review of the literature. *Critical Reviews in Oncology/Hematology*, 97, 96-106.
- MATHUPALA, S. P., KO, Y. H. & PEDERSEN, P. L. 2009. Hexokinase-2 bound to mitochondria: Cancer's stygian link to the “Warburg effect” and a pivotal target for effective therapy. *Seminars in Cancer Biology*, 19, 17-24.
- MCGROGAN, B. T., GILMARTIN, B., CARNEY, D. N. & MCCANN, A. 2008. Taxanes, microtubules and chemoresistant breast cancer. *Biochim Biophys Acta*, 1785, 96-132.

- MCKENNA, D. J., TOWERS, G. N. & ABBOTT, F. 1984. Monoamine oxidase inhibitors in South American hallucinogenic plants: tryptamine and β -carboline constituents of ayahuasca. *Journal of ethnopharmacology*, 10, 195-223.
- MCQUEEN, E., DOYLE, A. & SMIRK, F. 1954. Mechanism of hypotensive action of reserpine, an alkaloid of *Rauwolfia serpentina*. *Nature*, 174, 1015-1015.
- MEI, L.-H., GAN, H.-H., WANG, H.-F., XU, G., YE, X.-G. & YANG, G. 2024. Lipidomics revealed alterations in glycerophospholipid metabolism in skin squamous cell carcinoma. *Frontiers in Molecular Biosciences*, 11.
- MIKKOLA, S. 2020. Nucleotide Sugars in Chemistry and Biology. *Molecules*, 25, 5755.
- MILANO, G., INNOCENTI, F. & MINAMI, H. 2022. Liposomal irinotecan (Onivyde): Exemplifying the benefits of nanotherapeutic drugs. *Cancer Science*, 113, 2224-2231.
- MILLER, E. E., EVANS, A. E. & COHN, M. 1993. Inhibition of rate of tumor growth by creatine and cyclocreatine. *Proceedings of the National Academy of Sciences*, 90, 3304-3308.
- MITTAL, L., ARYAL, U. K., CAMARILLO, I. G., RAMAN, V. & SUNDARARAJAN, R. 2020. Effective electrochemotherapy with curcumin in MDA-MB-231-human, triple negative breast cancer cells: A global proteomics study. *Bioelectrochemistry*, 131, 107350.
- MIYASHITA, T. & REED, J. C. 1995. Tumor suppressor p53 is a direct transcriptional activator of the human bax gene. *Cell*, 80, 293-9.
- MOHAMMED, H., RUSSELL, I. A., STARK, R., RUEDA, O. M., HICKEY, T. E., TARULLI, G. A., SERANDOUR, A. A., BIRRELL, S. N., BRUNA, A., SAADI, A., MENON, S., HADFIELD, J., PUGH, M., RAJ, G. V., BROWN, G. D., D'SANTOS, C., ROBINSON, J. L. L., SILVA, G., LAUNCHBURY, R., PEROU, C. M., STINGL, J., CALDAS, C., TILLEY, W. D. & CARROLL, J. S. 2015. Progesterone receptor modulates ER α action in breast cancer. *Nature*, 523, 313-317.
- MONTALVO, R. N., DOERR, V., MIN, K., SZETO, H. H. & SMUDER, A. J. 2020. Doxorubicin-induced oxidative stress differentially regulates proteolytic signaling in cardiac and skeletal muscle. *American Journal of Physiology-Regulatory, Integrative and Comparative Physiology*, 318, R227-R233.
- MONTERO, A. J. & JASSEM, J. 2011. Cellular Redox Pathways as a Therapeutic Target in the Treatment of Cancer. *Drugs*, 71, 1385-1396.

MORIKAWA, T., NAKANISHI, Y., NINOMIYA, K., MATSUDA, H., NAKASHIMA, S., MIKI, H., MIYASHITA, Y., YOSHIKAWA, M., HAYAKAWA, T. & MURAOKA, O. 2014. Dimeric pyrrolidinoindoline-type alkaloids with melanogenesis inhibitory activity in flower buds of *Chimonanthus praecox*. *Journal of natural medicines*, 68, 539-549.

MOSMANN, T. 1983. Rapid colorimetric assay for cellular growth and survival: Application to proliferation and cytotoxicity assays. *Journal of Immunological Methods*, 65, 55-63.

MURRAY-STEWART, T. R., WOSTER, P. M. & CASERO, R. A., JR 2016. Targeting polyamine metabolism for cancer therapy and prevention. *Biochemical Journal*, 473, 2937-2953.

MYBIS. *Psychotria montana* [Online]. Malaysia Biodiversity Information System (MyBIS) by Malaysia Biodiversity Centre (MBC). Available: <https://www.mybis.gov.my/sp/29387> [Accessed].

MYBIS. *Psychotria rostrata* [Online]. Malaysia Biodiversity Information System (MyBIS) by Malaysia Biodiversity Centre (MBC). Available: <https://www.mybis.gov.my/sp/43583> [Accessed].

NAGY, J., VASILE, E., FENG, D., SUNDBERG, C., BROWN, L., MANSEAU, E., DVORAK, A. & DVORAK, H. VEGF-A induces angiogenesis, arteriogenesis, lymphangiogenesis, and vascular malformations. Cold Spring Harbor symposia on quantitative biology, 2002. Cold Spring Harbor Laboratory Press, 227-238.

NAJI A, G. J. M. A. *Muscarinic Antagonists* [Online]. In: StatPearls [Internet]. Treasure Island (FL): StatPearls Publishing. Available: <https://www.ncbi.nlm.nih.gov/books/NBK557541/> [Accessed 2025].

NAJJAR, A., OLĞAÇ, A., NTIE-KANG, F. & SIPPL, W. 2019. Fragment-based drug design of nature-inspired compounds. *Physical Sciences Reviews*, 4.

NAKANO, K. & VOUSDEN, K. H. 2001. PUMA, a novel proapoptotic gene, is induced by p53. *Mol Cell*, 7, 683-94.

NAKATA, H., WANG, S.-L., CHUNG, D. C., WESTWICK, J. K. & TILLOTSON, L. G. 1998. Oncogenic ras induces gastrin gene expression in colon cancer. *Gastroenterology*, 115, 1144-1153.

- NAMBIAR, D. K., DEEP, G., SINGH, R. P., AGARWAL, C. & AGARWAL, R. 2014. Silibinin inhibits aberrant lipid metabolism, proliferation and emergence of androgen-independence in prostate cancer cells via primarily targeting the sterol response element binding protein 1. *Oncotarget*, 5, 10017-33.
- NASCIMENTO, R. R. G., PIMENTA, A. T. A., LIMA NETO, P. D., C. JUNIOR, J. R., COSTA-LOTUFO, L. V., FERREIRA, E. G., TINOCO, L. W., BRAZ-FILHO, R., SILVEIRA, E. R. & LIMA, M. A. S. 2015. New Alkaloids from *Margaritopsis carrascoana* (Rubiaceae). *Journal of the Brazilian Chemical Society*, 26.
- NAZEMALHOSSEINI MOJARAD, E., KUPPEN, P. J., AGHDAEI, H. A. & ZALI, M. R. 2013. The CpG island methylator phenotype (CIMP) in colorectal cancer. *Gastroenterol Hepatol Bed Bench*, 6, 120-8.
- NEAMTU, A.-A., MAGHIAR, T.-A., ALAYA, A., OLAH, N.-K., TURCUS, V., PELEA, D., TOTOLICI, B. D., NEAMTU, C., MAGHIAR, A. M. & MATHE, E. 2022. A Comprehensive View on the Quercetin Impact on Colorectal Cancer. *Molecules*, 27, 1873.
- NEWMAN, D. J. & CRAGG, G. M. 2020. Natural Products as Sources of New Drugs over the Nearly Four Decades from 01/1981 to 09/2019. *Journal of Natural Products*, 83, 770-803.
- NEWSHOLME, P., REBELATO, E., ABDULKADER, F., KRAUSE, M., CARPINELLI, A. & CURI, R. 2012. Reactive oxygen and nitrogen species generation, antioxidant defenses, and β -cell function: a critical role for amino acids. *J Endocrinol*, 214, 11-20.
- NG, R., ETHIRAJAN, S., O'NEILL, M. & STATLAND, B. 1987. Increased activities of creatine kinase and lactate dehydrogenase isoenzymes in a patient with metastatic ovarian tumor. *Clinical chemistry*, 33, 1484-1485.
- NICOLETTI, I., MIGLIORATI, G., PAGLIACCI, M. C., GRIGNANI, F. & RICCARDI, C. 1991. A rapid and simple method for measuring thymocyte apoptosis by propidium iodide staining and flow cytometry. *Journal of Immunological Methods*, 139, 271-279.
- NIE, M., CHEN, N., PANG, H., JIANG, T., JIANG, W., TIAN, P., YAO, L., CHEN, Y., DEBERARDINIS, R. J., LI, W., YU, Q., ZHOU, C. & HU, Z. 2022. Targeting acetylcholine signaling modulates persistent drug tolerance in EGFR-mutant lung cancer and impedes tumor relapse. *The Journal of Clinical Investigation*, 132.

- NIEMI, R. J., ROINE, A. N., HäKKINEN, M. R., KUMPULAINEN, P. S., KEINÄNEN, T. A., VEPSÄLÄINEN, J. J., LEHTIMÄKI, T., OKSALA, N. K. & MÄENPÄÄ, J. U. 2017. Urinary polyamines as biomarkers for ovarian cancer. *International Journal of Gynecologic Cancer*, 27.
- NIKITOVIC, D., BERDIKI, A., SPYRIDAKI, I., KRASANAKIS, T., TSATSAKIS, A. & TZANAKAKIS, G. N. 2018. Proteoglycans—biomarkers and targets in cancer therapy. *Frontiers in endocrinology*, 9, 69.
- NITISS, J. & WANG, J. C. 1988. DNA topoisomerase-targeting antitumor drugs can be studied in yeast. *Proceedings of the National Academy of Sciences*, 85, 7501-7505.
- NOGALES, E. 2001. Structural insights into microtubule function. *Annual review of biophysics and biomolecular structure*, 30, 397-420.
- NOGALES, E., GRAYER WOLF, S., KHAN, I. A., LUDUEÑA, R. F. & DOWNING, K. H. 1995. Structure of tubulin at 6.5 Å and location of the taxol-binding site. *Nature*, 375, 424-427.
- NORDEN, A. D., YOUNG, G. S., SETAYESH, K., MUZIKANSKY, A., KLUFAS, R., ROSS, G. L., CIAMPA, A. S., EBBELING, L. G., LEVY, B., DRAPPATZ, J., KESARI, S. & WEN, P. Y. 2008. Bevacizumab for recurrent malignant gliomas. *Neurology*, 70, 779-787.
- NORELDEEN, H. A. A., LIU, X. & XU, G. 2020. Metabolomics of lung cancer: Analytical platforms and their applications. *Journal of Separation Science*, 43, 120-133.
- OCTAVIA, Y., TOCCHETTI, C. G., GABRIELSON, K. L., JANSSENS, S., CRIJNS, H. J. & MOENS, A. L. 2012. Doxorubicin-induced cardiomyopathy: From molecular mechanisms to therapeutic strategies. *Journal of Molecular and Cellular Cardiology*, 52, 1213-1225.
- OH, S. Y., SOHN, Y. W., PARK, J. W., PARK, H. J., JEON, H. M., KIM, T. K., LEE, J. S., JUNG, J. E., JIN, X., CHUNG, Y. G., CHOI, Y. K., YOU, S., LEE, J. B. & KIM, H. 2007. Selective cell death of oncogenic Akt-transduced brain cancer cells by etoposide through reactive oxygen species mediated damage. *Mol Cancer Ther*, 6, 2178-87.
- OKANYA, P. W., MOHR, K. I., GERTH, K., JANSEN, R. & MÜLLER, R. 2011. Marinoquinolines A–F, Pyrroloquinolines from *Ohtaekwangia kribbensis* (Bacteroidetes). *Journal of Natural Products*, 74, 603-608.
- OLIVER, J. A., ORTIZ, R., JIMÉNEZ-LUNA, C., CABEZA, L., PERAZZOLI, G., CABA, O., MESAS, C., MELGUIZO, C. & PRADOS, J. 2020. MMR-proficient and MMR-deficient

colorectal cancer cells: 5-Fluorouracil treatment response and correlation to CD133 and MGMT expression. *Journal of Biosciences*, 45, 121.

ONG, H. C., FAEZAH, A. W. & MILOW, P. 2012. Medicinal Plants Used By the Jah Hut Orang Asli at Kampung Pos Penderas, Pahang, Malaysia. *Studies on Ethno-Medicine*, 6, 11 - 15.

ONITILO, A. A., ENGEL, J. M., GREENLEE, R. T. & MUKESH, B. N. 2009. Breast cancer subtypes based on ER/PR and Her2 expression: comparison of clinicopathologic features and survival. *Clinical medicine & research*, 7, 4-13.

ORGANIZATION, W. H. 2022. *Cancer* [Online]. Available: <https://www.who.int/news-room/fact-sheets/detail/cancer> [Accessed 0707 2022].

OTEGUI, N., HOURY, M., AROZARENA, I., SERRANO, D., REDIN, E., EXPOSITO, F., LEON, S., VALENCIA, K., MONTUENGA, L. & CALVO, A. 2023. Cancer Cell-Intrinsic Alterations Associated with an Immunosuppressive Tumor Microenvironment and Resistance to Immunotherapy in Lung Cancer. *Cancers*, 15, 3076.

OTTAGGIO, L., BESTOSO, F., ARMIROTTI, A., BALBI, A., DAMONTE, G., MAZZEI, M., SANCANDI, M. & MIELE, M. 2008. Taxanes from Shells and Leaves of *Corylus avellana*. *Journal of Natural Products*, 71, 58-60.

PAN, H., XIA, K., ZHOU, W., XUE, J., LIANG, X., CHENG, L., WU, N., LIANG, M., WU, D. & LING, L. 2013. Low serum creatine kinase levels in breast cancer patients: a case-control study. *PLoS One*, 8, e62112.

PAN, X., WILSON, M., MIRBAHAI, L., MCCONVILLE, C., ARVANITIS, T. N., GRIFFIN, J. L., KAUPPINEN, R. A. & PEET, A. C. 2011. In Vitro Metabonomic Study Detects Increases in UDP-GlcNAc and UDP-GalNAc, as Early Phase Markers of Cisplatin Treatment Response in Brain Tumor Cells. *Journal of Proteome Research*, 10, 3493-3500.

PANEQUE, A., FORTUS, H., ZHENG, J., WERLEN, G. & JACINTO, E. 2023. The Hexosamine Biosynthesis Pathway: Regulation and Function. *Genes*, 14, 933.

PANG, Z., CHONG, J., ZHOU, G., DE LIMA MORAIS, D. A., CHANG, L., BARRETTE, M., GAUTHIER, C., JACQUES, P.-É., LI, S. & XIA, J. 2021. MetaboAnalyst 5.0: narrowing the gap between raw spectra and functional insights. *Nucleic Acids Research*, 49, W388-W396.

- PANG, Z., ZHOU, G., EWALD, J., CHANG, L., HACARIZ, O., BASU, N. & XIA, J. 2022. Using MetaboAnalyst 5.0 for LC–HRMS spectra processing, multi-omics integration and covariate adjustment of global metabolomics data. *Nature Protocols*, 17, 1735-1761.
- PARRY, K. P. & SMITH, G. F. 1978. Quadrigemines-A and-B, two minor alkaloids of *Hodgkinsonia frutescens* F. Muell. *Journal of the Chemical Society, Perkin Transactions 1*, 1671-1682.
- PARSONS, D. W., JONES, S., ZHANG, X., LIN, J. C.-H., LEARY, R. J., ANGENENDT, P., MANKOO, P., CARTER, H., SIU, I.-M., GALLIA, G. L., OLIVI, A., MCLENDON, R., RASHEED, B. A., KEIR, S., NIKOLSKAYA, T., NIKOLSKY, Y., BUSAM, D. A., TEKLEAB, H., DIAZ, L. A., HARTIGAN, J., SMITH, D. R., STRAUSBERG, R. L., MARIE, S. K. N., SHINJO, S. M. O., YAN, H., RIGGINS, G. J., BIGNER, D. D., KARCHIN, R., PAPADOPOULOS, N., PARMIGIANI, G., VOGELSTEIN, B., VELCULESCU, V. E. & KINZLER, K. W. 2008. An Integrated Genomic Analysis of Human Glioblastoma Multiforme. *Science*, 321, 1807-1812.
- PASSOS, C. S., SIMões-PIRES, C. A., NURISSO, A., SOLDI, T. C., KATO, L., DE OLIVEIRA, C. M., DE FARIA, E. O., MARCOURT, L., GOTTFRIED, C. & CARRUPT, P.-A. 2013. Indole alkaloids of *Psychotria* as multifunctional cholinesterases and monoamine oxidases inhibitors. *Phytochemistry*, 86, 8-20.
- PATEL, R., FORD, C. A., RODGERS, L., RUSHWORTH, L. K., FLEMING, J., MUI, E., ZHANG, T., WATSON, D., LYNCH, V., MACKAY, G., SUMPTON, D., SANSOM, O. J., VANDE VOORDE, J. & LEUNG, H. Y. 2022. Cyclocreatine Suppresses Creatine Metabolism and Impairs Prostate Cancer Progression. *Cancer Research*, 82, 2565-2575.
- PATRA, K. C. & HAY, N. 2014. The pentose phosphate pathway and cancer. *Trends in Biochemical Sciences*, 39, 347-354.
- PAUL, J., MAXWELL, A. & REYNOLDS, W. 2003. Novel bis (monoterpenoid) indole alkaloids from *Psychotria bahiensis*. *Journal of natural products*, 66, 752-754.
- PAWLOWSKA, E., SZCZEPANSKA, J., SZATKOWSKA, M. & BLASIAK, J. 2018. An Interplay between Senescence, Apoptosis and Autophagy in Glioblastoma Multiforme—Role in Pathogenesis and Therapeutic Perspective. *International Journal of Molecular Sciences*, 19, 889.

- PEDERSEN, A. G., BACH, F. W., NISSEN, M. & BACH, F. 1985. Creatine kinase BB and beta-2-microglobulin as markers of CNS metastases in patients with small-cell lung cancer. *Journal of Clinical Oncology*, 3, 1364-1372.
- PELICANO, H., MARTIN, D., XU, R., AND & HUANG, P. 2006. Glycolysis inhibition for anticancer treatment. *Oncogene*, 25, 4633-4646.
- PIMENTA, A. Á. T., BRAZ-FILHO, R., DELPRETE, P. G., DE SOUZA, E. B., SILVEIRA, E. R. & LIMA, M. A. S. 2010. Unusual monoterpene indole alkaloids from *Psychotria stachyoides* Benth. *Biochemical Systematics and Ecology*, 38, 846-849.
- PIMENTEL, J. M., ZHOU, J. Y. & WU, G. S. 2023. The Role of TRAIL in Apoptosis and Immunosurveillance in Cancer. *Cancers (Basel)*, 15.
- PIRZKALL, A., MCGUE, C., SARASWATHY, S., CHA, S., LIU, R., VANDENBERG, S., LAMBORN, K. R., BERGER, M. S., CHANG, S. M. & NELSON, S. J. 2009. Tumor regrowth between surgery and initiation of adjuvant therapy in patients with newly diagnosed glioblastoma. *Neuro-Oncology*, 11, 842-852.
- POMMIER, Y. 2006. Topoisomerase I inhibitors: camptothecins and beyond. *Nature Reviews Cancer*, 6, 789-802.
- POMMIER, Y. 2013. Drugging Topoisomerases: Lessons and Challenges. *ACS Chemical Biology*, 8, 82-95.
- POMMIER, Y., BARCELO, J. M., RAO, V. A., SORDET, O., JOBSON, A. G., THIBAUT, L., MIAO, Z. H., SEILER, J. A., ZHANG, H., MARCHAND, C., AGAMA, K., NITISS, J. L. & REDON, C. 2006. Repair of topoisomerase I-mediated DNA damage. *Prog Nucleic Acid Res Mol Biol*, 81, 179-229.
- POMMIER, Y., LEO, E., ZHANG, H. & MARCHAND, C. 2010. DNA Topoisomerases and Their Poisoning by Anticancer and Antibacterial Drugs. *Chemistry & Biology*, 17, 421-433.
- POMMIER, Y., POURQUIER, P., URASAKI, Y., WU, J. & LACO, G. S. 1999. Topoisomerase I inhibitors: selectivity and cellular resistance. *Drug Resistance Updates*, 2, 307-318.
- POMMIER, Y., REDON, C., RAO, V. A., SEILER, J. A., SORDET, O., TAKEMURA, H., ANTONY, S., MENG, L., LIAO, Z., KOHLHAGEN, G., ZHANG, H. & KOHN, K. W. 2003. Repair of and checkpoint response to topoisomerase I-mediated DNA damage. *Mutation Research/Fundamental and Molecular Mechanisms of Mutagenesis*, 532, 173-203.

POPOVICI-MULLER, J., SAUNDERS, J. O., SALITURO, F. G., TRAVINS, J. M., YAN, S., ZHAO, F., GROSS, S., DANG, L., YEN, K. E., YANG, H., STRALEY, K. S., JIN, S., KUNII, K., FANTIN, V. R., ZHANG, S., PAN, Q., SHI, D., BILLER, S. A. & SU, S. M. 2012. Discovery of the First Potent Inhibitors of Mutant IDH1 That Lower Tumor 2-HG in Vivo. *ACS Medicinal Chemistry Letters*, 3, 850-855.

PRYOR, D. E., O'BRATE, A., BILCER, G., DÍAZ, J. F., WANG, Y., WANG, Y., KABAKI, M., JUNG, M. K., ANDREU, J. M. & GHOSH, A. K. 2002. The microtubule stabilizing agent laulimalide does not bind in the taxoid site, kills cells resistant to paclitaxel and epothilones, and may not require its epoxide moiety for activity. *Biochemistry*, 41, 9109-9115.

QAZZAZ, M. E., RAJA, V. J., LIM, K. H., KAM, T. S., LEE, J. B., GERSHKOVICH, P. & BRADSHAW, T. D. 2016. In vitro anticancer properties and biological evaluation of novel natural alkaloid jerantinine B. *Cancer Lett*, 370, 185-97.

QUASTHOFF, S. & HARTUNG, H. P. 2002. Chemotherapy-induced peripheral neuropathy. *Journal of neurology*, 249, 9-17.

RA, Y.-M., YIM, J.-S., SONG, K.-H., KO, D.-G., CHOI, I.-S., CHOI, W.-J. & YOON, D.-S. 2007. The Effects of Genistein to Expression of Fatty Acid Synthase in Breast Cancer Cells. *jbc*, 10, 127-133.

RAJENDRAN, R., GARVA, R., KRSTIC-DEMONACOS, M. & DEMONACOS, C. 2011. Sirtuins: molecular traffic lights in the crossroad of oxidative stress, chromatin remodeling, and transcription. *J Biomed Biotechnol*, 2011, 368276.

RAPPORT, M. M., GREEN, A. A. & PAGE, I. H. 1948. Crystalline Serotonin. *Science*, 108, 329-330.

RASTI, M. & AZIMI, T. 2015. TP53 Binding to BRCA1 and RAD51 in MCF7 and MDA-MB-468 Breast Cancer Cell Lines In vivo and In vitro. *Avicenna J Med Biotechnol*, 7, 76-9.

RAUL, F. 2007. Revival of 2-(difluoromethyl)ornithine (DFMO), an inhibitor of polyamine biosynthesis, as a cancer chemopreventive agent¹. *Biochemical Society Transactions*, 35, 353-355.

RAVEENDRAN NAIR, P. K., RODRIGUEZ, S., RAMACHANDRAN, R., ALAMO, A., MELNICK, S. J., ESCALON, E., GARCIA, P. I., WNUK, S. F. & RAMACHANDRAN, C.

2004. Immune stimulating properties of a novel polysaccharide from the medicinal plant *Tinospora cordifolia*. *International Immunopharmacology*, 4, 1645-1659.
- RAVIZZA, R., GARIBOLDI, M. B., PASSARELLI, L. & MONTI, E. 2004. Role of the p53/p21 system in the response of human colon carcinoma cells to Doxorubicin. *BMC Cancer*, 4, 92.
- RECK, M., MOK, T. S., NISHIO, M., JOTTE, R. M., CAPPUZZO, F., ORLANDI, F., STROYAKOVSKIY, D., NOGAMI, N., RODRÍGUEZ-ABREU, D. & MORO-SIBILOT, D. 2019. Atezolizumab plus bevacizumab and chemotherapy in non-small-cell lung cancer (IMpower150): key subgroup analyses of patients with EGFR mutations or baseline liver metastases in a randomised, open-label phase 3 trial. *The Lancet Respiratory Medicine*, 7, 387-401.
- RECK, M., RODRÍGUEZ-ABREU, D., ROBINSON, A. G., HUI, R., CSÖSZI, T., FÜLÖP, A., GOTTFRIED, M., PELED, N., TAFRESHI, A. & CUFFE, S. 2016. Pembrolizumab versus chemotherapy for PD-L1-positive non-small-cell lung cancer. *New England Journal of Medicine*, 375, 1823-1833.
- ŘEHÁČEK, Z. & SAJDL, P. 1990. *Ergot Alkaloids: Chemistry, Biological Effects, Biotechnology*, Elsevier.
- REITZER, L. J., BM, W. & KENNEL, D. 1979. Evidence that glutamine, not sugar, is the major energy source for cultured HeLa cells.
- REN, H., SHI, C. & ZHAO, H. 2020. Computational Tools for Discovering and Engineering Natural Product Biosynthetic Pathways. *iScience*, 23.
- RHEE, S. G. 2006. H₂O₂, a Necessary Evil for Cell Signaling. *Science*, 312, 1882-1883.
- RIGANTI, C., GAZZANO, E., POLIMENI, M., ALDIERI, E. & GHIGO, D. 2012. The pentose phosphate pathway: An antioxidant defense and a crossroad in tumor cell fate. *Free Radical Biology and Medicine*, 53, 421-436.
- RIVIER, L. & LINDGREN, J.-E. 1972. "Ayahuasca," the South American hallucinogenic drink: An ethnobotanical and chemical investigation. *Economic Botany*, 26, 101-129.
- ROBINSON, M. J., CORBETT, A. H. & OSHEROFF, N. 1993. Effects of topoisomerase II-targeted drugs on enzyme-mediated DNA cleavage and ATP hydrolysis: evidence for distinct drug interaction domains on topoisomerase II. *Biochemistry*, 32, 3638-3643.

- RODAK, O., PERIS-DÍAZ, M. D., OLBROMSKI, M., PODHORSKA-OKOŁÓW, M. & DZIĘGIEL, P. 2021. Current Landscape of Non-Small Cell Lung Cancer: Epidemiology, Histological Classification, Targeted Therapies, and Immunotherapy. *Cancers*, 13, 4705.
- ROTH, A., KUBALLA, B., BOUNTHANH, C., CABALION, P., SÉVENET, T., BECK, J. P. & ANTON, R. 1986. Cytotoxic activity of polyindoline alkaloids of *Psychotria forsteriana* (Rubiaceae) (1). *Planta Med*, 450-3.
- ROTHER, C., JOHN, T. & WONG, A. 2024. Biomarkers for immunotherapy resistance in non-small cell lung cancer. *Front Oncol*, 14, 1489977.
- RUTLEDGE, P. J. & CHALLIS, G. L. 2015. Discovery of microbial natural products by activation of silent biosynthetic gene clusters. *Nature Reviews Microbiology*, 13, 509-523.
- RYCZKO, M. C., PAWLING, J., CHEN, R., ABDEL RAHMAN, A. M., YAU, K., COPELAND, J. K., ZHANG, C., SURENDRA, A., GUTTMAN, D. S., FIGEYS, D. & DENNIS, J. W. 2016. Metabolic Reprogramming by Hexosamine Biosynthetic and Golgi N-Glycan Branching Pathways. *Scientific Reports*, 6, 23043.
- SAAD, H.-E. A., EL-SHARKAWY, S. H. & SHIER, W. T. 1995. Biological Activities of Pyrrolidinoindoline Alkaloids from *Calycodendron milnei*. *Planta Med*, 61, 313-316.
- SAHA, T., MONDAL, J., KHISTE, S., LUSIC, H., HU, Z.-W., JAYABALAN, R., HODGETTS, K. J., JANG, H., SENGUPTA, S., LEE, S. E., PARK, Y., LEE, L. P. & GOLDMAN, A. 2021. Nanotherapeutic approaches to overcome distinct drug resistance barriers in models of breast cancer. *Nanophotonics*, 10, 3063-3073.
- SAHENK, Z., BAROHN, R., NEW, P. & MENDELL, J. R. 1994. Taxol neuropathy: electrodiagnostic and sural nerve biopsy findings. *Archives of neurology*, 51, 726-729.
- SATO, K., HIDA, S., TAKAYANAGI, H., YOKOCHI, T., KAYAGAKI, N., TAKEDA, K., YAGITA, H., OKUMURA, K., TANAKA, N., TANIGUCHI, T. & OGASAWARA, K. 2001. Antiviral response by natural killer cells through TRAIL gene induction by IFN- α/β *European Journal of Immunology*, 31, 3138-3146.
- SATRIANO, J. 2004. Arginine pathways and the inflammatory response: Interregulation of nitric oxide and polyamines: Review article. *Amino Acids*, 26, 321-9.
- SCALBERT, A., BRENNAN, L., FIEHN, O., HANKEMEIER, T., KRISTAL, B. S., VAN OMMEN, B., PUJOS-GUILLOT, E., VERHEIJ, E., WISHART, D. & WOPEREIS, S. 2009.

Mass-spectrometry-based metabolomics: limitations and recommendations for future progress with particular focus on nutrition research. *Metabolomics*, 5, 435-458.

SCHALLENBERGER, M. A., NEWHOUSE, T., BARAN, P. S. & ROMESBERG, F. E. 2010. The psychotrimine natural products have antibacterial activity against Gram-positive bacteria and act via membrane disruption. *The Journal of Antibiotics*, 63, 685-687.

SCHIFF, P. B., FANT, J. & HORWITZ, S. B. 1979. Promotion of microtubule assembly in vitro by taxol. *Nature*, 277, 665-667.

SCHLATTNER, U., TOKARSKA-SCHLATTNER, M. & WALLIMANN, T. 2006. Mitochondrial creatine kinase in human health and disease. *Biochim Biophys Acta*, 1762, 164-80.

SCHONN, I., HENNESEN, J. & DARTSCH, D. C. 2010. Cellular responses to etoposide: cell death despite cell cycle arrest and repair of DNA damage. *Apoptosis*, 15, 162-72.

SCHULTES, R. E. & HOFMANN, A. 1979. *Plants of the Gods: Their Sacred, Healing and Hallucinogenic Powers*, New York, McGraw-Hill Book Company.

SCOTT, A., MCCAPRA, F. & HALL, E. 1964. Chimonanthine. A one-step synthesis and biosynthetic model. *Journal of the American Chemical Society*, 86, 302-303.

SCOTT, B. J., QUTOB, S., LIU, Q. Y. & NG, C. E. 2009. APM2 is a novel mediator of cisplatin resistance in a variety of cancer cell types regardless of p53 or MMR status. *International journal of cancer*, 125, 1193-1204.

SCOTT, T. Z. & MOVASSAGHI, M. 2024. Unified, Biosynthesis-Inspired, Completely Stereocontrolled Total Synthesis of All Highest-Order [n + 1] Oligocyclotryptamine Alkaloids. *Journal of the American Chemical Society*, 146, 23574-23581.

SEZER, A., KILICKAP, S., GüMüş, M., BONDARENKO, I., ÖZGÜROĞLU, M., GOGISHVILI, M., TURK, H. M., CICIN, I., BENTSION, D., GLADKOV, O., CLINGAN, P., SRIURANPONG, V., RIZVI, N., GAO, B., LI, S., LEE, S., MCGUIRE, K., CHEN, C.-I., MAKHARADZE, T., PAYDAS, S., NECHAEVA, M., SEEBACH, F., WEINREICH, D. M., YANCOPOULOS, G. D., GULLO, G., LOWY, I. & RIETSCHER, P. 2021. Cemiplimab monotherapy for first-line treatment of advanced non-small-cell lung cancer with PD-L1 of at least 50%: a multicentre, open-label, global, phase 3, randomised, controlled trial. *The Lancet*, 397, 592-604.

- SHI, D., SHI, G., HUANG, G., ZHANG, J. & LARTIGAU, E. 2009. Chemosensitivity of radioresistant cells in the multicellular spheroids of A549 lung adenocarcinoma. *J Exp Clin Cancer Res*, 28, 72.
- SHI, L., YANG, S., BI, J., YIN, G. & WANG, Y. 2012. Chemical constituents from the branches and leaves of *Chimonanthus praecox* with antiviral activity investigations. *Nat. Prod. Res. Dev*, 24, 1335-1338.
- SHI, Y., WANG, Y., HUANG, W., WANG, Y., WANG, R. & YUAN, Y. 2019. Integration of Metabolomics and Transcriptomics To Reveal Metabolic Characteristics and Key Targets Associated with Cisplatin Resistance in Nonsmall Cell Lung Cancer. *Journal of Proteome Research*, 18, 3259-3267.
- SILVA, C., PERESTRELO, R., SILVA, P., TOMÁS, H. & CÂMARA, J. S. 2019. Breast Cancer Metabolomics: From Analytical Platforms to Multivariate Data Analysis. A Review. *Metabolites*, 9, 102.
- SINGER, W. D., JORDAN, M., WILSON, L. & HIMES, R. H. 1989. Binding of vinblastine to stabilized microtubules. *Molecular pharmacology*, 36, 366-370.
- SKOROKHODOVA, A. Y., STASENKO, A. A., KRASILNIKOVA, N. V., GULEVICH, A. Y. & DEBABOV, V. G. 2022. Engineering *Escherichia coli* for Efficient Aerobic Conversion of Glucose to Malic Acid through the Modified Oxidative TCA Cycle. *Fermentation*, 8, 738.
- SKOULIDIS, F., GOLDBERG, M. E., GREENAWALT, D. M., HELLMANN, M. D., AWAD, M. M., GAINOR, J. F., SCHROCK, A. B., HARTMAIER, R. J., TRABUCCO, S. E., GAY, L., ALI, S. M., ELVIN, J. A., SINGAL, G., ROSS, J. S., FABRIZIO, D., SZABO, P. M., CHANG, H., SASSON, A., SRINIVASAN, S., KIROV, S., SZUSTAKOWSKI, J., VITAZKA, P., EDWARDS, R., BUFILL, J. A., SHARMA, N., OU, S. I., PELED, N., SPIGEL, D. R., RIZVI, H., AGUILAR, E. J., CARTER, B. W., ERASMUS, J., HALPENNY, D. F., PLODKOWSKI, A. J., LONG, N. M., NISHINO, M., DENNING, W. L., GALAN-COBO, A., HAMDY, H., HIRZ, T., TONG, P., WANG, J., RODRIGUEZ-CANALES, J., VILLALOBOS, P. A., PARRA, E. R., KALHOR, N., SHOLL, L. M., SAUTER, J. L., JUNGBLUTH, A. A., MINO-KENUDSON, M., AZIMI, R., ELAMIN, Y. Y., ZHANG, J., LEONARDI, G. C., JIANG, F., WONG, K. K., LEE, J. J., PAPADIMITRAKOPOULOU, V. A., WISTUBA, II, MILLER, V. A., FRAMPTON, G. M., WOLCHOK, J. D., SHAW, A. T., JÄNNE, P. A., STEPHENS, P. J., RUDIN, C. M., GEESE, W. J., ALBACKER, L. A. & HEYMACH, J. V. 2018. STK11/LKB1

Mutations and PD-1 Inhibitor Resistance in KRAS-Mutant Lung Adenocarcinoma. *Cancer Discov*, 8, 822-835.

SMANSKI, M. J., ZHOU, H., CLAESEN, J., SHEN, B., FISCHBACH, M. A. & VOIGT, C. A. 2016. Synthetic biology to access and expand nature's chemical diversity. *Nature Reviews Microbiology*, 14, 135-149.

SMITH, C. D., CRAFT, D. W., SHIROMOTO, R. S. & YAN, P. O. 1986. Alternative cell line for virus isolation. *Journal of Clinical Microbiology*, 24, 265-268.

SMITH, H. L., SOUTHGATE, H., TWEDDLE, D. A. & CURTIN, N. J. 2020. DNA damage checkpoint kinases in cancer. *Expert Reviews in Molecular Medicine*, 22, e2.

SOLDEVILLA, B., LÓPEZ-LÓPEZ, A., LENS-PARDO, A., CARRETERO-PUCHE, C., LOPEZ-GONZALVEZ, A., LA SALVIA, A., GIL-CALDERON, B., RIESCO-MARTINEZ, M. C., ESPINOSA-OLARTE, P., SARMENTERO, J., RUBIO-CUESTA, B., RINCÓN, R., BARBAS, C. & GARCIA-CARBONERO, R. 2021. Comprehensive Plasma Metabolomic Profile of Patients with Advanced Neuroendocrine Tumors (NETs). Diagnostic and Biological Relevance. *Cancers*, 13, 2634.

SOLEIMANI, A., RAHMANI, F., FERNS, G. A., RYZHIKOV, M., AVAN, A. & HASSANIAN, S. M. 2020. Role of the NF- κ B signaling pathway in the pathogenesis of colorectal cancer. *Gene*, 726, 144132.

SONKAR, K., AYYAPPAN, V., TRESSLER, C. M., ADELAJA, O., CAI, R., CHENG, M. & GLUNDE, K. 2019. Focus on the glycerophosphocholine pathway in choline phospholipid metabolism of cancer. *NMR Biomed*, 32, e4112.

SOULE, H. D., VAZGUEZ, J., LONG, A., ALBERT, S. & BRENNAN, M. 1973. A human cell line from a pleural effusion derived from a breast carcinoma. *J Natl Cancer Inst*, 51, 1409-16.

SPERANDIO, S., POKSAY, K., DE BELLE, I., LAFUENTE, M. J., LIU, B., NASIR, J. & BREDESEN, D. E. 2004. Paraptosis: mediation by MAP kinases and inhibition by AIP-1/Alix. *Cell Death Differ*, 11, 1066-75.

SPETH, P. A. J., VAN HOESEL, Q. G. C. M. & HAANEN, C. 1988. Clinical Pharmacokinetics of Doxorubicin. *Clinical Pharmacokinetics*, 15, 15-31.

- SPICER, A. P., KABACK, L. A., SMITH, T. J. & SELDIN, M. F. 1998. Molecular Cloning and Characterization of the Human and Mouse UDP-Glucose Dehydrogenase Genes *. *Journal of Biological Chemistry*, 273, 25117-25124.
- STACHEL, S. J., STOCKWELL, S. A. & VAN VRANKEN, D. L. 1999. The fluorescence of scorpions and cataractogenesis. *Chemistry & biology*, 6, 531-539.
- STEFANI, C., MIRICESCU, D., STANESCU-SPINU, I.-I., NICA, R. I., GREABU, M., TOTAN, A. R. & JINGA, M. 2021. Growth Factors, PI3K/AKT/mTOR and MAPK Signaling Pathways in Colorectal Cancer Pathogenesis: Where Are We Now? *International Journal of Molecular Sciences*, 22, 10260.
- STEVEN, A. & OVERMAN, L. E. 2007. Total Synthesis of Complex Cyclotryptamine Alkaloids: Stereocontrolled Construction of Quaternary Carbon Stereocenters. *Angewandte Chemie International Edition*, 46, 5488-5508.
- STOLL, A. 1945. Über Ergotamin.(10. Mitteilung über Mutterkornalkaloide). *Helvetica Chimica Acta*, 28, 1283-1308.
- STUPP, R., MASON, W. P., BENT, M. J. V. D., WELLER, M., FISHER, B., TAPHOORN, M. J. B., BELANGER, K., BRANDES, A. A., MAROSI, C., BOGDAHN, U., CURSCHMANN, J., JANZER, R. C., LUDWIN, S. K., GORLIA, T., ALLGEIER, A., LACOMBE, D., CAIRNCROSS, J. G., EISENHAUER, E. & MIRIMANOFF, R. O. 2005. Radiotherapy plus Concomitant and Adjuvant Temozolomide for Glioblastoma. *New England Journal of Medicine*, 352, 987-996.
- SU, X.-L., SU, W., WANG, Y., WANG, Y.-H., MING, X. & KONG, Y. 2016. The pyrrolidinoindoline alkaloid Psm2 inhibits platelet aggregation and thrombus formation by affecting PI3K/Akt signaling. *Acta Pharmacologica Sinica*, 37, 1208-1217.
- SUMNER, L., LEI, Z., NIKOLAU, B., SAITO, K., ROESSNER, U. & TRENGOVE, R. 2014. Proposed quantitative and alphanumeric metabolite identification metrics. *Metabolomics*, 10.
- SUMNER, L. W., AMBERG, A., BARRETT, D., BEALE, M. H., BEGER, R., DAYKIN, C. A., FAN, T. W., FIEHN, O., GOODACRE, R., GRIFFIN, J. L., HANKEMEIER, T., HARDY, N., HARNLY, J., HIGASHI, R., KOPKA, J., LANE, A. N., LINDON, J. C., MARRIOTT, P., NICHOLLS, A. W., REILY, M. D., THADEN, J. J. & VIAN, M. R. 2007. Proposed minimum

reporting standards for chemical analysis Chemical Analysis Working Group (CAWG) Metabolomics Standards Initiative (MSI). *Metabolomics*, 3, 211-221.

SUNG, H., FERLAY, J., SIEGEL, R. L., LAVERSANNE, M., SOERJOMATARAM, I., JEMAL, A. & BRAY, F. 2021. Global Cancer Statistics 2020: GLOBOCAN Estimates of Incidence and Mortality Worldwide for 36 Cancers in 185 Countries. *CA: A Cancer Journal for Clinicians*, 71, 209-249.

SUTHERLAND, R. L., HALL, R. E. & TAYLOR, I. W. 1983. Cell proliferation kinetics of MCF-7 human mammary carcinoma cells in culture and effects of tamoxifen on exponentially growing and plateau-phase cells. *Cancer Res*, 43, 3998-4006.

SUZUKI, T., KUBOTA, T. & KOBAYASHI, J. I. 2011. Eudistomidins H–K, new β -carboline alkaloids from the Okinawan marine tunicate Eudistoma glaucus. *Bioorganic & medicinal chemistry letters*, 21, 4220-4223.

SWAMY, M., PATHAK, S., GRZES, K. M., DAMEROW, S., SINCLAIR, L. V., VAN AALTEN, D. M. & CANTRELL, D. A. 2016. Glucose and glutamine fuel protein O-GlcNAcylation to control T cell self-renewal and malignancy. *Nat Immunol*, 17, 712-20.

SWIFT, L. P., REPHAELI, A., NUDELMAN, A., PHILLIPS, D. R. & CUTTS, S. M. 2006. Doxorubicin-DNA adducts induce a non-topoisomerase II-mediated form of cell death. *Cancer research*, 66, 4863-4871.

TABATA, H. 2004. Paclitaxel Production by Plant-Cell-Culture Technology. In: ZHONG, J.-J. (ed.) *Biomanufacturing*. Berlin, Heidelberg: Springer Berlin Heidelberg.

TACAR, O., SRIAMORNSAK, P. & DASS, C. R. 2013. Doxorubicin: an update on anticancer molecular action, toxicity and novel drug delivery systems. *Journal of Pharmacy and Pharmacology*, 65, 157-170.

TAKAYAMA, H., MORI, I., KITAJIMA, M., AIMI, N. & LAJIS, N. H. 2004. New Type of Trimeric and Pentameric Indole Alkaloids from *Psychotria rostrata*. *Organic Letters*, 6, 2945-2948.

TANG, S., NING, Q., YANG, L., MO, Z. & TANG, S. 2020. Mechanisms of immune escape in the cancer immune cycle. *International Immunopharmacology*, 86, 106700.

TAPIERO, H., MATHÉ, G., COUVREUR, P. & TEW, K. D. 2002. II. Glutamine and glutamate. *Biomedicine & Pharmacotherapy*, 56, 446-457.

- TASKAR, K. S., RUDRARAJU, V., MITTAPALLI, R. K., SAMALA, R., THORSHEIM, H. R., LOCKMAN, J., GRIL, B., HUA, E., PALMIERI, D., POLLI, J. W., CASTELLINO, S., RUBIN, S. D., LOCKMAN, P. R., STEEG, P. S. & SMITH, Q. R. 2012. Lapatinib Distribution in HER2 Overexpressing Experimental Brain Metastases of Breast Cancer. *Pharmaceutical Research*, 29, 770-781.
- TAVERNA, P., LIU, L., HANSON, A. J., MONKS, A. & GERSON, S. L. 2000. Characterization of MLH1 and MSH2 DNA mismatch repair proteins in cell lines of the NCI anticancer drug screen. *Cancer Chemotherapy and Pharmacology*, 46, 507-516.
- TAYLOR, C. M., RAZAFIMANDIMBISON, S. G., BARRABÉ, L., JARDIM, J. G. & BARBOSA, M. R. V. 2017. Eumachia expanded, a pantropical genus distinct from Psychotria (Rubiaceae, Palicoureeae). *Candollea*, 72, 289-318, 30.
- TAYLOR, W. I. & FARNSWORTH, N. R. The Catharanthus alkaloids: Botany, chemistry, pharmacology, and clinical use. 1975.
- TAYMAZ-NIKEREL, H., KARABEKMEZ, M. E., ERASLAN, S. & KIRDAR, B. 2018. Doxorubicin induces an extensive transcriptional and metabolic rewiring in yeast cells. *Scientific Reports*, 8, 13672.
- TENNANT, D. A., DURÁN, R. V. & GOTTLIEB, E. 2010. Targeting metabolic transformation for cancer therapy. *Nature reviews cancer*, 10, 267-277.
- THORNBURG, C. C., BRITT, J. R., EVANS, J. R., AKEE, R. K., WHITT, J. A., TRINH, S. K., HARRIS, M. J., THOMPSON, J. R., EWING, T. L., SHIPLEY, S. M., GROTHAUS, P. G., NEWMAN, D. J., SCHNEIDER, J. P., GRKOVIC, T. & O'KEEFE, B. R. 2018. NCI Program for Natural Product Discovery: A Publicly-Accessible Library of Natural Product Fractions for High-Throughput Screening. *ACS Chemical Biology*, 13, 2484-2497.
- TIAN, X., LIU, M., HUANG, X., ZHU, Q., LIU, W., CHEN, W., ZOU, Y., CAI, Y., HUANG, S., CHEN, A., ZHAN, T., HUANG, M., CHEN, X., HAN, Z. & TAN, J. 2020. Noscapine Induces Apoptosis in Human Colon Cancer Cells by Regulating Mitochondrial Damage and Warburg Effect via PTEN/PI3K/mTOR Signaling Pathway. *OncoTargets and Therapy*, 13, 5419-5428.
- TONELLI, C., CHIO, I. I. C. & TUVESON, D. A. 2018. Transcriptional Regulation by Nrf2. *Antioxid Redox Signal*, 29, 1727-1745.

TOWLE, M. J., SALVATO, K. A., BUDROW, J., WELS, B. F., KUZNETSOV, G., AALFS, K. K., WELSH, S., ZHENG, W., SELETSKY, B. M., PALME, M. H., HABGOOD, G. J., SINGER, L. A., DIPIETRO, L. V., WANG, Y., CHEN, J. J., QUINCY, D. A., DAVIS, A., YOSHIMATSU, K., KISHI, Y., YU, M. J. & LITTLEFIELD, B. A. 2001. In vitro and in vivo anticancer activities of synthetic macrocyclic ketone analogues of halichondrin B. *Cancer Res*, 61, 1013-21.

TOWLE, M. J., SALVATO, K. A., WELS, B. F., AALFS, K. K., ZHENG, W., SELETSKY, B. M., ZHU, X., LEWIS, B. M., KISHI, Y., YU, M. J. & LITTLEFIELD, B. A. 2011. Eribulin Induces Irreversible Mitotic Blockade: Implications of Cell-Based Pharmacodynamics for In vivo Efficacy under Intermittent Dosing Conditions. *Cancer Research*, 71, 496-505.

TURNER, I. M. 2019. THREE NEW COMBINATIONS IN EUMACHIA (RUBIACEAE–PALICOUREEAE) FROM SOUTHEAST ASIA. *Edinburgh Journal of Botany*, 76, 23-27.

TZVETKOV, N. T., KIRILOV, K., MATIN, M. & ATANASOV, A. G. 2023. Natural product drug discovery and drug design: two approaches shaping new pharmaceutical development. *Nephrology Dialysis Transplantation*, 39, 375-378.

UK, C. R. *Breast cancer statistics* [Online]. Available: <https://www.cancerresearchuk.org/health-professional/cancer-statistics/statistics-by-cancer-type/breast-cancer#heading-Three> [Accessed 3006 2022].

UK, C. R. *Nab-paclitaxel (Abraxane)* [Online]. Available: <https://www.cancerresearchuk.org/about-cancer/treatment/drugs/nab-paclitaxel> [Accessed 0108 2024].

UK, C. R. *Research and clinical trials* [Online]. Available: <https://www.cancerresearchuk.org/about-cancer/breast-cancer/research-clinical-trials> [Accessed 3006 2022].

UK, C. R. *Targeted and immunotherapy drugs for advanced bowel cancer* [Online]. Available: <https://www.cancerresearchuk.org/about-cancer/bowel-cancer/advanced/treatment/targeted-cancer-drugs-treatment> [Accessed 0707 2022].

UK, C. R. *Types of breast cancer and related conditions* [Online]. Available: <https://www.cancerresearchuk.org/about-cancer/breast-cancer/stages-types-grades/types> [Accessed 3006 2022].

UK, C. R. 2022. *Bowel cancer statistics* [Online]. Available: <https://www.cancerresearchuk.org/health-professional/cancer-statistics/statistics-by-cancer-type/bowel-cancer> [Accessed 3006 2022].

VAN DE SANTOS, L., FETT-NETO, A. G., KERBER, V. A., ELISABETSKY, E., QUIRION, J.-C. & HENRIQUES, A. T. 2001. Indole monoterpene alkaloids from leaves of *Psychotria suterella* Müll. Arg.(Rubiaceae). *Biochemical Systematics and Ecology*, 29, 1185-1187.

VAN DEN BERG, R. A., HOEFSLOOT, H. C., WESTERHUIS, J. A., SMILDE, A. K. & VAN DER WERF, M. J. 2006. Centering, scaling, and transformations: improving the biological information content of metabolomics data. *BMC Genomics*, 7, 142.

VAN MEER, G., VOELKER, D. R. & FEIGENSON, G. W. 2008. Membrane lipids: where they are and how they behave. *Nature Reviews Molecular Cell Biology*, 9, 112-124.

VAN MEIR, E. G., HADJIPANAYIS, C. G., NORDEN, A. D., SHU, H.-K., WEN, P. Y. & OLSON, J. J. 2010. Exciting New Advances in Neuro-Oncology: The Avenue to a Cure for Malignant Glioma. *CA: A Cancer Journal for Clinicians*, 60, 166-193.

VASCONCELOS-DOS-SANTOS, A., LOPONTE, H. F. B. R., MANTUANO, N. R., OLIVEIRA, I. A., DE PAULA, I. F., TEIXEIRA, L. K., DE-FREITAS-JUNIOR, J. C. M., GONDIM, K. C., HEISE, N., MOHANA-BORGES, R., MORGADO-DÍAZ, J. A., DIAS, W. B. & TODESCHINI, A. R. 2017. Hyperglycemia exacerbates colon cancer malignancy through hexosamine biosynthetic pathway. *Oncogenesis*, 6, e306-e306.

VASSEUR, S. & MANIÉ, S. N. 2015. ER stress and hexosamine pathway during tumourigenesis: A pas de deux? *Seminars in Cancer Biology*, 33, 34-39.

VELMA, V., DASARI, S. R. & TCHOUNWOU, P. B. 2016. Low Doses of Cisplatin Induce Gene Alterations, Cell Cycle Arrest, and Apoptosis in Human Promyelocytic Leukemia Cells. *Biomarker Insights*, 11, BMI.S39445.

VERMES, I., HAANEN, C., STEFFENS-NAKKEN, H. & REUTELINGSPERGER, C. 1995. A novel assay for apoptosis. Flow cytometric detection of phosphatidylserine expression on early apoptotic cells using fluorescein labelled Annexin V. *J Immunol Methods*, 184, 39-51.

VERMEULEN, L., DE SOUSA E MELO, F., VAN DER HEIJDEN, M., CAMERON, K., DE JONG, J. H., BOROVSKI, T., TUYNMAN, J. B., TODARO, M., MERZ, C., RODERMOND, H., SPRICK, M. R., KEMPER, K., RICHEL, D. J., STASSI, G. & MEDEMA, J. P. 2010. Wnt

activity defines colon cancer stem cells and is regulated by the microenvironment. *Nature Cell Biology*, 12, 468-476.

VERNOLE, P., TEDESCHI, B., TENTORI, L., LEVATI, L., ARGENTIN, G., CICCETTI, R., FORINI, O., GRAZIANI, G. & D'ATRI, S. 2006. Role of the mismatch repair system and p53 in the clastogenicity and cytotoxicity induced by bleomycin. *Mutation Research/Fundamental and Molecular Mechanisms of Mutagenesis*, 594, 63-77.

VEROTTA, L., ORSINI, F., SBACCHI, M., SCHEILDLER, M., AMADOR, T. & ELISABETSKY, E. 2002. Synthesis and antinociceptive activity of chimonanthines and pyrrolidinoindoline-type alkaloids. *Bioorganic & medicinal chemistry*, 10, 2133-2142.

VEROTTA, L., PILATI, T., TATò, M., ELISABETSKY, E., AMADOR, T. A. & NUNES, D. S. 1998. Pyrrolidinoindoline Alkaloids from *Psychotria colorata*1. *J Nat Prod*, 61, 392-6.

VON LINTIG, F. C., DREILINGER, A. D., VARKI, N. M., WALLACE, A. M., CASTEEL, D. E. & BOSS, G. R. 2000. Ras activation in human breast cancer. *Breast Cancer Research and Treatment*, 62, 51-62.

WAGENAAR, M. M. 2008. Pre-fractionated Microbial Samples – The Second Generation Natural Products Library at Wyeth. *Molecules*, 13, 1406-1426.

WALL, M. E. & WANI, M. C. 1996. Camptothecin and taxol: from discovery to clinic. *Journal of Ethnopharmacology*, 51, 239-254.

WALLIMANN, T., WYSS, M., BRDICZKA, D., NICOLAY, K. & EPPENBERGER, H. 1992. Intracellular compartmentation, structure and function of creatine kinase isoenzymes in tissues with high and fluctuating energy demands: the 'phosphocreatine circuit' for cellular energy homeostasis. *Biochemical Journal*, 281, 21.

WALSH, J. G., CULLEN, S. P., SHERIDAN, C., LÜTHI, A. U., GERNER, C. & MARTIN, S. J. 2008. Executioner caspase-3 and caspase-7 are functionally distinct proteases. *Proceedings of the National Academy of Sciences*, 105, 12815-12819.

WANG, F., TRAVINS, J., DELABARRE, B., PENARD-LACRONIQUE, V., SCHALM, S., HANSEN, E., STRALEY, K., KERNYTSKY, A., LIU, W., GLISER, C., YANG, H., GROSS, S., ARTIN, E., SAADA, V., MYLONAS, E., QUIVORON, C., POPOVICI-MULLER, J., SAUNDERS, J. O., SALITURO, F. G., YAN, S., MURRAY, S., WEI, W., GAO, Y., DANG, L., DORSCH, M., AGRESTA, S., SCHENKEIN, D. P., BILLER, S. A., SU, S. M., DE

BOTTON, S. & YEN, K. E. 2013. Targeted Inhibition of Mutant IDH2 in Leukemia Cells Induces Cellular Differentiation. *Science*, 340, 622-626.

WANG, J., SOISSON, S. M., YOUNG, K., SHOOP, W., KODALI, S., GALGOCI, A., PAINTER, R., PARTHASARATHY, G., TANG, Y. S., CUMMINGS, R., HA, S., DORSO, K., MOTYL, M., JAYASURIYA, H., ONDEYKA, J., HERATH, K., ZHANG, C., HERNANDEZ, L., ALLOCCO, J., BASILIO, Á., TORMO, J. R., GENILLOUD, O., VICENTE, F., PELAEZ, F., COLWELL, L., LEE, S. H., MICHAEL, B., FELCETTO, T., GILL, C., SILVER, L. L., HERMES, J. D., BARTIZAL, K., BARRETT, J., SCHMATZ, D., BECKER, J. W., CULLY, D. & SINGH, S. B. 2006. Platensimycin is a selective FabF inhibitor with potent antibiotic properties. *Nature*, 441, 358-361.

WANG, J. C. 1985. DNA topoisomerases. *Annual review of biochemistry*, 54, 665-697.

WANG, S., FU, J.-L., HAO, H.-F., JIAO, Y.-N., LI, P.-P. & HAN, S.-Y. 2021a. Metabolic reprogramming by traditional Chinese medicine and its role in effective cancer therapy. *Pharmacological Research*, 170, 105728.

WANG, T., FAHRMANN, J. F., LEE, H., LI, Y.-J., TRIPATHI, S. C., YUE, C., ZHANG, C., LIFSHITZ, V., SONG, J., YUAN, Y., SOMLO, G., JANDIAL, R., ANN, D., HANASH, S., JOVE, R. & YU, H. 2018. JAK/STAT3-Regulated Fatty Acid β -Oxidation Is Critical for Breast Cancer Stem Cell Self-Renewal and Chemoresistance. *Cell Metabolism*, 27, 136-150.e5.

WANG, W.-X., CAO, L., XIONG, J., XIA, G. & HU, J.-F. 2011. Constituents from *Chimonanthus praecox* (wintersweet). *Phytochemistry Letters*, 4, 271-274.

WANG, X., LIU, R., ZHU, W., CHU, H., YU, H., WEI, P., WU, X., ZHU, H., GAO, H., LIANG, J., LI, G. & YANG, W. 2019. UDP-glucose accelerates SNAIL mRNA decay and impairs lung cancer metastasis. *Nature*, 571, 127-131.

WANG, X., WANG, Z., WANG, K., GAO, M., ZHANG, H. & XU, X. 2021b. Metabolomics analysis of multidrug resistance in colorectal cancer cell and multidrug resistance reversal effect of verapamil. *Biomedical Chromatography*, 35, e4976.

WANG, Y., CHEN, W., LI, K., WU, G., ZHANG, W., MA, P. & FENG, S. 2021c. Tissue-based metabolomics reveals metabolic signatures and major metabolic pathways of gastric cancer with help of transcriptomic data from TCGA. *Bioscience Reports*, 41.

- WANI, M. C., TAYLOR, H. L., WALL, M. E., COGGON, P. & MCPHAIL, A. T. 1971. Plant antitumor agents. VI. Isolation and structure of taxol, a novel antileukemic and antitumor agent from *Taxus brevifolia*. *Journal of the American Chemical Society*, 93, 2325-2327.
- WASIELEWSKI, M., ELSTRODT, F., KLIJN, J. G., BERNIS, E. M. & SCHUTTE, M. 2006. Thirteen new p53 gene mutants identified among 41 human breast cancer cell lines. *Breast Cancer Res Treat*, 99, 97-101.
- WELLEN, K. E., LU, C., MANCUSO, A., LEMONS, J. M. S., RYCZKO, M., DENNIS, J. W., RABINOWITZ, J. D., COLLIER, H. A. & THOMPSON, C. B. 2010. The hexosamine biosynthetic pathway couples growth factor-induced glutamine uptake to glucose metabolism. *Genes & Development*, 24, 2784-2799.
- WHITTERIDGE, D. 1948. The role of acetylcholine in synaptic transmission; a critical review. *J Neurol Neurosurg Psychiatry*, 11, 134-40.
- WICK, W., WELLER, M., VAN DEN BENT, M., SANSON, M., WEILER, M., VON DEIMLING, A., PLASS, C., HEGI, M., PLATTEN, M. & REIFENBERGER, G. 2014. MGMT testing--the challenges for biomarker-based glioma treatment. *Nature reviews. Neurology*, 10, 372-385.
- WICKSTRÖM, M., DYBERG, C., MILOSEVIC, J., EINVIK, C., CALERO, R., SVEINBJÖRNSSON, B., SANDÉN, E., DARABI, A., SIESJÖ, P., KOOL, M., KOGNER, P., BARYAWNO, N. & JOHNSEN, J. I. 2015. Wnt/ β -catenin pathway regulates MGMT gene expression in cancer and inhibition of Wnt signalling prevents chemoresistance. *Nature Communications*, 6, 8904.
- WILSON, L., JORDAN, M. A., MORSE, A. & MARGOLIS, R. L. 1982. Interaction of vinblastine with steady-state microtubules in vitro. *Journal of Molecular Biology*, 159, 125-149.
- WILSON, N. S., DIXIT, V. & ASHKENAZI, A. 2009. Death receptor signal transducers: nodes of coordination in immune signaling networks. *Nat Immunol*, 10, 348-55.
- WOJTOWICZ, W., WRÓBEL, A., PYZIAK, K., TARKOWSKI, R., BALCERZAK, A., BĘBENEK, M. & MŁYNARZ, P. 2020. Evaluation of MDA-MB-468 Cell Culture Media Analysis in Predicting Triple-Negative Breast Cancer Patient Sera Metabolic Profiles. *Metabolites*, 10.

- WOLFE, A. L., ZHOU, Q., TOSKA, E., GALEAS, J., KU, A. A., KOCH, R. P., BANDYOPADHYAY, S., SCALTRITI, M., LEBRILLA, C. B., MCCORMICK, F. & KIM, S. E. 2021. UDP-glucose pyrophosphorylase 2, a regulator of glycogen synthesis and glycosylation, is critical for pancreatic cancer growth. *Proceedings of the National Academy of Sciences*, 118, e2103592118.
- WOO-MING, R. B. & STUART, K. L. 1975. Calycanthine from *Palicourea alpina*. *Phytochemistry*, 14, 2529.
- WORLEY, B. & POWERS, R. 2013. Multivariate Analysis in Metabolomics. *Curr Metabolomics*, 1, 92-107.
- WU, C., KHAN, S. A., PENG, L.-J. & LANGE, A. J. 2006. Roles for fructose-2, 6-bisphosphate in the control of fuel metabolism: beyond its allosteric effects on glycolytic and gluconeogenic enzymes. *Advances in enzyme regulation*, 46, 72-88.
- WU, G. 2009. Amino acids: metabolism, functions, and nutrition. *Amino Acids*, 37, 1-17.
- WU, G. & MORRIS, S. M., JR. 1998. Arginine metabolism: nitric oxide and beyond. *Biochem J*, 336 (Pt 1), 1-17.
- WU, H., WANG, L., ZHAN, X., WANG, B., WU, J. & ZHOU, A. 2020a. A UPLC-Q-TOF/MS-based plasma metabolomics approach reveals the mechanism of Compound Kushen Injection-based intervention against non-small cell lung cancer in Lewis tumor-bearing mice. *Phytomedicine*, 76, 153259.
- WU, K., YANG, Q., MU, Y., ZHOU, L., LIU, Y., ZHOU, Q. & HE, B. 2012. Berberine inhibits the proliferation of colon cancer cells by inactivating Wnt/ β -catenin signaling. *Int J Oncol*, 41, 292-298.
- WU, X.-X., YUE, G. G.-L., DONG, J.-R., LAM, C. W.-K., WONG, C.-K., QIU, M.-H. & LAU, C. B.-S. 2020b. Actein Inhibits Tumor Growth and Metastasis in HER2-Positive Breast Tumor Bearing Mice via Suppressing AKT/mTOR and Ras/Raf/MAPK Signaling Pathways. *Frontiers in Oncology*, 10.
- WYLLIE, A. H. 1980. Glucocorticoid-induced thymocyte apoptosis is associated with endogenous endonuclease activation. *Nature*, 284, 555-556.

- WYLLIE, A. H., KERR, J. F. R. & CURRIE, A. R. 1980. Cell Death: The Significance of Apoptosis. In: BOURNE, G. H., DANIELLI, J. F. & JEON, K. W. (eds.) *International Review of Cytology*. Academic Press.
- WYSS, M. & KADDURAH-DAOUK, R. 2000. Creatine and Creatinine Metabolism. *Physiological Reviews*, 80, 1107-1213.
- XIE, G. & RAUFMAN, J.-P. 2016. Muscarinic receptor signaling and colon cancer progression. *Journal of Cancer Metastasis and Treatment*, 2, 195-200.
- XU, H., LIU, R., HE, B., BI, C. W., BI, K. & LI, Q. 2016. Polyamine Metabolites Profiling for Characterization of Lung and Liver Cancer Using an LC-Tandem MS Method with Multiple Statistical Data Mining Strategies: Discovering Potential Cancer Biomarkers in Human Plasma and Urine. *Molecules*, 21, 1040.
- YALCIN, A., TELANG, S., CLEM, B. & CHESNEY, J. 2009. Regulation of glucose metabolism by 6-phosphofructo-2-kinase/fructose-2, 6-bisphosphatases in cancer. *Experimental and molecular pathology*, 86, 174-179.
- YAMAMOTO, M., SUZUKI, S. O. & HIMENO, M. 2010. Resveratrol-induced autophagy in human U373 glioma cells. *Oncol Lett*, 1, 489-493.
- YANG, F., TEVES, S. S., KEMP, C. J. & HENIKOFF, S. 2014. Doxorubicin, DNA torsion, and chromatin dynamics. *Biochim Biophys Acta*, 1845, 84-9.
- YANG, S., LI, W., SUN, H., WU, B., JI, F., SUN, T., CHANG, H., SHEN, P., WANG, Y. & ZHOU, D. 2015. Resveratrol elicits anti-colorectal cancer effect by activating miR-34c-KITLG in vitro and in vivo. *BMC Cancer*, 15, 969.
- YANG, T., HUI, R., NOUWS, J., SAULER, M., ZENG, T. & WU, Q. 2022. Untargeted metabolomics analysis of esophageal squamous cell cancer progression. *Journal of Translational Medicine*, 20, 127.
- YAO, N., LI, W., XU, G., DUAN, N., YU, G. & QU, J. 2023. Choline metabolism and its implications in cancer. *Frontiers in Oncology*, 13.
- YE, Z., ZENG, Z., SHEN, Y., YANG, Q., CHEN, D., CHEN, Z. & SHEN, S. 2019. ODC1 promotes proliferation and mobility via the AKT/GSK3 β / β -catenin pathway and modulation of acidotic microenvironment in human hepatocellular carcinoma. *OncoTargets and Therapy*, 12, 4081-4092.

- YVON, A.-M. C., WADSWORTH, P. & JORDAN, M. A. 1999. Taxol suppresses dynamics of individual microtubules in living human tumor cells. *Molecular biology of the cell*, 10, 947-959.
- ZAMBRANO, A., MOLT, M., URIBE, E. & SALAS, M. 2019. Glut 1 in Cancer Cells and the Inhibitory Action of Resveratrol as A Potential Therapeutic Strategy. *International Journal of Molecular Sciences*, 20, 3374.
- ZAMPELLA, E. J., BRADLEY JR, E. L. & PRETLOW II, T. G. 1982. Glucose-6-phosphate dehydrogenase: A possible clinical indicator for prostatic carcinoma. *Cancer*, 49, 384-387.
- ZANCAN, P., ROSAS, A. O., MARCONDES, M. C., MARINHO-CARVALHO, M. M. & SOLA-PENNA, M. 2007. Clotrimazole inhibits and modulates heterologous association of the key glycolytic enzyme 6-phosphofructo-1-kinase. *Biochemical pharmacology*, 73, 1520-1527.
- ZHANG, J., HUMMERSON, M., MATTHEWS, C. S., STEVENS, M. F. G. & BRADSHAW, T. D. 2014. N3-Substituted Temozolomide Analogs Overcome Methylguanine-DNA Methyltransferase and Mismatch Repair Precipitating Apoptotic and Autophagic Cancer Cell Death. *Oncology*, 88, 28-48.
- ZHANG, J., STEVENS, M. F. G., LAUGHTON, C. A., MADHUSUDAN, S. & BRADSHAW, T. D. 2010. Acquired Resistance to Temozolomide in Glioma Cell Lines: Molecular Mechanisms and Potential Translational Applications. *Oncology*, 78, 103-114.
- ZHANG, J., WANG, X., VIKASH, V., YE, Q., WU, D., LIU, Y. & DONG, W. 2016. ROS and ROS-Mediated Cellular Signaling. *Oxidative Medicine and Cellular Longevity*, 2016, 4350965.
- ZHANG, J. W., GAO, J. M., XU, T., ZHANG, X. C., MA, Y. T., JARUSSOPHON, S. & KONISHI, Y. 2009a. Antifungal activity of alkaloids from the seeds of *Chimonanthus praecox*. *Chemistry & biodiversity*, 6, 838-845.
- ZHANG, L. & BU, P. 2022. The two sides of creatine in cancer. *Trends in Cell Biology*, 32, 380-390.
- ZHANG, L., ZHANG, J., HU, C., CAO, J., ZHOU, X., HU, Y., HE, Q. & YANG, B. 2009b. Efficient activation of p53 pathway in A549 cells exposed to L2, a novel compound targeting p53-MDM2 interaction. *Anti-Cancer Drugs*, 20, 416-424.

ZHANG, L., ZHU, Z., YAN, H., WANG, W., WU, Z., ZHANG, F., ZHANG, Q., SHI, G., DU, J., CAI, H., ZHANG, X., HSU, D., GAO, P., PIAO, H.-L., CHEN, G. & BU, P. 2021. Creatine promotes cancer metastasis through activation of Smad2/3. *Cell Metabolism*, 33, 1111-1123.e4.

ZHANG, W., CAI, S., QIN, L., FENG, Y., DING, M., LUO, Z., SHAN, J. & DI, L. 2024. Alkaloids of Aconiti Lateralis Radix Praeparata inhibit growth of non-small cell lung cancer by regulating PI3K/Akt-mTOR signaling and glycolysis. *Communications Biology*, 7, 1118.

ZHANG, Y., WANG, G., LV, H., LUO, J. & KONG, L. 2015. Two new β -carboline alkaloids from the roots of Gypsophila oldhamiana. *Natural Product Research*, 29, 1207-1211.

ZHAO, F., GAO, Z., JIAO, W., CHEN, L., CHEN, L. & YAO, X. 2012. In vitro anti-inflammatory effects of beta-carboline alkaloids, isolated from Picrasma quassioides, through inhibition of the iNOS pathway. *Planta Med*, 78, 1906-11.

ZHOU, H., HE, H.-P., WANG, Y.-H. & HAO, X.-J. 2010. A New Dimeric Alkaloid from the Leaf of Psychotria calocarpa. *Helvetica Chimica Acta*, 93, 1650-1652.

ZHU, Q.-H., HE, J.-F. & FENG, J.-Y. 2007. Optimization of the process parameters of synthesis of vinblastine imprinted polymer. *European polymer journal*, 43, 4043-4051.

ZHUKOVA, O. S., GERASIMOVA, G. K., SHUBINA, I. Z. & KISELEVSKII, M. V. 2007. Combined effect of cisplatin and lymphokine-activated killer cells on A549 cells of non-small cell lung cancer. *Bulletin of Experimental Biology and Medicine*, 144, 231-234.

ZOIS, C. E., FAVARO, E. & HARRIS, A. L. 2014. Glycogen metabolism in cancer. *Biochemical Pharmacology*, 92, 3-11.

ZUBAREV, R. A. & MAKAROV, A. 2013. Orbitrap Mass Spectrometry. *Analytical Chemistry*, 85, 5288-5296.

ZULUETA DÍAZ, Y. L. M., AMBROGGIO, E. E. & FANANI, M. L. 2020. Miltefosine inhibits the membrane remodeling caused by phospholipase action by changing membrane physical properties. *Biochim Biophys Acta Biomembr*, 1862, 183407.

Appendices

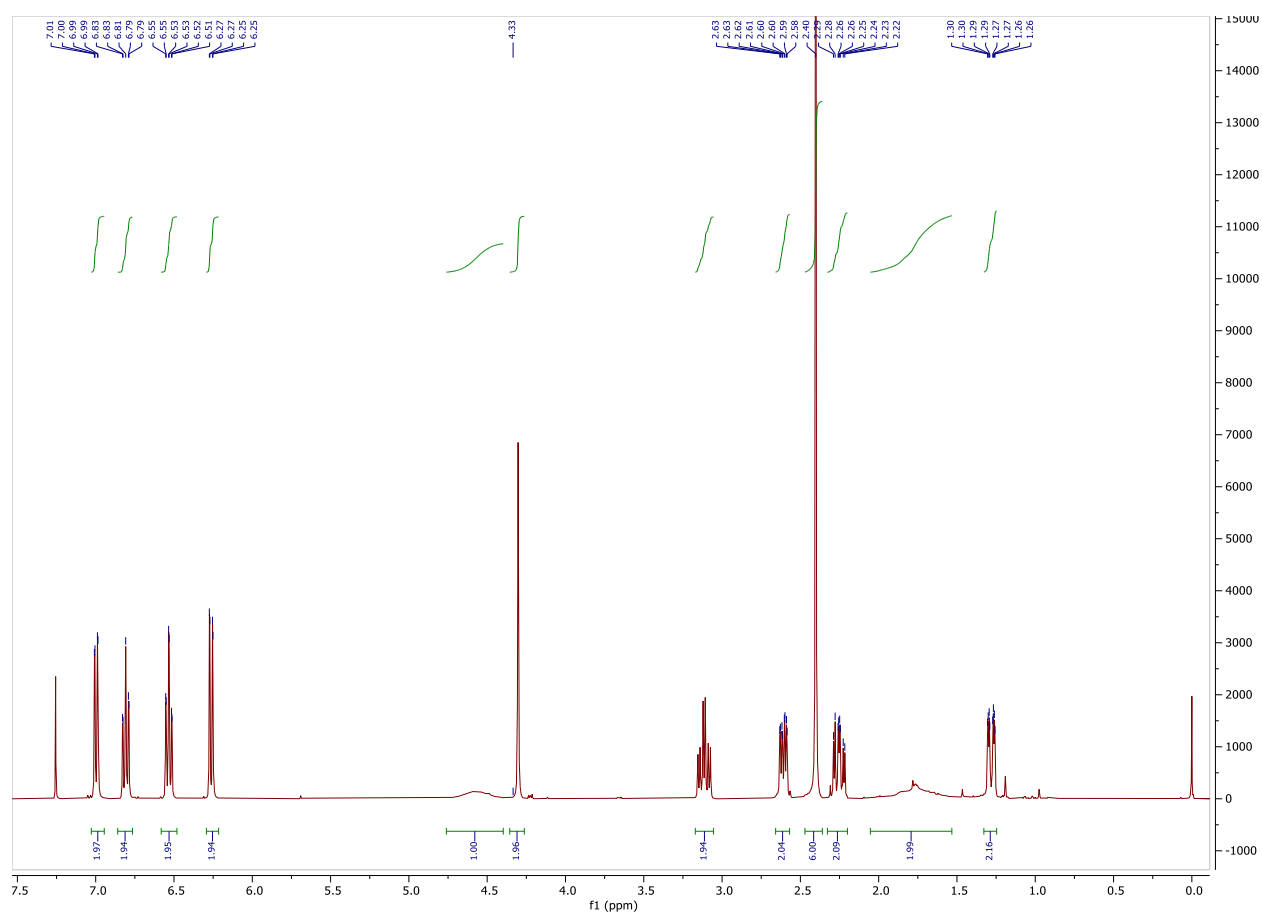


Figure S1. ^1H NMR Spectrum of (-)-Calycanthine (**1**)

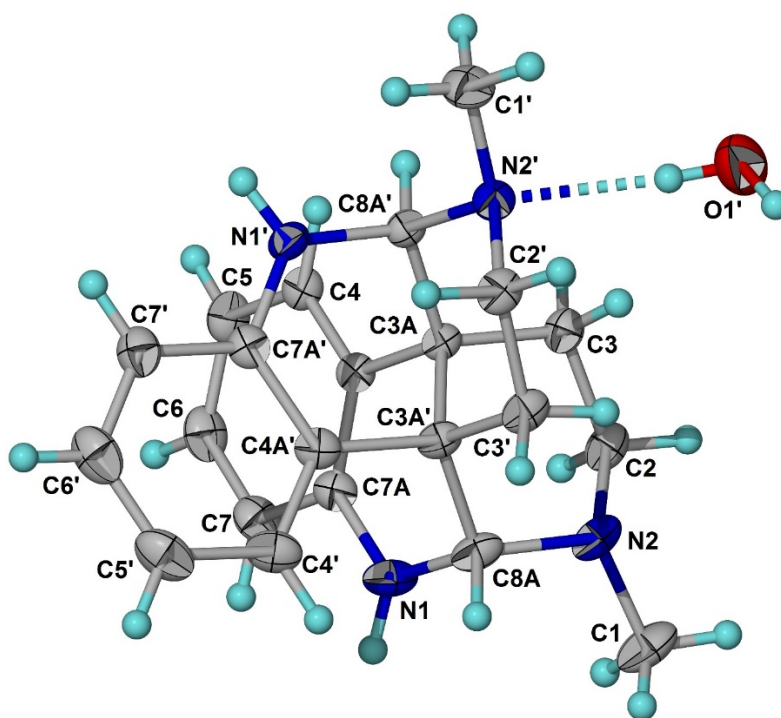


Figure S2. X-ray Crystal Structure of (–)-Calycanthine (**1**)

Crystallographic data of (–)-Calycanthine (**1**): Colorless block crystals, $C_{22}H_{26}N_4 \cdot H_2O$, $M_r = 364.48$, orthorhombic, space group $P2_12_12_1$, $a = 10.43715(15)$ Å, $b = 12.9710(2)$ Å, $c = 13.8569(2)$ Å, $V = 1875.95(5)$ Å³, $Z = 4$, $D_{\text{calcd}} = 1.291$ gcm^{–3}, crystal size 0.5 x 0.5 x 0.2 mm³, $F(000) = 784$, Cu K α radiation ($\lambda = 1.54184$ Å), $T = 293(2)$ K, 4650 reflections measured ($9.34^\circ \leq 2\theta \leq 147.878^\circ$), 3212 unique ($R_{\text{int}} = 0.0161$, $R_{\text{sigma}} = 0.0233$) which were used in all calculations. The final R_1 value was 0.0431 [$I > 2\sigma(I)$] and wR_2 was 0.1123.

Crystal data and structure refinement for (–)-Calycanthine (**1**)

Molecular formula	$C_{22}H_{26}N_4 \cdot H_2O$
Molecular weight, M_r	364.48
Temperature during diffraction experiment, T	293(2) K
X-ray source	Cu K α ($\lambda = 1.54184$)
Crystal system	Orthorhombic
Space group	$P2_12_12_1$
a	10.43715(15) Å
b	12.9710(2) Å
c	13.8569(2) Å
α	90°
β	90°
γ	90°
Volume, V	1875.95(5) Å ³
No. of molecule per unit cell, Z	4
Density (calcd)	1.291 g/cm ³

μ	0.638 mm ⁻¹
F(000)	784
Crystal size	0.5 × 0.5 × 0.2 mm
2 θ range for data collection	9.34 to 147.878°
Index ranges	$-12 \leq h \leq 12$, $-15 \leq k \leq 15$, $-16 \leq l \leq 16$
Reflections collected	4650
Independent reflections	3212 [$R_{\text{int}} = 0.0161$, $R_{\text{sigma}} = 0.0233$]
Data/restraints/parameters	3212/0/249
Goodness-of-fit on F^2	1.073
Final R indexes [$I \geq 2\sigma(I)$]	$R_1 = 0.0431$, $wR_2 = 0.1101$
Final R indexes [all data]	$R_1 = 0.0449$, $wR_2 = 0.1123$
Largest diff. peak/hole / e Å ⁻³	0.17/−0.31

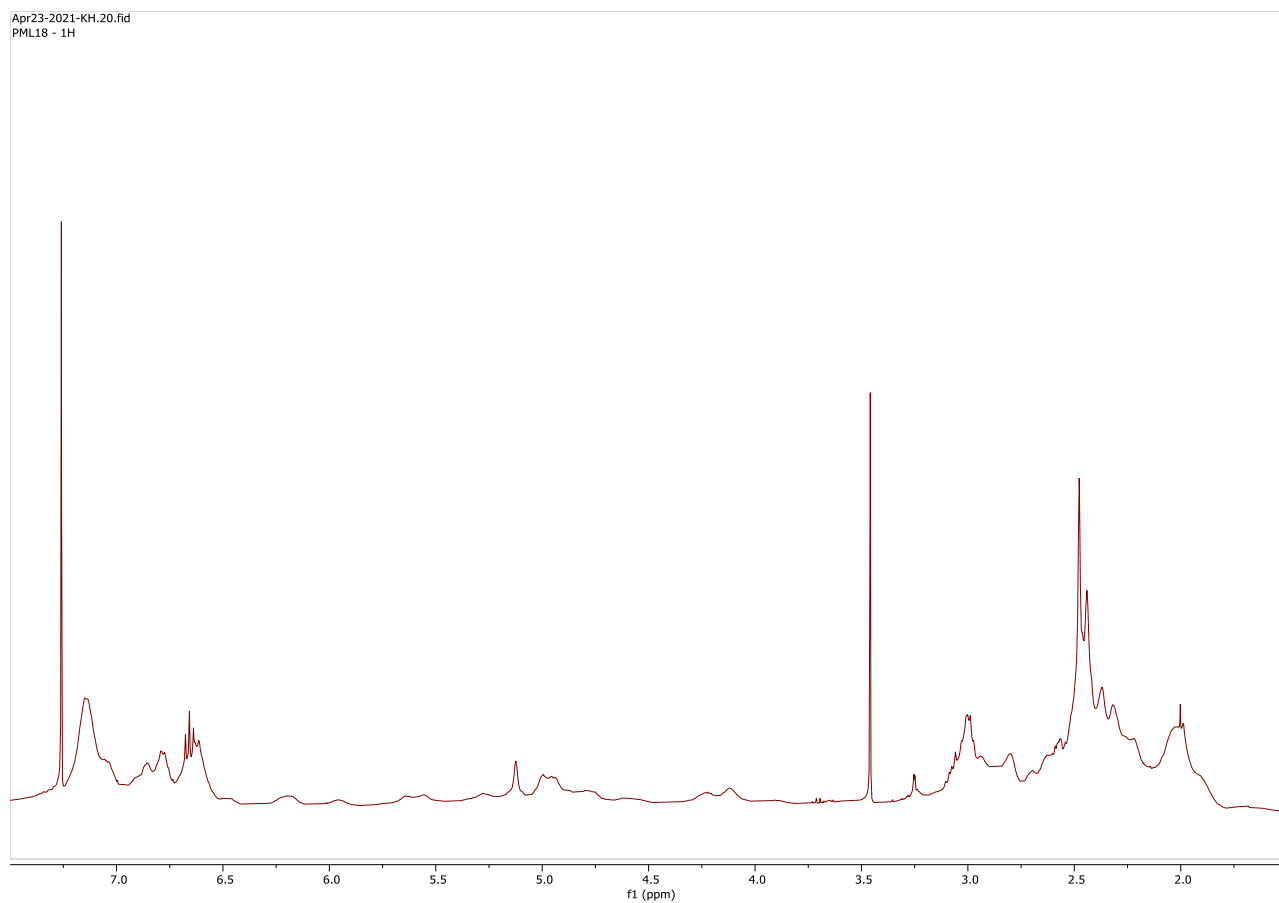


Figure S3. ^1H NMR Spectrum of Oleoidine (**2**) at rt in CDCl_3

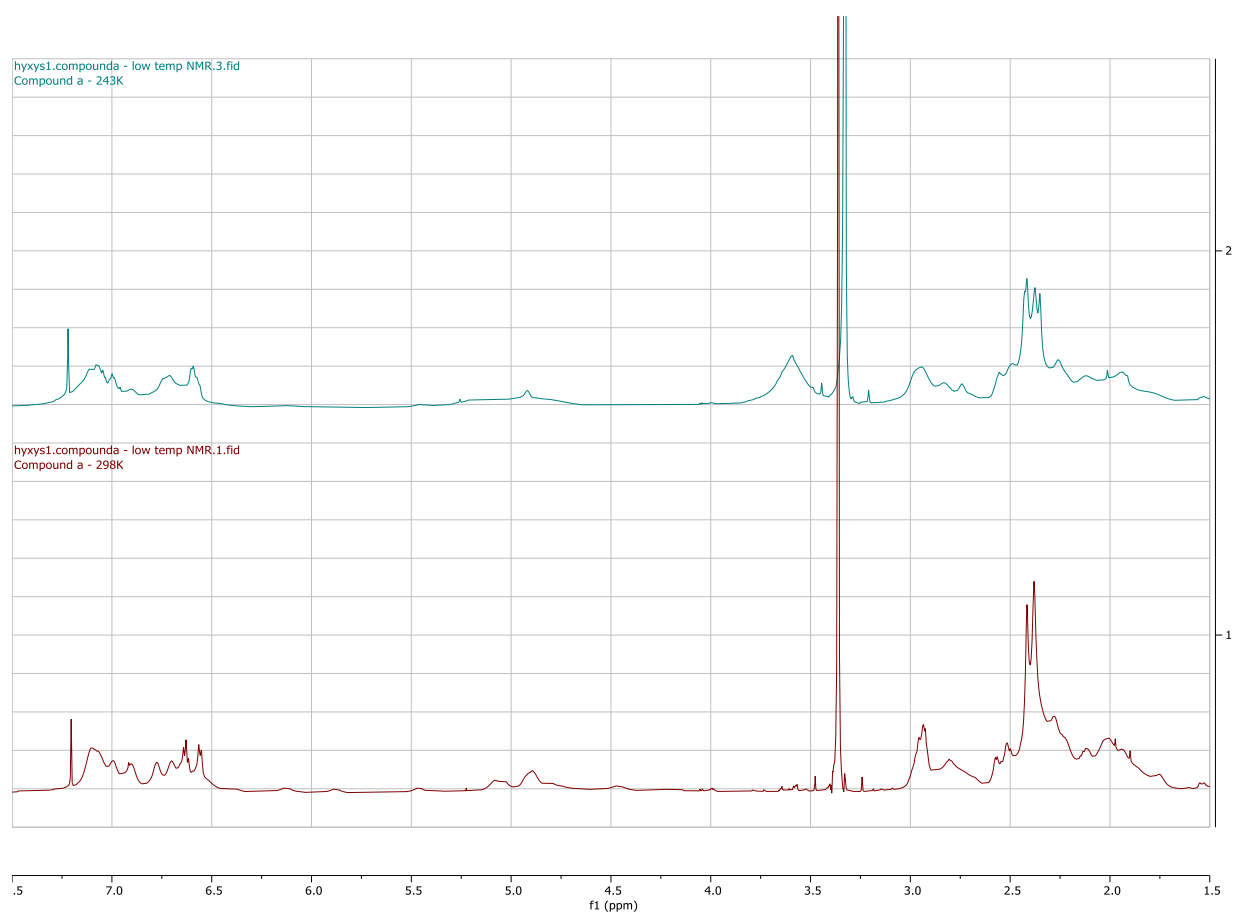


Figure S4. ^1H NMR Spectra of Oleoidine (**2**) at 243 K and 298 K in CD_3OD

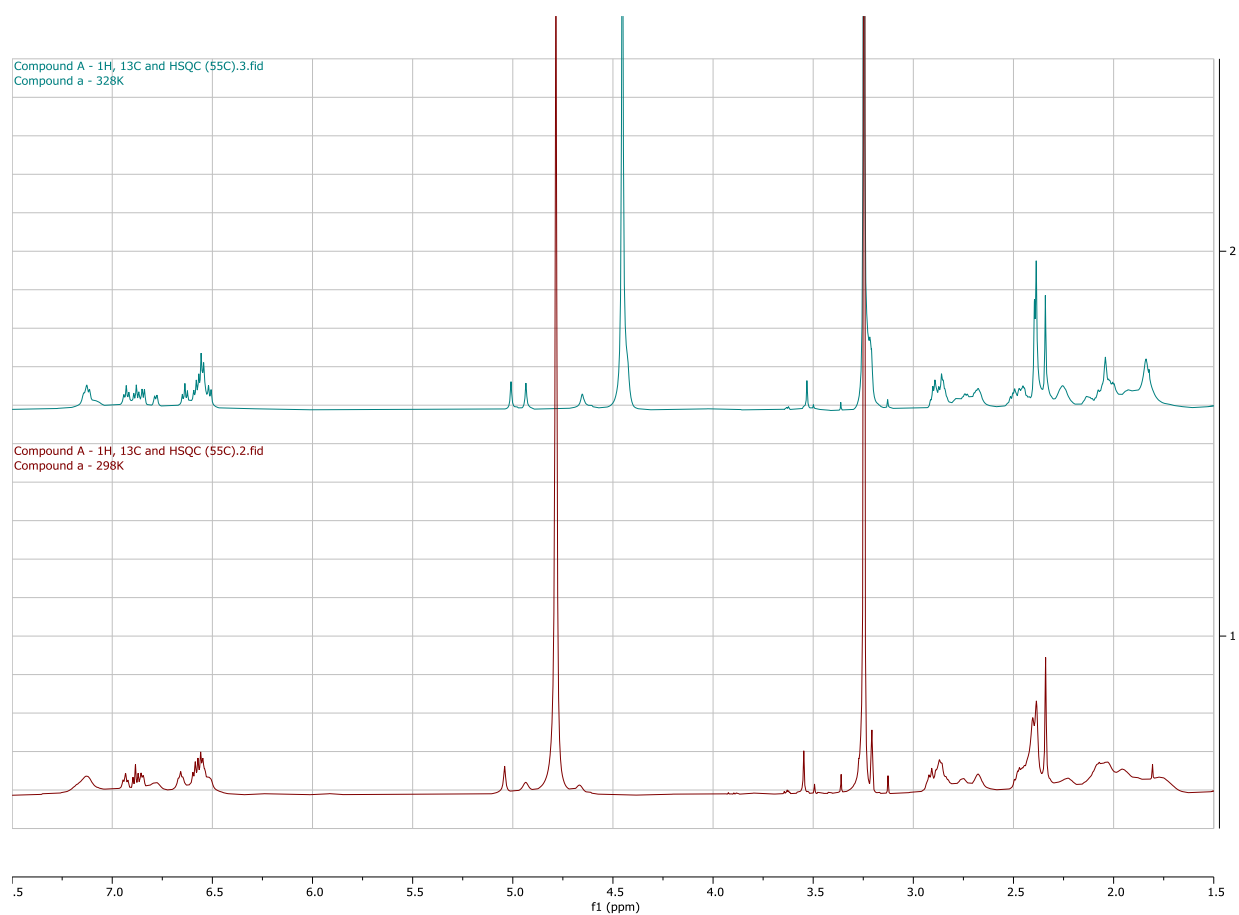


Figure S5. ^1H NMR Spectra of Oleoidine (**2**) at 328 K and 298 K in CD_3OD

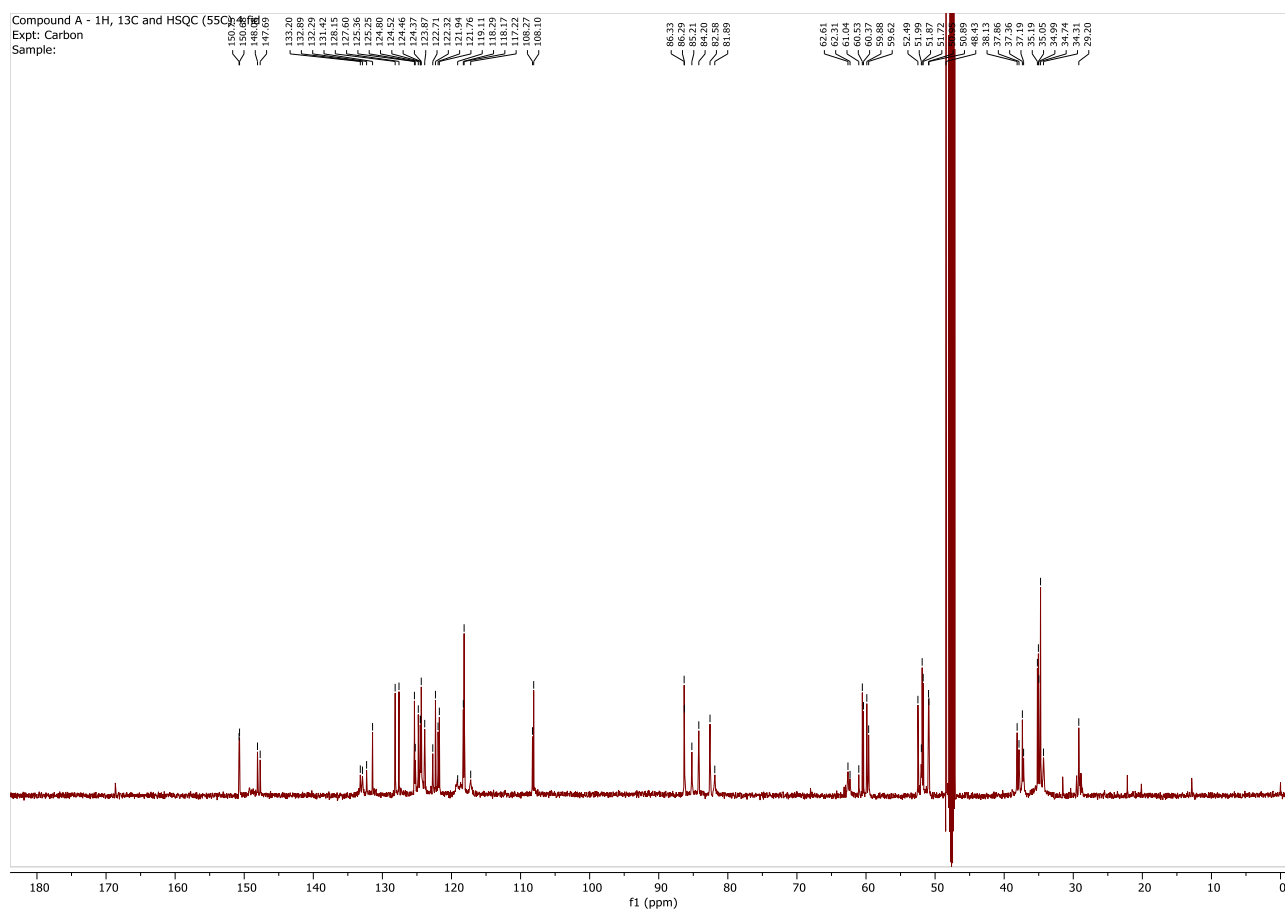


Figure S6. ¹³C NMR Spectrum of Oleoidine (**2**) at 328 K in CD₃OD

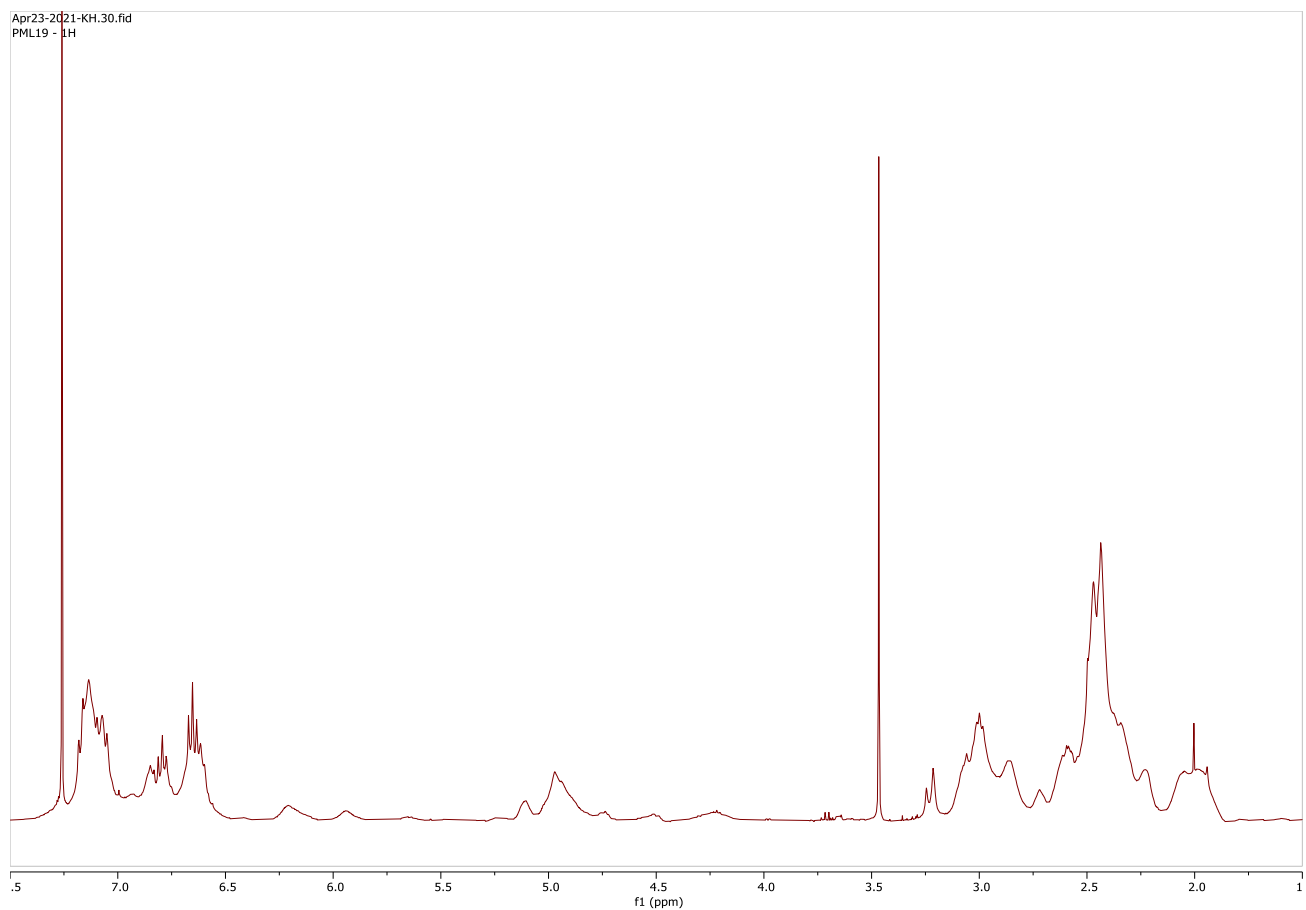


Figure S7. ^1H NMR Spectrum of Caledonine (**3**) at rt in CDCl_3

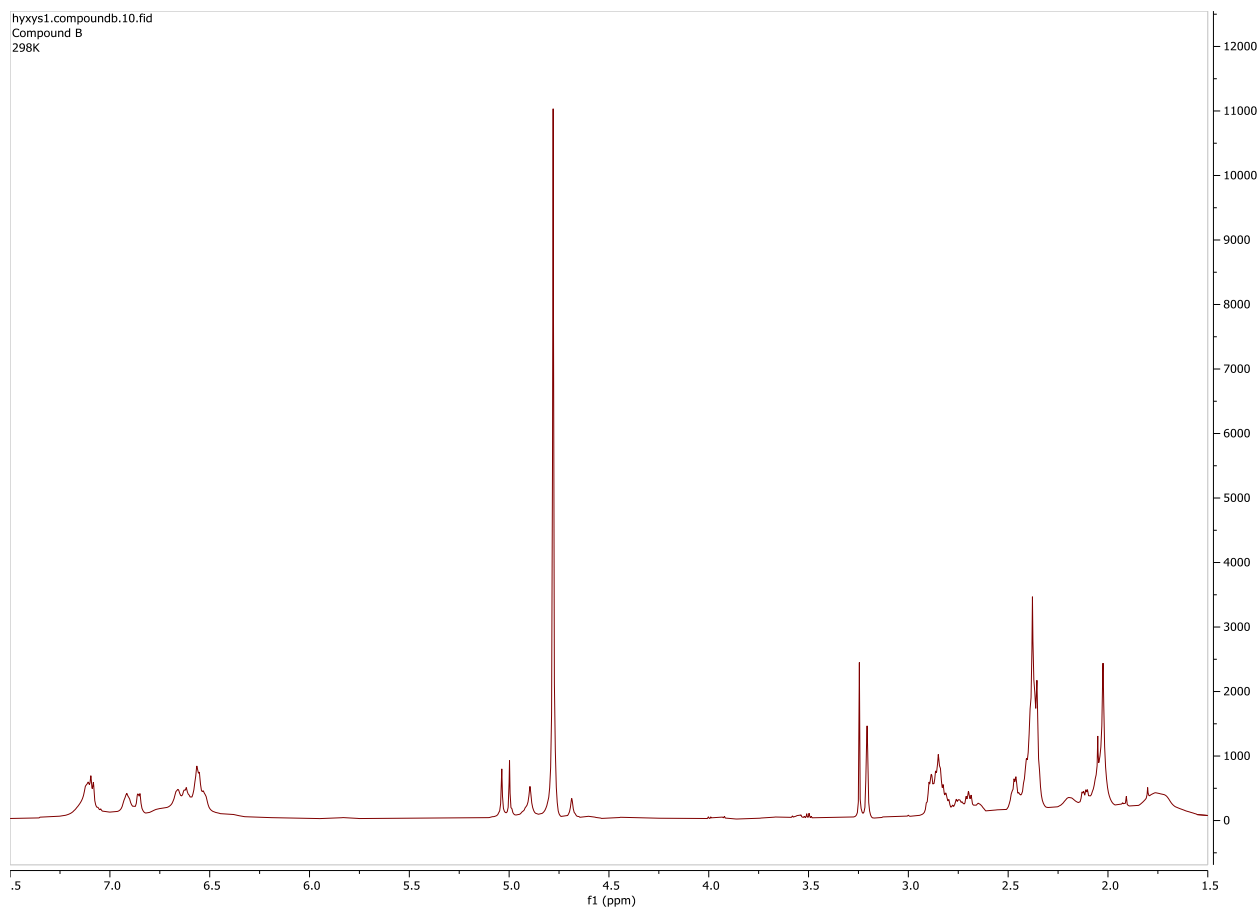


Figure S8. ^1H NMR Spectrum of Caledonine (**3**) at rt in CD_3OD

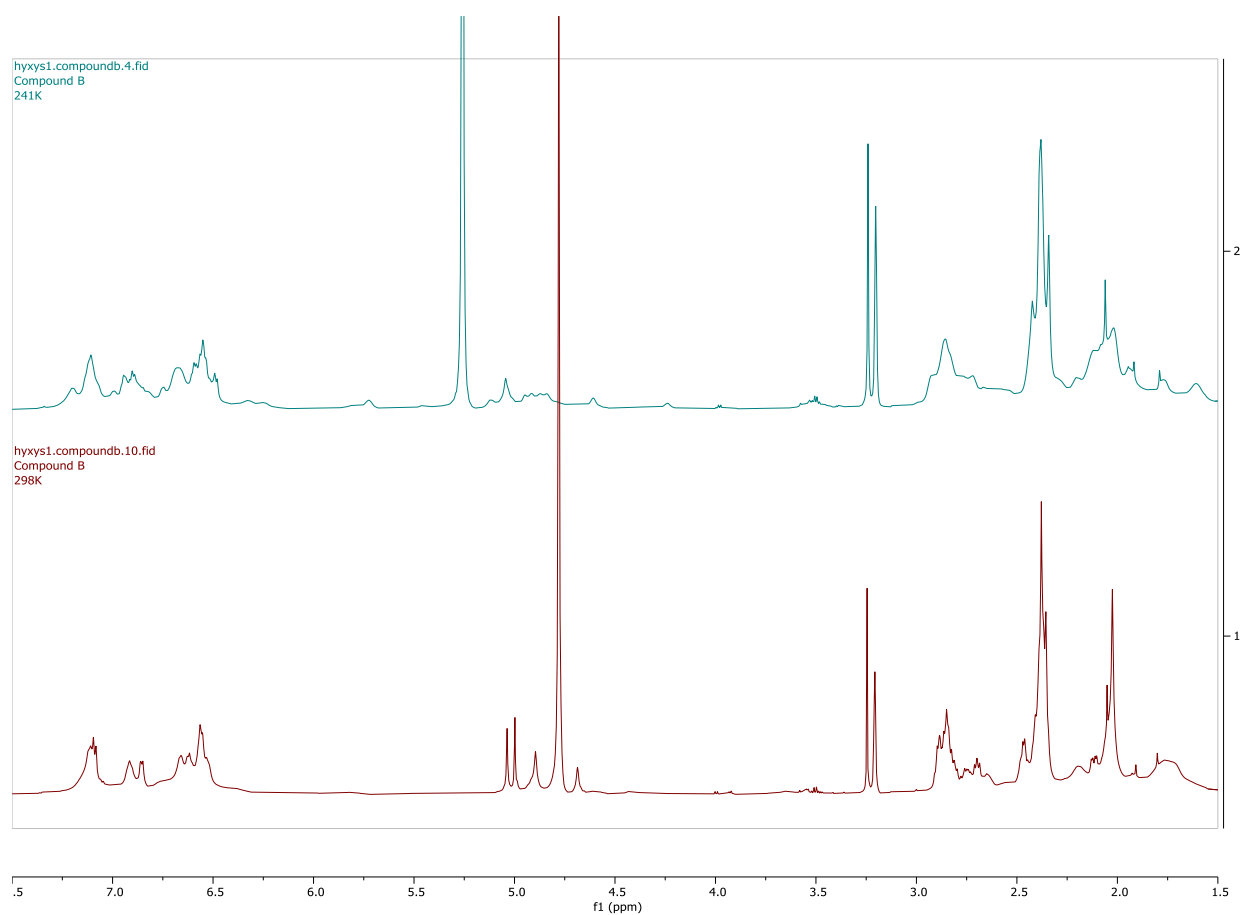


Figure S9. ¹H NMR Spectra of Caledonine (**3**) at 241 K and 298 K in CD₃OD

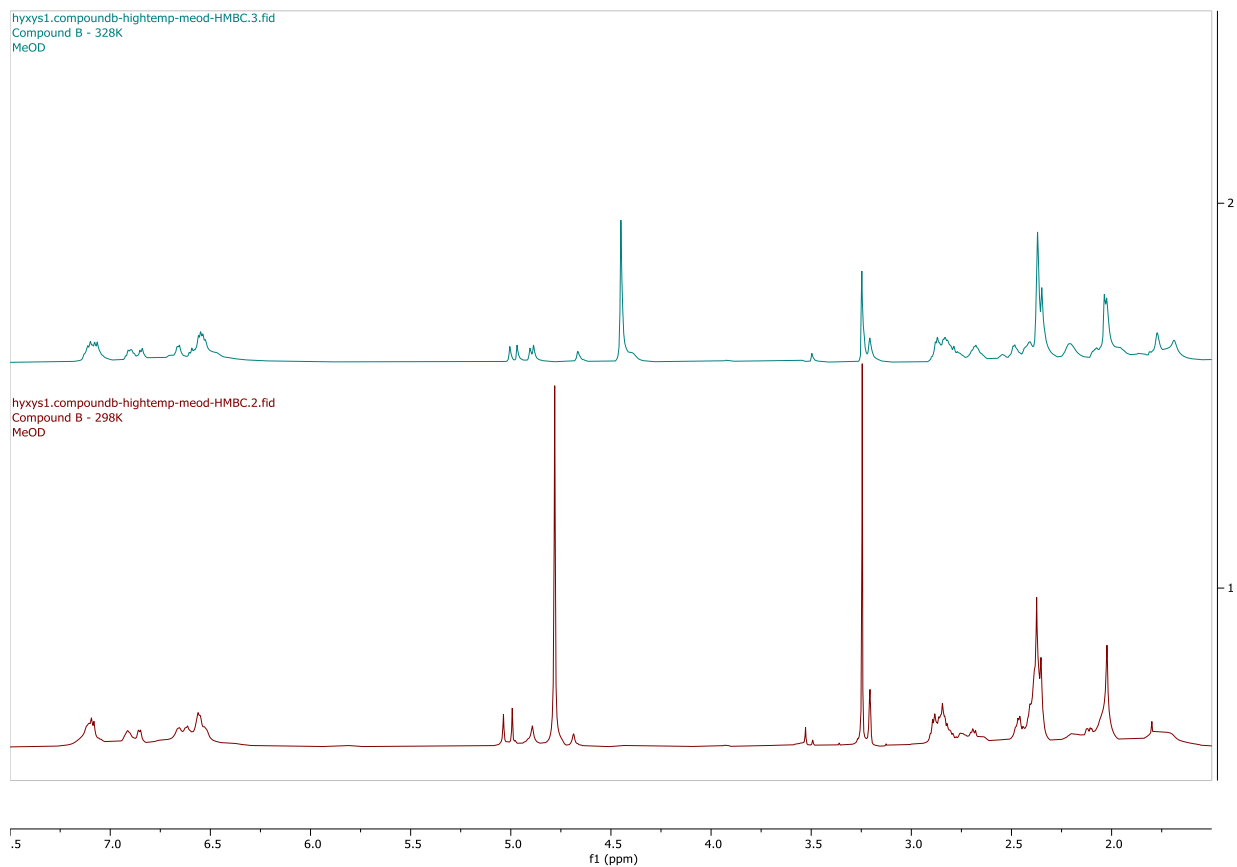


Figure S10. ^1H NMR Spectra of Caledonine (**3**) at 328 K and 298 K in CD_3OD

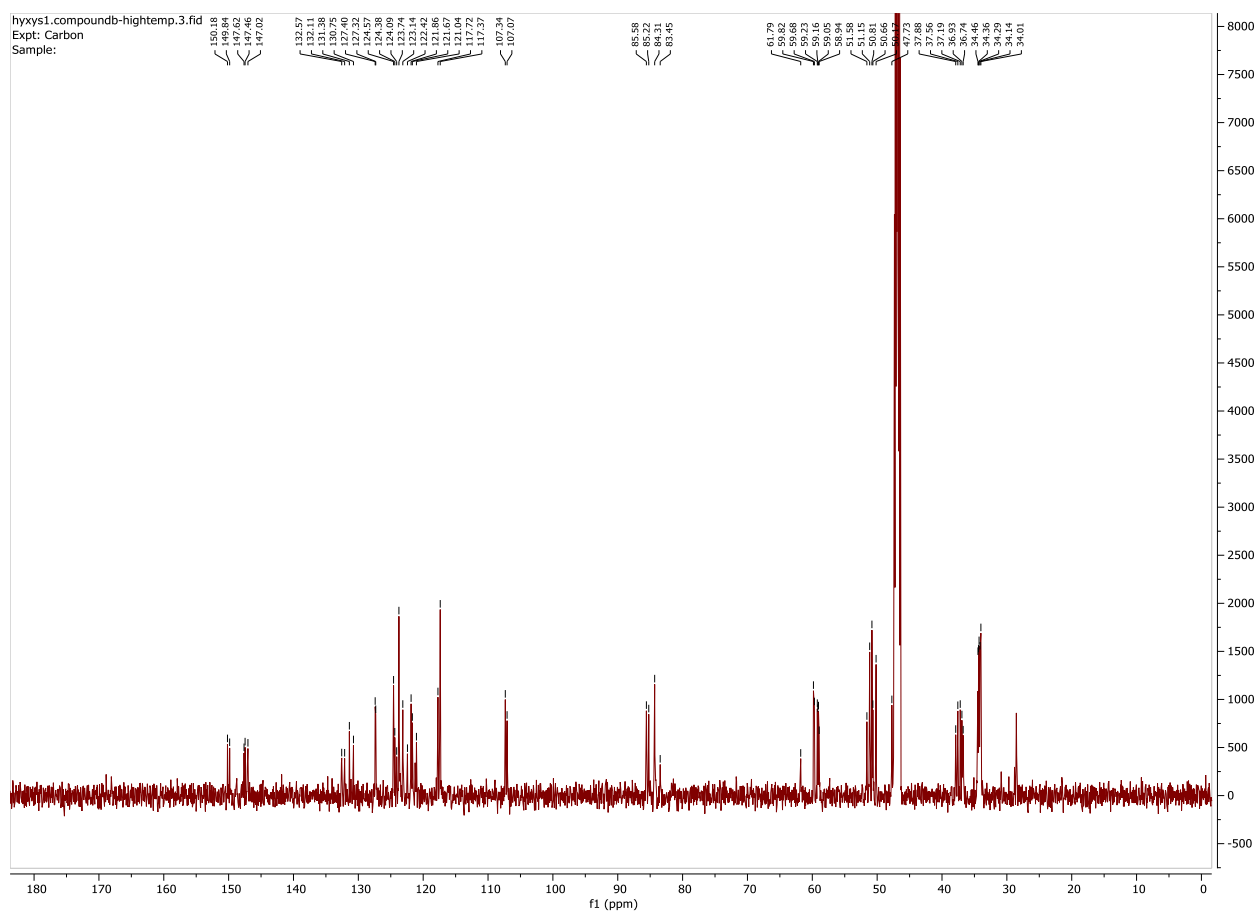


Figure S11. ^{13}C NMR Spectrum of Caledonine (**3**) at 328 K in CD_3OD

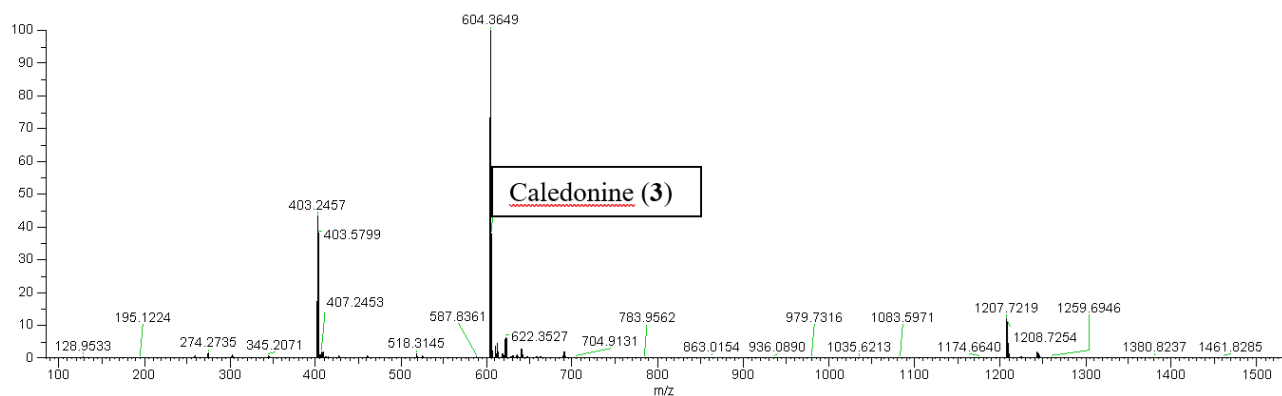
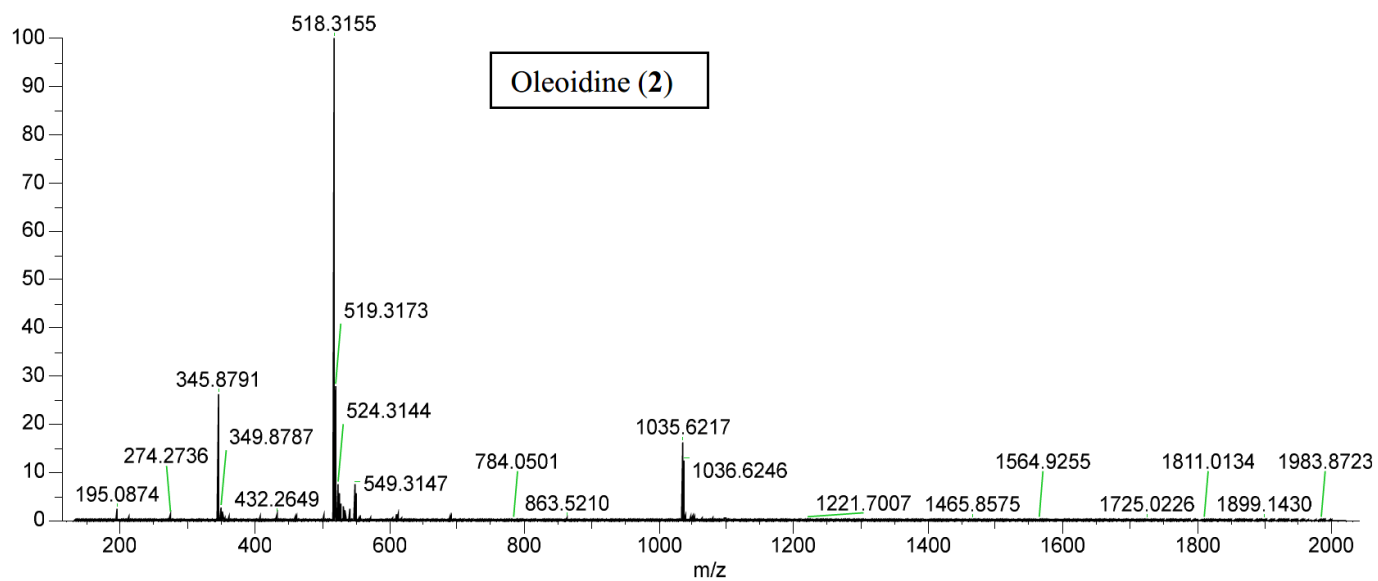
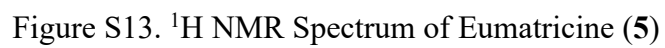


Figure S12. Mass Spectra of Oleoidine (2) and Caledonine (3)



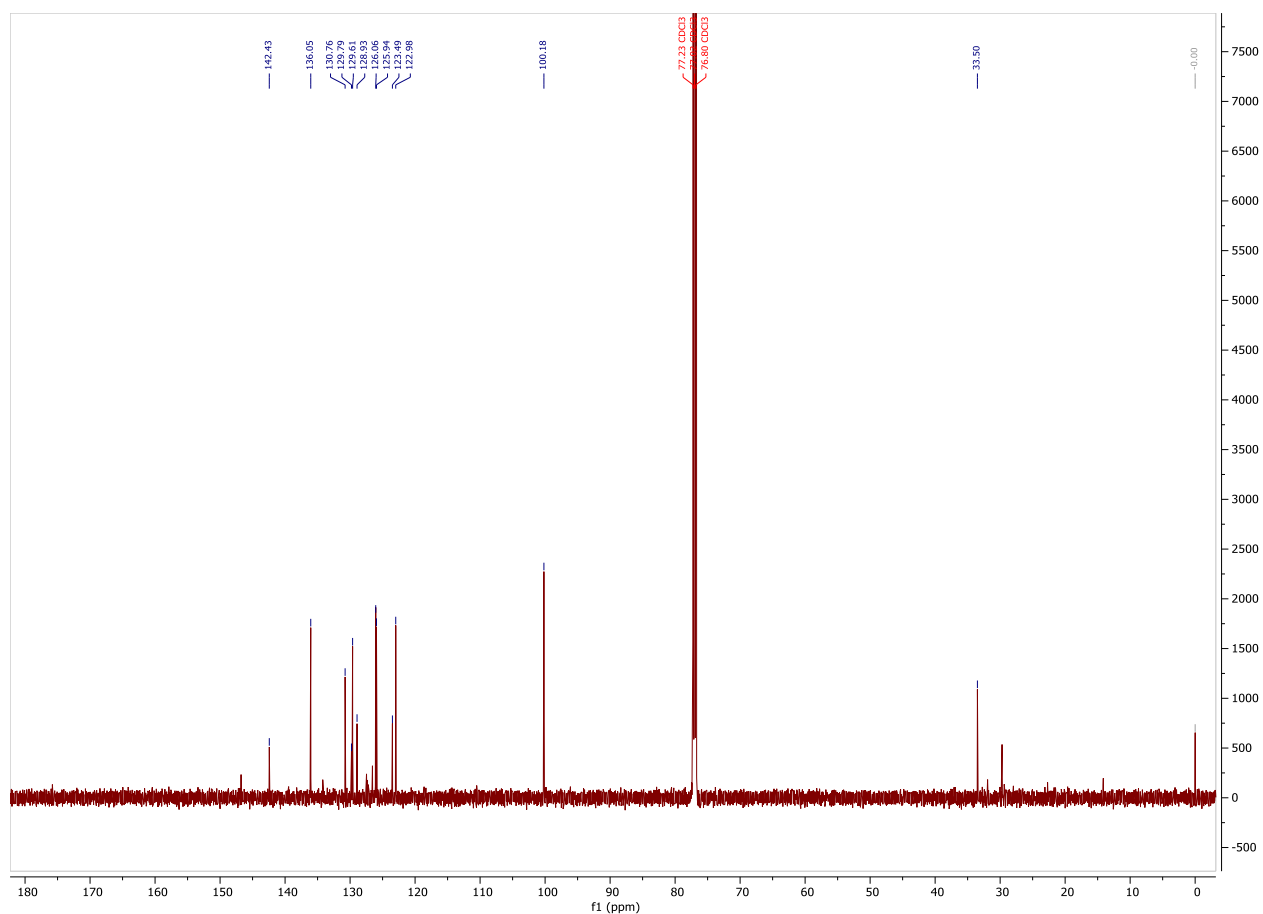


Figure S14. ^{13}C NMR Spectrum of Eumatricine (5)

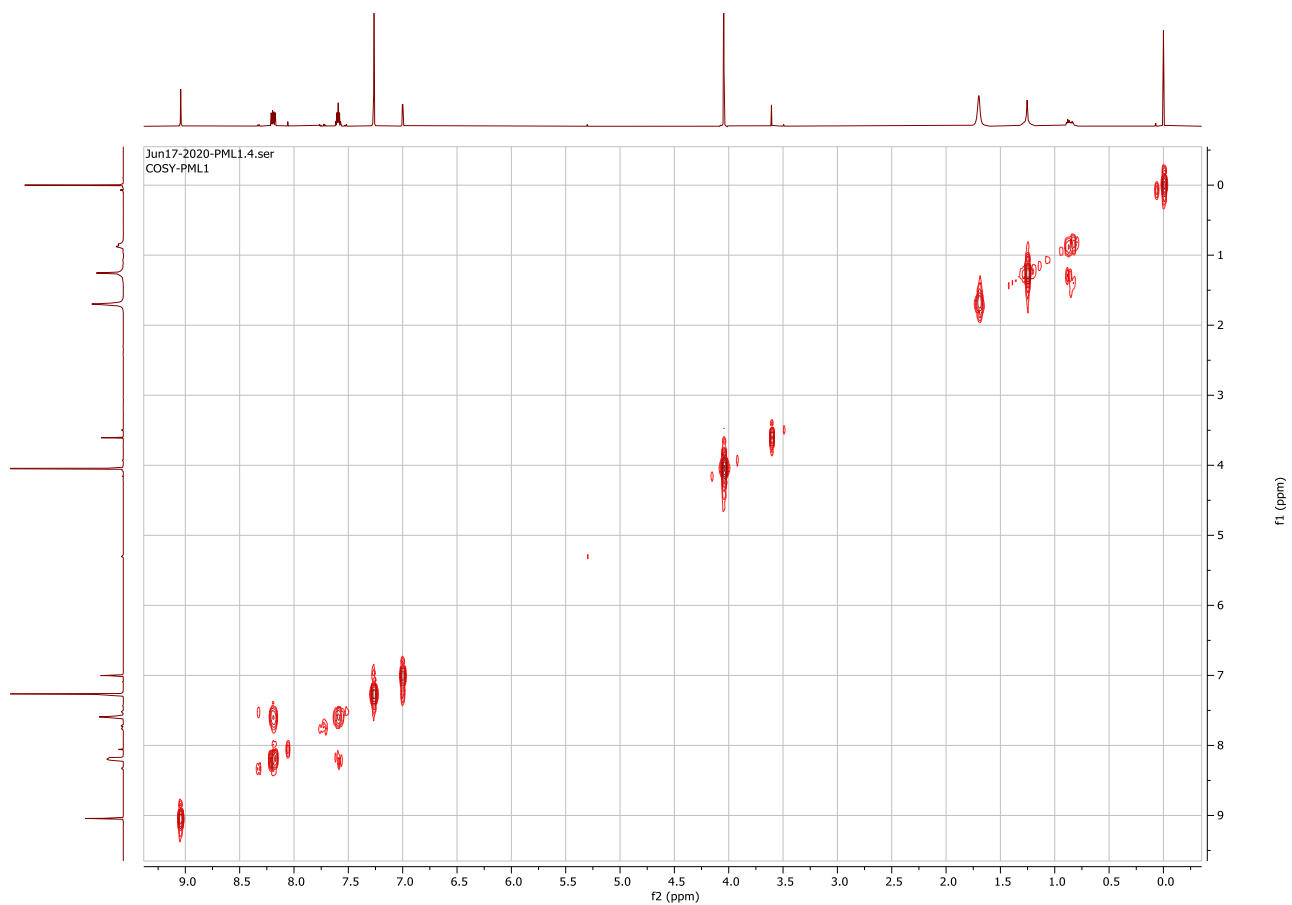


Figure S15. COSY Spectrum of Eumatricine (**5**)

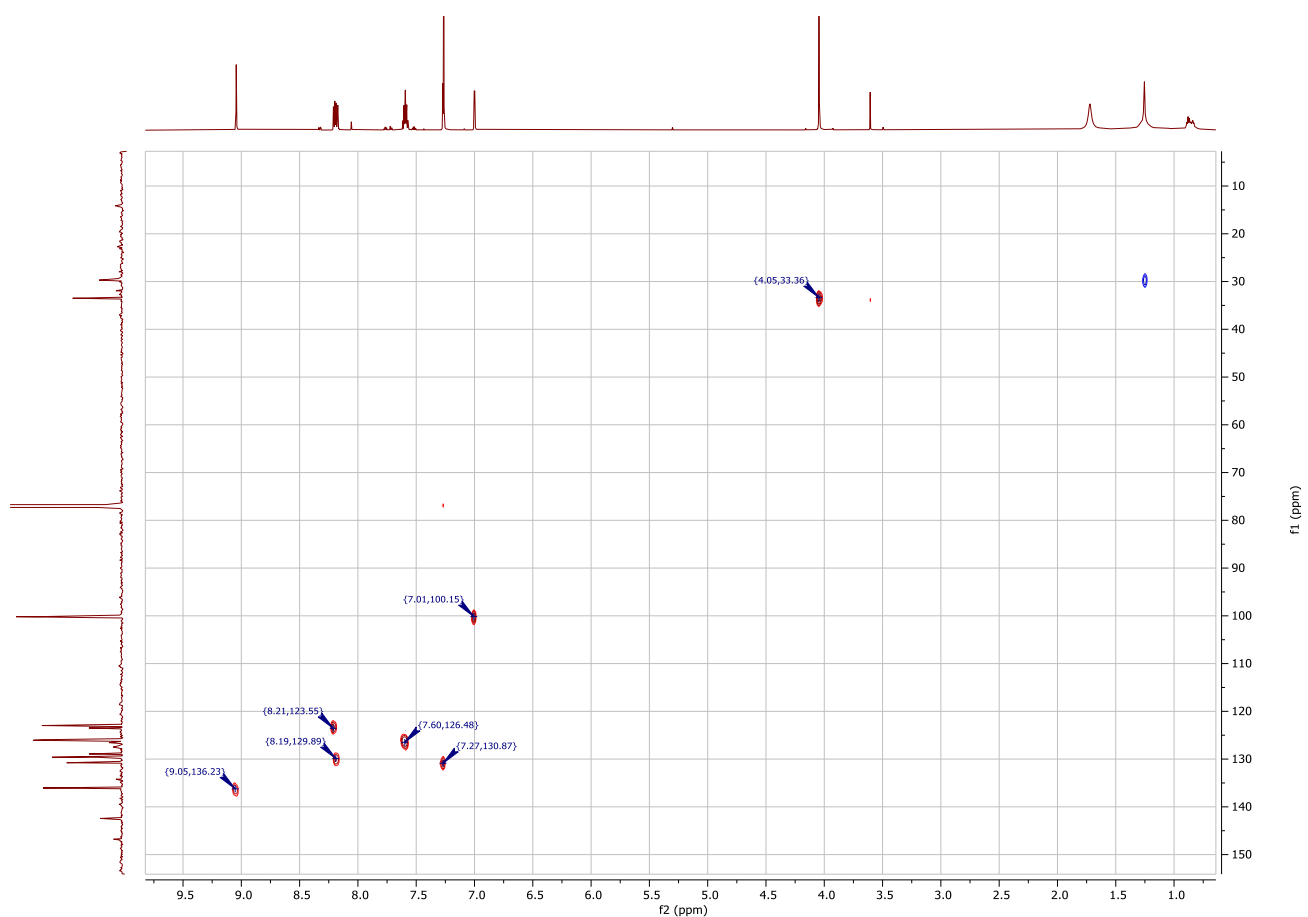


Figure S16. HSQC Spectrum of Eumatricine (5)

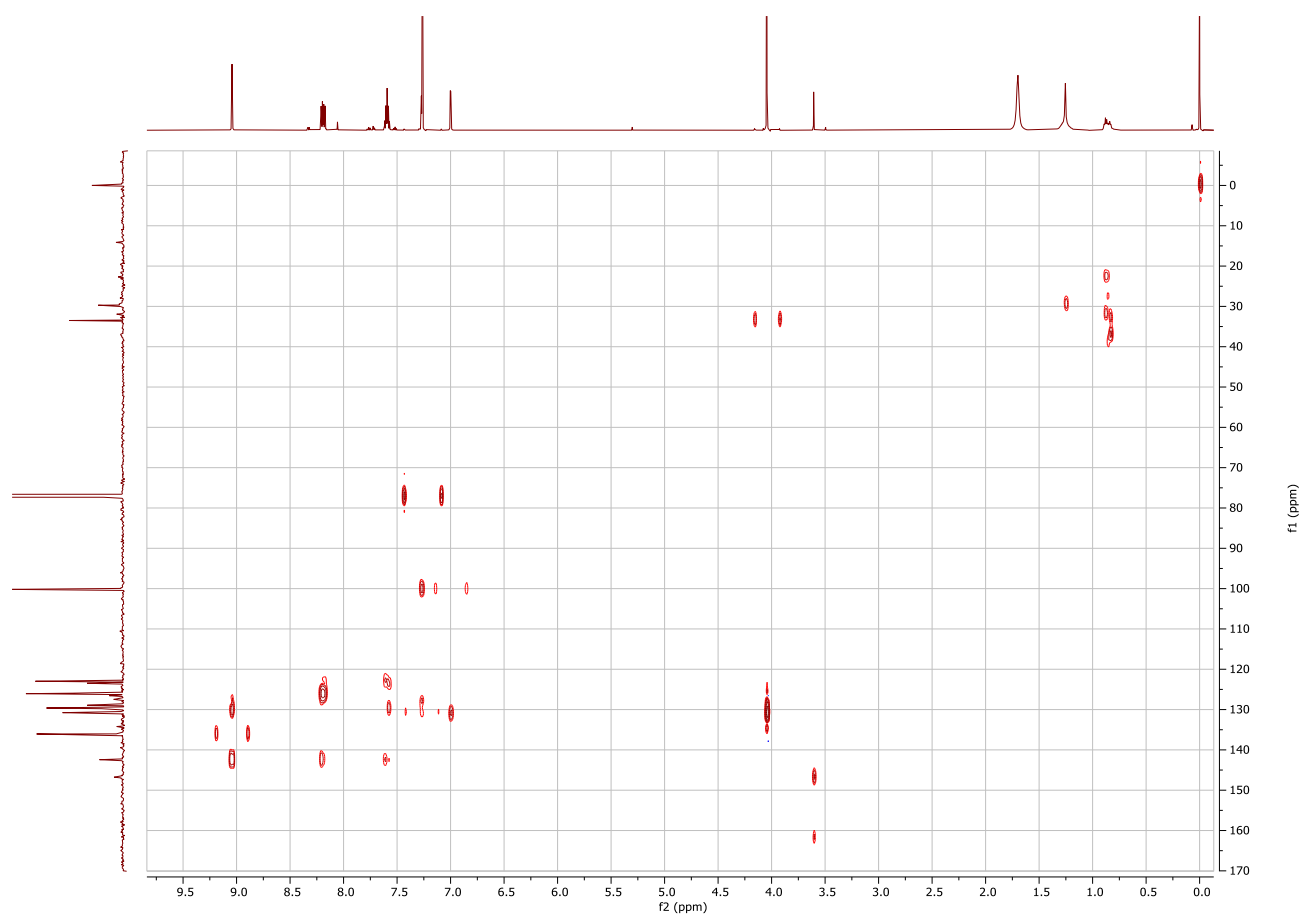


Figure S17. HMBC Spectrum of Eumatricine (**5**)

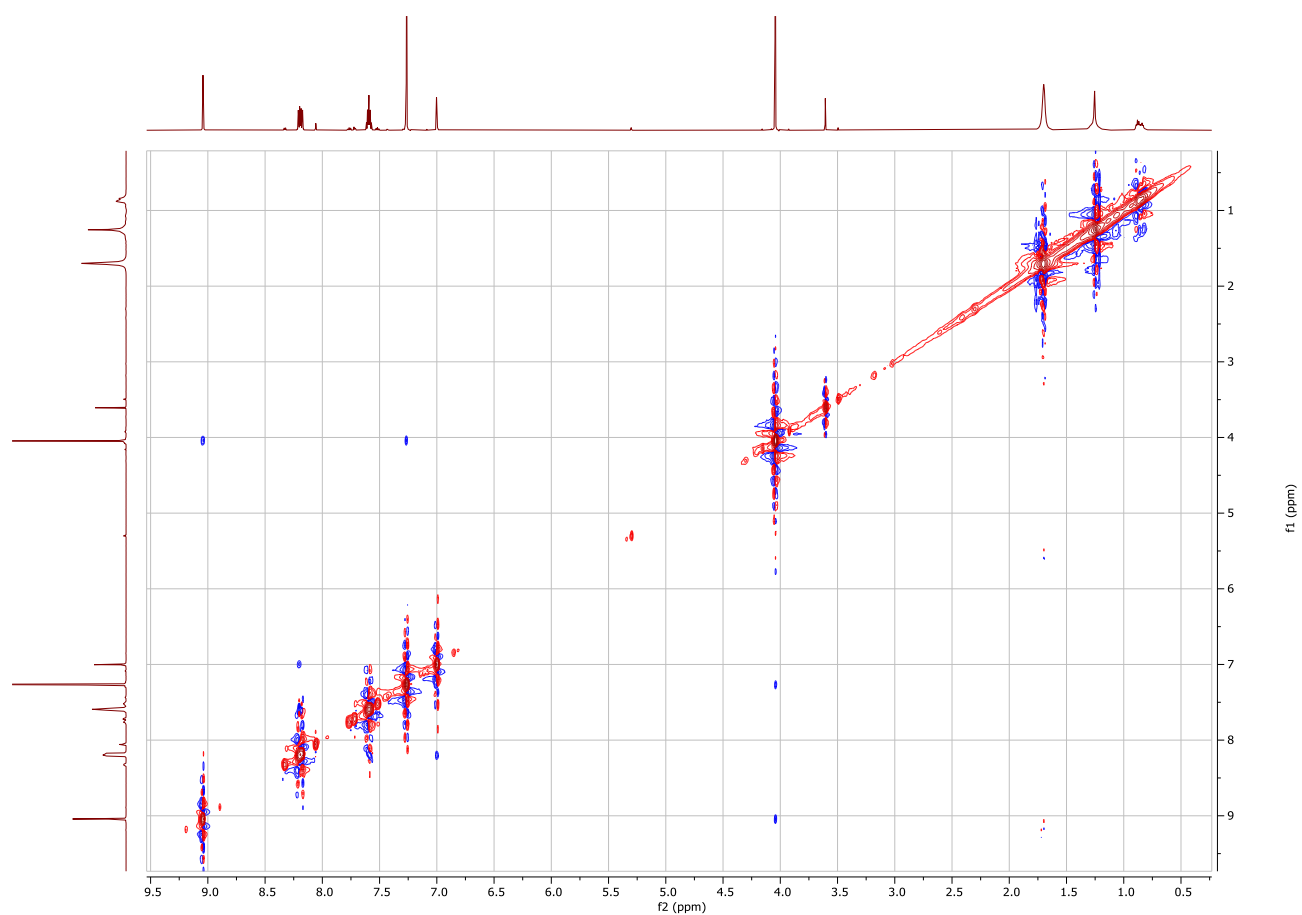
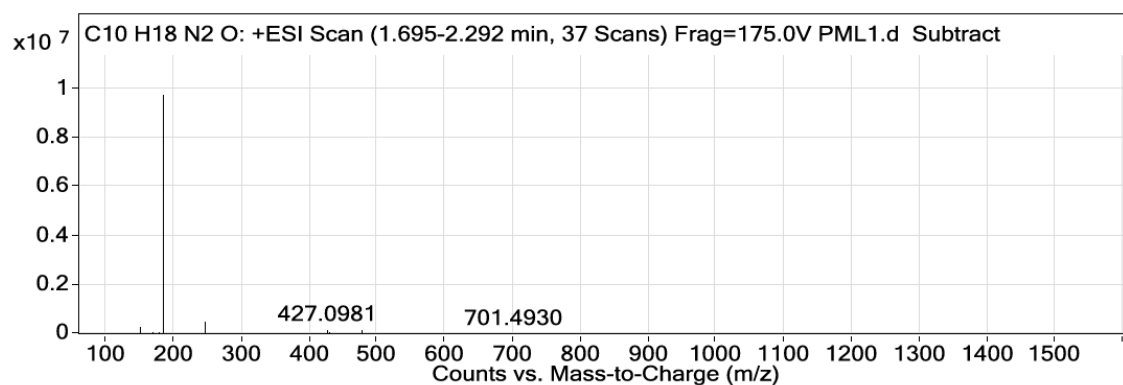


Figure S18. NOESY Spectrum of Eumatricine (**5**)



Peak List

m/z	z	Abund	Formula	Ion
149.0237	1	269279		
183.0932	1	9766457	C12 H10 N2	(M+H)+
183.1489		353347.53	C10 H18 N2 O	(M+H)+
184.0956	1	1664578.38	C12 H10 N2	(M+H)+
185.0984	1	87381.25	C12 H10 N2	(M+H)+
245.079	1	512324.81		
246.0819	1	62618.72		
427.0981	1	190984.48		

Figure S19. Mass Spectrum of Eumatricine (5)